eCAM Evidence-Based Complementary and Alternative Medicine

When Modern Technology Meets Ancient Traditional Chinese Medicine

Guest Editors: Calvin Yu-Chian Chen, James David Adams, Tingjun Hou, and Gerhard Litscher

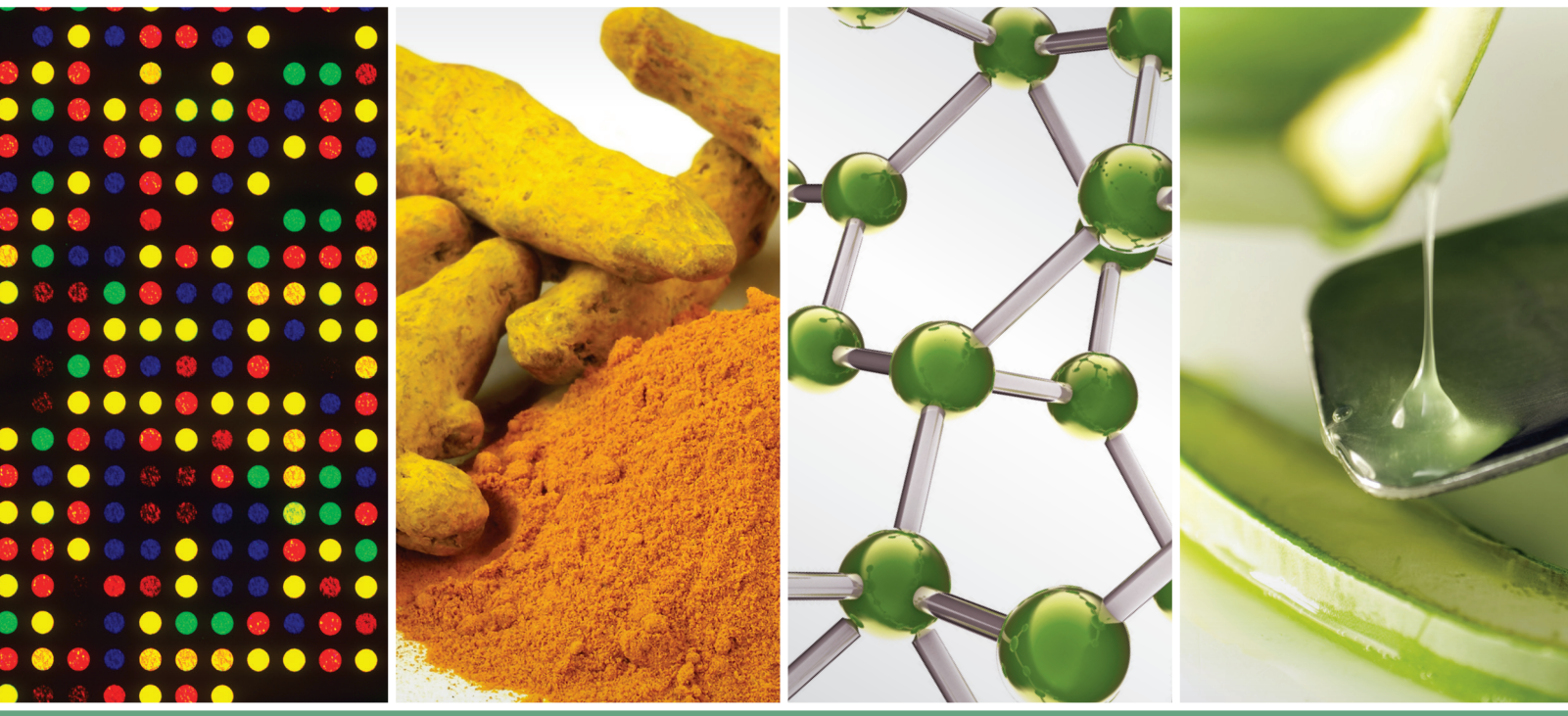

When Modern Technology Meets Ancient Traditional Chinese Medicine

Evidence-Based Complementary and Alternative Medicine

When Modern Technology Meets Ancient Traditional Chinese Medicine

Guest Editors: Calvin Yu-Chian Chen, James David Adams, Tingjun Hou, and Gerhard Litscher

Editorial Board

Contents

Hindawi Publishing Corporation
Evidence-Based Complementary and Alternative Medicine
Volume 2015, Article ID 156581, 2 pages
http://dx.doi.org/10.1155/2015/156581

Editorial

When Modern Technology Meets Ancient Traditional Chinese Medicine

Calvin Yu-Chian Chen,[1,2,3,4] James David Adams,[5] Tingjun Hou,[6] and Gerhard Litscher[3,7]

[1]*Human Genetic Center, Department of Medical Research, China Medical University Hospital, Taichung 40447, Taiwan*
[2]*Research Center for Chinese Medicine & Acupuncture, China Medical University, Taichung 40402, Taiwan*
[3]*School of Medicine, College of Medicine, China Medical University, Taichung 40402, Taiwan*
[4]*Department of Biomedical Informatics, Asia University, Taichung 41354, Taiwan*
[5]*Department of Pharmacology and Pharmaceutical Sciences, University of Southern California, School of Pharmacy, Los Angeles, CA, USA*
[6]*College of Pharmaceutical Sciences, Zhejiang University, Hangzhou, Zhejiang 310058, China*
[7]*TCM Research Center Graz, Medical University of Graz, 8036 Graz, Austria*

Correspondence should be addressed to Calvin Yu-Chian Chen; ycc929@mit.edu

Received 25 August 2014; Accepted 25 August 2014

In this issue, we select several papers related to how modern technology modernizes ancient traditional Chinese medicine such as acupuncture, herbal medicine, and other alternative treatments. There are 9 papers collected in this special issue. In this issue, we particularly picked some research articles which use computational techniques to approach ancient traditional Chinese medicine (TCM). No doubt TCM has a very strong clinical and experience base lasting for thousands of years. However, TCM is still a complementary and alternative medicine (CAM) because of its mysterious theoretical basis, including qi and blood. However, there are plenty of investigations that have identified the efficiency of TCM and acupuncture. In this issue, we present the issue of peroxisome proliferator-activated receptors (PPARs), acute lymphoblastic leukemia (ALL), protein phosphatase 2A (PP2A), diabetic nephropathy, antihepatic steatosis components within Coptidis Rhizoma alkaloids extract (CAE), dermal microcirculation blood perfusion characterization of meridian channels (acupoints), acute spinal cord injury, and nucleoside analogues (NAs) and a review paper of cerebrospinal fluid pharmacology.

The paper by K.-C. Chen and C. Y.-C. Chen raises an interesting issue about PPARs related to regulation of lipid metabolism, inflammation, cell proliferation, differentiation, and glucose homeostasis and control of related ligand-dependent transcription networks of genes. They screen potent compounds from TCM databases. Biological activity prediction using multiple linear regression (MLR), support vector machines (SVM), and Bayes network toolbox (BNT) models is utilized in this paper for more evidence of these potent TCM compounds. Furthermore, a molecular dynamics simulation is performed with a high speed workstation. The investigation shows that these TCMs might be potent leads for PPARs. Another paper contributed by Y.-L. Hsiao et al. uses different approach and method. They screen potent leads from Shanghai Innovative Research Center of Traditional Chinese Medicine (http://www.sirc-tcm.sh.cn/en/index.html) and use the MLR model and SVM model for further investigation. More evidence is also shown with CoMFA and CoMSIA models. Protein phosphatase 2A (PP2A) is an important phosphatase which regulates various cellular processes, such as protein synthesis, cell growth, cellular signalling, apoptosis, metabolism, and stress responses. K.-C. Chen et al. discover few potent TCM compounds from TCM databases by screening more than 61000 TCM compound databases. The disordered part of a protein might influence the efficacy of a drug; thus they analyse the disordered part in the first stage. It is a very new and important concept for screening and docking. However, in most of the recent studies, it seems that it is still not in practice yet. Their Figure 1 indicates that the structure of the binding domain is stable as the major

residues of the binding domain do not lie in the disordered region. This study also performs a time-consuming molecular dynamics experiment for further clarity.

L. Zhang et al. show their ability in text mining of the classical medical literature for medicines that show potential in diabetic nephropathy. They mention in the conclusion, "The methods developed in this study offer a targeted approach to identifying traditional herbs and/or formulae as candidates for further investigation in the search for new drugs for modern disease. However, more effort is still required to improve our techniques, especially with regard to compound formulae." H. Fan et al. publish a paper entitled "*In Vitro Screening for Antihepatic Steatosis Active Components within Coptidis Rhizoma Alkaloids Extract Using Liver Cell Extraction with HPLC Analysis and a Free Fatty Acid-Induced Hepatic Steatosis HepG2 Cell Assay*" and show significant results, finding two potent and active compounds within CAE. This indicates that the screening method they developed is a feasible, rapid, and useful tool for studying TCMs in treating hepatic steatosis.

Y. Wu et al. contribute a significant review article entitled "*Cerebrospinal Fluid Pharmacology: An Improved Pharmacology Approach for Chinese Herbal Medicine Research.*" They make an important conclusion we quote here, "In summary, CSFP provides a new strategy not only to eliminate some barriers of CHM research for treating ND, but also to broaden the pharmacology research for bridging the gap between CHM and modern medicine. Moreover, the advancements in CSFP will bring about a conceptual move in active ingredients discovery of CHM and make a significant contribution to CHM modernization and globalization."

D. Zhou et al. contribute a research article entitled "*Microcirculation Perfusion Monitor on the Back of the Health Volunteers.*" They observe some of the characteristics of the dermal microcirculation blood perfusion of the governor meridian. All of the features of the governor meridian have not been shown. In future research, they plan to accomplish the characterization of all of the features of the governor meridian as well as the other twelve regular meridians and draw the specific dermal microcirculation blood perfusion graphs of the fourteen meridians in order to provide evidence that microcirculation changes after interventions or under pathological conditions.

M. Du et al. publish an interesting paper entitled "*A Brief Analysis of Traditional Chinese Medical Elongated Needle Therapy on Acute Spinal Cord Injury and Its Mechanism.*" From their investigation, we learn that elongated needle therapy has an obvious effect on acute spinal cord injury in rabbits. Its mechanism involves inhibiting the expression of the Fas $\rightarrow$ caspase-3 cascade, thereby inhibiting cell apoptosis after spinal cord injury.

L. Min et al. show their powerful ability in mathematic modelling investigation in TCM. We quote their important results, "The modelling analysis with the experimental data analysis motivates to propose the previous three hypotheses, which may interpret some clinical experience judgements. The dynamics of anti-HBV infection therapy are very complex. It is difficult to set up mathematical model to describe them accurately. However, modelling dynamics of anti-HBV infection therapy would enable a better understanding, prediction, and design of anti-HBV infection treatments."

Overall, we can see that modern technology is used for investigating TCM related studies. We also hope more modern techniques can be applied in TCM studies to speed up the modernization of TCM.

Acknowledgments

Firstly we express our sincere thanks and gratitude to the Editorial Board of this journal for their approval of this concept and continuous help in the successful publication of this special issue. We would also like to thank contributors to this special issue for their scientifically sound papers. With great pleasure and respect we extend our thanks to the reviewers for critical assessment of each paper, their constructive criticisms, and timely responses that made this special issue possible.

Calvin Yu-Chian Chen
James David Adams
Tingjun Hou
Gerhard Litscher

Hindawi Publishing Corporation
Evidence-Based Complementary and Alternative Medicine
Volume 2014, Article ID 192452, 19 pages
http://dx.doi.org/10.1155/2014/192452

Research Article

In Silico Identification of Potent PPAR-γ Agonists from Traditional Chinese Medicine: A Bioactivity Prediction, Virtual Screening, and Molecular Dynamics Study

Kuan-Chung Chen[1] and Calvin Yu-Chian Chen[2,3]

[1] *School of Pharmacy, China Medical University, Taichung 40402, Taiwan*
[2] *School of Medicine, College of Medicine, China Medical University, Taichung 40402, Taiwan*
[3] *Department of Biomedical Informatics, Asia University, Taichung 41354, Taiwan*

Correspondence should be addressed to Calvin Yu-Chian Chen; ycc929@MIT.edu

Received 17 December 2013; Accepted 25 January 2014; Published 26 May 2014

Academic Editor: Fuu-Jen Tsai

The peroxisome proliferator-activated receptors (PPARs) related to regulation of lipid metabolism, inflammation, cell proliferation, differentiation, and glucose homeostasis by controlling the related ligand-dependent transcription of networks of genes. They are used to be served as therapeutic targets against metabolic disorder, such as obesity, dyslipidemia, and diabetes; especially, PPAR-γ is the most extensively investigated isoform for the treatment of dyslipidemic type 2 diabetes. In this study, we filter compounds of traditional Chinese medicine (TCM) using bioactivities predicted by three distinct prediction models before the virtual screening. For the top candidates, the molecular dynamics (MD) simulations were also utilized to investigate the stability of interactions between ligand and PPAR-γ protein. The top two TCM candidates, 5-hydroxy-L-tryptophan and abrine, have an indole ring and carboxyl group to form the H-bonds with the key residues of PPAR-γ protein, such as residues Ser289 and Lys367. The secondary amine group of abrine also stabilized an H-bond with residue Ser289. From the figures of root mean square fluctuations (RMSFs), the key residues were stabilized in protein complexes with 5-Hydroxy-L-tryptophan and abrine as control. Hence, we propose 5-hydroxy-L-tryptophan and abrine as potential lead compounds for further study in drug development process with the PPAR-γ protein.

1. Introduction

The peroxisome proliferator-activated receptors (PPARs) belonged to the nuclear receptor superfamily of ligand-inducible transcription factors. They are "fatty acid sensors" related to regulation of lipid metabolism, inflammation, cell proliferation, differentiation, and glucose homeostasis by controlling the related ligand-dependent transcription of networks of genes [1–3]. There are three different isoforms of PPARs in mammal, which are PPAR-α, PPAR-γ, and PPAR-δ/β. They have different tissue distributions and responses to different ligands [4–6]. PPARs are used to be served as therapeutic targets against metabolic disorder, such as obesity, dyslipidemia, and diabetes; especially, PPAR-γ is the most extensively investigated isoform for the treatment of dyslipidemic type 2 diabetes [7–10]. It is a well-known receptor located in fat for antidiabetic insulin sensitizers and has the functions related to adipogenesis, lipogenesis, and glucose homeostasis [11–13]. In rat stroke models, PPAR-γ has been served as a brain protector against ischemic cerebral infraction [14].

Nowadays, increasing numbers of drug are designed with a target protein against a specific disease [15–18], as increasing numbers of distinct mechanism of diseases have been

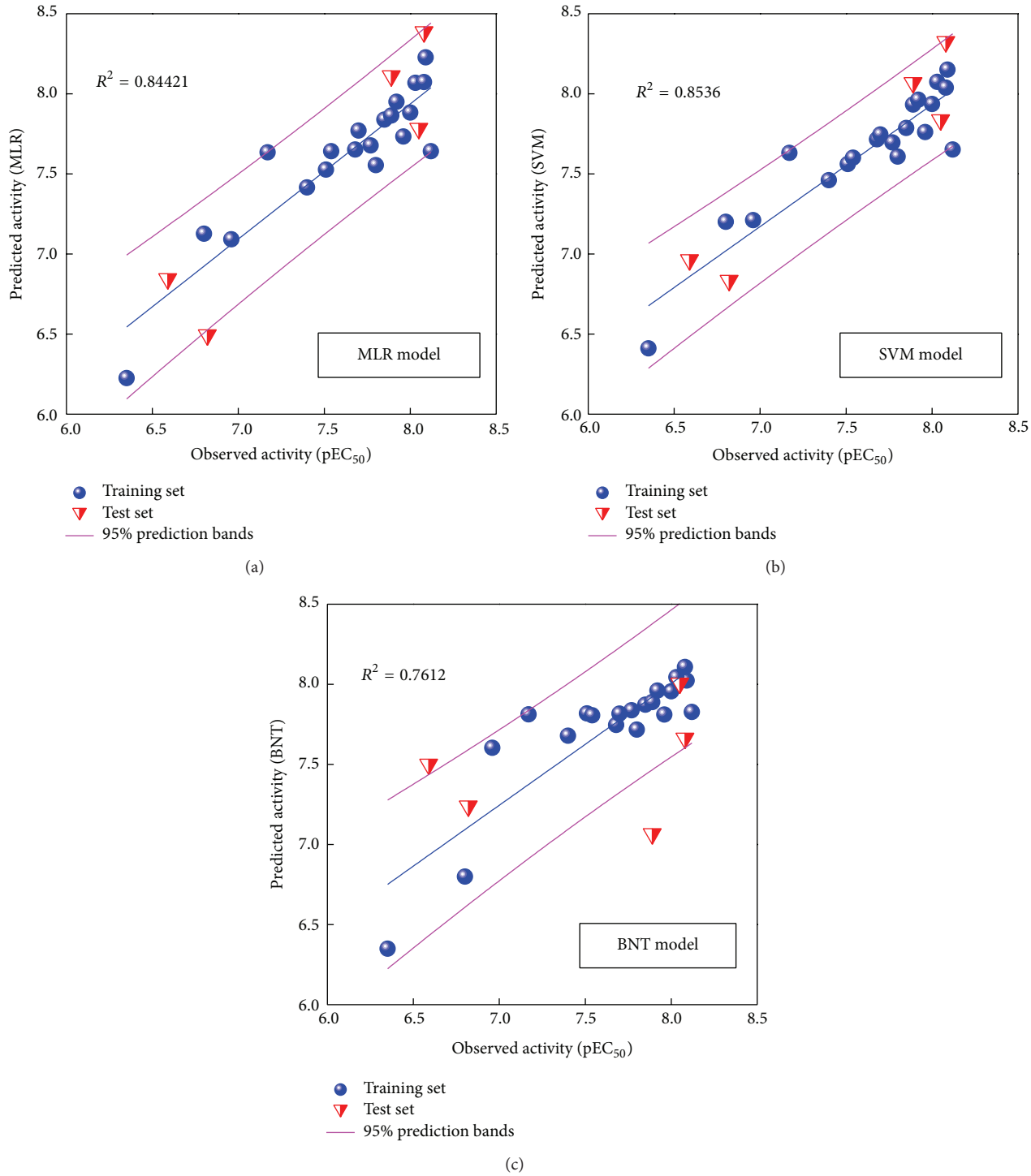

Figure 1: Comparative plots of observed versus predicted activity for (a) MLR, (b) SVM, and (c) BNT models. Correlation trend (blue line) and 95% prediction boundaries (enclosed by magenta lines) were shown.

identified by the researches [19–26]. Recently, the compounds from traditional Chinese herb have been proven to have the therapeutic effects [27–30]. In previous researches, many compounds of traditional Chinese medicine (TCM) have been indicated as potential candidates of lead compounds against cancer [31–34], neuropathic pain [35], stroke [36, 37], and virus infection [38, 39].

In the former study, we aim to detect potential candidates from TCM compounds as agonists targeting PPAR-α, PPAR-δ, and PPAR-γ [40]. However, a compound which had

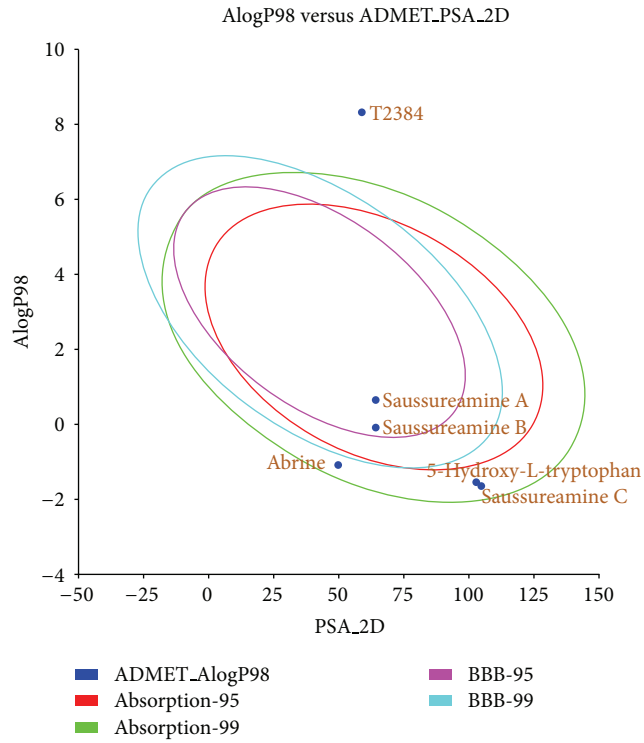

Figure 2: Human intestinal absorption model for top TCM compounds and T2384.

Table 1: Docking results, predicted pEC_{50}, and ADMET properties for top TCM compounds and T2384.

Name	Dock score	Predicted pEC_{50}			CYP2D6[a] probability	Hepatotoxicity probability	PPB level[b]
		MLR	SVM	BNT			
5-Hydroxy-L-tryptophan	148.721	5.89	6.62	6.59	0.069	0.291	0
Abrine	142.592	6.31	6.63	6.44	0.049	0.642	0
Saussureamine C	135.304	5.90	7.27	7.91	0.415	0.450	0
Saussureamine B	124.688	8.85	7.63	8.00	0.356	0.708	0
Saussureamine A	103.030	7.59	7.81	7.64	0.336	0.754	0
*T2384	77.618	7.52	7.06	8.50	0.069	0.953	2

*Control.
[a]Inhibition probability of cytochrome P450 2D6 enzyme.
[b]Plasma protein binding: 0: binding is <90%; 1: binding is >90%; 3: binding is >95%.

a higher binding affinity with target protein may not always obtain a higher bioactivity. In this paper, we aimed to focus on the target protein of PPAR-γ and filter TCM compounds using bioactivities predicted by three distinct prediction models before the virtual screening. The molecular dynamics (MD) simulations were also utilized to investigate the stability of interactions between ligand and PPAR-γ protein in the docking pose under dynamic conditions. We attempt to identify the potent TCM compounds with higher bioactivities and binding affinity for PPAR-γ protein and discuss the functional group of these candidates and common binding residues of PPAR-γ protein in their docking pose.

2. Materials and Methods

2.1. Data Collection. After TCM compounds from TCM database, Taiwan [41], were filtered by Lipinski et al.'s rule of five [42], a total of 9,029 nonduplicate compounds were prepared by Prepare Ligand module in Discovery Studio 2.5 (DS2.5) to adjust the ionization state to physiological setting for virtual screening. For calculating the pharmacokinetics properties, ADMET Descriptors model in DS2.5 was employed to calculate the aqueous solubility, CYP2D6 binding, hepatotoxicity, and plasma protein binding (PPB) as absorption, distribution, metabolism, excretion, and toxicity (ADMET) properties for each compound.

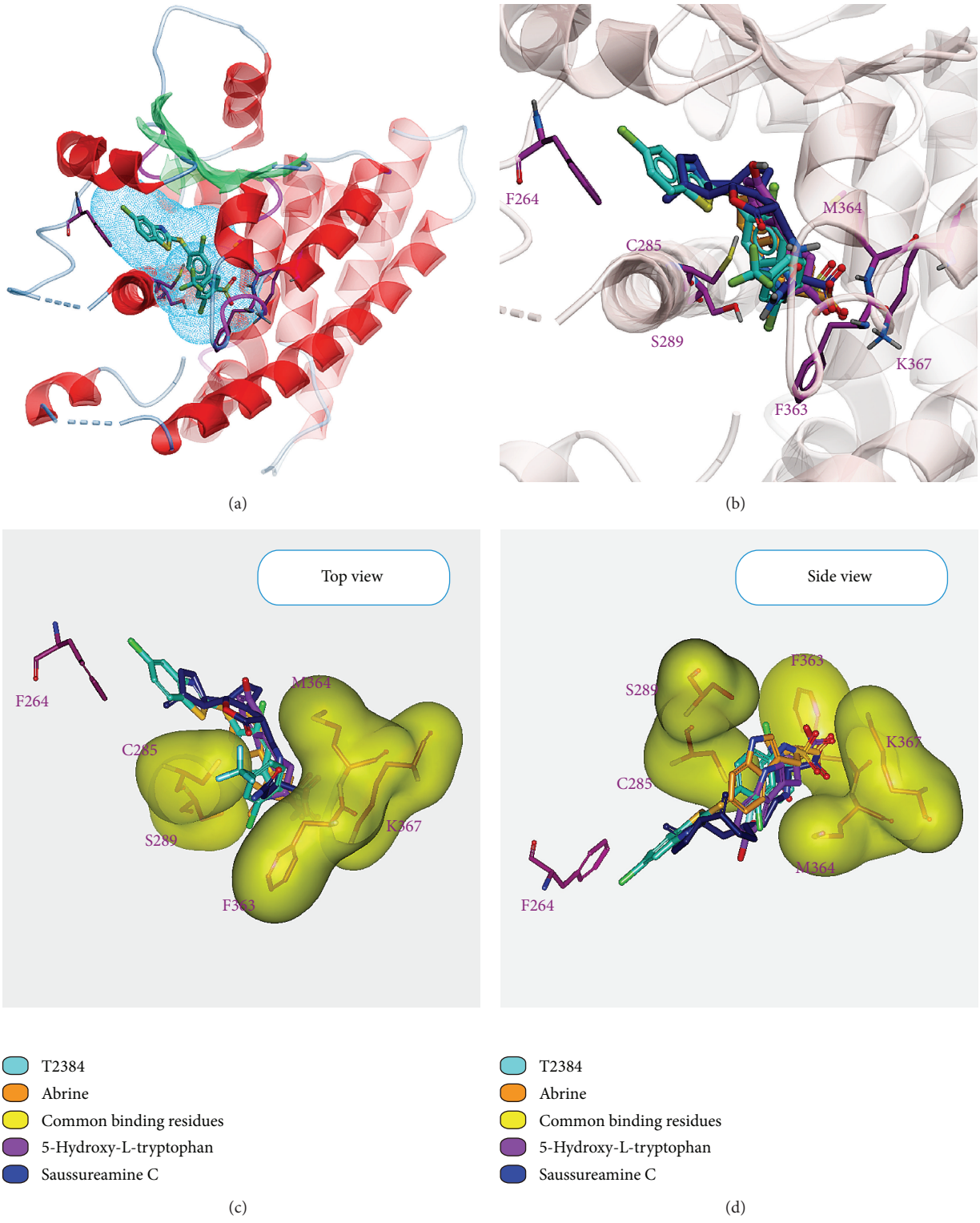

Figure 3: Binding sites and common binding residues for PPAR-γ protein. PPAR-γ protein with (a) binding site defined by T2384, (b) docking poses of top TCM compounds and T2384 in the binding site. (c) Top view, (d) side view of docking poses with common binding residues.

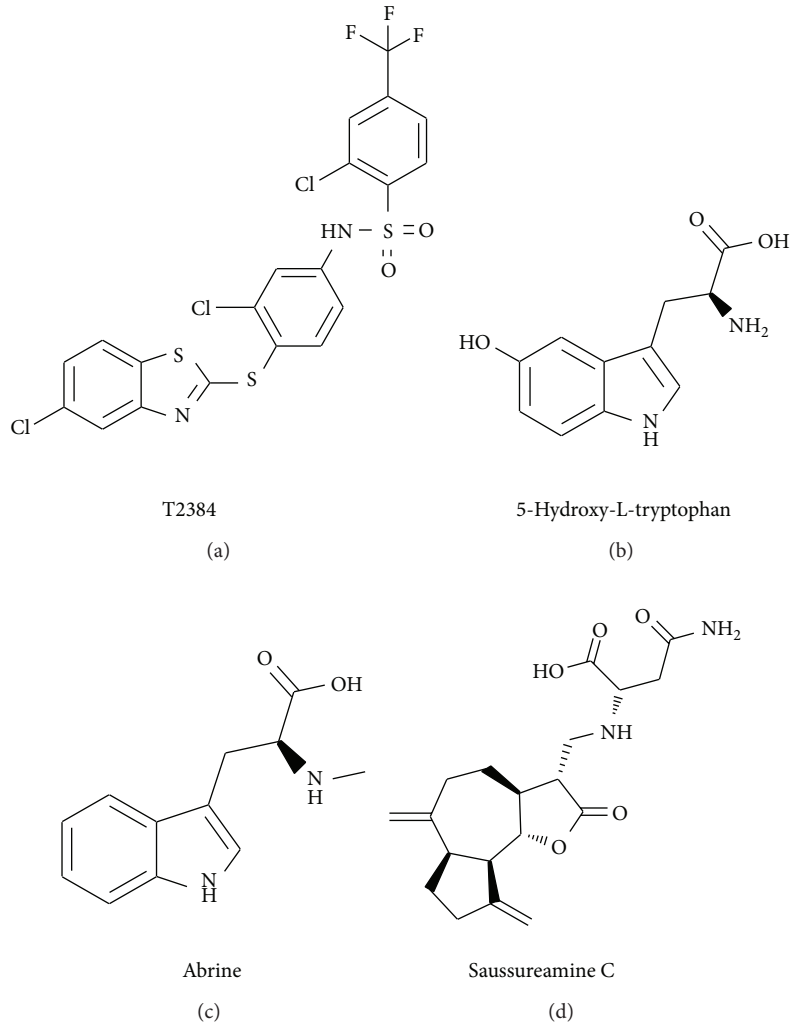

Figure 4: Chemical scaffold of control and top three candidates: (a) T2384, (b) 5-hydroxy-L-tryptophan, (c) abrine, and (d) saussureamine C.

The X-ray crystallography structure of the human peroxisome proliferator-activated receptor gamma (PPAR-γ) protein was obtained from RCSB Protein Data Bank with PDB ID: 3K8S [43]. After protein preparation, the chain A of PPAR-γ protein was used as target protein for virtual screening, and T2384, cocrystallized in PPAR-γ protein, was used as control.

2.2. Biological Activity Prediction Using Multiple Linear Regression (MLR), Support Vector Machine (SVM), and Bayes Network Toolbox (BNT) Models. For the prediction of biological activity for the TCM compounds, three distinct prediction models were constructed with the pEC_{50} ($\log(1/EC_{50})$) value of 20 compounds from Rikimaru et al.'s study [2] as training set. The genetic function approximation module [44] of DS 2.5 was utilized to determine the suitable molecular descriptors for constructing the prediction models, and the fitness of individual model was estimated by square correlation coefficient (R^2). Cross-validation test was used to validate the prediction model. For three distinct prediction models, multiple linear regression and Bayes network toolbox were performed using MATLAB, and support vector machine was performed using LibSVM developed by Chang and Lin [45].

2.3. Docking Simulation. For virtual screening, LigandFit protocol [46] in DS 2.5 was employed to dock each compound into an active site using a shape filter and Monte Carlo ligand conformation generation, and each docked pose was minimized with Chemistry at HARvard Macromolecular Mechanics (CHARMM) force field [47] and evaluated with a set of scoring functions. In addition, LigPlot

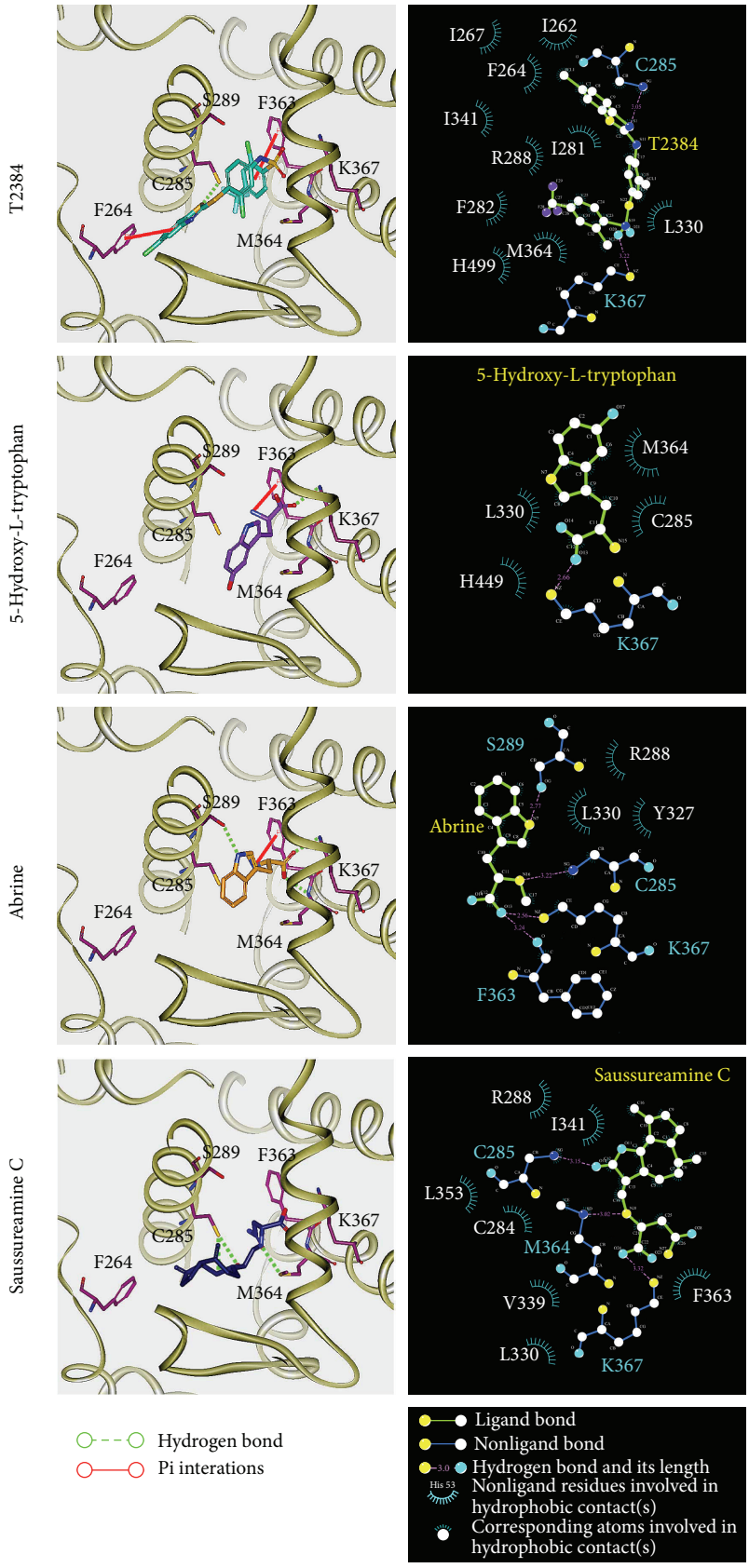

Figure 5: Docking pose of PPAR-γ complexes with T2384, 5-hydroxy-L-tryptophan, abrine, and saussureamine C, respectively. Hydrophobic contacts between PPAR-γ protein and each compound determined by LIGPLOT program.

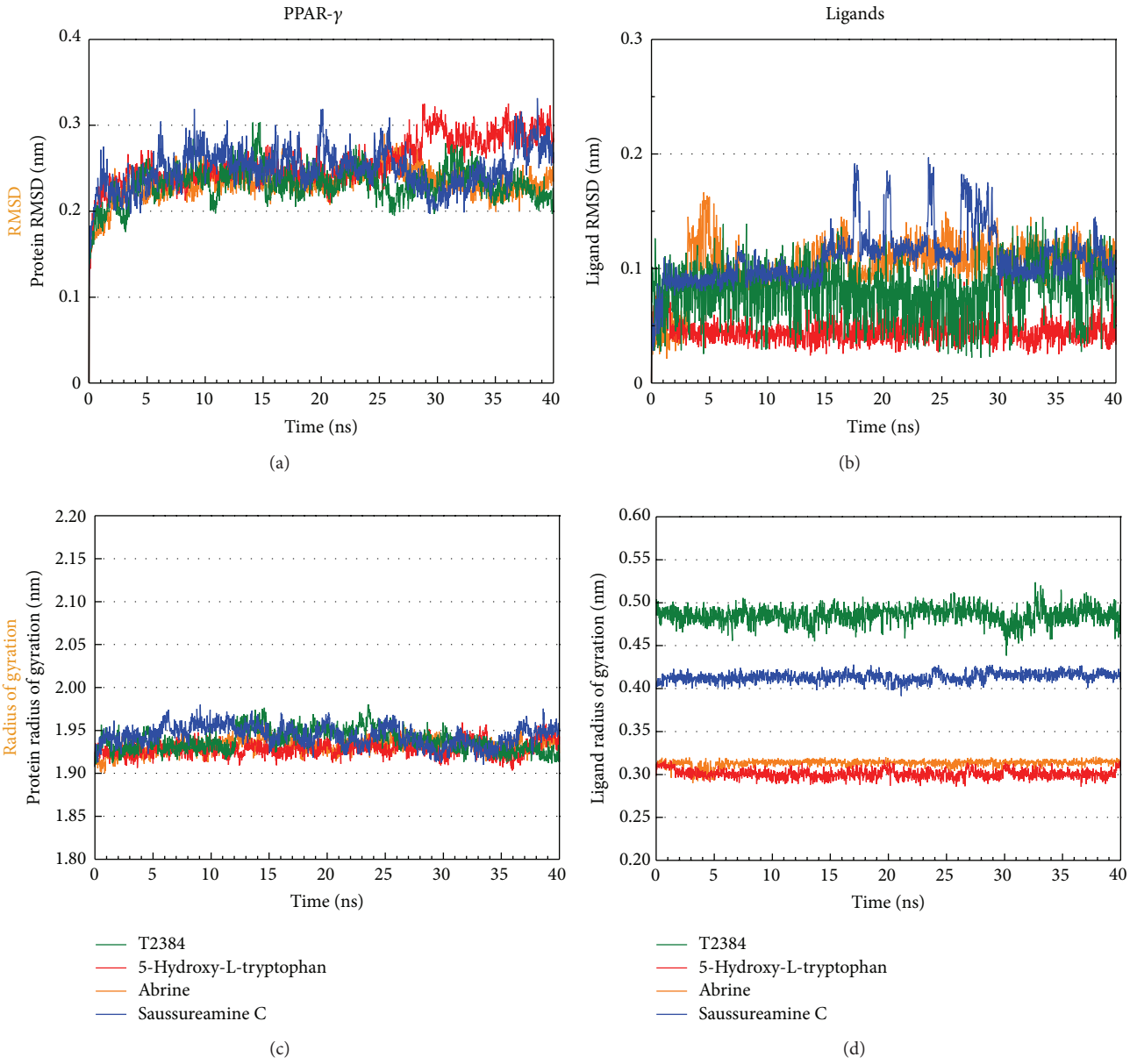

Figure 6: RMSDs and radii of gyration for PPAR-γ protein and ligands over 40 ns MD simulation.

v.2.2.25 program [48] was employed to identify the interactions between protein and ligand in each docking pose.

2.4. Molecular Dynamics Simulation. Before the molecular dynamics simulation by Gromacs [49], each protein-ligand complex in docking pose has been reprepared. Each ligand was reprepared by SwissParam program [50], and the protein was reprepared with charmm27 force field by Gromacs. The protein-ligand complex was solvated using a water model of TIP3P with a minimum distance of 1.2 Å from the complex and then minimized by steepest descent algorithm [51] with maximum of 5,000 steps. Then a single 10 ps constant temperature (NVT ensemble) equilibration was performed using Berendsen weak thermal coupling method followed by a 40 ns production simulation. For each MD simulation, it adopts the particle mesh Ewald (PME) option with a time step of 2 fs. A series of protocols in Gromacs were employed to analyze the MD trajectories.

3. Results and Discussion

3.1. Biological Activity Predictions. The genetic approximation algorithm determined the six optimum molecular

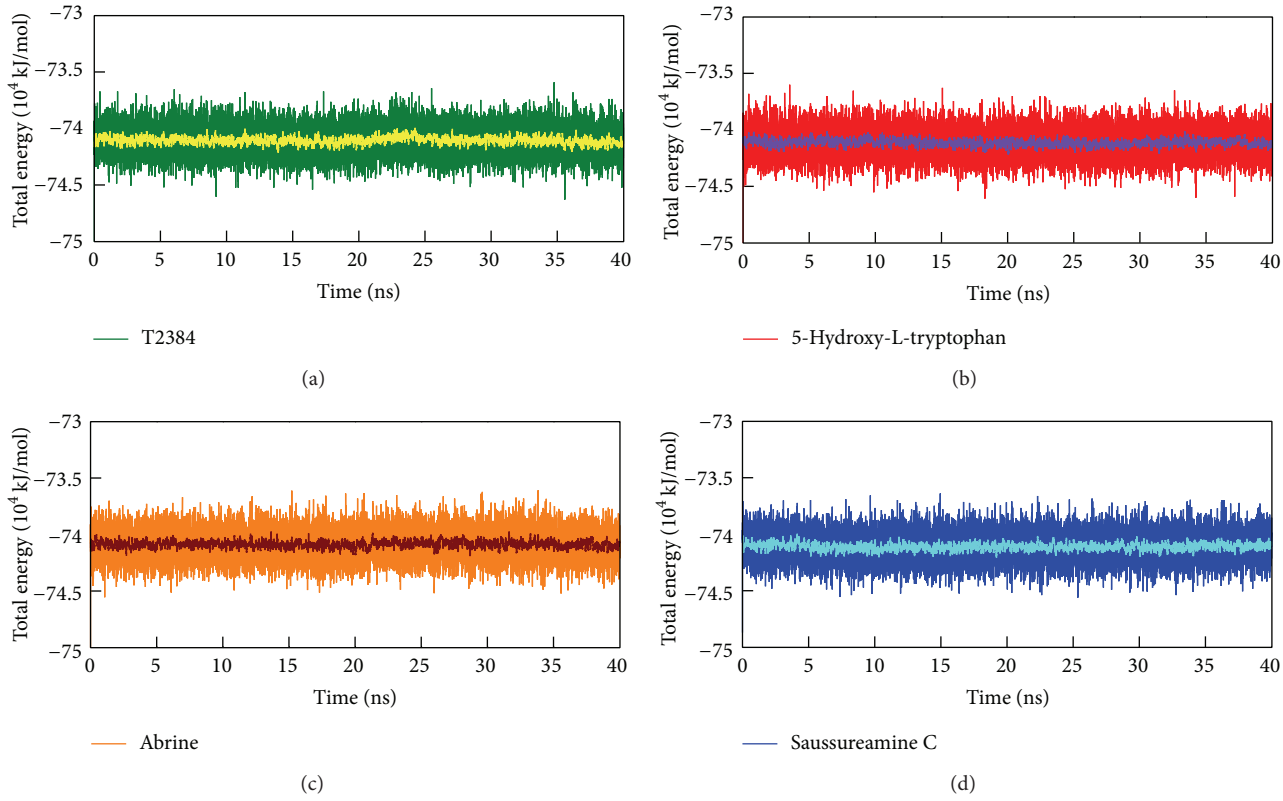

FIGURE 7: Total energy of PPAR-γ complexes with (a) T2384, (b) 5-hydroxy-L-tryptophan, (c) abrine, and (d) saussureamine C over 40 ns MD simulation. The average fluctuations in a cycle of 21 frames were illustrated by yellow (T2384), violet (5-hydroxy-L-tryptophan), wine (abrine), and cyan (saussureamine C) line, respectively.

descriptors for constructing prediction models with 20 compounds of training set. The selected descriptors were ES_Sum_sssCH, ES_Count_aaN, BIC, IAC_Mean, CHI_3_P, and JY. These six optimum molecular descriptors can be broadly divided into two groups, which are electronic and special topological descriptors. For electronic topological descriptors, it includes ES_Sum_sssCH, ES_Count_aaN for calculating the sums of the electrotopological state (E-state) values and the counts of each atom type, respectively. For special topological descriptors, BIC and IAC_Mean are bonding information content and mean information of atomic composition, which both belong to Graph-Theoretical InfoContent descriptors [52]. CHI_3_P is a Kier and Hall molecular connectivity index [53]. JY is a Balaban index [54]. According to these selected descriptors, the functional formula of multiple linear regression (MLR) model was constructed as follows:

$$\begin{aligned} \mathrm{pEC}_{50} = {} & -5.987 + 1.987 \times \mathrm{ES\_Sum\_sssCH} \\ & - 0.812 \times \mathrm{ES\_Count\_aaN} + 8.608 \times \mathrm{BIC} \\ & - 2.047 \times \mathrm{IAC\_Mean} + 0.812 \times \mathrm{CHI\_3\_P} \\ & + 2.159 \times \mathrm{JY}. \end{aligned} \quad (1)$$

The support vector machine (SVM) and Bayes network toolbox (BNT) models were also constructed with the identical training set and descriptors. The correlation of predicted and observed activities shown in Figure 1 illustrates the correlation trend and 95% prediction bands for each prediction model. The square correlation coefficients (R^2) of training set for MLR, SVM, and BNT models are 0.8442, 0.8536, and 0.7612, respectively. These prediction models are acceptable for predicting activity of PPAR-γ protein.

3.2. Docking Simulation. The potent compounds, which have acceptable predicted activities in all three prediction models, have been virtual screening with the target protein. After filtering by the absorption properties, the top TCM candidates ranked by Dock score were listed in Table 1 with their predicted activities and pharmacokinetics properties. Human intestinal absorption model displayed in Figure 2 suggested that the top five TCM candidates may have good absorption.

For the docking simulation, the binding site of PPAR-γ protein was defined by the volume and position of control, T2384 (Figure 3(a)). We visually inspected docking poses of top ranked TCM candidates (Figure 3(b)), 5-hydroxy-L-tryptophan, abrine, and saussureamine C interacting with

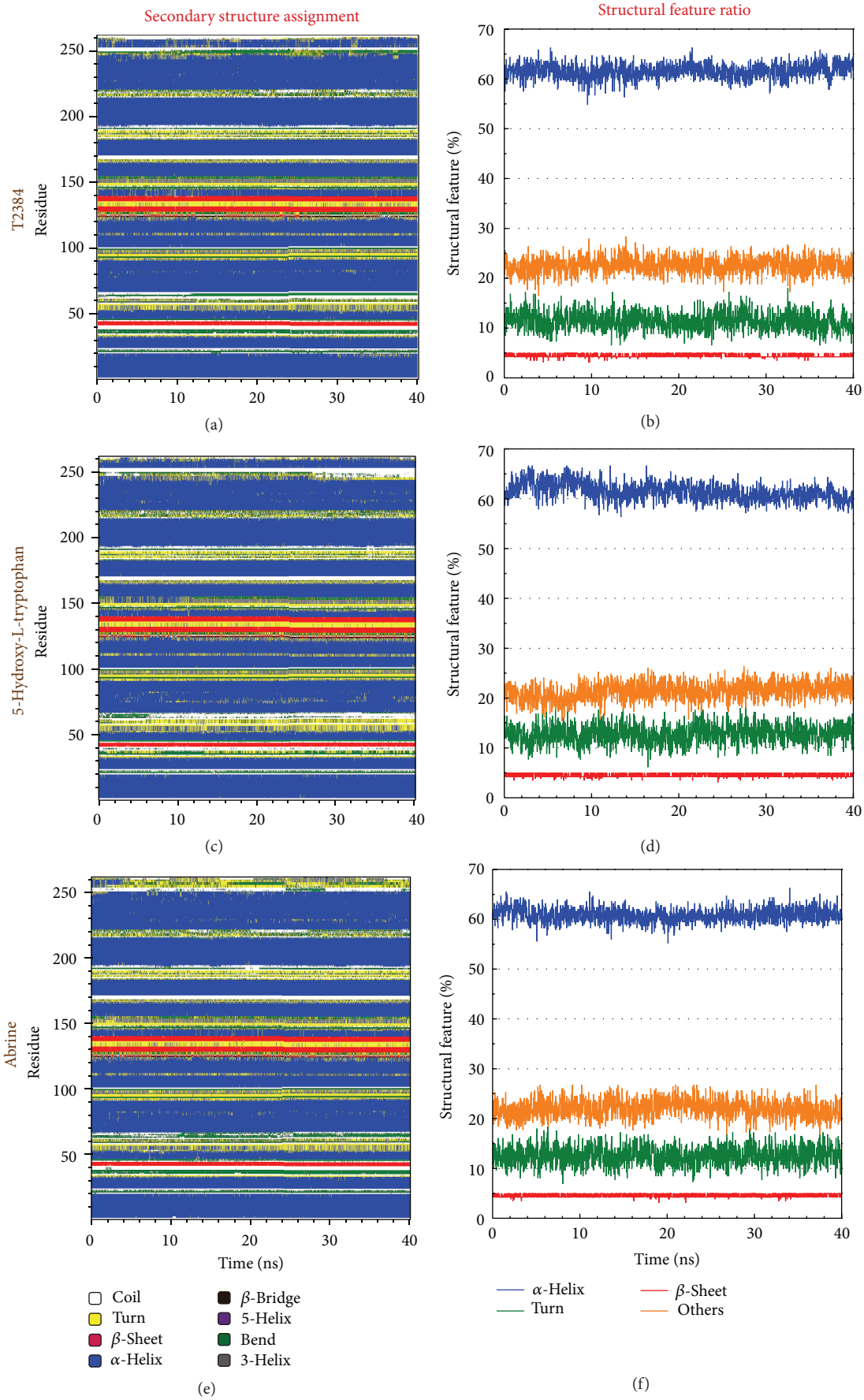

Figure 8: Continued.

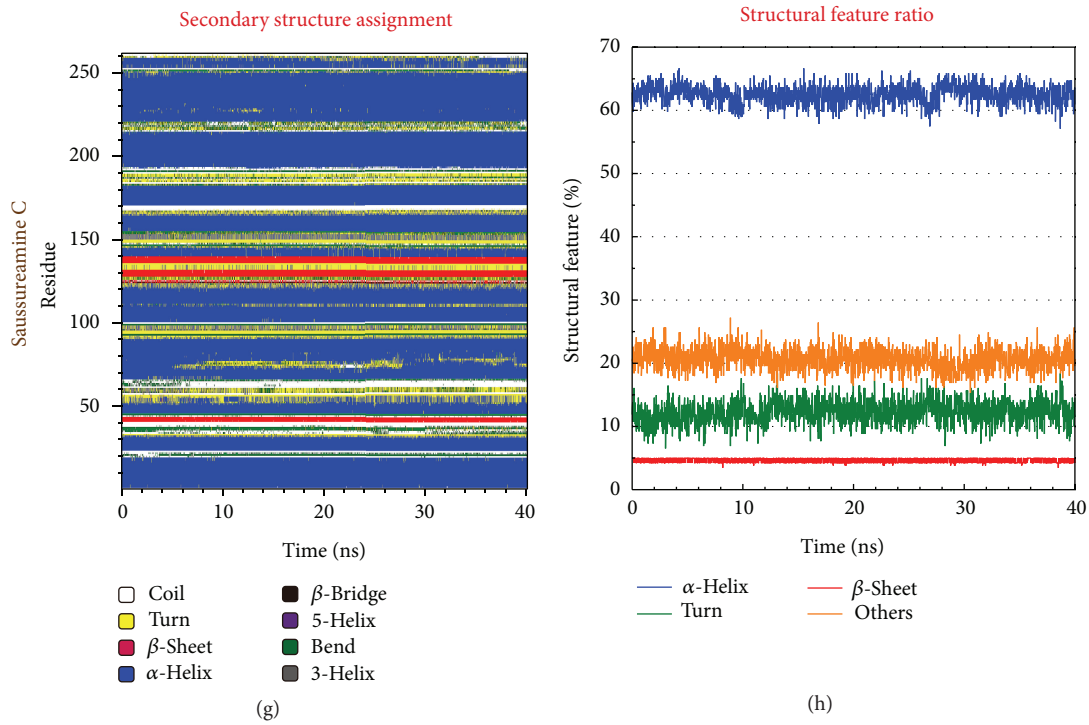

FIGURE 8: Secondary structure assignments and secondary structural feature ratio variations of PPAR-γ complexes over 40 ns MD simulation. Residues 1–65 in y-axis correspond to residues 207–271, residues 66-250 in y-axis correspond to residues 276–460, and residues 251–262 in y-axis correspond to residues 465–476.

similar PPAR-γ binding site residues as control (Figures 3(c)-3(d)). Figure 4 displays the structure of T2384 and top three candidates. According to the docking poses shown in Figure 5, T2384 has π interactions with residues Phe264 and Phe363, hydrogen bonds (H-bonds) with residues Cys285 and Lys367, and hydrophobic contact with other nine residues.

Compared with T2384 in PPAR-γ protein, the top three TCM candidates have been docked with similar docking poses. Due to the molecular size of three TCM compounds, none of them have interaction with Phe264 as T2384. Except saussureamine C, both of 5-hydroxy-L-tryptophan and abrine have π interaction with residue Phe363 as control. However, saussureamine C still has hydrophobic contact with residue Phe363. All top three candidates have similar H-bond with residue Lys367 and hydrophobic contacts with some common residues, such as Leu330 and Met364. Except that 5-hydroxy-L-tryptophan has hydrophobic contact instead of H-bond with residue Cys285, the other two candidates have the similar H-bond with residues Cys285 as T2384. In addition, abrine and saussureamine C also have H-bond with Ser289 and Met364, respectively.

3.3. Molecular Dynamics Simulation. The docking poses in the docking simulation illustrate that the top three TCM candidates have similar interactions with the target proteins as T2384. However, the structure of PPAR-γ protein is fixed during the progress of docking simulation. As this reason, the molecular dynamics (MD) simulations for each protein-ligand complex were performed to investigate the stability of interactions between ligand and target protein in the docking pose under dynamic conditionsand investigate the possible variations for each protein-ligand complex after docking.

The root mean square deviations (RMSDs) and radii of gyration for each protein and ligand in the complexes were illustrated in Figure 6. For RMSD, it calculates the deviation of the structure compared with the starting structure over 40 ns of MD simulation. They indicate that all protein-ligand complexes tend to be stable after 30 ns of MD simulation. Radius of gyration, which measures the mass of the atom relative to the center of mass of the complex, is indicative of the compactness of each complex. As shown in Figure 6, there is no significant variation for the compactness of each complex. Figure 7 illustrates the variation of total energy for each protein-ligand complex over the course of 40 ns MD simulation with the average fluctuations in a cycle of 21 frames shown in the center of each graph. Total energy trajectories indicate that these systems were stabilized for PPAR-γ protein in the complex with T2384 and top three TCM candidates over the course of 40 ns MD simulation. Figure 8 displays the variation of secondary structure of PPAR-γ protein and secondary structural feature ratio over the course of 40 ns MD simulation for each complex with T2384 and top three TCM candidates. It indicates that docking with three TCM

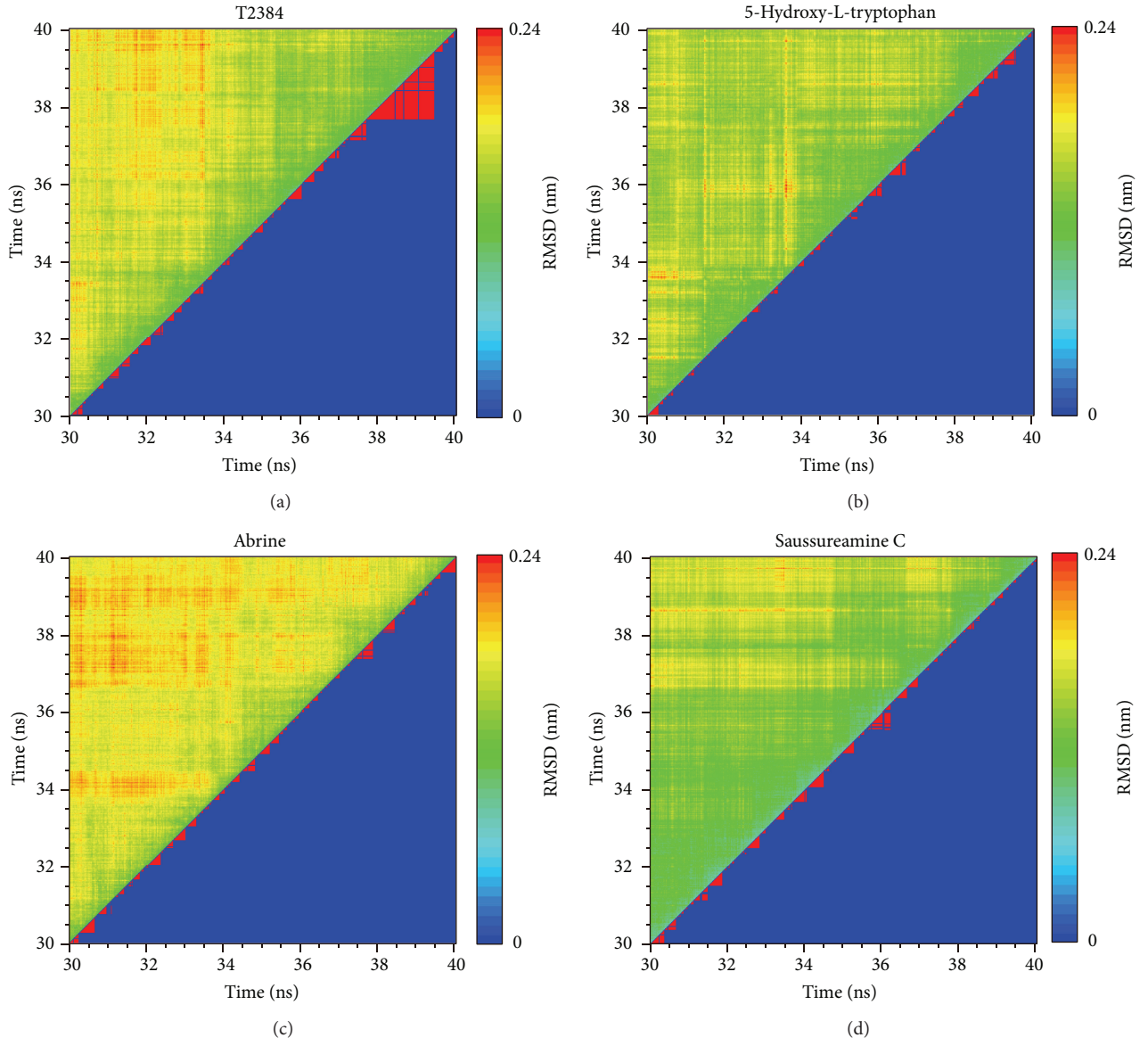

Figure 9: RMSD values (upper left half) and graphical depiction of the clusters (lower right half) of PPAR-γ complexes during 30–40 ns MD simulation.

candidates may not cause the significant differences from docking with the control in the secondary structure of PPAR-γ protein.

The representative structures of each complex after MD simulation were identified by the cluster analysis with a RMSD cutoff of 0.1 nm. In Figure 9, it illustrates the RMSD values and graphical depiction of the clusters over 30–40 ns MD simulation. The representative structures of each complex were identified by middle RMSD structure in the major cluster over 30–40 ns MD simulation, which are 38.88 ns (T2384), 39.86 ns (5-hydroxy-L-tryptophan), 39.80 ns (abrine), and 39.96 ns (saussureamine C), respectively. The snapshots and ligand interaction diagrams for each docking pose of the representative structures are illustrated in Figure 10. For T2384, it maintains the H-bonds with residues Cys285 and Lys367 in a nonstatic condition, which may retain the docking pose of T2384 in the binding pocket of PPAR-γ protein. In addition, the ligand interaction diagram also indicates that T2384 has interactions with common residues in docking simulation. For 5-hydroxy-L-tryptophan, it keeps the H-bond with residue Lys367 in a nonstatic condition and also has an H-bond with residue Ser289 as the docking pose of abrine in the docking simulation. Similarly, abrine has H-bonds with residues Ser289 and Lys367 as well as has an H-bond and π interaction with residue Tyr327. The docking pose of saussureamine C in the docking simulation is not stable

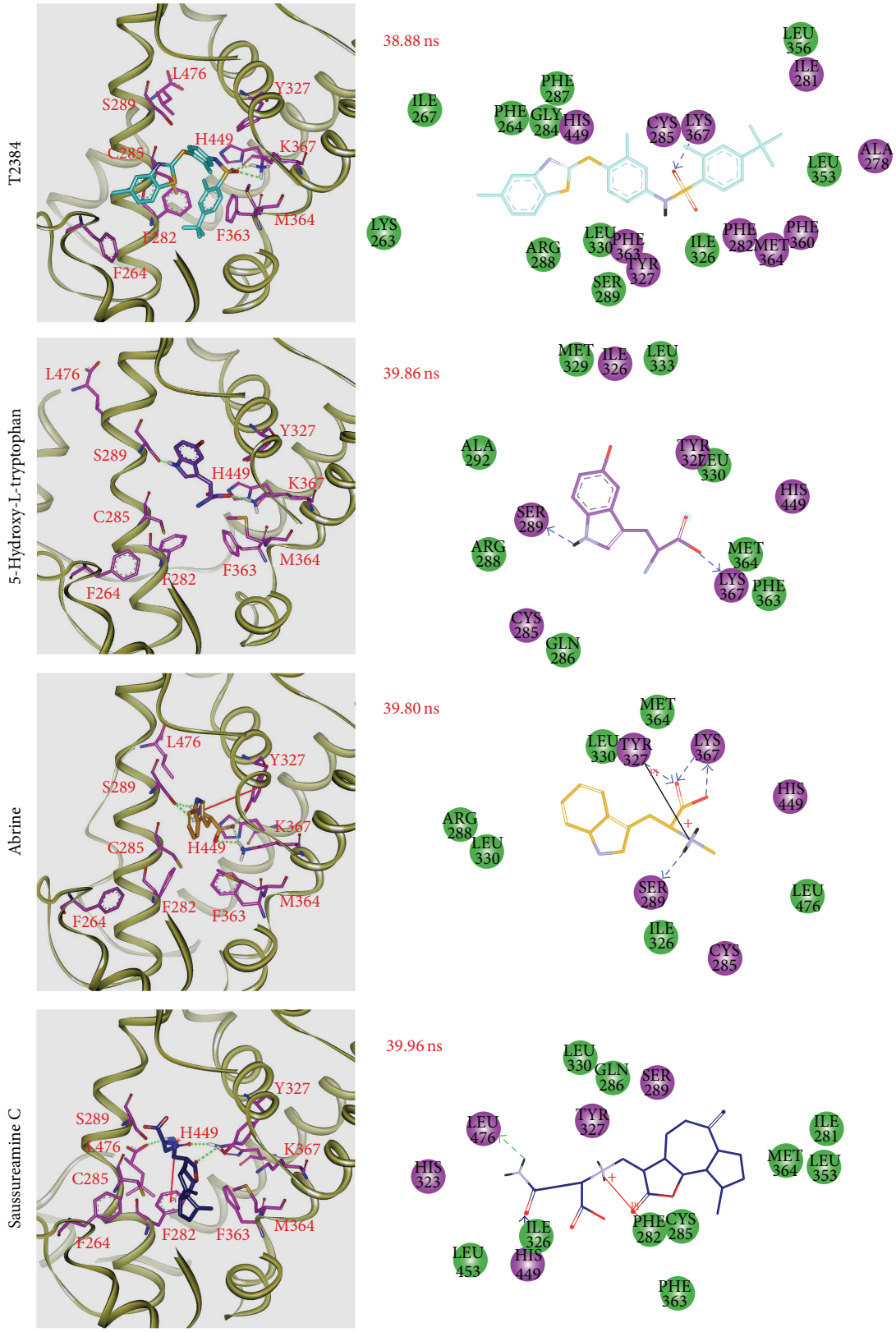

FIGURE 10: Docking poses of middle RMSD structure in the major cluster during 30–40 ns of MD simulation. Snapshots and ligand interaction diagrams for PPAR-γ protein complexes with T2384 (38.88 ns), 5-hydroxy-L-tryptophan (39.86 ns), abrine (39.80 ns), and saussureamine C (39.96 ns). For 2D diagrams, residues with magenta cycles are involved in hydrogen-bond, charge, or polar interactions, and residues with green cycles are involved in van der Waals interactions.

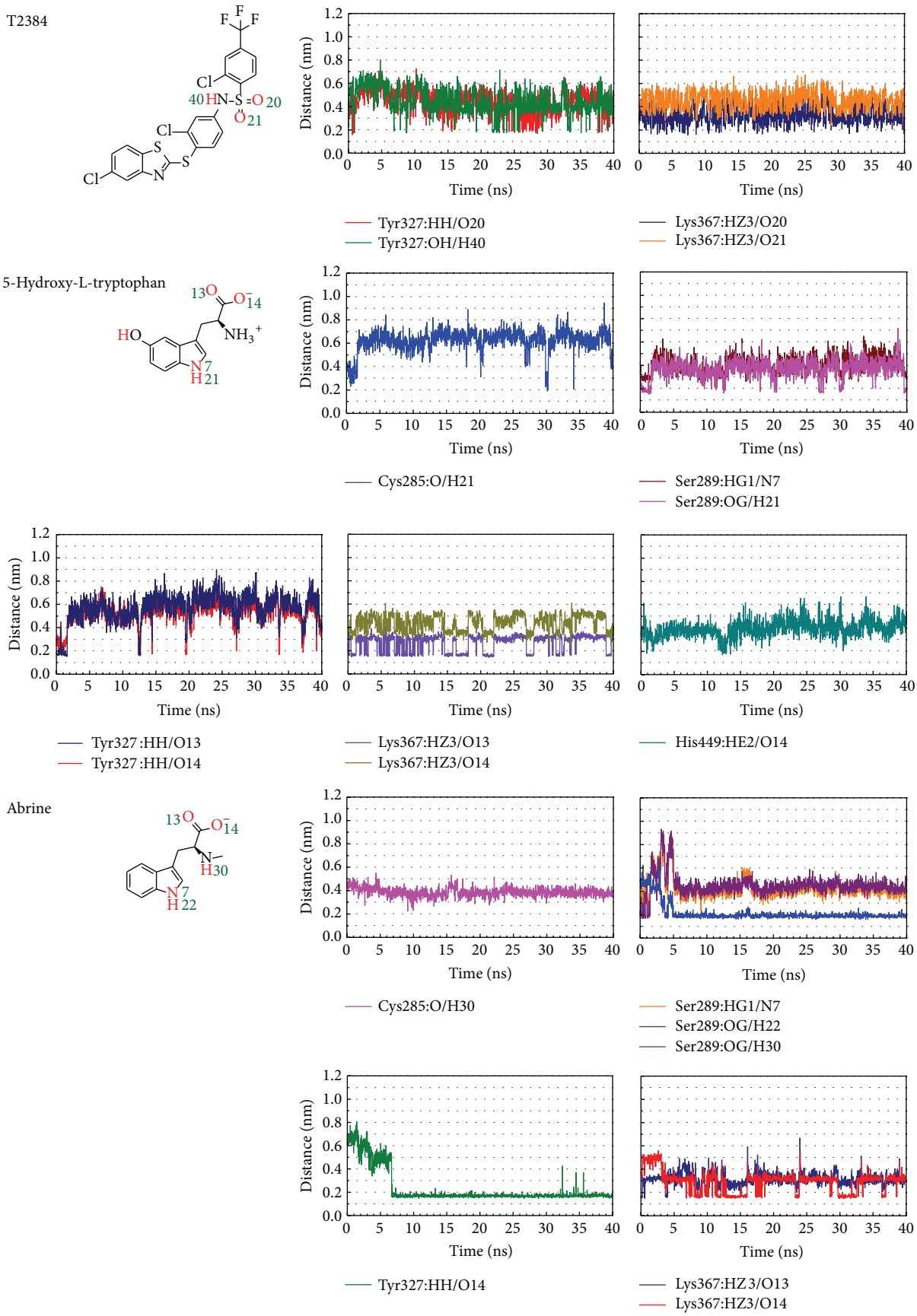

(a)

Figure 11: Continued.

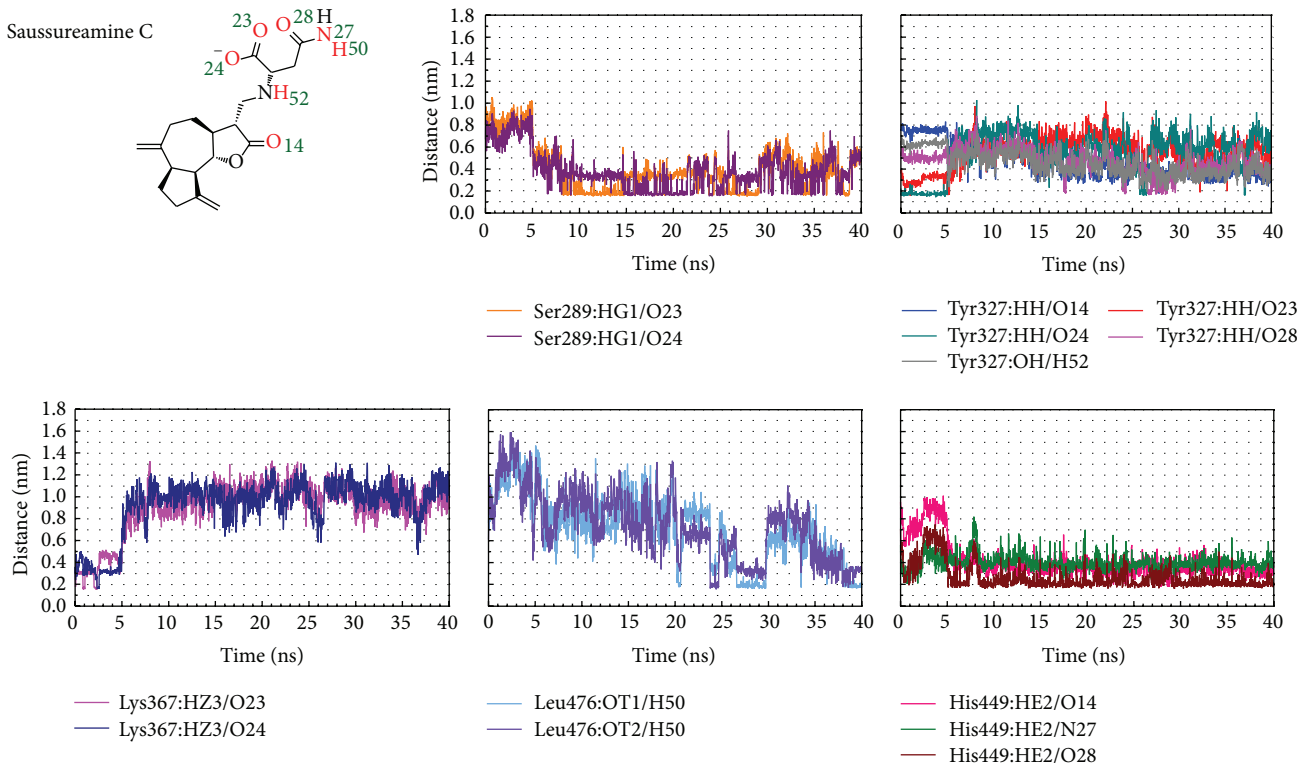

Figure 11: Distances of potential H-bonds between PPAR-γ protein and each compound during 40 ns MD simulation.

in a nonstatic condition. In the representative structures after MD simulation, it has H-bonds with residues His449 and Leu476, as well as a π interaction with residue Phe282.

The H-bonds occupancies for key residues of PPAR-γ protein in each complex are shown in Table 2 with cutoff of 0.3 nm. Figure 11 displays the variation of these distances over the course of 40 ns MD simulation. For T2384, the potential H-bonds with key residues of PPAR-γ protein are formed by its sulfonamide group. 5-Hydroxy-L-tryptophan and abrine form H-bonds with residue Lys367 by the carboxyl group. They form H-bonds with residue Ser289 by the indole group in the beginning of MD simulation, but the H-bond for abrine has shifted from the indole group to secondary amine group after 5 ns of MD simulation. In addition, the carboxyl group of abrine also forms a stable H-bond with residue Tyr327 after 7 ns of MD simulation. For saussureamine C, the docking pose in the docking simulation had changed after MD simulation. The H-bonds formed by the carboxyl group are shifted from residue Lys367 to residue Ser289 after 5 ns of MD simulation. In addition, it forms stable H-bonds with residue His449 by its sulfonamide group and heterocycle group after MD simulation.

The root mean square fluctuations (RMSFs) shown in Figure 12 illustrate the stability of each residue over 30–40 ns MD simulation. Residues Cys285, Lys367, and His449 are stabilized by all top three TCM candidates and T2384. As abrine forms stable H-bond with residues Ser289 and Tyr327, the RMSFs of Ser289 and Tyr327 are much lower in the complex with abrine than with others. For saussureamine C, as the H-bonds with residue Tyr327 are shifted between the heterocycle group, secondary amine group, and sulfonamide group, it causes the highest value of RMSF for residue Tyr327 in the complex with saussureamine C.

To consider the variation of each ligand during MD simulation, variation of torsion angles during 40 ns of MD simulation for each ligand in the PPAR-γ complexes is shown in Figure 13. As T2384 is the cocrystallized compound in the PPAR-γ protein, the docking pose is stable during 40 ns of MD simulation. For 5-hydroxy-L-tryptophan, the docking pose which is also stable during 40 ns of MD simulation except for the hydroxyl group in the indole ring has a 180-degree shift after MD simulation. For abrine, the variation of torsions 10 and 11 at the initial period of MD simulation may be the reason that the H-bond has shifted from the indole group to secondary amine group, and carboxyl group forms a stable H-bond with residue Tyr327 after MD simulation. Torsions 14 and 16 for saussureamine C indicate that the docking pose of saussureamine C has a fluctuation during 15–30 ns of MD; it can also be seen in the ligand RMSD (Figure 6) and the distance variation with residue Tyr327 (Figure 11). The variation of torsion 19 shows that the sulfonamide group of saussureamine C is flexible over MD simulation.

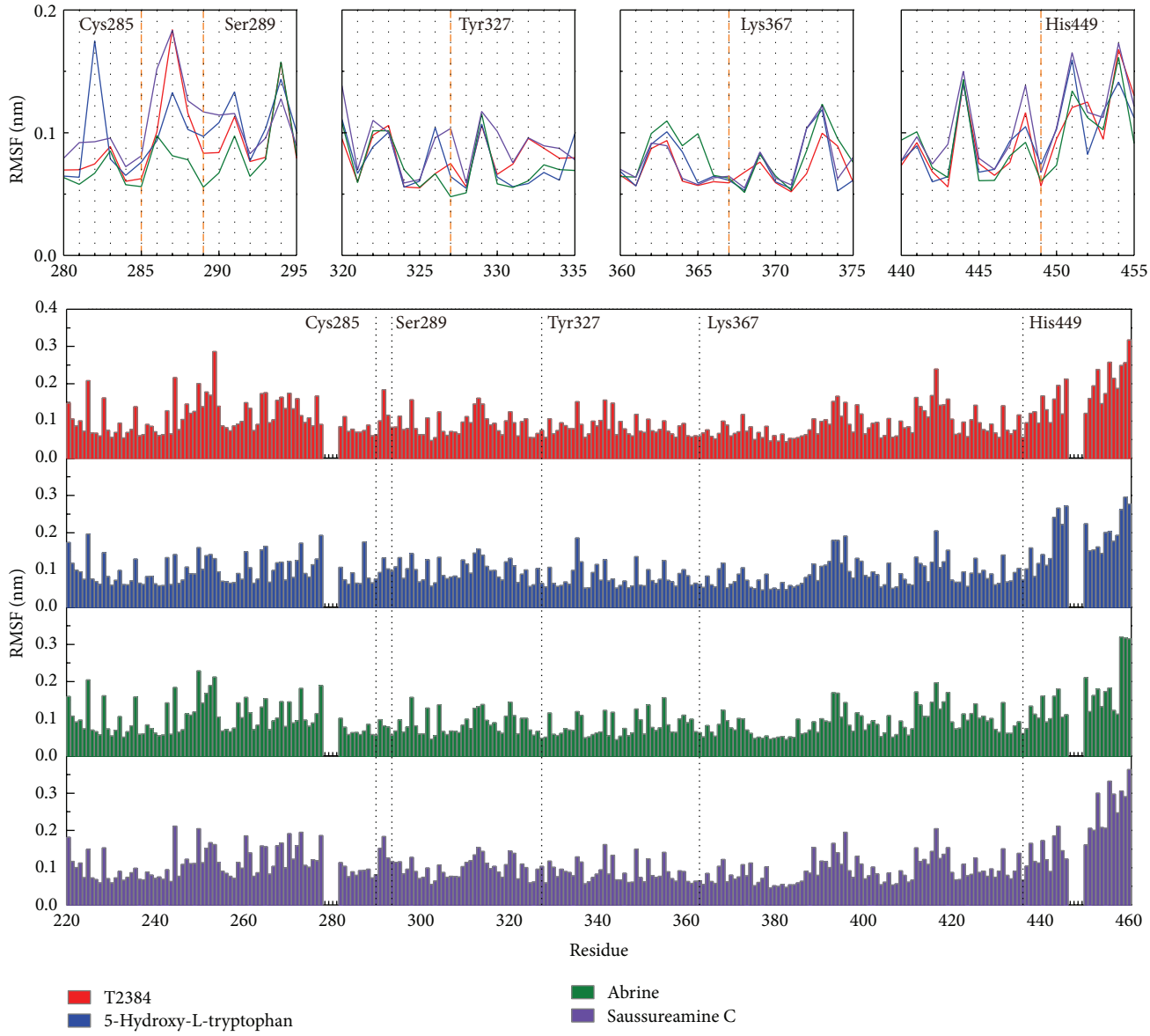

FIGURE 12: RMSFs for residues 207–476 of PPAR-γ complexes with each compound over 30–40 ns MD simulation. Common binding residues were illustrated with dash lines.

4. Conclusion

This study aims to investigate the potent TCM candidates for PPAR-γ protein. The biologically activities of candidates were predicted by three distinct prediction models (MLR, SVM and BNT) based on their ligand characteristics. After docking simulation, the docking poses of top TCM compounds ranked by the scoring function were validated by the MD simulation. For the top three TCM candidates, both of 5-hydroxy-L-tryptophan and abrine have an indole ring and carboxyl group to form the H-bonds with the key residues of PPAR-γ protein. The secondary amine group of abrine also stabilized an H-bond with residue Ser289. The key residues were stabilized in protein complexes with 5-Hydroxy-L-tryptophan and abrine as control. For saussureamine C, the interactions of docking pose in the docking simulation are not stable after MD simulation. Hence, we propose 5-hydroxy-L-tryptophan and abrine as potential lead compounds for further study in drug development process with the PPAR-γ protein.

Conflict of Interests

The authors declare that there is no conflict of interests regarding the publication of this paper.

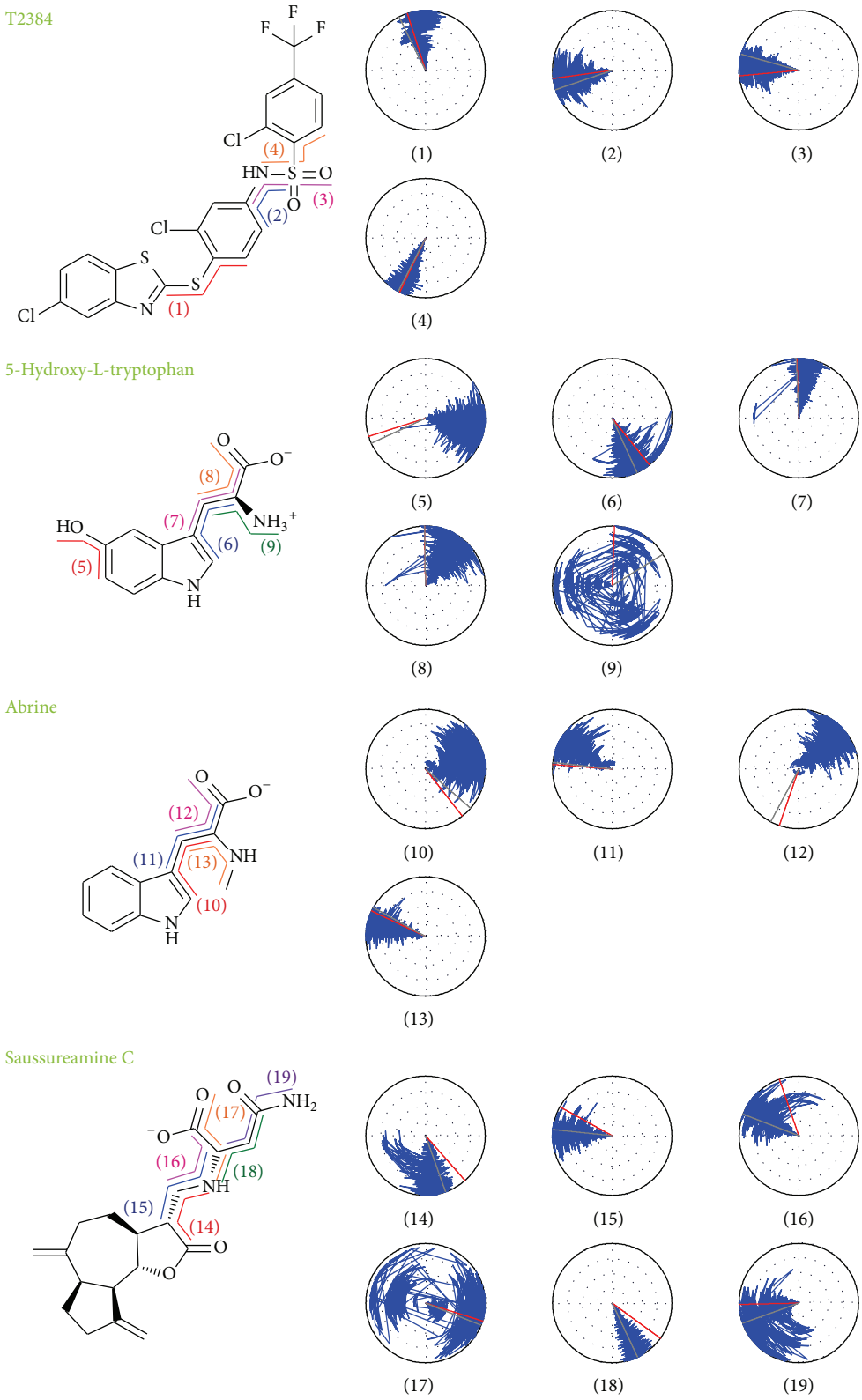

Figure 13: Variation of ligand torsion angles for each of PPAR-γ complexes during 40 ns of MD simulation. Red and gray lines represent the ligand torsion angle at docking simulation and first conformation of MD simulation, respectively.

Table 2: H-bond occupancy for key residues of PPAR-γ protein with top three candidates and T2384 overall 40 ns molecular dynamics simulation.

Name	H-bond interaction	Occupancy
T2384	Tyr327:HH/O20	8.70%
	Tyr327:OH/H40	5.55%
	Lys367:HZ3/O20	39.30%
	Lys367:HZ3/O21	0.75%
5-Hydroxy-L-tryptophan	Cys285:O/H21	1.30%
	Ser289:HG1/N7	7.05%
	Ser289:OG/H26	0.15%
	Ser289:OG/H21	14.54%
	Tyr327:HH/O13	5.25%
	Tyr327:HH/O14	4.55%
	Lys367:HZ3/O13	49.93%
	Lys367:HZ3/O14	0.90%
	His449:HE2/O14	7.60%
Abrine	Cys285:O/H30	1.00%
	Ser289:HG1/N7	1.45%
	Ser289:OG/H22	3.00%
	Ser289:OG/H30	90.05%
	Tyr327:HH/O14	83.15%
	Lys367:HZ3/O13	41.15%
	Lys367:HZ3/O14	37.75%
Saussureamine C	Ser289:HG1/O23	32.40%
	Ser289:HG1/O24	30.05%
	Tyr327:HH/O14	4.95%
	Tyr327:HH/O23	6.20%
	Tyr327:HH/O24	14.65%
	Tyr327:HH/O28	6.60%
	Tyr327:OH/H52	6.65%
	Lys367:HZ3/O23	2.65%
	Lys367:HZ3/O24	2.70%
	His449:HE2/O14	14.65%
	His449:HE2/O24	3.50%
	His449:HE2/N27	3.90%
	His449:HE2/O28	77.60%
	Leu476:OT1/H50	13.85%
	Leu476:OT2/H50	7.00%

H-bond occupancy cutoff: 0.3 nm.

Acknowledgments

The research was supported by Grants from the National Science Council of Taiwan (NSC102-2325-B039-001, NSC102-2221-E-468-027-), Asia University (Asia101-CMU-2, 102-Asia-07), and China Medical University Hospital (DMR-102-105, DMR-103-058, DMR-103-001, and DMR-103-096). This study is also supported in part by Taiwan Department of Health Clinical Trial and Research Center of Excellence (DOH102-TD-B-111-004), Taiwan Department of Health Cancer Research Center of Excellence (MOHW103-TD-B-111-03), and CMU under the Aim for Top University Plan of the Ministry of Education, Taiwan.

References

[1] R. M. Evans, G. D. Barish, and Y.-X. Wang, "PPARs and the complex journey to obesity," *Nature Medicine*, vol. 10, no. 4, pp. 355–361, 2004.

[2] K. Rikimaru, T. Wakabayashi, H. Abe et al., "A new class of non-thiazolidinedione, non-carboxylic-acid-based highly selective peroxisome proliferator-activated receptor (PPAR) γ agonists: design and synthesis of benzylpyrazole acylsulfonamides," *Bioorganic and Medicinal Chemistry*, vol. 20, no. 2, pp. 714–733, 2012.

[3] J. N. Feige, L. Gelman, L. Michalik, B. Desvergne, and W. Wahli, "From molecular action to physiological outputs: peroxisome proliferator-activated receptors are nuclear receptors at the crossroads of key cellular functions," *Progress in Lipid Research*, vol. 45, no. 2, pp. 120–159, 2006.

[4] L. Poulsen, M. Siersbaek, and S. Mandrup, "PPARs: fatty acid sensors controlling metabolism," *Seminars in Cell & Developmental Biology*, vol. 23, no. 6, pp. 631–639, 2012.

[5] M. Ahmadian, J. M. Suh, N. Hah et al., "PPARgamma signaling and metabolism: the good, the bad and the future," *Nature Medicine*, vol. 19, no. 5, pp. 557–566, 2013.

[6] A. Bugge and S. Mandrup, "Molecular mechanisms and genome-wide aspects of PPAR subtype specific transactivation," *PPAR Research*, vol. 2010, Article ID 169506, 12 pages, 2010.

[7] A. R. Miller, "Today's challenges and tomorrow's opportunities: ligands to peroxisome proliferator-activated receptors as therapies for type 2 diabetes and the metabolic syndrome," *Drug Development Research*, vol. 67, no. 7, pp. 574–578, 2006.

[8] J. M. Lehmann, L. B. Moore, T. A. Smith-Oliver, W. O. Wilkison, T. M. Willson, and S. A. Kliewer, "An antidiabetic thiazolidinedione is a high affinity ligand for peroxisome proliferator-activated receptor γ (PPARγ)," *The Journal of Biological Chemistry*, vol. 270, no. 22, pp. 12953–12956, 1995.

[9] N. Kubota, Y. Terauchi, H. Miki et al., "PPARγ mediates high-fat diet-induced adipocyte hypertrophy and insulin resistance," *Molecular Cell*, vol. 4, no. 4, pp. 597–609, 1999.

[10] B. M. Forman, J. Chen, and R. M. Evans, "The peroxisome proliferator-activated receptors: ligands and activators," *Annals of the New York Academy of Sciences*, vol. 804, pp. 266–275, 1996.

[11] W. W. Cheatham, "Peroxisome proliferator-activated receptor translational research and clinical experience," *The American Journal of Clinical Nutrition*, vol. 91, no. 1, pp. 262S–266S, 2010.

[12] A. M. Sharma and B. Staels, "Review: peroxisome proliferator-activated receptor γ and adipose tissue—understanding obesity-related changes in regulation of lipid and glucose metabolism," *The Journal of Clinical Endocrinology and Metabolism*, vol. 92, no. 2, pp. 386–395, 2007.

[13] Y.-T. Li, L. Li, J. Chen et al., "7-chloroarctinone-b as a new selective PPARγ antagonist potently blocks adipocyte differentiation," *Acta Pharmacologica Sinica*, vol. 30, no. 9, pp. 1351–1358, 2009.

[14] J.-S. Wu, W.-M. Cheung, Y.-S. Tsai et al., "Ligand-activated peroxisome proliferator-activated receptor-γ protects against ischemic cerebral infarction and neuronal apoptosis by 14-3-3ε upregulation," *Circulation*, vol. 119, no. 8, pp. 1124–1134, 2009.

[15] C.-L. Jao, S.-L. Huang, and K.-C. Hsu, "Angiotensin I-converting enzyme inhibitory peptides: inhibition mode, bioavailability, and antihypertensive effects," *BioMedicine*, vol. 2, no. 4, pp. 130–136, 2012.

[16] M. Lin, S. Tsai, F. Wang, F.-H. Liu, J.-N. Syu, and F.-Y. Tang, "Leptin induces cell invasion and the upregulation of matrilysin in human colon cancer cells," *BioMedicine*, vol. 3, no. 4, pp. 174–180, 2013.

[17] K.-P. Su, "Inflammation in psychopathology of depression: clinical, biological, and therapeutic implications," *BioMedicine*, vol. 2, no. 2, pp. 68–74, 2012.

[18] M. A. Leissring, E. Malito, S. Hedouin et al., "Designed inhibitors of insulin-degrading enzyme regulate the catabolism and activity of insulin," *PLoS ONE*, vol. 5, no. 5, Article ID e10504, 2010.

[19] Y. Jiang, X. Li, W. Yang et al., "PKM2 regulates chromosome segregation and mitosis progression of tumor cells," *Molecular Cell*, vol. 53, no. 1, pp. 75–87, 2014.

[20] I. C. Chou, W.-D. Lin, C.-H. Wang et al., "Association analysis between Tourette's syndrome and two dopamine genes (DAT1, DBH) in Taiwanese children," *BioMedicine*, vol. 3, no. 2, pp. 88–91, 2013.

[21] T. Yamamoto, W.-C. Hung, T. Takano, and A. Nishiyama, "Genetic nature and virulence of community-associated methicillin-resistant *Staphylococcus aureus*," *BioMedicine*, vol. 3, no. 1, pp. 2–18, 2013.

[22] C.-H. Wang, W.-D. Lin, D.-T. Bau, I.-C. Chou, C.-H. Tsai, and F.-J. Tsai, "Appearance of acanthosis nigricans may precede obesity: an involvement of the insulin/IGF receptor signaling pathway," *BioMedicine*, vol. 3, no. 2, pp. 82–87, 2013.

[23] W. Chen, Z. Wang, C. Jiang, and Y. Ding, "PP2A-mediated anticancer therapy," *Gastroenterology Research and Practice*, vol. 2013, Article ID 675429, 10 pages, 2013.

[24] Y.-M. Chang, B. K. Velmurugan, W.-W. Kuo et al., "Inhibitory effect of alpinate Oxyphyllae fructus extracts on Ang II-induced cardiac pathological remodeling-related pathways in H9c2 cardiomyoblast cells," *BioMedicine*, vol. 3, no. 4, pp. 148–152, 2013.

[25] Y. M. Leung, K. L. Wong, S. W. Chen et al., "Down-regulation of voltage-gated Ca^{2+} channels in Ca^{2+} store-depleted rat insulinoma RINm5F cells," *BioMedicine*, vol. 3, no. 3, pp. 130–139, 2013.

[26] S. P. Mahamuni, R. D. Khose, F. Menaa, and S. L. Badole, "Therapeutic approaches to drug targets in hyperlipidemia," *BioMedicine*, vol. 2, no. 4, pp. 137–146, 2012.

[27] K. C. Chen, S. S. Chang, F. J. Tsai, and C. Y. Chen, "Han ethnicity-specific type 2 diabetic treatment from traditional Chinese medicine?" *Journal of Biomolecular Structure & Dynamics*, vol. 31, no. 11, pp. 1219–1235, 2013.

[28] K.-C. Chen, M.-F. Sun, S.-C. Yang et al., "Investigation into potent inflammation inhibitors from traditional Chinese medicine," *Chemical Biology & Drug Design*, vol. 78, no. 4, pp. 679–688, 2011.

[29] K. C. Chen, Y. R. Jian, M. F. Sun, T. T. Chang, C. C. Lee, and C. Y. Chen, "Investigation of silent information regulator 1 (Sirt1) agonists from Traditional Chinese Medicine," *Journal of Biomolecular Structure & Dynamics*, vol. 31, no. 11, pp. 1207–1218, 2013.

[30] S.-C. Hsu, J.-H. Lin, S.-W. Weng et al., "Crude extract of Rheum palmatum inhibits migration and invasion of U-2 OS human osteosarcoma cells by suppression of matrix metalloproteinase-2 and -9," *BioMedicine*, vol. 3, no. 3, pp. 120–129, 2013.

[31] C.-Y. Chen and C. Y.-C. Chen, "Insights into designing the dual-targeted HER2/HSP90 inhibitors," *Journal of Molecular Graphics & Modelling*, vol. 29, no. 1, pp. 21–31, 2010.

[32] S.-C. Yang, S.-S. Chang, H.-Y. Chen, and C. Y.-C. Chen, "Identification of potent EGFR inhibitors from TCM Database@-Taiwan," *PLoS Computational Biology*, vol. 7, no. 10, Article ID e1002189, 2011.

[33] Y. A. Tsou, K. C. Chen, H. C. Lin, S. S. Chang, and C. Y. C. Chen, "Uroporphyrinogen decarboxylase as a potential target for specific components of traditional Chinese medicine: a virtual screening and molecular dynamics study," *PLoS ONE*, vol. 7, no. 11, 2012.

[34] Y. A. Tsou, K. C. Chen, S. S. Chang, Y. R. Wen, and C. Y. Chen, "A possible strategy against head and neck cancer: *in silico* investigation of three-in-one inhibitors," *Journal of Biomolecular Structure & Dynamics*, vol. 31, no. 12, pp. 1358–1369, 2013.

[35] W. I. Tou, S. S. Chang, C. C. Lee, and C. Y. C. Chen, "Drug design for neuropathic pain regulation from traditional Chinese medicine," *Scientific Reports*, vol. 3, article 844, 2013.

[36] K.-C. Chen, K.-W. Chang, H.-Y. Chen, and C. Y.-C. Chen, "Traditional Chinese medicine, a solution for reducing dual stroke risk factors at once?" *Molecular BioSystems*, vol. 7, no. 9, pp. 2711–2719, 2011.

[37] T.-T. Chang, K.-C. Chen, K.-W. Chang et al., "*In silico* pharmacology suggests ginger extracts may reduce stroke risks," *Molecular BioSystems*, vol. 7, no. 9, pp. 2702–2710, 2011.

[38] H. J. Huang, Y. R. Jian, and C. Y. Chen, "Traditional Chinese medicine application in HIV: an *in silico* study," *Journal of Biomolecular Structure & Dynamics*, vol. 32, no. 1, pp. 1–12, 2014.

[39] S.-S. Chang, H.-J. Huang, and C. Y.-C. Chen, "Two birds with one stone? Possible dual-targeting H1N1 inhibitors from traditional Chinese medicine," *PLoS Computational Biology*, vol. 7, no. 12, Article ID e1002315, 2011.

[40] K. C. Chen, S. S. Chang, H. J. Huang, T. L. Lin, Y. J. Wu, and C. Y. Chen, "Three-in-one agonists for PPAR-alpha, PPAR-gamma, and PPAR-delta from traditional Chinese medicine," *Journal of Biomolecular Structure & Dynamics*, vol. 30, no. 6, pp. 662–683, 2012.

[41] C. Y.-C. Chen, "TCM Database@Taiwan: the world's largest traditional Chinese medicine database for drug screening *in silico*," *PLoS ONE*, vol. 6, no. 1, Article ID e15939, 2011.

[42] C. A. Lipinski, F. Lombardo, B. W. Dominy, and P. J. Feeney, "Experimental and computational approaches to estimate solubility and permeability in drug discovery and development settings," *Advanced Drug Delivery Reviews*, vol. 46, no. 1–3, pp. 3–26, 2001.

[43] Y. Li, Z. Wang, N. Furukawa et al., "T2384, a novel antidiabetic agent with unique peroxisome proliferator-activated receptor γ binding properties," *The Journal of Biological Chemistry*, vol. 283, no. 14, pp. 9168–9176, 2008.

[44] D. Rogers and A. J. Hopfinger, "Application of genetic function approximation to quantitative structure-activity relationships and quantitative structure-property relationships," *Journal of Chemical Information and Computer Sciences*, vol. 34, no. 4, pp. 854–866, 1994.

[45] C. Chang and C.-J. Lin, "LIBSVM: a library for support vector machines," *ACM Transactions on Intelligent Systems and Technology*, vol. 2, no. 3, pp. 1–27, 2011.

[46] C. M. Venkatachalam, X. Jiang, T. Oldfield, and M. Waldman, "LigandFit: a novel method for the shape-directed rapid docking of ligands to protein active sites," *Journal of Molecular Graphics & Modelling*, vol. 21, no. 4, pp. 289–307, 2003.

[47] B. R. Brooks, R. E. Bruccoleri, B. D. Olafson, D. J. States, S. Swaminathan, and M. Karplus, "CHARMM: a program for macromolecular energy minimization and dynamics calculations," *Journal of Computational Chemistry*, vol. 4, pp. 187–217, 1983.

[48] A. C. Wallace, R. A. Laskowski, and J. M. Thornton, "LIGPLOT: a program to generate schematic diagrams of protein-ligand interactions," *Protein Engineering*, vol. 8, no. 2, pp. 127–134, 1995.

[49] B. Hess, C. Kutzner, D. van der Spoel, and E. Lindahl, "GRGMACS 4: algorithms for highly efficient, load-balanced, and scalable molecular simulation," *Journal of Chemical Theory and Computation*, vol. 4, no. 3, pp. 435–447, 2008.

[50] V. Zoete, M. A. Cuendet, A. Grosdidier, and O. Michielin, "SwissParam: a fast force field generation tool for small organic molecules," *Journal of Computational Chemistry*, vol. 32, no. 11, pp. 2359–2368, 2011.

[51] R. Fletcher, *Optimization*, Academic Press, New York, NY, USA, 1969.

[52] D. Bonchev, *Information Theoretic Indices for Characterization of Chemical Structures*, Research Studies Press, 1983.

[53] L. B. Kier and L. H. Hall, *Molecular Connectivity in Chemistry and Drug Research*, Academic Press, New York, NY, USA, 1976.

[54] A. T. Balaban, "Highly discriminating distance-based topological index," *Chemical Physics Letters*, vol. 89, no. 5, pp. 399–404, 1982.

Hindawi Publishing Corporation
Evidence-Based Complementary and Alternative Medicine
Volume 2014, Article ID 601064, 21 pages
http://dx.doi.org/10.1155/2014/601064

Research Article

Treatment of Acute Lymphoblastic Leukemia from Traditional Chinese Medicine

Ya-Li Hsiao,[1] Pei-Chun Chang,[1] Hung-Jin Huang,[2] Chia-Chen Kuo,[1] and Calvin Yu-Chian Chen[1,2]

[1] *Department of Biomedical Informatics, Asia University, Taichung 41354, Taiwan*
[2] *School of Medicine, College of Medicine, China Medical University, Taichung 40402, Taiwan*

Correspondence should be addressed to Calvin Yu-Chian Chen; ycc929@MIT.edu

Received 3 January 2014; Accepted 7 January 2014; Published 22 May 2014

Academic Editor: Fuu-Jen Tsai

Acute lymphoblastic leukemia (ALL) is a cancer that immature white blood cells continuously overproduce in the bone marrow. These cells crowd out normal cells in the bone marrow bringing damage and death. Methotrexate (MTX) is a drug used in the treatment of various cancer and autoimmune diseases. In particular, for the treatment of childhood acute lymphoblastic leukemia, it had significant effect. MTX competitively inhibits dihydrofolate reductase (DHFR), an enzyme that participates in the tetrahydrofolate synthesis so as to inhibit purine synthesis. In addition, its downstream metabolite methotrexate polyglutamates (MTX-PGs) inhibit the thymidylate synthase (TS). Therefore, MTX can inhibit the synthesis of DNA. However, MTX has cytotoxicity and neurotoxin may cause multiple organ injury and is potentially lethal. Thus, the lower toxicity drugs are necessary to be developed. Recently, diseases treatments with Traditional Chinese Medicine (TCM) as complements are getting more and more attention. In this study, we attempted to discover the compounds with drug-like potential for ALL treatment from the components in TCM. We applied virtual screen and QSAR models based on structure-based and ligand-based studies to identify the potential TCM component compounds. Our results show that the TCM compounds adenosine triphosphate, manninotriose, raffinose, and stachyose could have potential to improve the side effects of MTX for ALL treatment.

1. Introduction

Dihydrofolate reductase (DHFR) is essential in cellular metabolism and cell growth. It catalyzes the conversion of dihydrofolate into tetrahydrofolate which is a carrier for the methyl group. The methyl group carried by tetrahydrofolate is required for de novo synthesis of varieties of essential metabolites including amino acids, lipids, pyrimidines, and purines. Methotrexate (MTX), a folate antagonist, arrests cell growth by competitively binding to DHFR, thereby, blocking de novo synthesis of nucleotide precursors and inhibiting DNA synthesis [1]. MTX has been found to be useful as an antineoplastic and immunosuppressive agent because it inhibits the proliferation of rapidly dividing malignant [2].

MTX tightly binding on DHFR is one of the most widely used drugs in cancer treatment and is especially effective in the treatment of acute lymphocytic leukemia [3]. In addition, its folate analogue is widely used in the treatment of acute lymphoblastic leukemia (ALL) [4], ovarian cancer [5], osteosarcoma [6], rheumatoid arthritis [7], psoriasis [8], and inflammatory bowel disease [9] and for prevention of graft-versus-host disease after transplantation [10].

In the cells, MTX acts by inhibiting two enzymes. First, as an analog of folate, MTX is a powerful competitive inhibitor with 1000-fold more potent than the natural substrate of DHFR. DHFR is responsible for converting dihydrofolate (FH2) to their active form tetrahydrofolate (FH4), which is a substrate of thymidylate synthase (TS). Second, MTX is converted to active methotrexate polyglutamates (MTX-PGs) by folylpolyglutamate synthase [11, 12]. The polyglutamated forms of MTX inhibit TS directly. Due to these inhibitions,

Table 1: Experimental pIC50 values for DHFR inhibitors [40].

Name	R1	R2	X	R3	pIC50
1	CH_3	CH_3	CH_2	H	4.71
2	CH_3	CH_3	CH_2	4′-CH_3	4.6091
3*	CH_3	CH_3	CH_2	4′-OCH_3	4.2306
4	CH_3	CH_3	CH_2	4′-F	4.6615
5*	CH_3	CH_3	CH_2	4′-Cl	4.5243
6	CH_3	CH_3	CH_2	3′,4′-diCl	4.8928
7*	CH_3	CH_3	–O-CH_2–	H	7.1612
8	CH_3	C_2H_5	–O-CH_2–	H	6.8097
9*	H	c-Pr	–O-CH_2–	H	6.2612
10	–$(CH_2)_3$–		–O-CH_2–	H	6.8729
11	– $(CH_2)_4$–		–O-CH_2–	H	6.762
12	– $(CH_2)_5$–		–O-CH_2–	H	5.7471
13	– $(CH_2)_6$–		–O-CH_2–	H	5.2733
14	– $(CH_2)_4$–		–O-CH_2CH_2–	H	7.5086
15	– $(CH_2)_5$–		–O-CH_2CH_2–	H	8.0458
16	– $(CH_2)_4$–		–O-$(CH_2)_3$-O–	H	7.699
17	– $(CH_2)_5$–		–O-$(CH_2)_3$-O–	H	7.4949
18	CH_3	CH_3	–O-$(CH_2)_3$-O–	H	8.2218
19	CH_3	CH_3	–O-$(CH_2)_4$-O–	H	7.5686
20	CH_3	C_2H_5	–O-$(CH_2)_3$-O–	H	8.0969
21	H	c-Pr	–O-$(CH_2)_3$-O–	H	8.1549
22	– $(CH_2)_4$–		–O-$(CH_2)_3$-O–	H	8.699
23*	– $(CH_2)_4$–		–O-$(CH_2)_4$-O–	H	7.3768
24	– $(CH_2)_5$–		–O-$(CH_2)_3$-O–	H	8.1549
25	– $(CH_2)_5$–		–O-$(CH_2)_4$-O–	H	6.8069
26	–$(CH_2)_6$–		–O-$(CH_2)_3$-O–	H	7.9586
27	–$(CH_2)_5$–		–O-$(CH_2)_3$-O–	F	7.8239
28	–$(CH_2)_5$–		–O-$(CH_2)_3$-O–	Cl	7.8539
29	–$(CH_2)_5$–		–O-$(CH_2)_3$-O–	NO_2	7.8239
30	–$(CH_2)_5$–		–O-$(CH_2)_3$-O–	Me	7.7447
31	–$(CH_2)_5$–		–O-$(CH_2)_3$-O–	t-Bu	7.6576
32	–$(CH_2)_5$–		–O-$(CH_2)_3$-O–	OMe	8.2218
33*	–$(CH_2)_5$–		–O-$(CH_2)_3$-O–	CN	8
34	–$(CH_2)_5$–		–O-$(CH_2)_3$-O–	$COCH_3$	7.8861
35	–$(CH_2)_5$–		–O-$(CH_2)_3$-O–	SO_2NH_2	8.2218
36*	–$(CH_2)_4$–		–O-$(CH_2)_3$-O–	F	8
37	–$(CH_2)_4$–		–O-$(CH_2)_3$-O–	Cl	8.1549
38	–$(CH_2)_4$–		–O-$(CH_2)_3$-O–	NO_2	8.0969
39*	–$(CH_2)_4$–		–O-$(CH_2)_3$-O–	Me	8
40	–$(CH_2)_4$–		–O-$(CH_2)_3$-O–	t-Bu	7.7696
41	–$(CH_2)_4$–		–O-$(CH_2)_3$-O–	OMe	7.9586
42	–$(CH_2)_4$–		–O-$(CH_2)_3$-O–	CN	8.0969
43	–$(CH_2)_4$–		–O-$(CH_2)_3$-O–	$COCH_3$	8.0458
44*	–$(CH_2)_4$–		–O-$(CH_2)_3$-N(Me)–	H	7.3872
45	–$(CH_2)_4$–		–O-$(CH_2)_3$–	H	7.4949
MTX					8.5229

* test set.

the cells will not be capable of de novo synthesis of purines and thymidylate, and thus DNA synthesis will be inhibited [13].

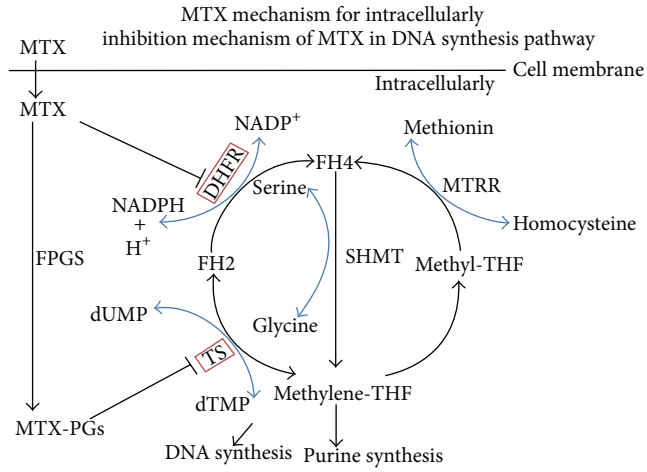

Figure 1: Inhibition mechanism of MTX in DNA synthesis pathway. MTX: methotrexate; FPGS: folylpolyglutamate synthetase; MTX-PGs: methotrexate polyglutamates; DHFR: dihydrofolate reductase; TS: thymidylate synthase; FH4: tetrahydrofolate; FH2: dihydrofolate; Methylene-THF: 5,10-methylenetetrahydrofolate; Methyl-THF: 5-methyltetrahydrofolate; dUMP: deoxyurindine-5′-monophosphate; dTMP: deoxythymidine-5′-monophosphate; MTRR: methionine synthase reductase; SHMT: serine hydroxymethyltransferase.

The primary action of MTX is inhibition of the enzyme DHFR, which converts dihydrofolate (FH2) to tetrahydrofolate (FH4) [11, 14]. MTX-PGs exert a stronger inhibition of DHFR and TS [15–17]. Thus, through direct inhibition by MTX and due to lack of FH4 and accumulation of FH2, deoxythymidine monophosphate synthesis and purine de novo synthesis is blocked, which eventually lead to leukemic cell death, bone marrow suppression, gastrointestinal mucositis, liver toxicity, and, rarely, alopecia [14, 15, 18, 19]. In fact, both MTX and natural folates undergo polyglutamylation catalyzed by the enzyme folylpolyglutamyl synthase. The MTX-PGs ensure intracellular retention and, furthermore, increase the affinity for the MTX-sensitive enzymes [16, 18, 20] (Figure 1).

However, MTX may lead to acute renal cytotoxicity [21] which is serious and potentially fatal in the spinal canal and may occur after the administration of neurotoxicity [22–25] and hematological toxicity [26] caused by animal somatic cells and human bone marrow chromosomal lesions [27] which led to the hematopoietic system abnormalities [28], gastrointestinal toxicity [29] made multiorgan dysfunction [30], nephrotoxicity [31] made renal failure [31, 32], and hepatotoxicity made liver fibrosis [33]. Higher concentrations of long-chain MTX-PGs have been in the risk of gastrointestinal and hepatic toxicity [12, 34, 35]. Thus, the lower toxicity drugs are necessary to be developed. Recently, the increasing numbers of mechanisms of different diseases have been clarified to detect the helpful target protein for diseases treatment [36–49], and diseases treatments with traditional Chinese medicine (TCM) as complements are getting more and more attention. The compounds extracted from traditional Chinese medicine have displayed their potential as

Table 2: DHFR and TS docking score of TCM candidates.

Index	TCM candidate	DHFR docking score	TS docking score
1	Adenosine triphosphate	226.6790	186.2170
2	Methyl 6-O-digalloyl-beta-D-glucopyranoside (II)	162.6260	154.1730
3	Methyl 4,6-di-O-galloyl-beta-D-glucopyranoside	153.7500	148.2880
4	Methyl 6-O-digalloyl-beta-D-glucopyranoside	151.7650	158.0350
5	Manninotriose	129.7870	114.6030
6	Forsythiaside	129.6030	27.9940
7	Isoacteoside	124.5900	30.6190
8	Rehmannioside B	119.9930	79.2920
9	Rehmannioside A	116.4330	71.3970
10	Raffinose	115.4940	134.2120
11	Cistanoside C	112.4270	—
12	Methyl 3,3,6-tri-O-galloyl-beta-D-glucopyranoside	109.9470	20.7830
13	Stachyose	107.0940	8.5760
14	Chlorogenic acid	103.8080	—
15	Jionoside D	103.5050	39.3430
16	Isochlorogenic acid	102.9470	—
17	Jionoside C	102.3940	—
18	Rutin	101.1310	78.816
*	MTX	97.0960	—
**	MTX-PGs	—	69.671

*control.
**Methotrexate polyglutamate.

Table 3: Predicted pharmacokinetic properties of TCM candidates and MTX.

Index	TCM candidate	Pharmacokinetic properties			
		Absorption	Solubility	Hepatotoxicity	PPB
1	Adenosine triphosphate	3	2	1	0
2	Chlorogenic acid	3	4	1	0
3	Cistanoside C	3	2	1	2
4	Forsythiaside	3	2	1	0
5	Isoacteoside	3	2	1	0
6	Isochlorogenic acid	3	4	1	0
7	Jionoside C	3	3	1	2
8	Jionoside D	3	2	1	2
9	Manninotriose	3	3	0	0
10	Methyl 4,6-di-O-galloyl-beta-D-glucopyranoside	3	2	1	0
11	Methyl 6-O-digalloyl-beta-D-glucopyranoside	3	2	1	0
12	Methyl 6-O-digalloyl-beta-D-glucopyranoside (II)	3	2	1	0
13	Methyl 3,3,6-tri-O-galloyl-beta-D-glucopyranoside	3	0	1	0
14	Raffinose	3	3	0	0
15	Rehmannioside A	3	4	1	0
16	Rehmannioside B	3	4	1	0
17	Rutin	3	1	1	2
18	Stachyose	3	1	0	0
Control	MTX	3	3	1	1

[1]Absorption (Human intestinal absorption), there are four prediction levels: 0 (good absorption), 1 (moderate absorption), 2 (poor absorption), 3 (very poor absorption).
[2]Solubility, there are gour prediction levels: 0 (extremely low), 1 (very low, but possible), 2 (low), 3 (good), 4 (optimal), 5 (too soluble), 6 (warning).
[3]Hepatotoxicity, there are four prediction levels: 0 (nontoxic), 1 (toxic).
[4]PPB (Plasma protein binding), there are there prediction levels: 0 (binding is <90%), 1 (binding is >90%), 2 (binding >95%).

Table 4: Partial Least Square (PLS) analysis for CoMFA and CoMSIA models.

	Cross Validation		Non-cross Validtion			Fraction				
	ONC	q^2	r^2	SEE	F	S	E	H	D	A
					CoMFA					
	7	0.5250	0.9630	0.2590	136.2760	0.7970	0.2030	—	—	—
					CoMSIA					
S	36	0.6350	0.9890	0.3040	19.6900	1.0000	0.0000	0.0000	0.0000	0.0000
E	—	—	—	—	—	—	—	—	—	—
H	2	0.6130	0.7760	0.5940	72.7070	0.0000	0.0000	1.0000	0.0000	0.0000
D	7	0.4180	0.7160	0.7130	13.3480	0.0000	0.0000	0.0000	1.0000	0.0000
A	1	0.0810	0.1600	1.1380	8.1640	0.0000	0.0000	0.0000	0.0000	1.0000
SE	37	0.6050	0.9890	0.3250	16.7260	0.9980	0.0200	0.0000	0.0000	0.0000
SH	2	0.5970	0.7790	0.5910	73.9120	0.3880	0.0000	0.6120	0.0000	0.0000
SD	36	0.6670	0.9890	0.3020	19.9580	0.6350	0.0000	0.0000	0.3650	0.0000
SA	30	0.7020	0.9890	0.2340	39.7820	0.7480	0.0000	0.0000	0.0000	0.2520
EH	7	0.6270	0.9540	0.2860	110.4680	0.0000	0.0500	0.9500	0.0000	0.0000
ED	7	0.4130	0.7090	0.7210	12.9020	0.0000	0.0180	0.0000	0.9820	0.0000
EA	2	0.0760	0.1830	1.1350	4.6860	0.0000	0.2000	0.0000	0.0000	0.8000
HD	2	0.5780	0.7940	0.5690	81.1680	0.0000	0.0000	0.7220	0.2780	0.0000
HA	2	0.5890	0.7910	0.5740	79.5410	0.0000	0.0000	0.7450	0.0000	0.2550
DA	9	0.4300	0.7290	0.7160	10.4430	0.0000	0.0000	0.0000	0.7800	0.2200
SHE	8	0.5850	0.9690	0.2400	139.5820	0.3570	0.0440	0.6000	0.0000	0.0000
SED	38	0.6500	0.9890	0.3490	14.1810	0.6340	0.0010	0.0000	0.3650	0.0000
SEA	31	0.7030	0.9880	0.2430	35.7980	0.7420	0.0110	0.0000	0.0000	0.2470
SHD	22	0.5780	0.9890	0.1830	89.3410	0.3070	0.0000	0.4490	0.2430	0.0000
SHA	2	0.5800	0.7950	0.5680	81.4850	0.3130	0.0000	0.4980	0.0000	0.1900
SDA	30	0.7170	0.9890	0.2320	40.3890	0.5640	0.0000	0.0000	0.2910	0.1450
EDA	11	0.4240	0.7380	0.7250	8.4650	0.0000	0.0200	0.0000	0.7640	0.2150
EHA*	**11**	**0.5770**	**0.9800**	**0.1990**	**148.9890**	**0.0000**	**0.0630**	**0.6910**	**0.0000**	**0.2460**
HAD	2	0.5550	0.8020	0.5580	85.2150	0.0000	0.0000	0.6150	0.2080	0.1770
SEHD	23	0.5970	0.9890	0.1870	81.1730	0.2940	0.0230	0.4520	0.2310	0.0000
SEHA	23	0.5970	0.9800	0.1880	80.4080	0.3000	0.0420	0.4620	0.0000	0.1960
SEDA	31	0.7110	0.9890	0.2420	36.1870	0.5640	0.0050	0.0000	0.2840	0.1470
SHDA	5	0.5630	0.9290	0.3470	102.3970	0.2600	0.0000	0.3980	0.1920	0.1510
EHDA*	**12**	**0.6070**	**0.9820**	**0.1940**	**143.5670**	**0.0000**	**0.0500**	**0.5880**	**0.2040**	**0.1580**
SEHDA	23	0.6120	0.9890	0.1880	80.3300	0.2690	0.0340	0.4020	0.1630	0.1330

OCN: Optimal number of components.
SEE: Standard error of estimate.
F: F-test value.
*Prediction model.
S: Steric.
H: Hydrophobic.
D: Hydrogen bond donor.
A: Hydrogen bone acceptor.
E: Electrostatic.

lead compounds against tumors [50–54], stroke [55–58], viral infection [59–63], metabolic syndrome [64–66], diabetes [67], inflammation [62], and other diseases [68, 69]. For this trend, we attempted to discover the compounds with drug-like potential and lower toxicity for ALL treatment from the components in traditional Chinese medicine.

2. Materials and Methods

2.1. Virtual Screening. The receptors, human dihydrofolate reductase (DHFR) and human thymidylate synthase (TS) proteins were downloaded from Protein Data Bank of 1U72 (PDB ID: 1U72) [70] and 1HVY (PDB ID: 1HVY) [71].

Table 5: Experimental and predicted pIC50 values of 45 DHFR inhibitors using the constructed CoMFA and CoMSIA models.

DHFR inhibitors no.	Experimental pIC50	CoMFA		CoMSIA_EHDA		CoMSIA_EHA	
		Predicted	Residual	Predicted	Residual	Predicted	Residual
1	4.710	4.652	0.0580	4.481	0.229	4.532	0.178
2	4.609	4.606	0.0031	4.635	−0.026	4.662	−0.053
3*	4.231	4.576	−0.3454	4.333	−0.102	4.407	−0.176
4	4.662	5.027	−0.3655	4.698	−0.037	4.701	−0.039
5*	4.524	4.571	−0.0467	4.807	−0.283	4.797	−0.273
6	4.893	4.476	0.4168	4.723	0.170	4.651	0.242
7*	7.161	6.810	0.3512	7.287	−0.126	7.359	−0.198
8	6.810	6.529	0.2807	6.722	0.088	6.723	0.087
9*	6.261	6.495	−0.2338	6.270	−0.009	6.240	0.021
10	6.873	6.648	0.2249	6.808	0.065	6.832	0.041
11	6.762	6.793	−0.0310	6.686	0.076	6.645	0.117
12	5.747	5.749	−0.0019	5.767	−0.020	5.705	0.042
13	5.273	5.346	−0.0727	5.245	0.028	5.279	−0.006
14	7.509	7.454	0.0546	7.494	0.015	7.522	−0.013
15	8.046	8.322	−0.2762	8.056	−0.010	8.052	−0.006
16	7.699	8.127	−0.4280	8.130	−0.431	8.110	−0.411
17	7.495	7.670	−0.1751	7.871	−0.376	7.820	−0.325
18	8.222	8.079	0.1428	8.130	0.092	8.105	0.117
19	7.569	7.561	0.0076	7.581	−0.012	7.609	−0.040
20	8.097	8.207	−0.1101	8.105	−0.008	8.240	−0.143
21	8.155	8.007	0.1479	8.242	−0.087	8.215	−0.060
22	8.699	8.127	0.5720	8.130	0.569	8.110	0.589
23*	7.377	7.636	−0.2592	7.325	0.052	7.318	0.059
24	8.155	7.670	0.4849	7.871	0.284	7.820	0.335
25	6.807	7.113	−0.3061	6.902	−0.095	6.824	−0.017
26	7.959	7.987	−0.0284	7.887	0.072	7.975	−0.016
27	7.824	7.763	0.0609	7.981	−0.157	7.955	−0.131
28	7.854	7.839	0.0149	7.906	−0.052	7.850	0.004
29	7.824	7.843	−0.0191	7.824	0.000	7.827	−0.003
30	7.745	7.914	−0.1693	7.736	0.009	7.733	0.012
31	7.658	8.069	−0.4114	7.665	−0.007	7.654	0.004
32	8.222	8.005	0.2168	7.848	0.374	7.814	0.408
33*	8.000	8.100	−0.1000	7.978	0.022	8.010	−0.010
34	7.886	7.455	0.4311	7.947	−0.061	7.811	0.075
35	8.222	7.981	0.2408	8.208	0.014	8.237	−0.015
36*	8.000	8.173	−0.1730	8.130	−0.130	8.139	−0.139
37	8.155	8.180	−0.0251	8.170	−0.015	8.187	−0.032
38	8.097	8.122	−0.0251	8.097	0.000	8.097	0.000
39*	8.000	7.990	0.0100	8.007	−0.007	8.054	−0.054
40	7.770	7.683	0.0866	7.832	−0.062	7.697	0.073
41	7.959	8.223	−0.2644	7.883	0.076	7.907	0.052
42	8.097	7.974	0.1229	8.040	0.057	8.150	−0.053
43	8.046	7.996	0.0498	8.052	−0.006	8.061	−0.015
44*	7.387	7.542	−0.1548	7.567	−0.180	7.590	−0.203
45	7.495	7.449	0.0459	7.484	0.011	7.516	−0.021

* test set.

Table 6: Predicted bioactivity (pIC50) of MTX and TCM candidates using MLR, Bayesian, SVM, CoMFA and CoMSIA models.

Name	MLR	Bayesian	SVM	CoMFA	CoMSIA_EHDA*	CoMSIA_EHA**
Adenosine triphosphate	6.4559	5.8145	8.7175	7.9640	7.8600	7.8350
Methyl 6-O-digalloyl-beta-D-glucopyranoside (II)	27.5044	5.1810	8.0157	6.9800	6.6030	5.5170
Methyl 4,6-di-O-galloyl-beta-D-glucopyranoside	27.7317	5.4868	8.4131	7.5490	6.5980	5.9300
Methyl 6-O-digalloyl-beta-D-glucopyranoside	26.7188	5.2477	7.8936	6.8980	6.6620	5.6840
Manninotriose	29.1034	5.1934	5.9247	7.6470	6.2450	5.3700
Forsythiaside	29.9821	5.3595	8.5713	7.7140	8.0830	7.8950
Isoacteoside	27.6319	6.3265	8.1255	7.6550	7.7990	7.5430
Rehmannioside B	26.7291	4.3032	7.3293	6.9990	6.8000	5.8300
Rehmannioside A	30.3632	4.4182	9.3324	6.7480	5.8070	4.6750
Raffinose	32.8592	5.1647	8.4766	6.9350	5.9620	4.2830
Cistanoside C	26.1802	5.7174	8.2029	7.6060	8.0200	7.9640
Methyl 3,3,6-tri-O-galloyl-beta-D-glucopyranoside	30.7405	6.0369	8.3193	6.7670	6.3240	6.6300
Stachyose	40.5491	5.9779	8.5055	7.4300	5.6830	4.4510
Chlorogenic acid	17.3951	4.2335	7.8897	7.8080	7.9640	7.7680
Jionoside D	26.0421	5.5238	8.2089	7.5080	7.4900	7.2820
Isochlorogenic acid	16.1484	4.4196	7.4839	7.1990	6.3590	6.4480
Jionoside C	23.7203	5.6640	8.2741	7.7600	7.0800	6.9110
Rutin	30.3096	5.6910	8.2465	6.5720	8.0190	7.6830

The pIC50 experimental values of MTX was 8.5229.
*EHDA model of CoMSIA.
**EHA model of CoMSIA.

We adopted the traditional Chinese medicine formulas that treat acute lymphoblastic leukemia from database "Shanghai Innovative Research Center of Traditional Chinese Medicine" (http://www.sirc-tcm.sh.cn/en/index.html) [72]. The component compounds of these formulas were integrated with the herbs data from the TCM Database@Taiwan [73] and became the ALL disease-specific compound library. Virtual screening of candidates from the compound library was conducted using the LigandFit Module of DS 2.5 under the Chemistry at HARvard Macromolecular Mechanics (CHARMm) force field. DockScore was selected as output values. Candidates were ranked according to DockScore and pharmacokinetic characteristics including absorption, solubility, blood brain barrier (BBB), and plasma protein binding (PPB) were predicted by ADMET protocols for each candidate.

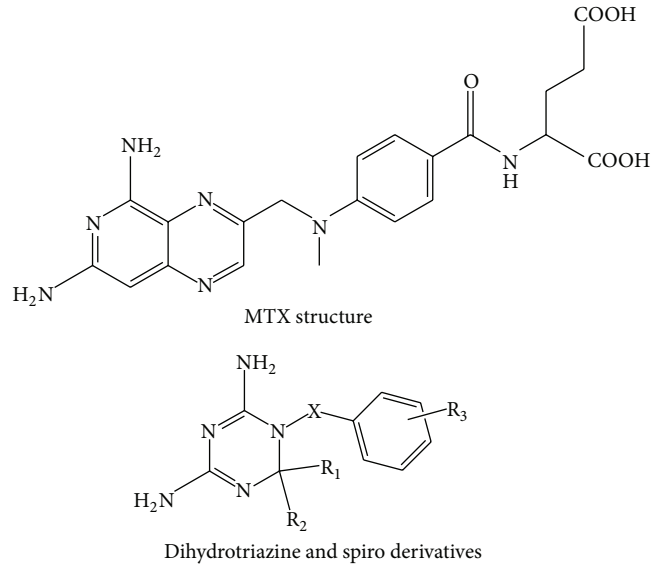

Figure 2: Chemical structure of DHFR inhibitors [40].

2.2. 2D-Quantitative Structure Activity Relationship (2D-QSAR) Models. In this study, 45 candidates (Figure 2) with known experimental pIC50 values [74] that have inhibitory activities toward DHFR were used in the QSAR studies (Table 1). The 45 known inhibitors were randomly divided into a training set of 36 candidates and a test set of 9 candidates. The chemical structures of these candidates were drawn by ChemDraw Ultra 10.0 (CambridgeSoft Inc., USA) and transformed to 3D molecule models by Chem3D Ultra 10.0 (CambridgeSoft Inc., USA). Molecular descriptors for each candidate were calculated using the DS 2.5 Calculate Molecular Property Module. Genetic function approximation (GFA) model was used to select representative descriptors that correlated ($r^2 > 0.8$) to bioactivity (pIC50) which were used to construct 2D-QSAR models. The training set was used to construct multiple linear regression (MLR), support vector machine (SVM), and Bayesian network (BN) models. The test set was used to test the accuracy of these models.

2.2.1. Multiple Linear Regression (MLR) Model. Multiple linear regression [75] attempts to model the relationship between two or more explanatory variables and a response

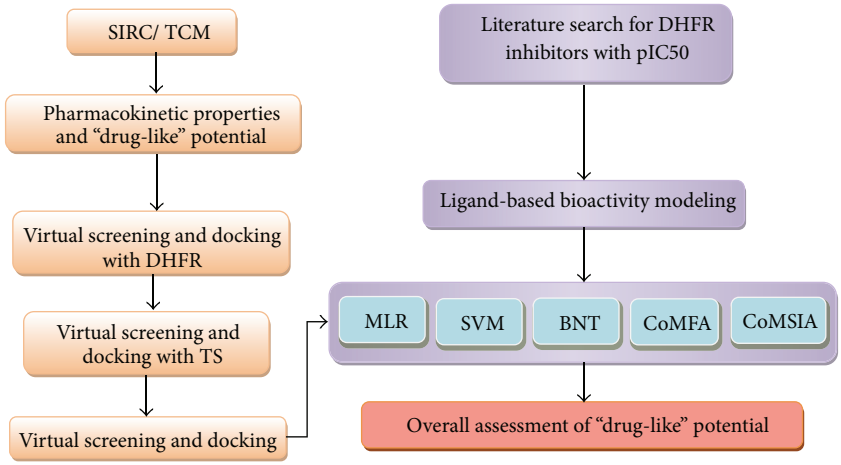

Figure 3: The experimental flowchart.

variable by fitting a linear equation to observed data. The model was built in the form of equation as follows:

$$\mathrm{pIC}_{50} = a_0 + a_1 x_1 + a_2 x_2 + \cdots + a_n x_n, \tag{1}$$

where x_i represents the ith molecular descriptor and a_i is its fitting coefficient. The generated MLR model was validated with test dataset. The square correlation coefficients (R^2) between predicted and actual pIC50 of the training set was used to verify accuracy of the model. This building model was applied to predict the pIC50 values of the TCM candidates.

2.2.2. Support Vector Machine (SVM) Model. SVM implement classification or regression analysis with linear or nonlinear algorithms [76]. The algorithm identifies a maximum-margin hyper-plane to discriminate two class training samples. Samples on the margin are called the support vectors. Lagrange multipliers and kernels were introduced to form the final pattern separating regression model. In this study, LibSVM [77–79] package was selected to build our regression SVM model. The selected kernel was the Gaussian radial basis function kernel equation:

$$K(x_i, x_k) = \exp\left[\frac{\|x_i - x_k\|^2}{2\sigma^2}\right]. \tag{2}$$

Cross-validation of the SVM model was also conducted following the default settings in LibSVM [80]. The generated regression SVM model was validated with test dataset. The square correlation coefficients (R^2) between predicted and actual pIC50 of the training set was used to verify accuracy of the model. This building model was applied to predict the pIC50 values of the TCM candidates.

2.2.3. Bayesian Network Model. We used the Bayes Net Toolbox (BNT) in Matlab (https://code.google.com/p/bnt) to create Bayesian network model [81] by the training data set. After data discretization, we applied linear regression analysis for each pIC50 category in the training dataset. For the ith pIC50 category with n candidates, let y_{ij} and x_{ijp} represent the pIC50 value and the pth descriptor value in the jth ligand, respectively. The regression model of the data sets $\{y_{ij}, x_{ij1}, \ldots, x_{ijp}\}_{j=1}^{n}$ is formulated as

$$y_i = X_i \beta_i + \varepsilon_i, \tag{3}$$

where

$$y_i = \begin{bmatrix} y_{i1} \\ y_{i2} \\ \vdots \\ y_{in} \end{bmatrix}, \qquad X_i = \begin{bmatrix} x_{i11} & \cdots & x_{i1p} \\ x_{i21} & \cdots & x_{i2p} \\ \vdots & \vdots & \vdots \\ x_{in1} & \cdots & x_{inp} \end{bmatrix}, \tag{4}$$

and β_i and ε_i are the regression coefficients and error term in the ith pIC50 category. We used ordinary least squares to estimate the unknown regression coefficient β_i:

$$\hat{\beta}_i = \left(X_i^T X_i\right)^{-1} X_i^T y_i. \tag{5}$$

The Banjo (Bayesian network inference with Java objects) is software for structure learning of static Bayesian networks (BN) [82]. It is implemented in Java. We used training dataset to discover the relationships in the BN structure among the descriptors and the pIC50 by the Banjo package. After that, we used test data to assess the accuracy of our algorithm. For the test data D, the pIC50 category (k) is predicted by the following formula:

$$k = \arg\max_{i=1}^{n} P(i \mid D), \tag{6}$$

where i represented the ith category of pIC50 and n represented the total number of the pIC50 categories. The marginal probability $P(i \mid D)$ can be calculated by BNT module. Finally, the pIC50 value is calculated as follows:

$$\mathrm{pIC50} = X_k \hat{\beta}_k. \tag{7}$$

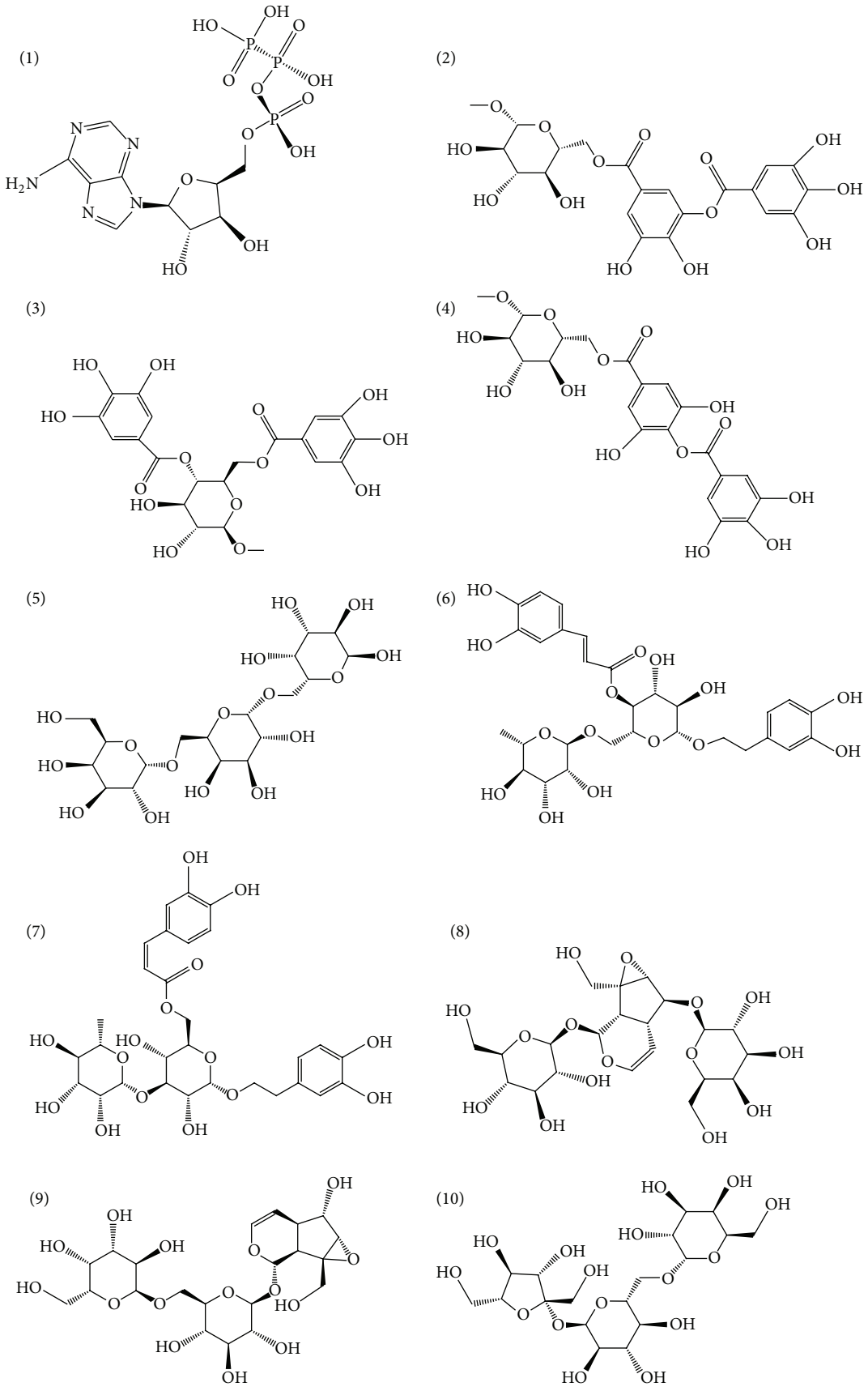

(a)

Figure 4: Continued.

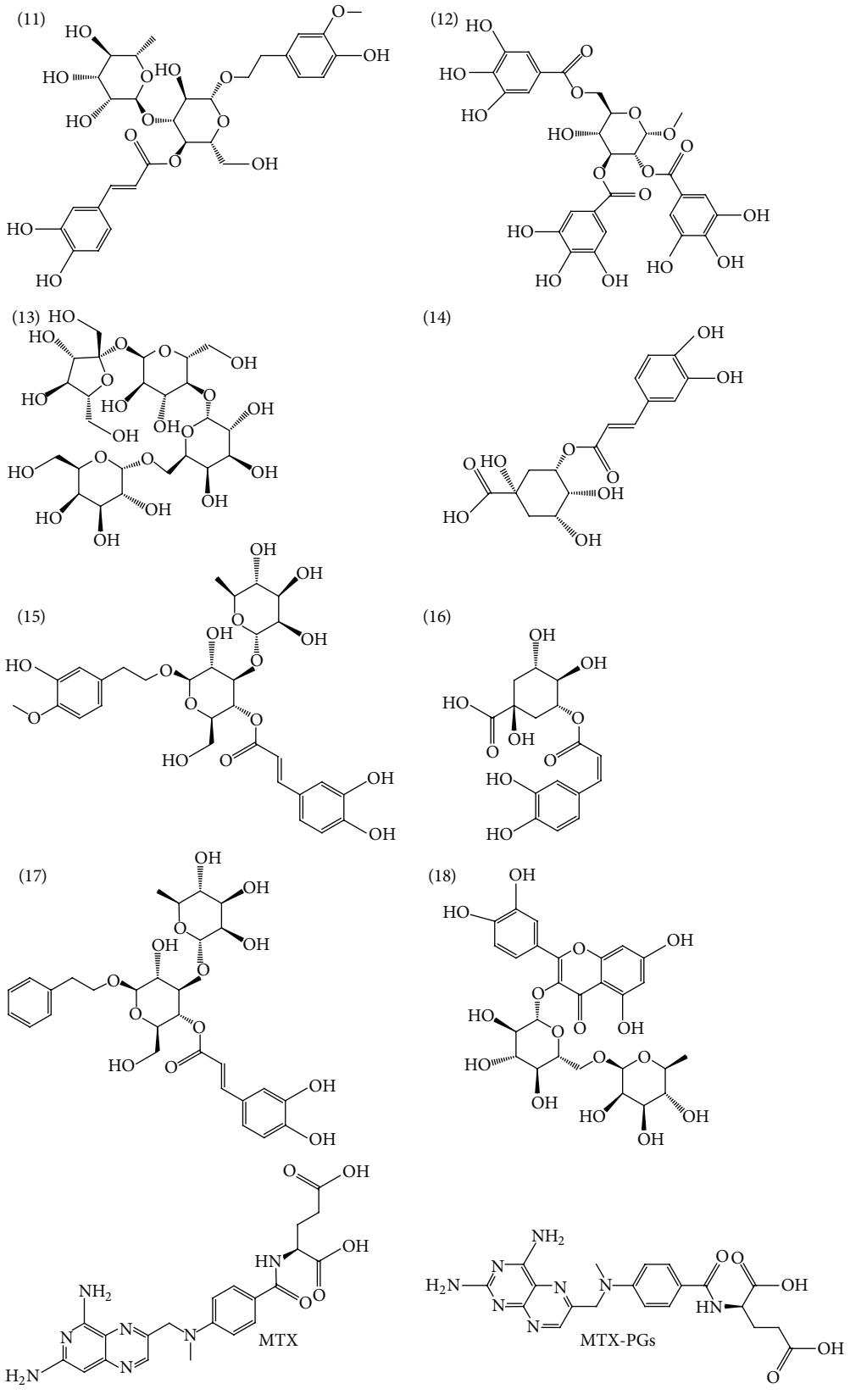

(b)

Figure 4: (a)-(b) The chemical scaffolds of MTX, MTX-PGs, and TCM candidates for acute lymphoblastic leukemia treatment.

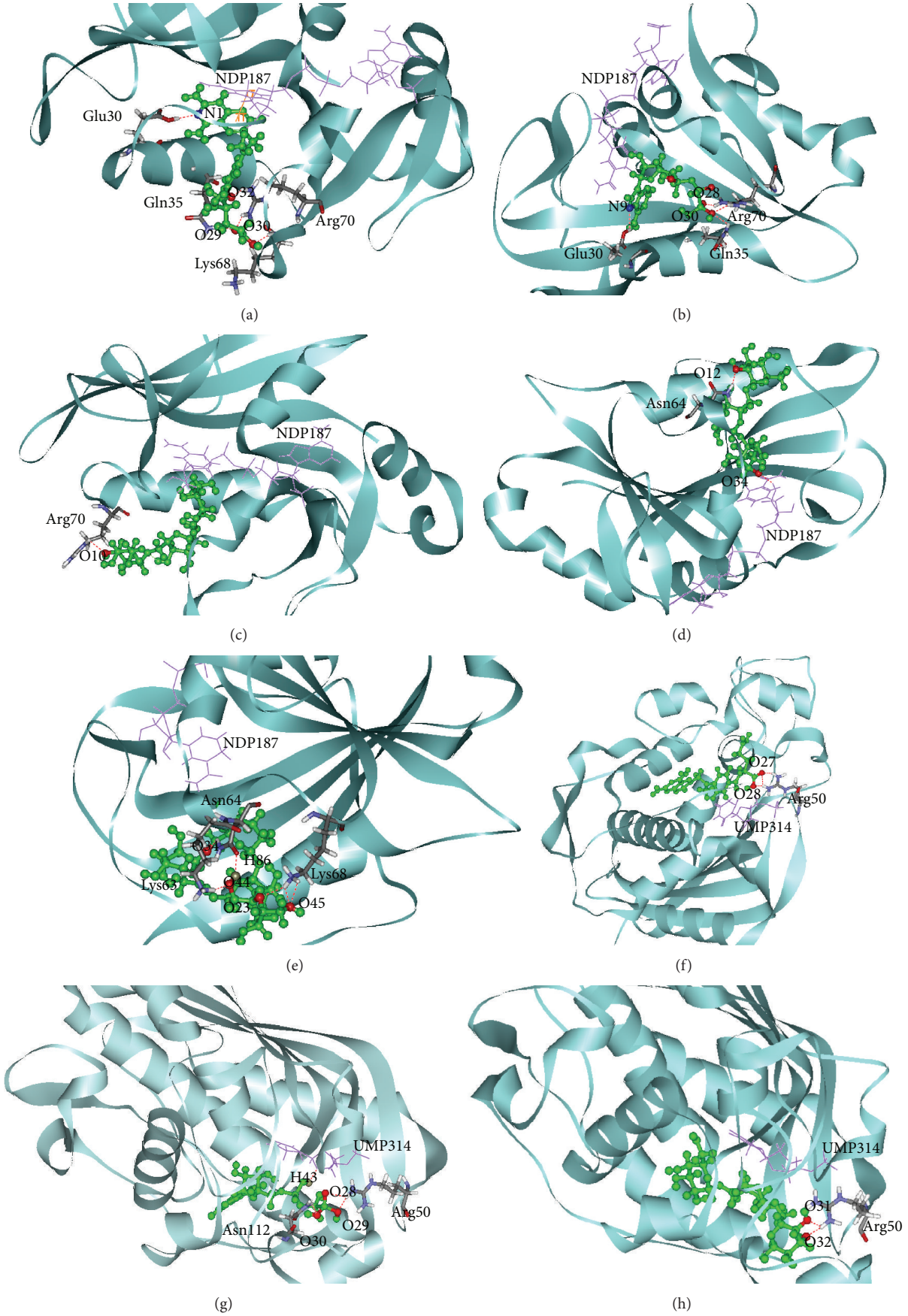

Figure 5: Continued.

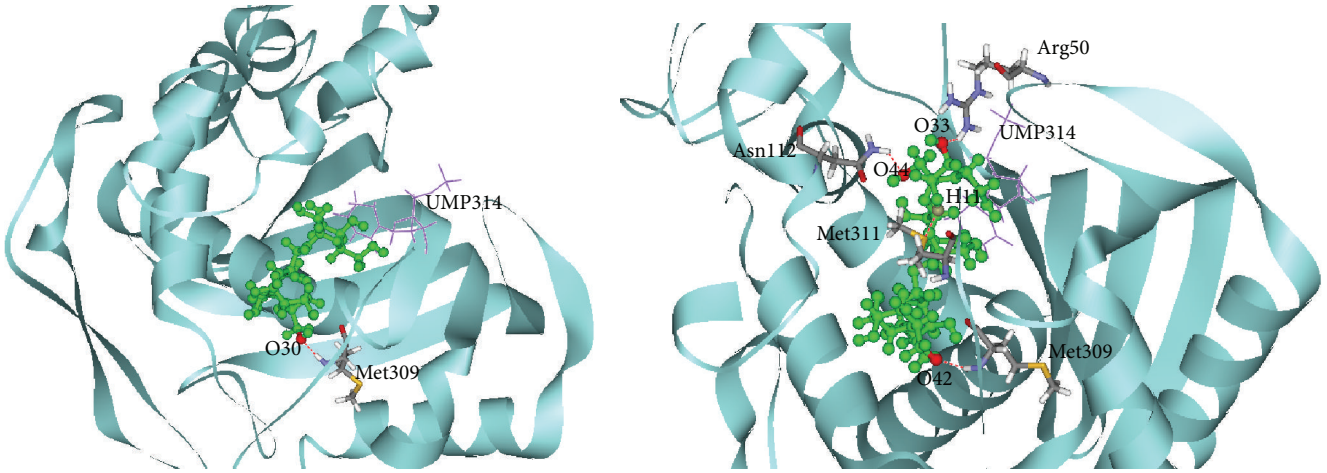

(i) (j)

Figure 5: Docking pose of MTX and TCM candidates with DHFR for (a), (b), (c), (d), and (e). Docking pose of MTX-PGs with TS for (f), (g), (h), (i), and (j). TCM candidates are shown in cyan. The cofactors are shown in purple. In H-bond interactions, nitrogen atoms are shown in blue, hydrogen atoms are shown in gray, oxygen atoms are shown in magenta, hydrogen bonds are shown in red dotted line, pi bonds are shown in orange solid line. (a) MTX, (b) and (g) adenosine triphosphate, (c) and (h) manninotriose, (d) and (i) raffinose, (e) and (j) stachyose, and (f) MTX-PGs.

The square correlation coefficients (R^2) between predicted and actual pIC50 of the training set were used to verify accuracy of the model. This building model was applied to predict the pIC50 values of the TCM candidates.

2.3. 3D-Quantitative Structure Activity Relationship (3D-QSAR) Models. Comparative molecular field analysis (CoMFA) and comparative molecular similarity indices analysis (CoMSIA) were performed by Sybyl-X 1.1.1 (Tripos Inc., St. Louis, MO, USA) for DHFR inhibitors. Lennard-Jones potential and Coulomb potential were employed to calculate steric and electrostatic interaction energies. The two 3D-QSAR models were further evaluated by cross-validated correlation coefficient (q^2) and non-cross-validated correlation coefficient (r^2). The correlation between the force field and biological activities was calculated by partial least squares (PLSs) method.

The flowchart for the entire experimental procedure for TCM candidates screening is illustrated in Figure 3.

3. Results and Discussion

3.1. Virtual Screening. The virtual screening was performed by the LigandFit Module of DS 2.5 in force field of CHARMm. The receptor binding sites were defined by the binding position of MTX on DHFR protein and by the binding position of MTX-PGs on TS protein. The compounds from our library were docked into the two receptors. In this protocol, the receptors were fixed, and the ligands that complement the binding sites were flexible in energy minimization process. The control compound used in this study was MTX which contains aromatic and heterocyclic rings (Figure 4).

The top eighteen results from DHFR docking score are tabulated in Table 2. The TS docking score for the eighteen candidates are also tabulated in Table 2. All the eighteen TCM candidates had higher Dock Scores than the control methotrexate (MTX) and MTX-PGs. Chemical scaffolds of MTX, MTX-PGs, and the eighteen TCM candidates are shown in Figure 4. Adsorption, solubility, hepatotoxicity, and plasma protein binding were assessed to evaluate pharmacokinetic properties of the selected candidates (Table 3). Considering the factor of hepatotoxicity, we selected the TCM compounds adenosine triphosphate, manninotriose, raffinose, and stachyose for advanced study. MTX and TCM candidates had very poor absorption for human intestine. Binding strength of the ligands to carrier proteins in the blood stream is indicated by the plasma protein binding (PPB) value [21]. MTX has more than 90% for PPB but adenosine triphosphate, manninotriose, raffinose, and stachyose were less than 90% for PPB.

Ligand-receptor interactions during docking are shown in Figures 5 and 6. MTX docked on DHFR (Figure 5(a)) through four hydrogen bondings of Glu30, Gln35, Lys68, and Arg70. Adenosne triphosphate formed three H-bonds with Glu30, Gln35, and Arg70 (Figure 5(b)). Manninotriose formed H-bond with Arg28 (Figure 5(c)). Raffinose formed H-bonds with Asn64 and NDP (Figure 5(d)). Stachyose formed H-bonds with Lys63, Asn64, and Lys68 (Figure 5(e)). MTX-PGs docked on TS (Figure 5(f)) by single H-bond with Arg50. Adenosne triphosphate, manninotriose, and stachyose docked on TS (Figures 5(g), 5(h), and 5(j)) by single H-bond with Arg50. Raffinose docked on TS by single H-bond with Met309 (Figure 5(i)).

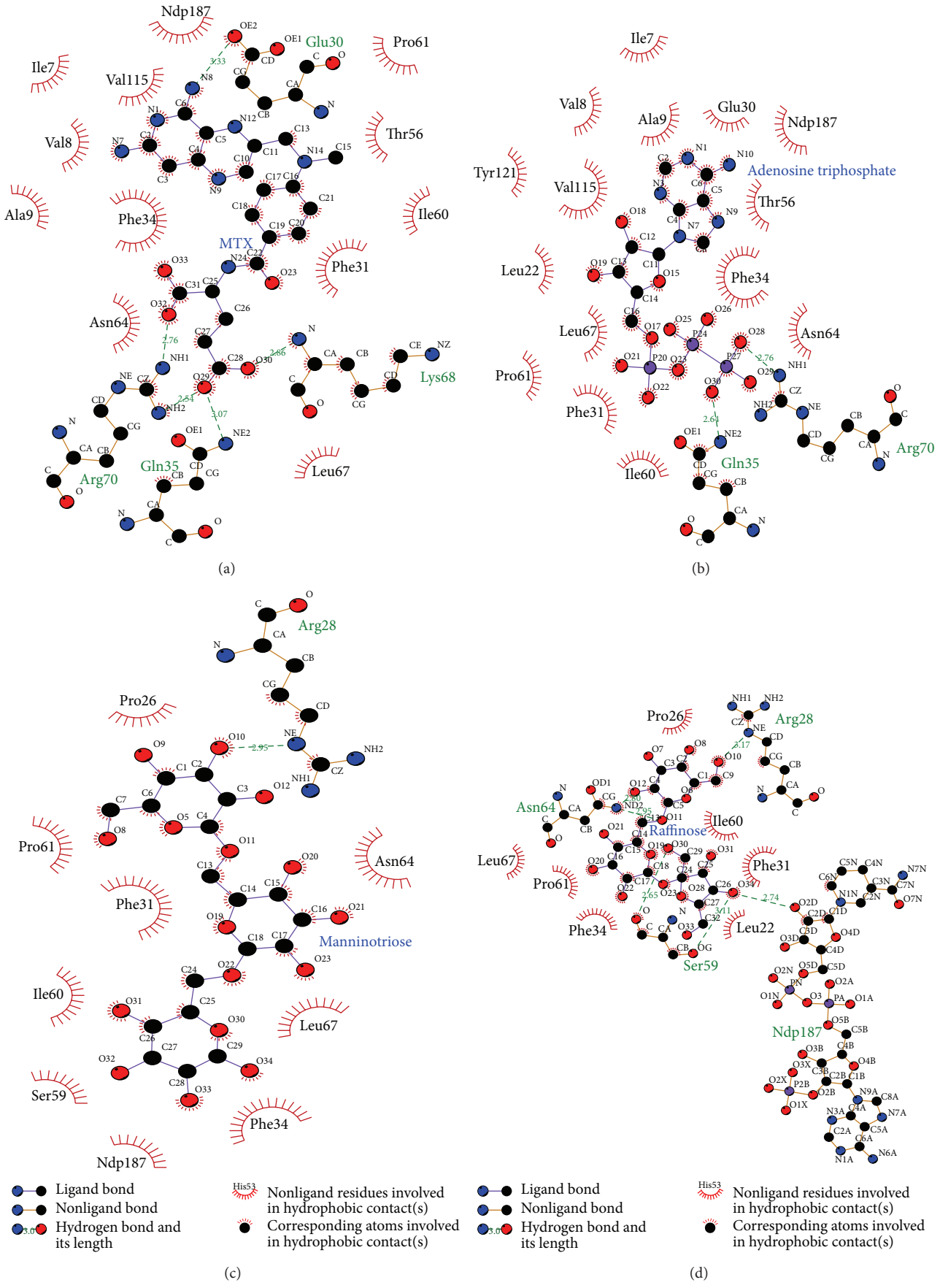

Figure 6: Continued.

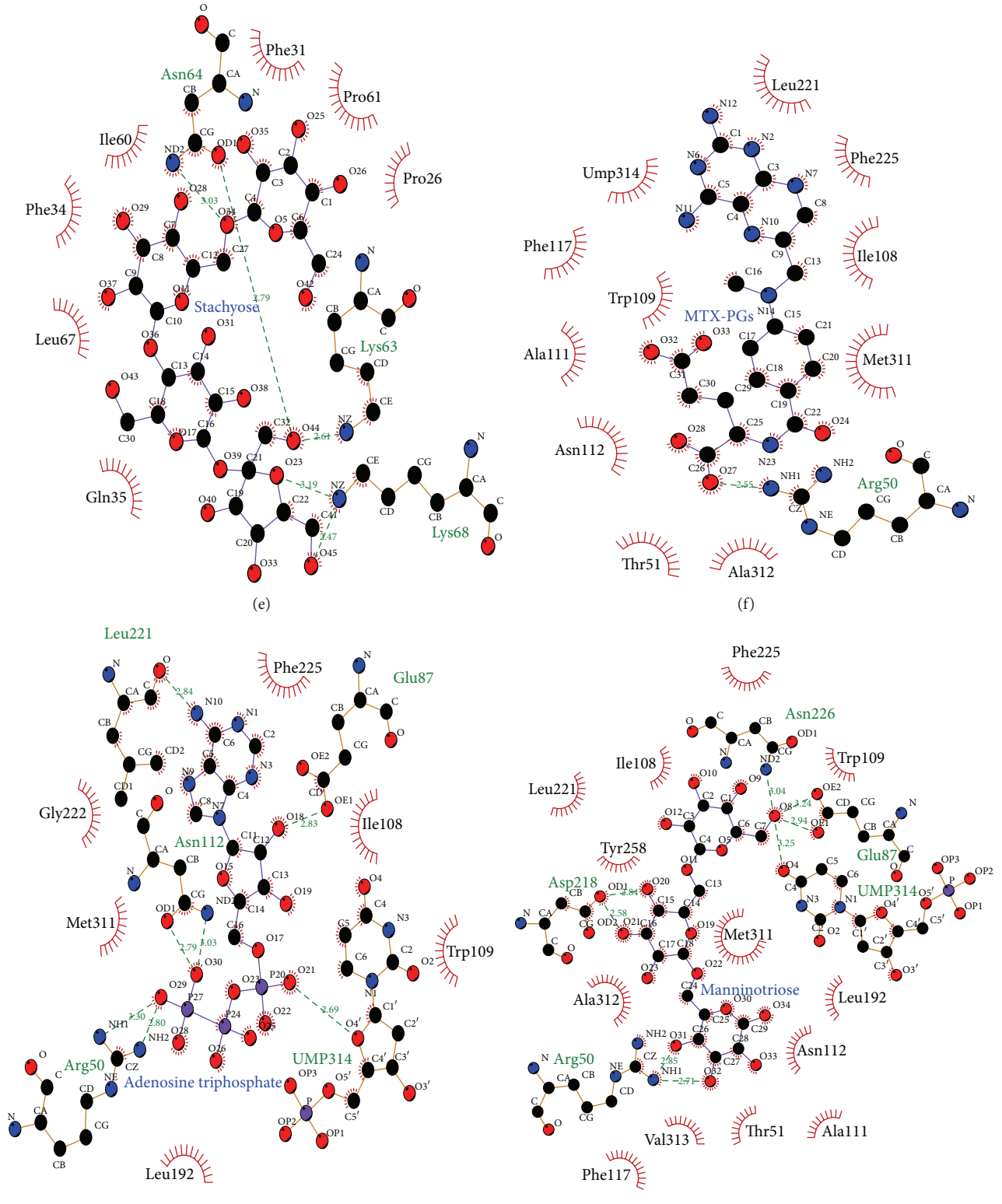

Figure 6: Continued.

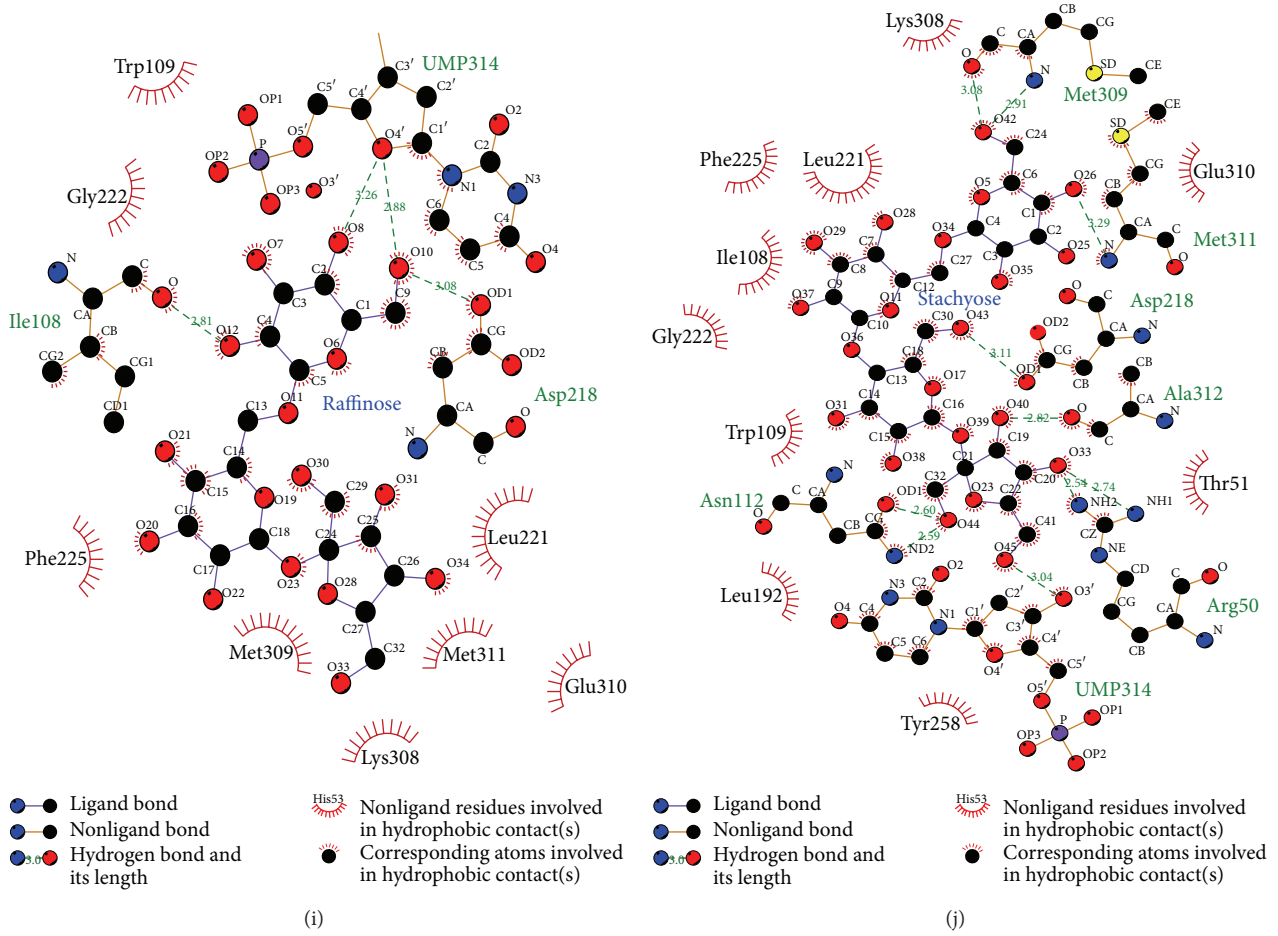

Figure 6: The Ligplot analysis of hydrophobic interactions between DHFR and TCM candidates and between TS and TCM candidates. (a) MTX with DHFR, (b) and (g) adenosine triphosphate with DHFR and TS, (c) and (h) manninotriose with DHFR and TS, (d) and (i) raffinose with DHFR and TS, (e) and (j) stachyose with DHFR and TS, and (f) MTX-PGs with DHFR and TS. Bonds: ligand bonds, nonligand bonds, hydrogen bonds, and hydrophobic are shown in purple, orange, olive green, and brick red, respectively. Atoms: nitrogen, oxygen, carbon, and sulfur are shown in blue, red, black, and yellow, respectively.

Analysis of hydrophobic interactions showed that MTX docking on DHFR was more stable than the TCM candidates. Comparing with chemical structures of the TCM candidates, it could be attributed to the larger size for MTX docking on DHFR (Figures 6(a), 6(b), 6(c), 6(d), and 6(e)). However, the TCM candidates docking on TS were more stable than MTX-PGs due to hydrophobic interactions (Figures 6(f), 6(g), 6(h), 6(i), and 6(j)).

3.2. Bioactivity Prediction Using QSAR Models. QSAR models were constructed using known DHFR inhibitors [40] and applied for predicting molecular properties of the TCM ligands. Molecular descriptors associated with bioactivity including BD_Count, Num_RotatableBonds, CHI_V_1, IAC_Mean, JX, JY, SC_3_C, Jurs_FNSA_1, Jurs_RPCS, Jurs_SASA, and Shadow_Xlength were used to construct MLR model, SVM model, and Bayesian network model.

Our MLR model was as follows.

GFATempModel_1 = 31.623 + 2.5173 * HBD_Count − 0.47471 * Num_RotatableBonds − 1.7664 * CHI_V_1 − 12.997 * IAC_Mean − 45.669 * JX + 36.62 * JY + 0.11612 * SC_3_C + 18.941 * Jurs_FNSA_1 − 4.8012 * Jurs_RPCS + 0.029451 * Jurs_SASA − 0.084377 * Shadow_Xlength.

In CoMFA model, the steric fields were the primary contributing factor. In CoMSIA, various factors were considered and modeled. The optimum CoMSIA models were "EHA model" and "EHDA model" based on high q^2, high r^2, and low SEE values (Table 4). The "EHA model" was consisting of electrostatic field and hydrophobic and hydrogen bond acceptor. The "EHDA model" was consisting of electrostatic field and hydrophobic and hydrogen bond donor, and hydrogen bond acceptor. The CoMFA model and CoMSIA model of EHDA and of EHA were with ONC of 7, 11, and 12, respectively.

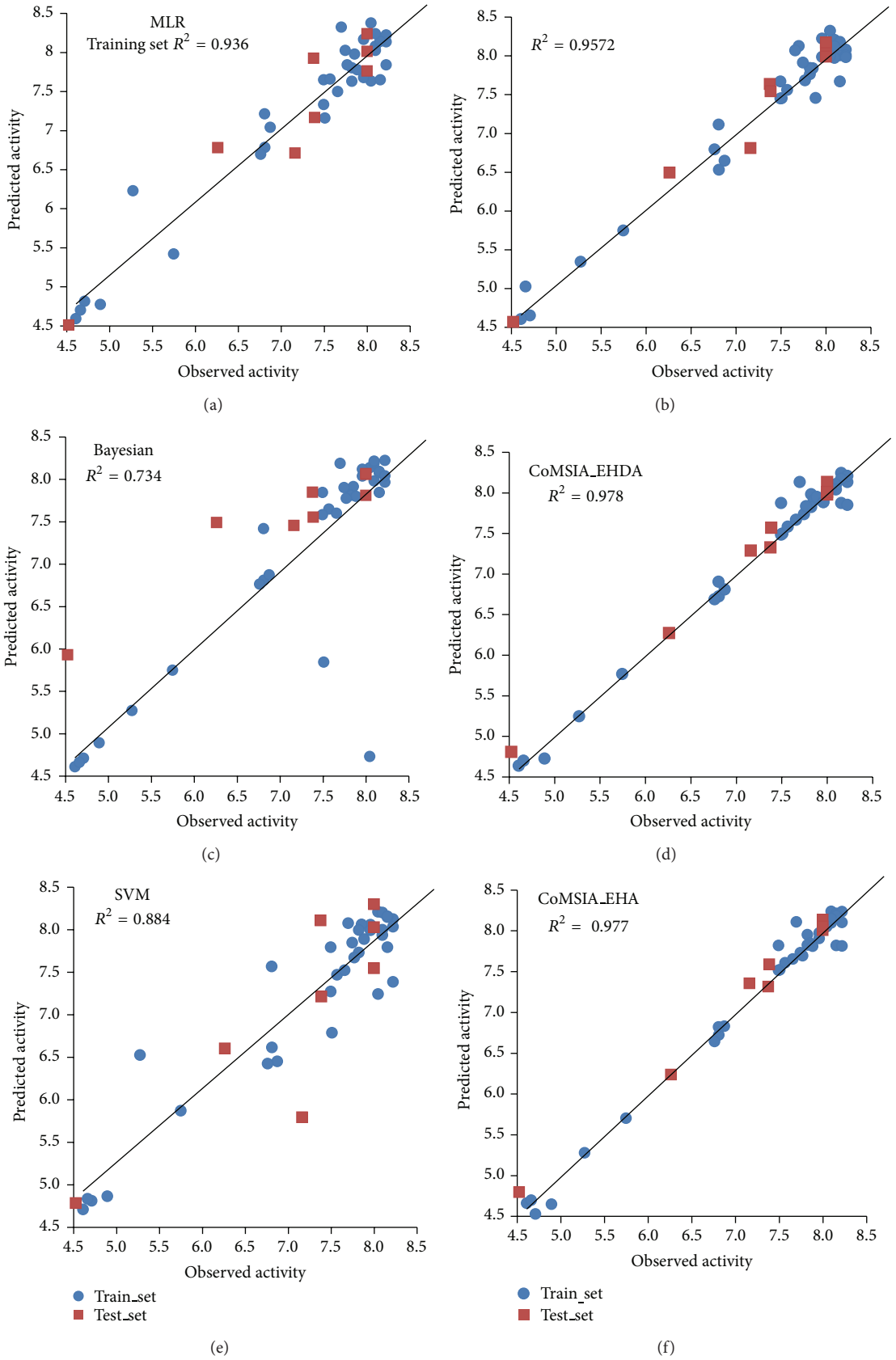

Figure 7: Correlation of observed and predicted activity (pIC50) using 2D-QSAR models and 3D-QSAR models. MLR, Bayesian network, and SVM were 2D-QSAR model. CoMFA, CoMSIA_EHDA, and CoMSIA_EHA were 3D-QSAR model.

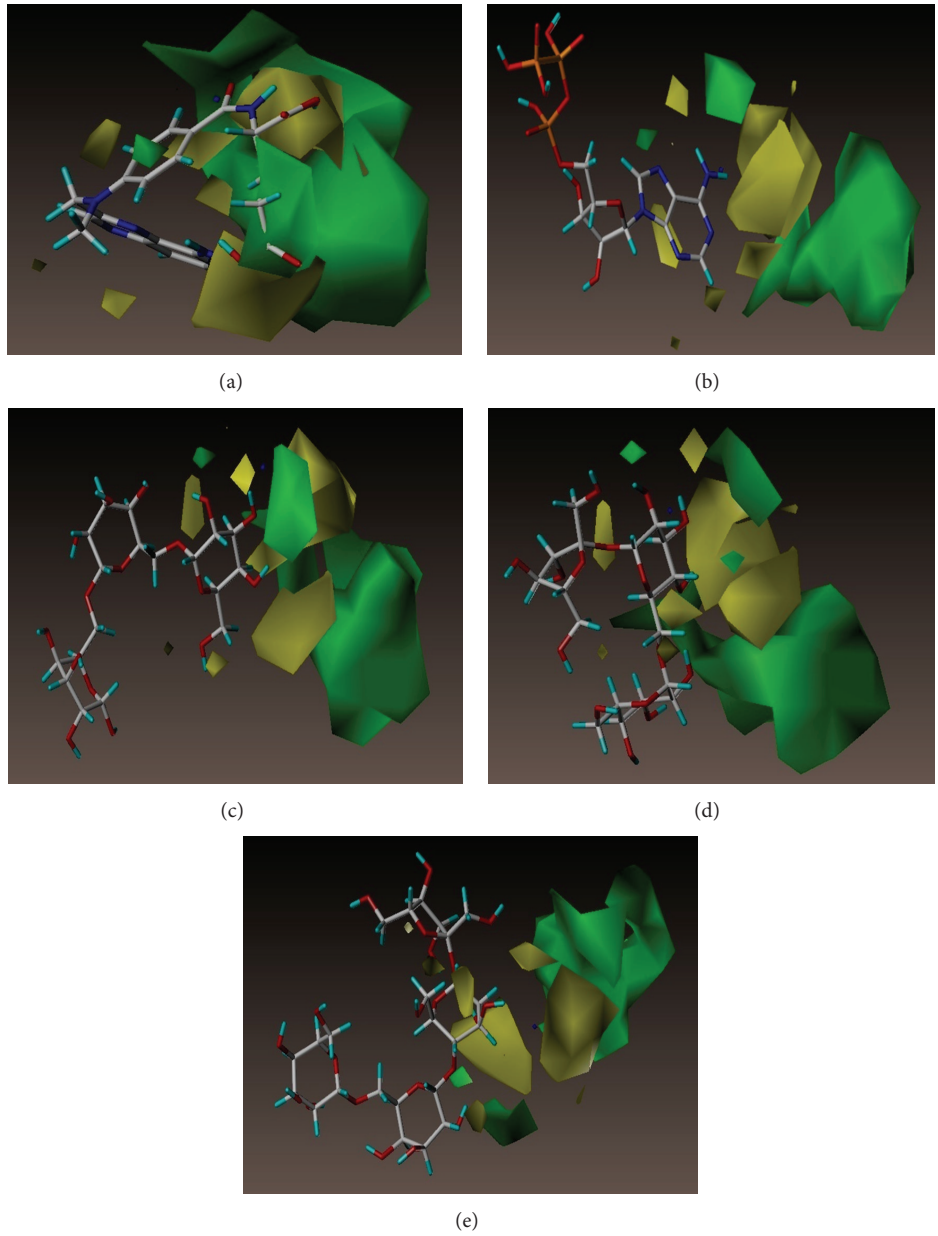

Figure 8: The CoMFA contour maps for DHFR. (a) MTX, (b) adenosine triphosphate, (c) manninotriose, (d) raffinose, and (e) stachyose. Green and yellow contours denote regions favoring and disfavoring steric fields, respectively. Blue and red contours denote regions favoring and disfavoring electrostatic fields, respectively.

Experimental and predicted pIC50 values of 45 DHFR inhibitors using CoMFA and CoMSIA models are shown in Table 5. Residuals calculated from the differences between observed and predicted pIC50 values ranged between −0.3655 and 0.4311 for the CoMFA, between −0.411 and 0.589 for the CoMSIA with "EHA model," and between −0.431 and 0.569 for CoMSIA with "EHDA model."

The correlations between the predicted and actual bioactivity for DHFR inhibitors are shown in Figure 7. The R^2 values are 0.936 for MLR, 0.734 for Bayesian network, 0.884 for SVM, 0.957 for CoMFA, 0.977 for CoMSIA with EHA model, and 0.978 for CoMSIA with EHDA model implicate high correlation. High correlation coefficients validated the reliability of the constructed CoMFA and CoMSIA models. The predicted bioactivity values of TCM candidates by 2D-QSAR and 3D-QSAR models are listed in Table 6.

3.3. The Contour Maps of CoMFA and CoMSIA Models. Ligand activities of MTX and the TCM candidates can be

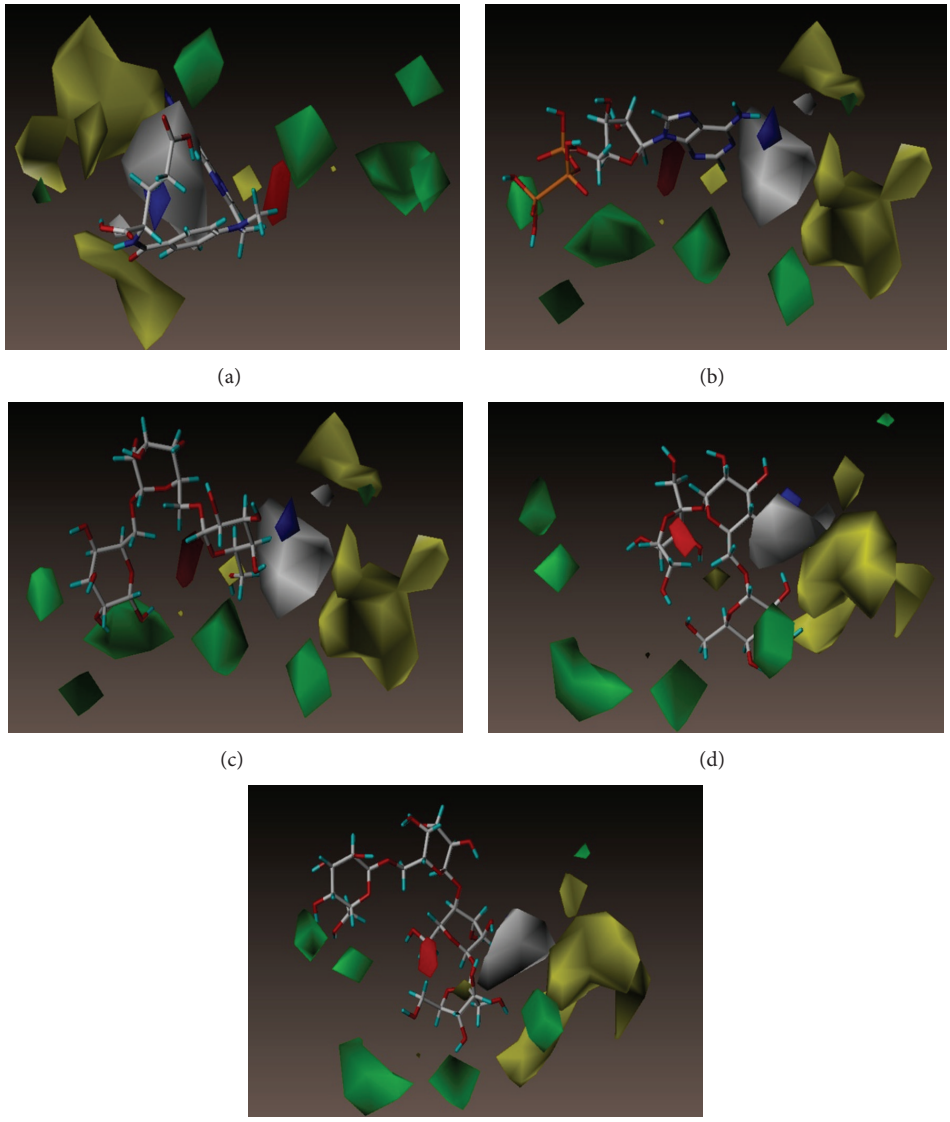

Figure 9: The CoMSIA contour maps of EHA model for DHFR. (a) MTX, (b) adenosine triphosphate, (c) manninotriose, (d) raffinose, and (e) stachyose. Blue and orange contours denote regions favoring and disfavoring electrostatic fields, respectively. Yellow and white contours denote regions favoring and disfavoring hydrophobic fields, respectively. Green and red contours denote regions favoring and disfavoring H-bond acceptor fields, respectively.

predicted based on the 3D-QSAR contour map, including features in steric field, hydrophobic field, and H-bond donor/acceptor characteristics. MTX and the TCM candidates contoured well to the steric features of the CoMFA in Figure 8. CoMSIA map provides more information with regard to bioactivity differences for "EHA model" and "EHDA model" in Figures 9 and 10, respectively. From the consistent results observed among the 3D-QSAR models validations, we inferred that adenosine triphosphate, manninotriose, raffinose, and stachyose of TCM candidates might have good biological activity for DHFR.

Contour to steric favoring and hydrophobic favoring regions was observed for adenosine triphosphate, manninotriose, raffinose, and stachyose. Consistent with the docking pose contour (Figures 8, 9, and 10), we propose that the four TCM candidates may maintain bioactivity for DHFR under dynamic conditions in physiological environments.

4. Conclusion

DHFR and TS proteins are key regulators in de novo synthesis of purines and thymidylate. Inhibiton of these proteins has the potential for treating acute lymphoblastic leukemia.

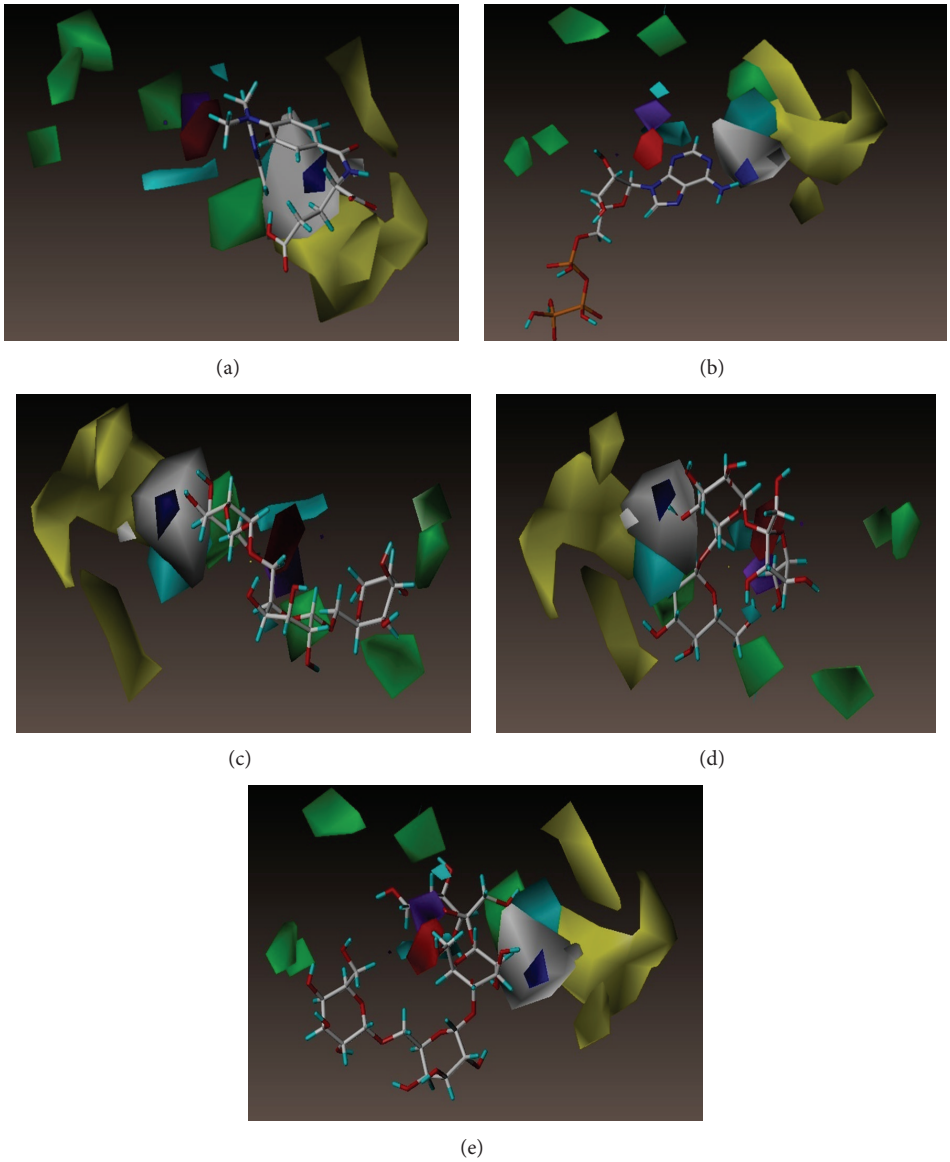

Figure 10: The CoMSIA contour maps of EHDA model for DHFR. (a) MTX, (b) adenosine triphosphate, (c) manninotriose, (d) raffinose, and (e) stachyose. Blue and orange contours denote regions favoring and disfavoring electrostatic fields, respectively. Yellow and white contours denote regions favoring and disfavoring hydrophobic fields, respectively. Green and red contours denote regions favoring and disfavoring H-bond acceptor fields, respectively. Cyan and purple contours denote regions favoring and disfavoring H-bond donor fields, respectively.

In this study, we applied virtual screen and QSAR models based on structure-based and ligand-based methods in order to identify the potential TCM compounds. The TCM compounds adenosine triphosphate, manninotriose, raffinose, and stachyose could bind on DHFR and TS specifically and had low hepatotoxicity. These TCM compounds had potential to improve the side effects of MTX for ALL treatment.

Conflict of Interests

The authors declare that they have no conflict of interests regarding the publication of this paper.

Acknowledgments

The research was supported by Grants from the National Science Council of Taiwan (NSC102-2632-E-468-001-MY3, NSC102-2325-B039-001, and NSC102-2221-E-468-027-), Asia University (101-ASIA-24, 101-ASIA-59, ASIA100-CMU-2, and ASIA101-CMU-2), and China Medical University Hospital (DMR-103-001, DMR-103-058, and DMR-103-096). This study is also supported in part by Taiwan Department of Health Clinical Trial and Research Center of Excellence (DOH102-TD-B-111-004) and Taiwan Department of Health Cancer Research Center of Excellence

(MOHW103-TD-B-111-03), and CMU under the Aim for Top University Plan of the Ministry of Education, Taiwan.

References

[1] L. H. Hartwell and M. B. Kastan, "Cell cycle control and cancer," *Science*, vol. 266, no. 5192, pp. 1821–1828, 1994.

[2] M. J. Chen, T. Shimada, and A. D. Moulton, "The functional human dihydrofolate reductase gene," *Journal of Biological Chemistry*, vol. 259, no. 6, pp. 3933–3943, 1984.

[3] Y. C. Hsieh, P. Tedeschi, R. A. Lawal et al., "Enhanced degradation of dihydrofolate reductase through inhibition of NAD kinase by nicotinamide analogs," *Molecular Pharmacology*, vol. 83, no. 2, pp. 339–353, 2013.

[4] M. Krajinovic and A. Moghrabi, "Pharmacogenetics of methotrexate," *Pharmacogenomics*, vol. 5, no. 7, pp. 819–834, 2004.

[5] G. Toffoli, A. Russo, F. Innocenti et al., "Effect of methylenetetrahydrofolate reductase 677C → T polymorphism on toxicity and homocysteine plasma level after chronic methotrexate treatment of ovarian cancer patients," *International Journal of Cancer*, vol. 103, no. 3, pp. 294–299, 2003.

[6] A. Patiño-García, M. Zalacaín, L. Marrodán, M. San-Julián, and L. Sierrasesúmaga, "Methotrexate in pediatric osteosarcoma: response and toxicity in relation to genetic polymorphisms and dihydrofolate reductase and reduced folate carrier 1 expression," *Journal of Pediatrics*, vol. 154, no. 5, pp. 688–693, 2009.

[7] P. Ranganathan, "An update on methotrexate pharmacogenetics in rheumatoid arthritis," *Pharmacogenomics*, vol. 9, no. 4, pp. 439–451, 2008.

[8] E. Campalani, M. Arenas, A. M. Marinaki, C. M. Lewis, J. N. W. N. Barker, and C. H. Smith, "Polymorphisms in folate, pyrimidine, and purine metabolism are associated with efficacy and toxicity of methotrexate in psoriasis," *Journal of Investigative Dermatology*, vol. 127, no. 8, pp. 1860–1867, 2007.

[9] K. R. Herrlinger, J. R. F. Cummings, M. C. N. M. Barnardo, M. Schwab, T. Ahmad, and D. P. Jewell, "The pharmacogenetics of methotrexate in inflammatory bowel disease," *Pharmacogenetics and Genomics*, vol. 15, no. 10, pp. 705–711, 2005.

[10] C. M. Ulrich, Y. Yasui, R. Storb et al., "Pharmacogenetics of methotrexate: toxicity among marrow transplantation patients varies with the methylenetetrahydrofolate reductase C677T polymorphism," *Blood*, vol. 98, no. 1, pp. 231–234, 2001.

[11] T. S. Mikkelsen, C. F. Thorn, J. J. Yang et al., "PharmGKB summary: methotrexate pathway," *Pharmacogenetics and Genomics*, vol. 21, no. 10, pp. 679–686, 2011.

[12] J. C. Barredo, T. W. Synold, J. Laver et al., "Differences in constitutive and post-methotrexate folylpolyglutamate synthetase activity in B-lineage and T-lineage leukemia," *Blood*, vol. 84, no. 2, pp. 564–569, 1994.

[13] L. Huang, W. J. E. Tissing, R. de Jonge, B. D. van Zelst, and R. Pieters, "Polymorphisms in folate-related genes: association with side effects of high-dose methotrexate in childhood acute lymphoblastic leukemia," *Leukemia*, vol. 22, no. 9, pp. 1798–1800, 2008.

[14] R. Gorlick, E. Goker, T. Trippett et al., "Intrinsic and acquired resistance to methotrexate in acute leukemia," *New England Journal of Medicine*, vol. 335, no. 14, pp. 1041–1048, 1996.

[15] B. A. Chabner, C. J. Allegra, and G. A. Curt, "Polyglutamation of methotrexate: is Methotrexate a prodrug?" *Journal of Clinical Investigation*, vol. 76, no. 3, pp. 907–912, 1985.

[16] K. Schmiegelow, "Advances in individual prediction of methotrexate toxicity: a review," *British Journal of Haematology*, vol. 146, no. 5, pp. 489–503, 2009.

[17] S. A. Jacobs, R. H. Adamson, and B. A. Chabner, "Stoichiometric inhibition of mammalian dihydrofolate reductase by the γ glutamyl metabolite of methotrexate, 4 amino 4 deoxy N10 methylpteroylglutamyl γ glutamate," *Biochemical and Biophysical Research Communications*, vol. 63, no. 3, pp. 692–698, 1975.

[18] A. K. Fotoohi and F. Albertioni, "Mechanisms of antifolate resistance and methotrexate efficacy in leukemia cells," *Leukemia and Lymphoma*, vol. 49, no. 3, pp. 410–426, 2008.

[19] J. C. White and I. D. Goldman, "Mechanism of action of methotrexate. IV. Free intracellular methotrexate required to suppress dihydrofolate reduction to tetrahydrofolate by Ehrlich ascites tumor cells in vitro," *Molecular Pharmacology*, vol. 12, no. 5, pp. 711–719, 1976.

[20] C. M. Baugh, C. L. Krumdieck, and M. G. Nair, "Polygammaglutamyl metabolites of methotrexate," *Biochemical and Biophysical Research Communications*, vol. 52, no. 1, pp. 27–34, 1973.

[21] I. C. Hung, S. S. Chang, P. C. Chang, C. C. Lee, and C. Y. C. Chen, "Memory enhancement by traditional Chinese medicine?" *Journal of Biomolecular Structure & Dynamics*, vol. 31, no. 12, pp. 1411–1439, 2013.

[22] S. Kishi, J. Griener, C. Cheng et al., "Homocysteine, pharmacogenetics, and neurotoxicity in children with leukemia," *Journal of Clinical Oncology*, vol. 21, no. 16, pp. 3084–3091, 2003.

[23] D. H. Mahoney Jr., J. J. Shuster, R. Nitschke et al., "Acute neurotoxicity in children with B-precursor acute lymphoid leukemia: an association with intermediate-dose intravenous methotrexate and intrathecal triple therapy—a pediatric oncology group study," *Journal of Clinical Oncology*, vol. 16, no. 5, pp. 1712–1722, 1998.

[24] G. Österlundh, I. Kjellmer, B. Lannering, L. Rosengren, U. A. Nilsson, and I. Márky, "Neurochemical markers of brain damage in cerebrospinal fluid during induction treatment of acute lymphoblastic leukemia in children," *Pediatric Blood and Cancer*, vol. 50, no. 4, pp. 793–798, 2008.

[25] A. Shuper, B. Stark, L. Kornreich, I. J. Cohen, G. Avrahami, and I. Yaniv, "Methotrexate-related neurotoxicity in the treatment of childhood acute lymphoblastic leukemia," *The Israel Medical Association Journal*, vol. 4, no. 11, pp. 1050–1053, 2002.

[26] I. Costea, A. Moghrabi, C. Laverdiere, A. Graziani, and M. Krajinovic, "Folate cycle gene variants and chemotherapy toxicity in pediatric patients with acute lymphoblastic leukemia," *Haematologica*, vol. 91, no. 8, pp. 1113–1116, 2006.

[27] R. C. Choudhury, S. K. Ghosh, and A. K. Palo, "Cytogenetic toxicity of methotrexate in mouse bone marrow," *Environmental Toxicology and Pharmacology*, vol. 8, no. 3, pp. 191–196, 2000.

[28] L. R. Belur, R. I. James, C. May et al., "Methotrexate preconditioning allows sufficient engraftment to confer drug resistance in mice transplanted with marrow expressing drug-resistant dihydrofolate reductase activity," *Journal of Pharmacology and Experimental Therapeutics*, vol. 314, no. 2, pp. 668–674, 2005.

[29] S. L. Whittle and R. A. Hughes, "Folate supplementation and methotrexate treatment in rheumatoid arthritis: a review," *Rheumatology*, vol. 43, no. 3, pp. 267–271, 2004.

[30] S. Saigal, R. K. Singh, and B. Poddar, "Acute methotrexate toxicity presenting as multiorgan failure and acute pneumonitis: a rare case report," *Indian Journal of Critical Care Medicine*, vol. 16, no. 4, pp. 225–227, 2012.

[31] B. C. Widemann and P. C. Adamson, "Understanding and managing methotrexate nephrotoxicity," *Oncologist*, vol. 11, no. 6, pp. 694–703, 2006.

[32] S. G. Yarlagadda and M. A. Perazella, "Drug-induced crystal nephropathy: an update," *Expert Opinion on Drug Safety*, vol. 7, no. 2, pp. 147–158, 2008.

[33] P. Halonen, J. Mattila, T. Ruuska, M. K. Salo, and A. Mäkipernaa, "Liver histology after current intensified therapy for childhood acute lymphoblastic leukemia: microvesicular fatty change and siderosis are the main findings," *Medical and Pediatric Oncology*, vol. 40, no. 3, pp. 148–154, 2003.

[34] T. Dervieux, D. Furst, D. O. Lein et al., "Polyglutamation of methotrexate with common polymorphisms in reduced folate carrier, aminoimidazole carboxamide ribonucleotide transformylase, and thymidylate synthase are associated with methotrexate effects in rheumatoid arthritis," *Arthritis and Rheumatism*, vol. 50, no. 9, pp. 2766–2774, 2004.

[35] M. L. Becker, R. Gaedigk, L. Van Haandel et al., "The effect of genotype on methotrexate polyglutamate variability in juvenile idiopathic arthritis and association with drug response," *Arthritis and Rheumatism*, vol. 63, no. 1, pp. 276–285, 2011.

[36] C.-H. Wang, W.-D. Lin, D.-T. Bau et al., "Appearance of acanthosis nigricans may precede obesity: an involvement of the insulin/IGF receptor signaling pathway," *BioMedicine*, vol. 3, no. 2, pp. 82–87, 2013.

[37] M.-C. Lin, S.-Y. Tsai, F.-Y. Wang et al., "Leptin induces cell invasion and the upregulation of matrilysin in human colon cancer cells," *BioMedicine*, vol. 3, no. 4, pp. 174–180, 2013.

[38] I. C. Chou, W.-D. Lin, C.-H. Wang et al., "Association analysis between Tourette's syndrome and two dopamine genes (DAT1, DBH) in Taiwanese children," *BioMedicine*, vol. 3, no. 2, pp. 88–91, 2013.

[39] T. Yamamoto, W.-C. Hung, T. Takano, and A. Nishiyama, "Genetic nature and virulence of community-associated methicillin-resistant Staphylococcus aureus," *BioMedicine*, vol. 3, no. 1, pp. 2–18, 2013.

[40] Y.-M. Chang, B. K. Velmurugan, W. W. Kuo et al., "Inhibitory effect of alpinate Oxyphyllae fructus extracts on Ang II-induced cardiac pathological remodeling-related pathways in H9c2 cardiomyoblast cells," *BioMedicine*, vol. 3, no. 4, pp. 148–152, 2013.

[41] S. P. Mahamuni, R. D. Khose, F. Menaa, and S. L. Badole, "Therapeutic approaches to drug targets in hyperlipidemia," *BioMedicine*, vol. 2, no. 4, pp. 137–146, 2012.

[42] Y.-T. Chang, W.-D. Lin, Z.-N. Chin et al., "Nonketotic hyperglycinemia: a case report and brief review," *BioMedicine*, vol. 2, no. 2, pp. 80–82, 2012.

[43] W.-Y. Lin, H.-P. Liu, J.-S. Chang et al., "Genetic variations within the PSORS1 region affect Kawasaki disease development and coronary artery aneurysm formation," *BioMedicine*, vol. 3, no. 2, pp. 73–81, 2013.

[44] I. C. Chou, W.-D. Lin, C.-H. Wang et al., "Möbius syndrome in a male with XX/XY mosaicism," *BioMedicine*, vol. 3, no. 2, pp. 102–104, 2013.

[45] D.-Y. Lin, F.-J. Tsai, C.-H. Tsai, and C.-Y. Huang, "Mechanisms governing the protective effect of 17β-estradiol and estrogen receptors against cardiomyocyte injury," *BioMedicine*, vol. 1, no. 1, pp. 21–28, 2011.

[46] C.-H. Wang, W.-D. Lin, and F.-J. Tsai, "Craniofacial dysmorphism, what is your diagnosis?" *BioMedicine*, vol. 2, no. 2, pp. 49–50, 2012.

[47] C. C. Lee, C.-H. Tsai, L. Wan et al., "Increased incidence of Parkinsonism among Chinese with β-glucosidase mutation in central Taiwan," *BioMedicine3*, no. 2, pp. 92–94, 2013.

[48] F.-J. Tsai, "Biomedicine brings the future nearer," *BioMedicine*, vol. 1, no. 1, p. 1, 2011.

[49] F.-J. Tsai, "Rare diseases: a mysterious puzzle," *BioMedicine*, vol. 3, no. 2, p. 65, 2013.

[50] Y. A. Tsou, K. C. Chen, S. S. Chang, Y. R. Wen, and C. Y. Chen, "A possible strategy against head and neck cancer: in silico investigation of three-in-one inhibitors," *Journal of Biomolecular Structure & Dynamics*, vol. 31, no. 12, pp. 1358–1369, 2013.

[51] Y. A. Tsou, K. C. Chen, H. C. Lin, S. S. Chang, and C. Y. C. Chen, "Uroporphyrinogen decarboxylase as a potential target for specific components of traditional Chinese Medicine: a virtual screening and molecular dynamics study," *PLoS ONE*, vol. 7, no. 11, 2012.

[52] S. C. Yang, S. S. Chang, H. Y. Chen, and C. Y. C. Chen, "Identification of Potent EGFR Inhibitors from TCM Database@Taiwan," *PLoS Computational Biology*, vol. 7, no. 10, 2011.

[53] C.-Y. Chen and C. Y.-C. Chen, "Insights into designing the dual-targeted HER2/HSP90 inhibitors," *Journal of Molecular Graphics and Modelling*, vol. 29, no. 1, pp. 21–31, 2010.

[54] H.-J. Huang, K.-J. Lee, H. W. Yu et al., "Structure-based and ligand-based drug design for HER 2 receptor," *Journal of Biomolecular Structure & Dynamics*, vol. 28, no. 1, pp. 23–37, 2010.

[55] W. Ieongtou, S. S. Chang, D. Wu et al., "Molecular level activation insights from a NR2A/NR2B agonist," *Journal of Biomolecular Structure & Dynamics*, 2013.

[56] K.-C. Chen and C. Yu-Chian Chen, "Stroke prevention by traditional Chinese medicine? A genetic algorithm, support vector machine and molecular dynamics approach," *Soft Matter*, vol. 7, no. 8, pp. 4001–4008, 2011.

[57] K.-C. Chen, K.-W. Chang, H.-Y. Chen, and C. Y.-C. Chen, "Traditional Chinese medicine, a solution for reducing dual stroke risk factors at once?" *Molecular BioSystems*, vol. 7, no. 9, pp. 2711–2719, 2011.

[58] T.-T. Chang, K.-C. Chen, K.-W. Chang et al., "In silico pharmacology suggests ginger extracts may reduce stroke risks," *Molecular BioSystems*, vol. 7, no. 9, pp. 2702–2710, 2011.

[59] H. J. Huang, Y. R. Jian, and C. Y. Chen, "Traditional Chinese medicine application in HIV: an in silico study," *Journal of Biomolecular Structure & Dynamics*, vol. 32, no. 1, pp. 1–12, 2014.

[60] C.-H. Lin, T.-T. Chang, M.-F. Sun et al., "Potent inhibitor design against H1N1 swine influenza: structure-based and molecular dynamics analysis for M2 inhibitors from traditional Chinese medicine database," *Journal of Biomolecular Structure & Dynamics*, vol. 28, no. 4, pp. 471–482, 2011.

[61] T.-T. Chang, M.-F. Sun, H.-Y. Chen et al., "Screening from the world's largest TCM database against H1N1 virus," *Journal of Biomolecular Structure & Dynamics*, vol. 28, no. 5, pp. 773–786, 2011.

[62] S.-S. Chang, H.-J. Huang, and C. Y.-C. Chen, "Two birds with one stone? Possible dual-targeting H1N1 inhibitors from traditional Chinese medicine," *PLoS Computational Biology*, vol. 7, no. 12, Article ID e1002315, 2011.

[63] C. Y. Chen, Y. H. Chang, D. T. Bau et al., "Ligand-based dual target drug design for H1N1: swine flu—a preliminary first study," *Journal of Biomolecular Structure & Dynamics*, vol. 27, no. 2, pp. 171–178, 2009.

[64] K. C. Chen, S. S. Chang, H. J. Huang et al., "Three-in-one agonists for PPAR-alpha, PPAR-gamma, and PPAR-delta from traditional Chinese medicine," *Journal of Biomolecular Structure & Dynamics*, vol. 30, no. 6, pp. 662–683, 2012.

[65] P.-C. Chang, J.-D. Wang, M.-M. Lee et al., "Lose weight with traditional Chinese medicine? Potential suppression of fat mass and obesity-associated protein," *Journal of Biomolecular Structure & Dynamics*, vol. 29, no. 3, pp. 471–483, 2011.

[66] H. J. Huang, K. J. Lee, H. W. Yu et al., "A novel strategy for designing the selective PPAR agonist by the "Sum of Activity" model," *Journal of Biomolecular Structure & Dynamics*, vol. 28, no. 2, pp. 187–200, 2010.

[67] K. C. Chen, S. S. Chang, F. J. Tsai, and C. Y. Chen, "Han ethnicity-specific type 2 diabetic treatment from traditional Chinese medicine?" *Journal of Biomolecular Structure & Dynamics*, vol. 31, no. 11, pp. 1219–1235, 2013.

[68] W. I. Tou, S. S. Chang, C. C. Lee, and C. Y. Chen, "Drug design for neuropathic pain regulation from traditional Chinese medicine," *Scientific Reports*, vol. 3, p. 844, 2013.

[69] K. C. Chen, Y. R. Jian, M. F. Sun et al., "Investigation of silent information regulator 1 (Sirt1) agonists from Traditional Chinese Medicine," *Journal of Biomolecular Structure & Dynamics*, vol. 31, no. 11, pp. 1207–1218, 2013.

[70] V. Cody, J. R. Luft, and W. Pangborn, "Understanding the role of Leu22 variants in methotrexate resistance: comparison of wild-type and Leu22Arg variant mouse and human dihydrofolate reductase ternary crystal complexes with methotrexate and NADPH," *Acta Crystallographica Section D: Biological Crystallography*, vol. 61, no. 2, pp. 147–155, 2005.

[71] J. Phan, S. Koli, W. Minor, R. B. Dunlap, S. H. Berger, and L. Lebioda, "Human thymidylate synthase is in the closed conformation when complexed with dUMP and raltitrexed, an antifolate drug," *Biochemistry*, vol. 40, no. 7, pp. 1897–1902, 2001.

[72] Shanghai Innovative Research Center of Traditional Chinese Medicine (SIRC/TCM), S.I.R.C.o.T.C.M., Add:No.1 Building, 439 Chunxiao Road,Zhangjiang Hi-tech Park,Shanghai, 2012.

[73] C. Y.-C. Chen, "TCM Database@Taiwan: the world's largest traditional Chinese medicine database for drug screening In Silico," *PLoS ONE*, vol. 6, no. 1, Article ID e15939, 2011.

[74] X. Ma, G. Xiang, C.-W. Yap, and W.-K. Chui, "3D-QSAR Study on dihydro-1,3,5-triazines and their spiro derivatives as DHFR inhibitors by comparative molecular field analysis (CoMFA)," *Bioorganic and Medicinal Chemistry Letters*, vol. 22, no. 9, pp. 3194–3197, 2012.

[75] B. K. Slinker and S. A. Glantz, "Multiple linear regression: accounting for multiple simultaneous determinants of a continuous dependent variable," *Circulation*, vol. 117, no. 13, pp. 1732–1737, 2008.

[76] V. Vapnik, "Pattern recognition using generalized portrait method," *Automation and Remote Control*, vol. 24, pp. 774–780, 1963.

[77] O. Ivanciuc, "Applications of support vector machines in chemistry," *Reviews in Computational Chemistry*, vol. 23, pp. 291–400, 2007.

[78] V. Vapnik, *The Nature of Statistical Learning Theory*, Springer, 1995.

[79] C.-C. Chang and C.-J. Lin, "LIBSVM: a Library for support vector machines," *ACM Transactions on Intelligent Systems and Technology*, vol. 2, no. 3, article 27, 2011.

[80] R. Burbidge, M. Trotter, B. Buxton, and S. Holden, "Drug design by machine learning: support vector machines for pharmaceutical data analysis," *Computers and Chemistry*, vol. 26, no. 1, pp. 5–14, 2001.

[81] J. Yu, V. A. Smith, P. P. Wang, A. J. Hartemink, and E. D. Jarvis, "Advances to Bayesian network inference for generating causal networks from observational biological data," *Bioinformatics*, vol. 20, no. 18, pp. 3594–3603, 2004.

[82] N. Friedman, M. Linial, I. Nachman, and D. Pe'er, "Using Bayesian networks to analyze expression data," *Journal of Computational Biology*, vol. 7, no. 3-4, pp. 601–620, 2000.

Hindawi Publishing Corporation
Evidence-Based Complementary and Alternative Medicine
Volume 2014, Article ID 436863, 10 pages
http://dx.doi.org/10.1155/2014/436863

Research Article

Potential Protein Phosphatase 2A Agents from Traditional Chinese Medicine against Cancer

Kuan-Chung Chen,[1] Hsin-Yi Chen,[2] and Calvin Yu-Chian Chen[2,3,4]

[1] *School of Pharmacy, China Medical University, Taichung 40402, Taiwan*
[2] *Department of Biomedical Informatics, Asia University, Taichung 41354, Taiwan*
[3] *School of Medicine, College of Medicine, China Medical University, Taichung 40402, Taiwan*
[4] *Computational and Systems Biology, Massachusetts Institute of Technology, Cambridge, MA 02139, USA*

Correspondence should be addressed to Calvin Yu-Chian Chen; ycc929@mit.edu

Received 18 January 2014; Accepted 30 January 2014; Published 29 April 2014

Academic Editor: Fuu-Jen Tsai

Protein phosphatase 2A (PP2A) is an important phosphatase which regulates various cellular processes, such as protein synthesis, cell growth, cellular signaling, apoptosis, metabolism, and stress responses. It is a holoenzyme composed of the structural A and catalytic C subunits and a regulatory B subunit. As an environmental toxin, okadaic acid, is a tumor promoter and binds to PP2A catalytic C subunit and the cancer-associated mutations in PP2A structural A subunit in human tumor tissue; PP2A may have tumor-suppressing function. It is a potential drug target in the treatment of cancer. In this study, we screen the TCM compounds in TCM Database@Taiwan to investigate the potent lead compounds as PP2A agent. The results of docking simulation are optimized under dynamic conditions by MD simulations after virtual screening to validate the stability of H-bonds between PP2A-α protein and each ligand. The top TCM candidates, trichosanatine and squamosamide, have potential binding affinities and interactions with key residues Arg89 and Arg214 in the docking simulation. In addition, these interactions were stable under dynamic conditions. Hence, we propose the TCM compounds, trichosanatine and squamosamide, as potential candidates as lead compounds for further study in drug development process with the PP2A-α protein.

1. Introduction

Protein phosphatase 2A (PP2A) is an important phosphatase which consists of a holoenzyme composed of the structural A and catalytic C subunits and a regulatory B subunit [1–3]. As each of these subunits exists many different isoforms, the holoenzymes of PP2A, can form various distinct trimeric ABC complexes. This enzyme can regulate various cellular processes, such as protein synthesis, cell growth, cellular signaling, apoptosis, metabolism, and stress responses [4, 5]. Many researches indicate the cancer-associated mutations in PP2A structural A subunit in human tumor tissue [6–8]. As a research in 1988 determined that an environmental toxin, okadaic acid, is a tumor promoter and binds to PP2A catalytic C subunit [9], PP2A may have tumor-suppressing function. As PP2A has tumor-suppressing function, it is a potential drug target in the treatment of cancer [10, 11].

Nowadays, the researchers have determined more and more distinct mechanisms of diseases [12–18]. According to these mechanisms, the researchers can identify the potential target protein for drug design against each disease [19–22]. The compounds extracted from traditional Chinese medicine (TCM) have been indicated in many *in silico* researches as potential lead compounds for the treatment of many different diseases, including tumours [23–26], diabetes [27], inflammation [28], influenza [29], metabolic syndrome [30], stroke [31–33], viral infection [34], and some other diseases [35, 36]. In this study, we aim to improve drug development of TCM compounds by investigating the potent lead compounds as PP2A agent from the TCM compounds in TCM Database@Taiwan [37]. As the disordered amino acids in the protein may cause the side effect and reduce the possibility of ligand binding to target protein [38, 39], we have predicted the disordered residues in sequence of PP2A-α

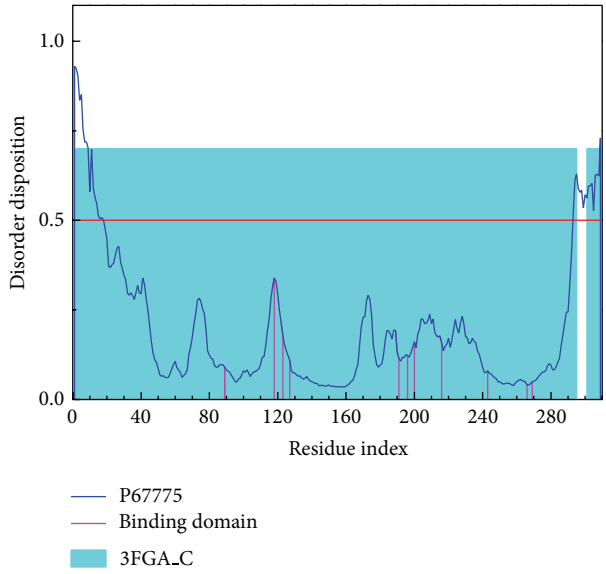

Figure 1: Disordered disposition predicted by PONDR-Fit.

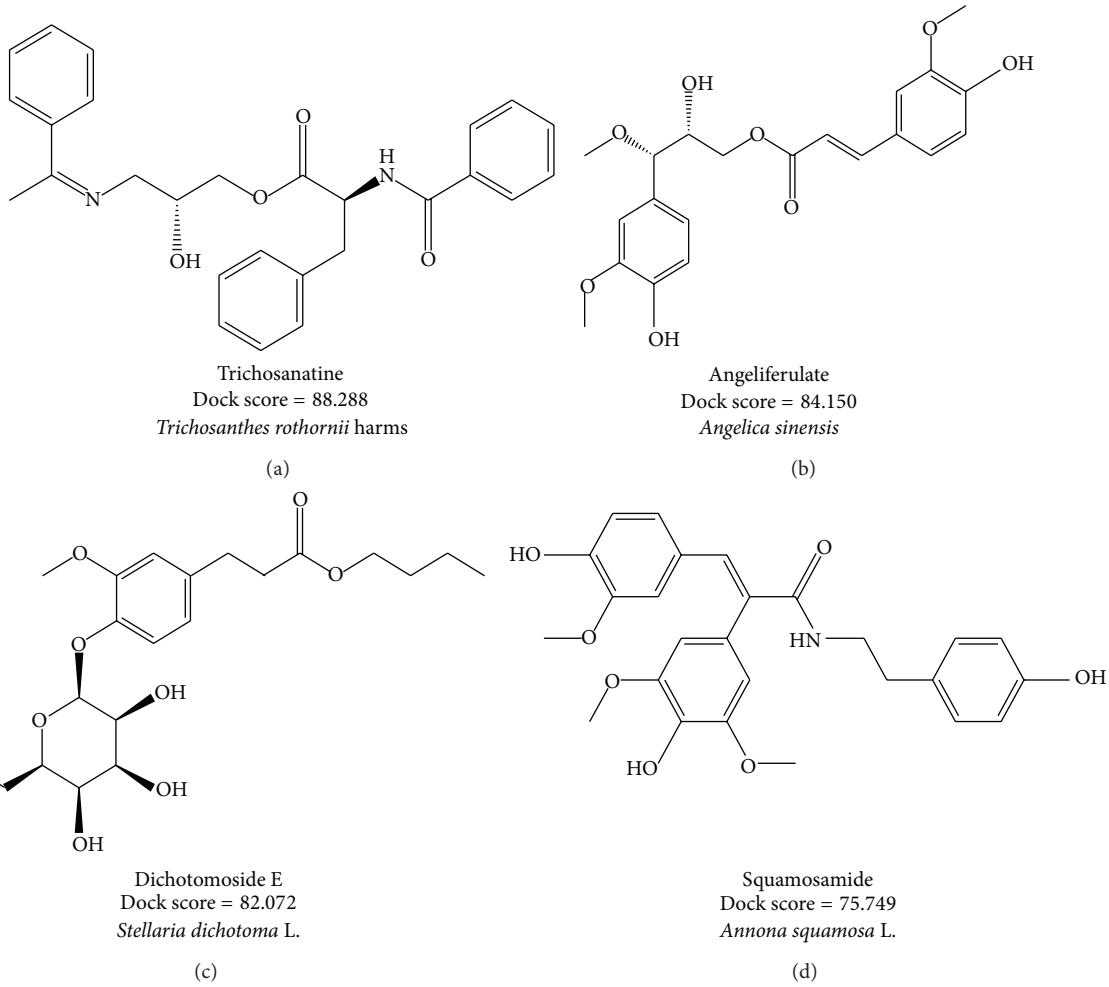

Figure 2: Chemical scaffold of top four TCM candidates with their scoring function and sources.

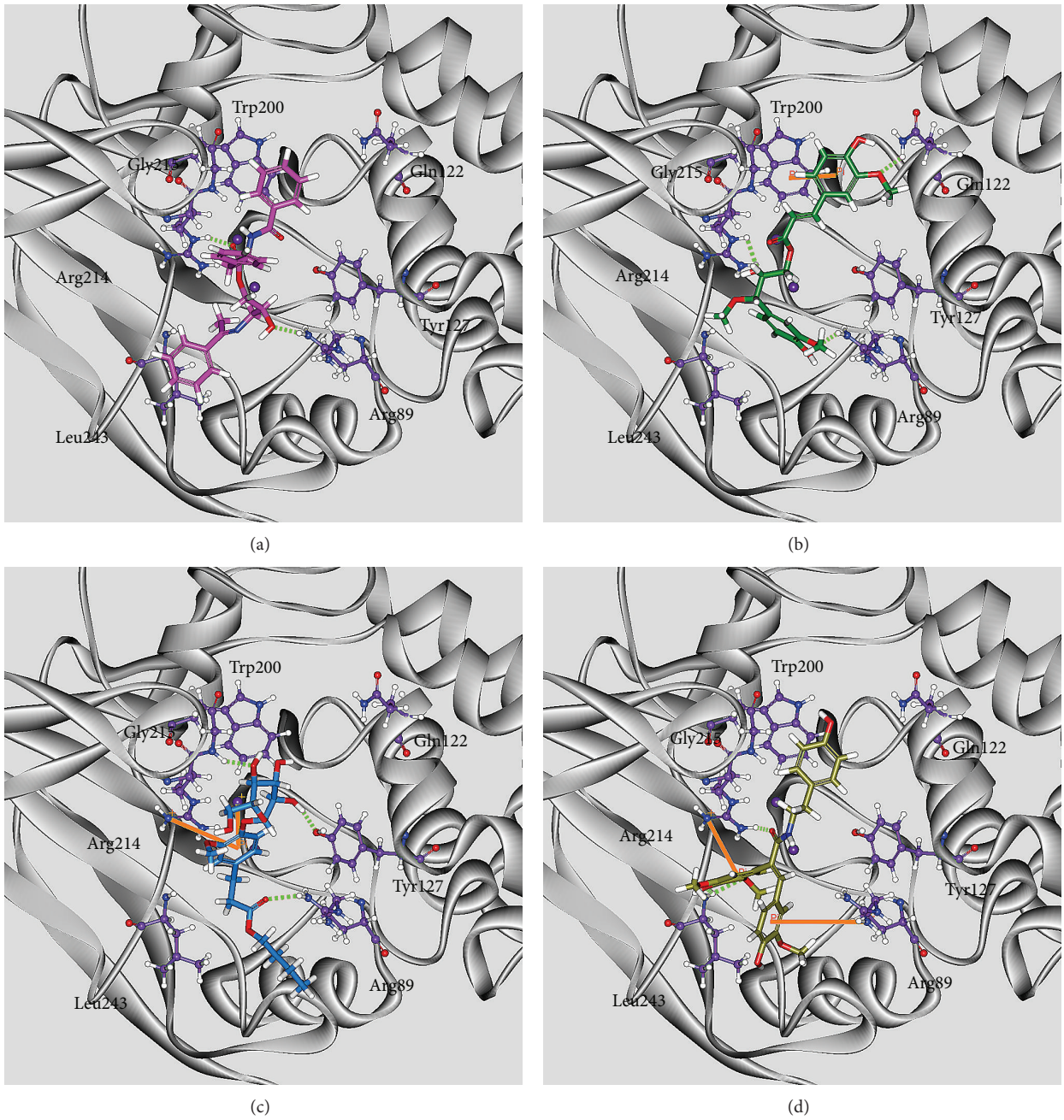

Figure 3: Docking pose of PP2A protein complexes with (a) trichosanatine, (b) angeliferulate, (c) dichotomoside E, and (d) squamosamide.

protein before virtual screening. After virtual screening of the TCM compounds, the results of docking simulation are optimized under dynamic conditions by MD simulations to validate the stability of H-bonds between PP2A-α protein and each ligand.

2. Materials and Methods

2.1. Data Collection. The X-ray crystallography structure of the human serine/threonine-protein phosphatase 2A (PP2A) catalytic subunit alpha isoform was obtained from RCSB Protein Data Bank with PDB ID: 3FGA [40]. We employed PONDR-Fit [41] protocol to predict the disordered residues in sequence of PP2A-α protein from Swiss-Prot (UniProtKB: P67775). For preparation, the protein was protonated with Chemistry at HARvard Macromolecular Mechanics (CHARMM) force field [42], and the crystal water was removed using Prepare Protein module in Discovery Studio 2.5 (DS2.5). The volume of the cocrystallized PP2A inhibitor, microcysteine, was employed to define the binding site for virtual screening. TCM compounds from TCM Database@Taiwan [37] were protonated using Prepare Ligand module in DS2.5 and filtered by Lipinski's Rule of Five [43] before virtual screening.

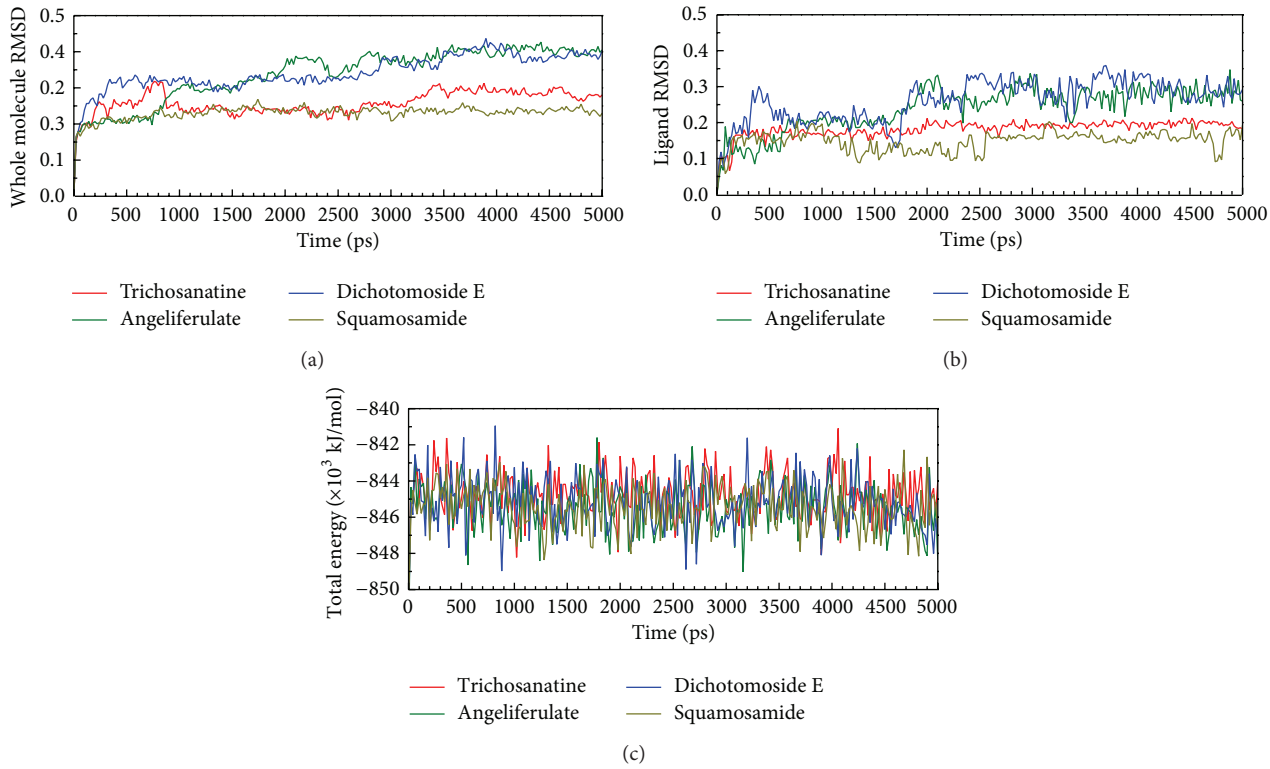

FIGURE 4: Root-mean-square deviations in units of nm and total energies over 5000 ps of MD simulation for PP2A protein complexes with trichosanatine, angeliferulate, dichotomoside E, and squamosamide.

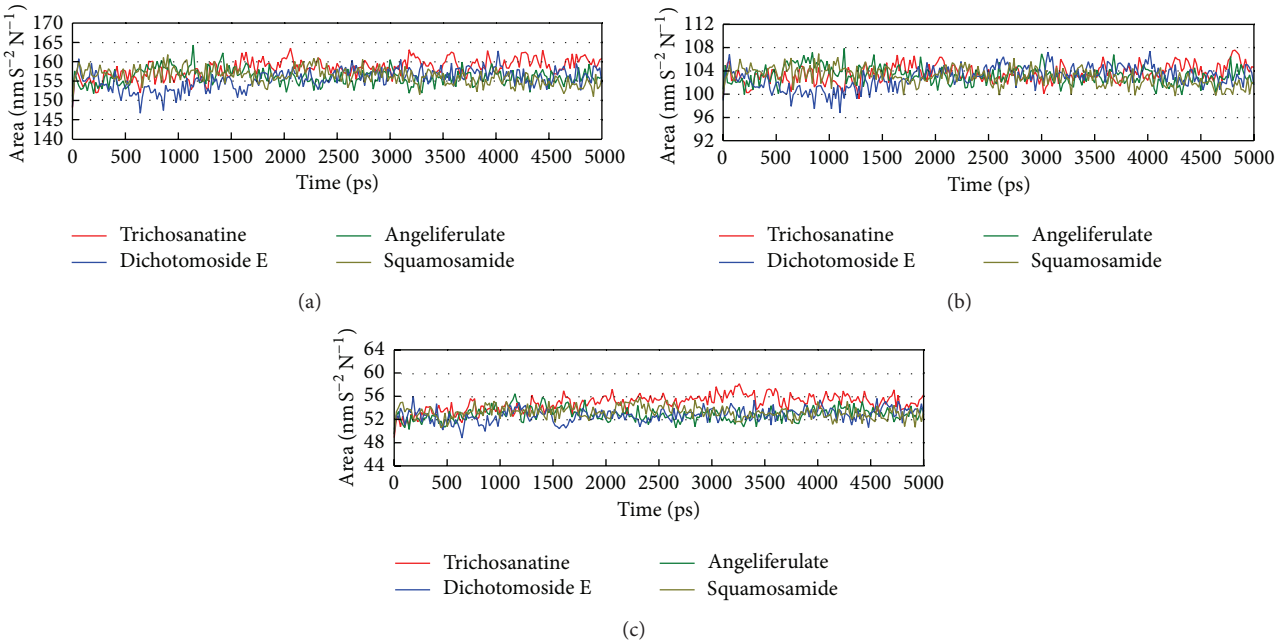

FIGURE 5: Variation of (a) total solvent accessible surface area, (b) hydrophobic surface area, and (c) hydrophilic surface area over 5000 ps of MD simulation for PP2A protein complexes with trichosanatine, angeliferulate, dichotomoside E, and squamosamide.

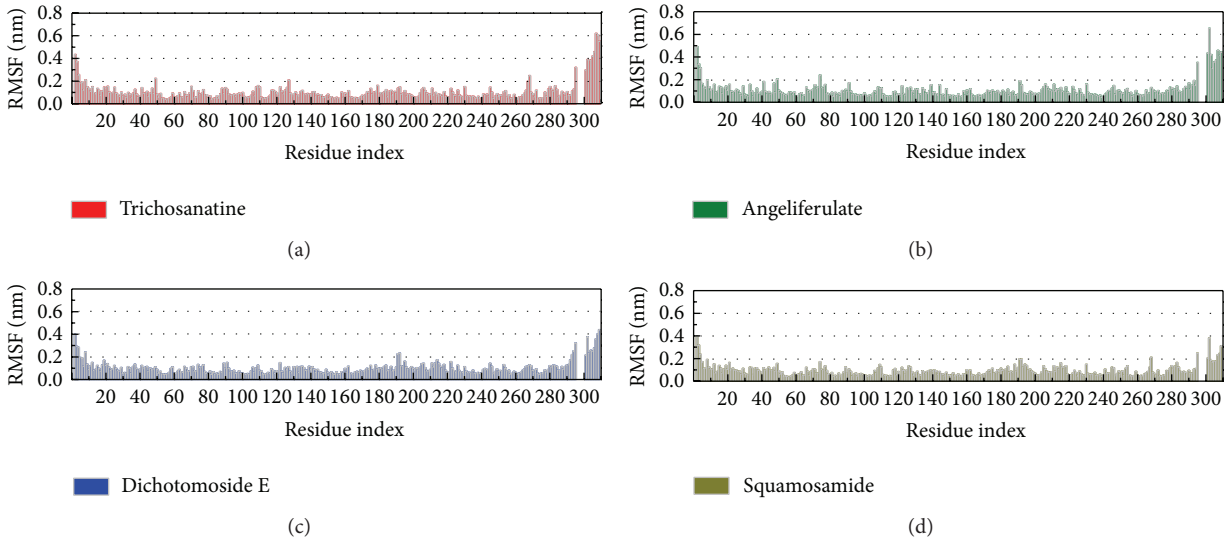

FIGURE 6: Root-mean-square fluctuation in units of nm for residues of PP2A protein complexes with trichosanatine, angeliferulate, dichotomoside E, and squamosamide during 5000 ps of MD simulation.

2.2. Docking Simulation. For virtual screening, the TCM compounds were docked into the binding site using a shape filter and Monte-Carlo ligand conformation generation using LigandFit protocol [44] in DS2.5. The docking poses were then optionally minimized with CHARMM force field [42] and then calculated their Dock Score energy function by the following equation:

$$\text{Dock Score} = -(\text{ligand/receptor interaction energy} + \text{ligand internal energy}). \quad (1)$$

Finally, the similar poses were rejected using the clustering algorithm.

2.3. Molecular Dynamics (MD) Simulation. The molecular dynamics (MD) simulation for each protein-ligand complex under dynamic conditions was performed by Gromacs 4.5.5 [45]. The topology and parameters for PP2A-α protein with charmm27 force field and ligands were performed by the pdb2gmx protocol of Gromacs and SwissParam program [46], respectively. Gromacs performed a cubic box with edge approx 12 Å from the molecules periphery and solvated with TIP3P water model for each protein-ligand complex. The common minimization algorithm, Steepest descents [47], was employed with a maximum of 5,000 steps to remove bad van der Waals contacts. After a neutral system using 0.145 M NaCl model was created by Gromacs; the steepest descents minimization with a maximum of 5,000 steps was employed again to remove bad van der Waals contacts. For the equilibration, the Linear Constraint algorithm for all bonds was employed for the position-restrained molecular dynamics with NVT equilibration, Berendsen weak thermal coupling method, and Particle Mesh Ewald method. A total of 5000 ps production simulation was then performed with time step in unit of 2 fs under Particle Mesh Ewald (PME) option and NPT ensembles. The 5000 ps of MD trajectories was then analyzed using a series of protocols in Gromacs.

3. Results and Discussion

3.1. Disordered Protein Prediction. The result of the disordered residues predicted by PONDR-Fit with the sequence of PP2A-α protein from Swiss-Prot (UniProtKB: P67775) is illustrated in Figure 1. For PP2A-α protein, Figure 1 indicates that the structure of binding domain is stable as the major residues of binding domain do not lie in the disordered region.

3.2. Docking Simulation. For virtual screening, Dock Score energy function is used to rank the top potential TCM compounds; the chemical scaffold of top four TCM candidates with high binding affinity is displayed in Figure 2 with its scoring function and sources. The top four TCM compounds, trichosanatine, angeliferulate, dichotomoside E, and squamosamide, were extracted from *Trichosanthes rosthornii* Harms, *Angelica sinensis*, *Stellaria dichotoma* L., and *Annona squamosa* L., respectively. After the virtual screening, the docking poses of top four TCM compounds in the binding domain of PP2A-α are displayed in Figure 3. All the top four TCM compounds have interactions with key residues Arg89 and Arg214. Trichosanatine exists hydrogen bonds (H-bonds) with key residues Arg89 and Arg214. Angeliferulate has H-bonds with residues Arg89, Gln122, Arg214, and a π interaction with residue Trp200. Dichotomoside E forms H-bonds with residues Arg89, Tyr127, Gly215, and a π interaction with residue Arg214. Squamosamide has both H-bond and π interaction with residue Arg214. In addition, there exist H-bonds with residue Leu243 and a π interaction with residue Arg89. Those interactions hold the top four TCM compounds in the binding domain of PP2A-α protein.

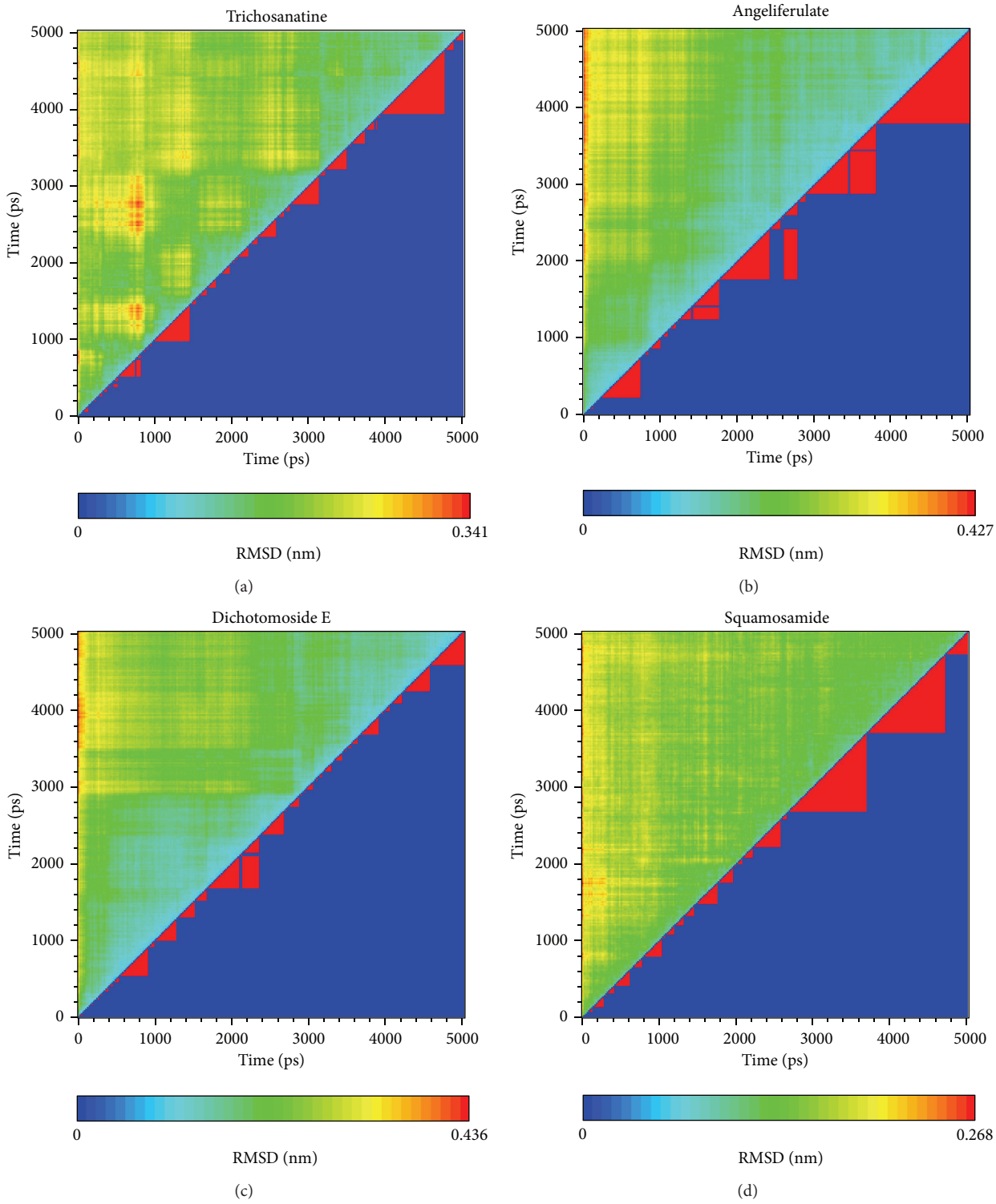

Figure 7: Root-mean-square deviation value (a) and graphical depiction of the clusters with cutoff 0.1 nm (d) for PP2A protein complexes with trichosanatine, angeliferulate, dichotomoside E, and squamosamide.

3.3. Molecular Dynamics Simulation. In LigandFit protocol, each compound was docked into binding site using a shape-based docking with rigid body of PP2A-α protein. The interactions between each compound and PP2A-α protein mention above may not be stable under dynamic conditions. We employed MD simulation for each protein-ligand complex to study the stability of interactions for each docking pose. The information of root-mean-square deviations (RMSDs) and total energies over 5000 ps of MD simulation is displayed in Figure 4. It indicates that the atomic fluctuations of protein

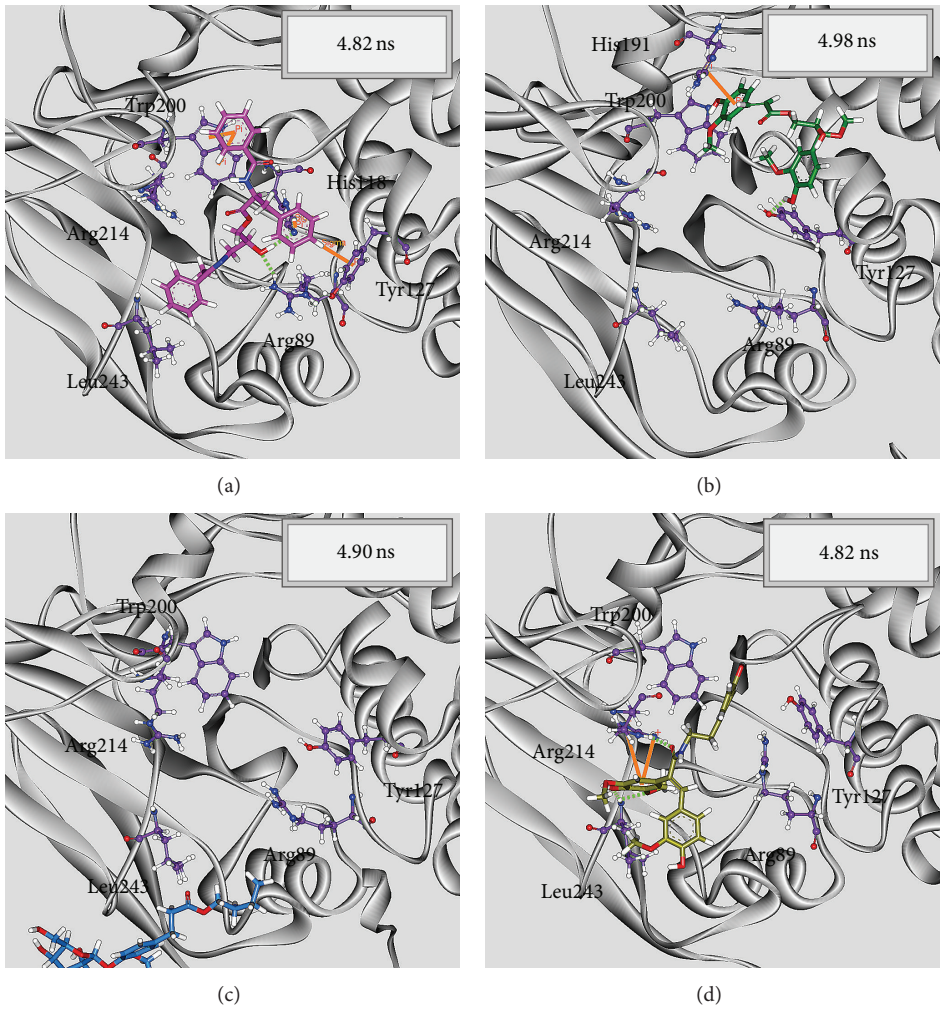

Figure 8: Docking poses of middle RMSD structure in the major cluster for PP2A protein complexes with trichosanatine, angeliferulate, dichotomoside E, and squamosamide.

complexes with top four TCM compounds tend to be stable after 4800 ps of MD simulation, and there is no significant variation in the total energies for each complex during MD simulation. To analyze the possible effect of each top TCM candidate for the PP2A-α protein, Figure 5 displays the variation of solvent accessible surface area for PP2A-α protein over 5000 ps of MD simulation. For top four TCM candidates, they have similar hydrophobic and hydrophilic surface areas when the MD simulation tends to be stable, which indicates that those compounds may not affect the sharpness of PP2A-α protein after they dock in the binding domain. Figure 6 illustrates the root-mean-square fluctuation of each residue of PP2A-α protein during 5000 ps of MD simulation. It indicates that they have similar deviation for key residues in the binding domain of PP2A-α protein during 5000 ps of MD simulation. In Figure 7, root-mean-square deviation value for each PP2A-α protein complex illustrates the RMSD values between each MD trajectory of 5000 ps of MD simulation, and graphical depiction of the clusters with cutoff 0.1 nm is employed to define the middle RMSD structure in the major cluster as the representative structures for each complex after MD simulation. The docking poses of the representative structures for each protein-ligand complex are illustrated in Figure 8. For angeliferulate and dichotomoside E, the interactions between protein and ligand mention in docking simulation are not stable under dynamic conditions, which indicates that those two TCM compounds cannot binding stabilized in the binding domain of PP2A-α protein. For trichosanatine, the representative docking poses in 4.82 ns indicate that it has similar docking pose as mentioned in docking simulation and maintains the H-bond with key residue Arg89. In addition, it forms H-bonds and π interactions with residues His118, Tyr127, and Trp200 after MD simulation. The docking pose of squamosamide in 4.82 ns of MD simulation also has similar docking pose as mentioned in docking simulation and maintains the H-bond and π interactions with key residue Arg214 and H-bond with Leu243. To analyze the stability of these H-bonds, the occupancy of H-bonds overall 5000 ps of molecular dynamics simulation are listed in Table 1, and the variations of distance

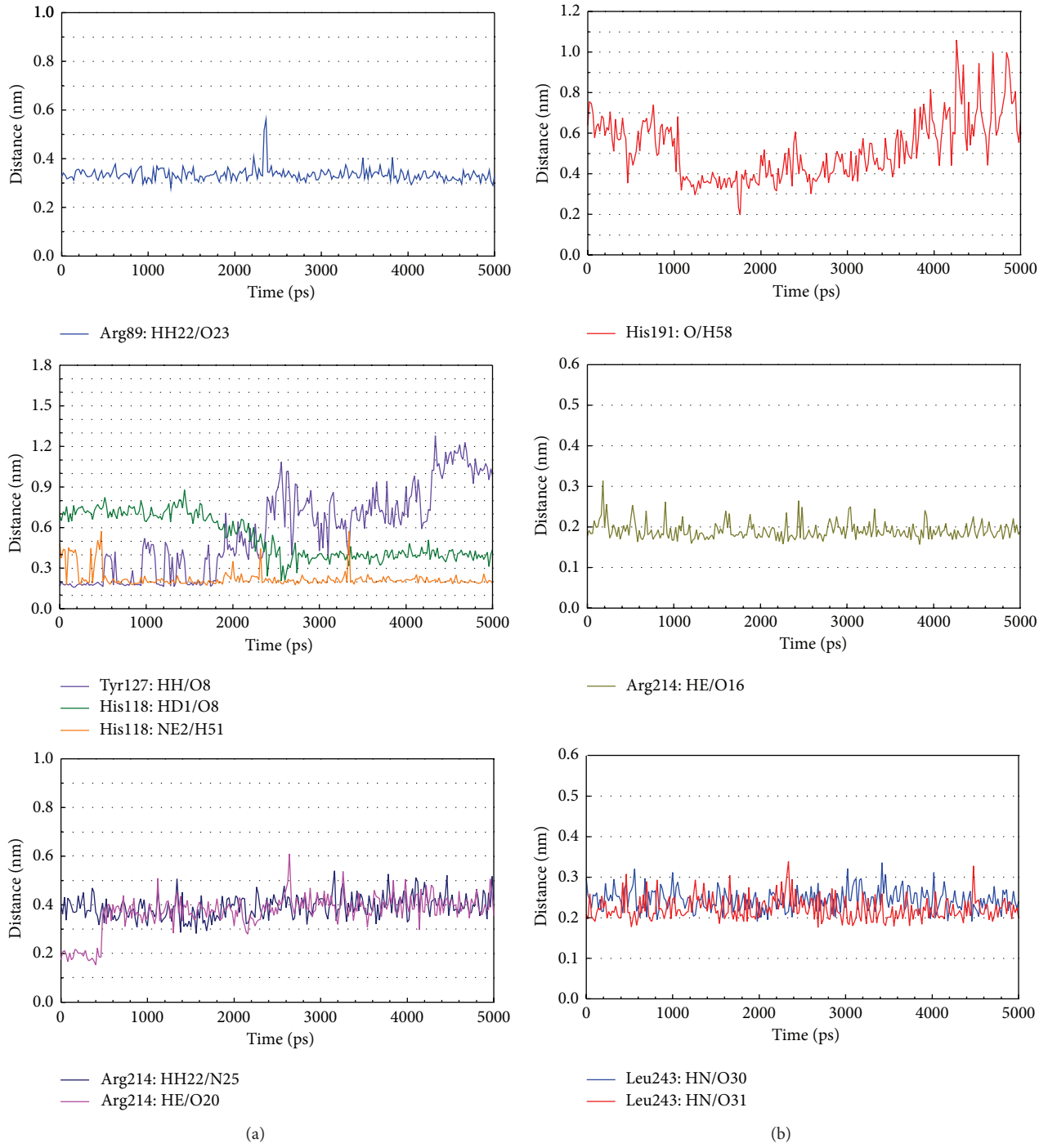

Figure 9: Distances of hydrogen bonds with common residues during 5000 ps of MD simulation for PP2A protein complexes with trichosanatine and squamosamide.

for each H-bond in the PP2A-α protein complexes with trichosanatine and squamosamide are illustrated in Figure 9. For trichosanatine, it has stable H-bonds with residues Arg89 and His118, and the distances with residues Arg214 are stable in 0.4 nm. For squamosamide, it has stable H-bonds with residues Arg214 and Leu243.

4. Conclusion

This study aims to investigate the potent TCM candidates as lead compounds of agent for PP2A-α protein. The top four TCM compounds have high binding affinities with PP2A-α protein in the docking simulation. However, the results of docking simulation are optimized under dynamic

Table 1: H-bond occupancy for key residues of PP2A protein with trichosanatine and squamosamide overall 5000 ps of molecular dynamics simulation.

Name	H-bond interaction		Occupancy
Trichosanatine	Arg89 : HH22	/O23	2%
	His118 : HD1	/O8	2%
	His118 : NE2	/H51	92%
	Tyr127 : HH	/O8	26%
	Arg214 : HE	/O20	11%
	Arg214 : HH22	/N25	1%
Squamosamide	His191 : O	/H58	1%
	Arg214 : HE	/O16	100%
	Leu243 : HN	/O30	98%
	Leu243 : HN	/O31	98%

H-bond occupancy cutoff: 0.3 nm.

conditions by MD simulations to validate the stability of H-bonds between PP2A-α protein and each ligand. Although angeliferulate and dichotomoside E have potent binding affinities with PP2A-α protein in the docking simulation, the interactions between protein and ligand mentioned in docking simulation are not stable under dynamic conditions. For the other two top TCM candidates, trichosanatine and squamosamide, there exist stable interactions with key residues Arg89 and Arg214 under dynamic conditions. Hence, we propose the TCM compounds, trichosanatine and squamosamide, as potential candidates as lead compounds for further study in drug development process with the PP2A-α protein.

Conflict of Interests

The authors declared that there is no conflict of interests.

Authors' Contribution

Kuan-Chung Chen and Hsin-Yi Chen had equal contribution.

Acknowledgments

The research was supported by Grants from the National Science Council of Taiwan (NSC102-2325-B039-001 and NSC102-2221-E-468-027-), Asia University (Asia101-CMU-2 and 102-Asia-07), and China Medical University Hospital (DMR-103-058, DMR-103-001, and DMR-103-096). This study is also supported in part by Taiwan Department of Health Clinical Trial and Research Center of Excellence (DOH102-TD-B-111-004) and Taiwan Department of Health Cancer Research Center of Excellence (MOHW103-TD-B-111-03).

References

[1] I. M. Porter, K. Schleicher, M. Porter, and J. R. Swedlow, "Bod1 regulates protein phosphatase 2A at mitotic kinetochores," *Nature Communications*, vol. 4, article 2677, 2013.

[2] S. Wera and B. A. Hemmings, "Serine/threonine protein phosphatases," *The Biochemical Journal*, vol. 311, part 1, pp. 17–29, 1995.

[3] M. C. Mumby and G. Walter, "Protein serine/threonine phosphatases: structure, regulation, and functions in cell growth," *Physiological Reviews*, vol. 73, no. 4, pp. 673–699, 1993.

[4] V. Janssens and J. Goris, "Protein phosphatase 2A: a highly regulated family of serine/threonine phosphatases implicated in cell growth and signalling," *The Biochemical Journal*, vol. 353, part 3, pp. 417–439, 2001.

[5] D. M. Virshup, "Protein phosphatase 2A: a panoply of enzymes," *Current Opinion in Cell Biology*, vol. 12, no. 2, pp. 180–185, 2000.

[6] R. Ruediger, M. Hentz, J. Fait, M. Mumby, and G. Walter, "Molecular model of the A subunit of protein phosphatase 2A: interaction with other subunits and tumor antigens," *Journal of Virology*, vol. 68, no. 1, pp. 123–129, 1994.

[7] G. A. Calin, M. G. di Iasio, E. Caprini et al., "Low frequency of alterations of the α (PPP2R1A) and β (PPP2R1B) isoforms of the subunit A of the serine-threonine phosphatase 2A in human neoplasms," *Oncogene*, vol. 19, no. 9, pp. 1191–1195, 2000.

[8] R. Ruediger, H. T. Pham, and G. Walter, "Disruption of protein phosphatase 2A subunit interaction in human cancers with mutations in the Aα subunit gene," *Oncogene*, vol. 20, no. 1, pp. 10–15, 2001.

[9] C. Bialojan and A. Takai, "Inhibitory effect of a marine-sponge toxin, okadaic acid, on protein phosphatases. Specificity and kinetics," *Biochemical Journal*, vol. 256, no. 1, pp. 283–290, 1988.

[10] W. Chen, Z. Wang, C. Jiang, and Y. Ding, "PP2A-mediated anticancer therapy," *Gastroenterology Research and Practice*, vol. 2013, Article ID 675429, 10 pages, 2013.

[11] A. H. Schönthal, "Role of serine/threonine protein phosphatase 2A in cancer," *Cancer Letters*, vol. 170, no. 1, pp. 1–13, 2001.

[12] Y. Jiang, X. Li, W. Yang et al., "PKM2 regulates chromosome segregation and mitosis progression of tumor cells," *Molecular Cell*, vol. 53, no. 1, pp. 75–87, 2014.

[13] I.-C. Chou, W.-D. Lin, C.-H. Wang et al., "Association analysis between Tourette's syndrome and two dopamine genes (DAT1, DBH) in Taiwanese children," *BioMedicine*, vol. 3, no. 2, pp. 88–91, 2013.

[14] T. Yamamoto, W.-C. Hung, T. Takano, and A. Nishiyama, "Genetic nature and virulence of community-associated methicillin-resistant *Staphylococcus aureus*," *BioMedicine*, vol. 3, no. 1, pp. 2–18, 2013.

[15] C.-H. Wang, W.-D. Lin, D.-T. Bau, I.-C. Choua, C.-H. Tsai, and F.-J. Tsai, "Appearance of acanthosis nigricans may precede obesity: an involvement of the insulin/IGF receptor signaling pathway," *BioMedicine*, vol. 3, no. 2, pp. 82–87, 2013.

[16] Y.-M. Chang, B. K. Velmurugan, W.-W. Kuo et al., "Inhibitory effect of alpinate Oxyphyllae fructus extracts on Ang II-induced cardiac pathological remodeling-related pathways in H9c2 cardiomyoblast cells," *BioMedicine*, vol. 3, no. 4, pp. 148–152, 2013.

[17] Y. M. Leung, K. L. Wong, S. W. Chen et al., "Down-regulation of voltage-gated Ca^{2+} channels in Ca^{2+} store-depleted rat insulinoma RINm5F cells," *BioMedicine*, vol. 3, no. 3, pp. 130–139, 2013.

[18] S. P. Mahamuni, R. D. Khose, F. Menaa, and S. L. Badole, "Therapeutic approaches to drug targets in hyperlipidemia," *BioMedicine*, vol. 2, no. 4, pp. 137–146, 2012.

[19] C.-L. Jao, S.-L. Huang, and K.-C. Hsu, "Angiotensin I-converting enzyme inhibitory peptides: inhibition mode, bioavailability, and antihypertensive effects," *BioMedicine*, vol. 2, no. 4, pp. 130–136, 2012.

[20] M.-C. Lin, S.-Y. Tsai, F.-Y. Wang, F.-H. Liu, J.-N. Syu, and F.-Y. Tang, "Leptin induces cell invasion and the upregulation of matrilysin in human colon cancer cells," *BioMedicine*, vol. 3, no. 4, pp. 174–180, 2013.

[21] K.-P. Su, "Inflammation in psychopathology of depression: clinical, biological, and therapeutic implications," *BioMedicine*, vol. 2, no. 2, pp. 68–74, 2012.

[22] M. A. Leissring, E. Malito, S. Hedouin et al., "Designed inhibitors of insulin-degrading enzyme regulate the catabolism and activity of insulin," *PLoS ONE*, vol. 5, no. 5, p. e10504, 2010.

[23] C.-Y. Chen and C. Y.-C. Chen, "Insights into designing the dual-targeted HER2/HSP90 inhibitors," *Journal of Molecular Graphics & Modelling*, vol. 29, no. 1, pp. 21–31, 2010.

[24] S.-C. Yang, S.-S. Chang, H.-Y. Chen, and C. Y.-C. Chen, "Identification of potent EGFR inhibitors from TCM database@Taiwan," *PLoS Computational Biology*, vol. 7, no. 10, Article ID e1002189, 2011.

[25] Y. A. Tsou, K. C. Chen, H. C. Lin, S. S. Chang, and C. Y. C. Chen, "Uroporphyrinogen decarboxylase as a potential target for specific components of traditional Chinese medicine: a virtual screening and molecular dynamics study," *PLoS ONE*, vol. 7, no. 11, Article ID e50087, 2012.

[26] Y. A. Tsou, K. C. Chen, S. S. Chang, Y. R. Wen, and C. Y. Chen, "A possible strategy against head and neck cancer: *in silico* investigation of three-in-one inhibitors," *Journal of Biomolecular Structure & Dynamics*, vol. 31, no. 12, pp. 1358–1369, 2013.

[27] K. C. Chen, S. S. Chang, F. J. Tsai, and C. Y. Chen, "Han ethnicity-specific type 2 diabetic treatment from traditional Chinese medicine?" *Journal of Biomolecular Structure & Dynamics*, vol. 31, no. 11, pp. 1219–1235, 2013.

[28] K.-C. Chen, M.-F. Sun, S.-C. Yang et al., "Investigation into potent inflammation inhibitors from traditional Chinese medicine," *Chemical Biology & Drug Design*, vol. 78, no. 4, pp. 679–688, 2011.

[29] S.-S. Chang, H.-J. Huang, and C. Y.-C. Chen, "Two birds with one stone? Possible dual-targeting H1N1 inhibitors from traditional Chinese medicine," *PLoS Computational Biology*, vol. 7, no. 12, Article ID e1002315, 2011.

[30] K. C. Chen, S. S. Chang, H. J. Huang, T. L. Lin, Y. J. Wu, and C. Y. Chen, "Three-in-one agonists for PPAR-alpha, PPAR-gamma, and PPAR-delta from traditional Chinese medicine," *Journal of Biomolecular Structure & Dynamics*, vol. 30, no. 6, pp. 662–683, 2012.

[31] K.-C. Chen and C. Yu-Chian Chen, "Stroke prevention by traditional Chinese medicine? A genetic algorithm, support vector machine and molecular dynamics approach," *Soft Matter*, vol. 7, no. 8, pp. 4001–4008, 2011.

[32] K.-C. Chen, K.-W. Chang, H.-Y. Chen, and C. Y.-C. Chen, "Traditional Chinese medicine, a solution for reducing dual stroke risk factors at once?" *Molecular BioSystems*, vol. 7, no. 9, pp. 2711–2719, 2011.

[33] T.-T. Chang, K.-C. Chen, K.-W. Chang et al., "*In silico* pharmacology suggests ginger extracts may reduce stroke risks," *Molecular BioSystems*, vol. 7, no. 9, pp. 2702–2710, 2011.

[34] H. J. Huang, Y. R. Jian, and C. Y. Chen, "Traditional Chinese medicine application in HIV: an *in silico* study," *Journal of Biomolecular Structure & Dynamics*, vol. 32, no. 1, pp. 1–12, 2014.

[35] W. I. Tou, S. S. Chang, C. C. Lee, and C. Y. Chen, "Drug design for neuropathic pain regulation from traditional Chinese medicine," *Scientific Reports*, vol. 3, article 844, 2013.

[36] K. C. Chen, Y. R. Jian, M. F. Sun, T. T. Chang, C. C. Lee, and C. Y. Chen, "Investigation of silent information regulator 1 (Sirt1) agonists from Traditional Chinese Medicine," *Journal of Biomolecular Structure & Dynamics*, vol. 31, no. 11, pp. 1207–1218, 2013.

[37] C. Y.-C. Chen, "TCM Database@Taiwan: the world's largest traditional Chinese medicine database for drug screening *in silico*," *PLoS ONE*, vol. 6, no. 1, Article ID e15939, 2011.

[38] W. I. Tou and C. Y. Chen, "May disordered protein cause serious drug side effect?" *Drug Discovery Today*, 2013.

[39] C. Y. Chen and W. I. Tou, "How to design a drug for the disordered proteins?" *Drug Discovery Today*, vol. 18, no. 19-20, pp. 910–915, 2013.

[40] Z. Xu, B. Cetin, M. Anger et al., "Structure and function of the PP2A-shugoshin interaction," *Molecular Cell*, vol. 35, no. 4, pp. 426–441, 2009.

[41] B. Xue, R. L. Dunbrack, R. W. Williams, A. K. Dunker, and V. N. Uversky, "PONDR-FIT: a meta-predictor of intrinsically disordered amino acids," *Biochimica et Biophysica Acta*, vol. 1804, no. 4, pp. 996–1010, 2010.

[42] B. R. Brooks, R. E. Bruccoleri, B. D. Olafson, D. J. States, S. Swaminathan, and M. Karplus, "CHARMM: a program for macromolecular energy minimization and dynamics calculations," *Journal of Computational Chemistry*, vol. 4, pp. 187–217, 1983.

[43] C. A. Lipinski, F. Lombardo, B. W. Dominy, and P. J. Feeney, "Experimental and computational approaches to estimate solubility and permeability in drug discovery and development settings," *Advanced Drug Delivery Reviews*, vol. 46, no. 1–3, pp. 3–26, 2001.

[44] C. M. Venkatachalam, X. Jiang, T. Oldfield, and M. Waldman, "LigandFit: a novel method for the shape-directed rapid docking of ligands to protein active sites," *Journal of Molecular Graphics and Modelling*, vol. 21, no. 4, pp. 289–307, 2003.

[45] B. Hess, C. Kutzner, D. van der Spoel, and E. Lindahl, "GRGMACS 4: algorithms for highly efficient, load-balanced, and scalable molecular simulation," *Journal of Chemical Theory and Computation*, vol. 4, no. 3, pp. 435–447, 2008.

[46] V. Zoete, M. A. Cuendet, A. Grosdidier, and O. Michielin, "SwissParam: a fast force field generation tool for small organic molecules," *Journal of Computational Chemistry*, vol. 32, no. 11, pp. 2359–2368, 2011.

[47] R. Fletcher, *Optimization*, Academic Press, New York, NY, USA, 1969.

Hindawi Publishing Corporation
Evidence-Based Complementary and Alternative Medicine
Volume 2014, Article ID 189125, 12 pages
http://dx.doi.org/10.1155/2014/189125

Research Article

Text Mining of the Classical Medical Literature for Medicines That Show Potential in Diabetic Nephropathy

Lei Zhang,[1] Yin Li,[2] Xinfeng Guo,[3] Brian H. May,[4] Charlie C. L. Xue,[4] Lihong Yang,[3] and Xusheng Liu[1]

[1] *Nephropathy Department, Guangdong Provincial Hospital of Chinese Medicine, 111 Dade Road, Guangzhou 510120, China*
[2] *Guangzhou University of Chinese Medicine, Guangzhou 510405, China*
[3] *Evidence-Based Medicine and Clinical Research Service Group, Guangdong Provincial Hospital of Chinese Medicine, 111 Dade Road, Guangzhou 510120, China*
[4] *Traditional and Complementary Medicine Research Program, Health Innovations Research Institute, WHO Collaborating Centre for Traditional Medicine, School of Health Sciences, RMIT University, Bundoora, VIC 3083, Australia*

Correspondence should be addressed to Xinfeng Guo; drguoguo@gmail.com and Xusheng Liu; liuxu801@126.com

Received 14 November 2013; Revised 29 December 2013; Accepted 29 December 2013; Published 13 March 2014

Academic Editor: Gerhard Litscher

Objectives. To apply modern text-mining methods to identify candidate herbs and formulae for the treatment of diabetic nephropathy. *Methods*. The method we developed includes three steps: (1) identification of candidate ancient terms; (2) systemic search and assessment of medical records written in classical Chinese; (3) preliminary evaluation of the effect and safety of candidates. *Results*. Ancient terms Xia Xiao, Shen Xiao, and Xiao Shen were determined as the most likely to correspond with diabetic nephropathy and used in text mining. A total of 80 Chinese formulae for treating conditions congruent with diabetic nephropathy recorded in medical books from Tang Dynasty to Qing Dynasty were collected. Sao si tang (also called Reeling Silk Decoction) was chosen to show the process of preliminary evaluation of the candidates. It had promising potential for development as new agent for the treatment of diabetic nephropathy. However, further investigations about the safety to patients with renal insufficiency are still needed. *Conclusions*. The methods developed in this study offer a targeted approach to identifying traditional herbs and/or formulae as candidates for further investigation in the search for new drugs for modern disease. However, more effort is still required to improve our techniques, especially with regard to compound formulae.

1. Introduction

Natural products used in traditional medicine have historically been invaluable for drug development [1, 2]. Successful examples of transformation of traditional medicines into modern drugs included quinine [3], huperzine [4], aspirin [5], and artemisinin [6, 7]. However, the path from traditional medicine to pharmaceutical product is fraught with challenges. The first step is "discovery" from traditional medicine [8]. Traditional Chinese medicine, which has been "clinically" tested for thousands of years, is a rich source of therapeutic leads for drug discovery. These ancient remedies were handed down from generation to generation and recorded in the classical literatures. Nowadays, the classical medical books have become the precious cultural heritage in China, and they are important sources for drug discovery from traditional medicine. As researchers in Western countries have focused on translational medicine to develop more effective clinical strategies from laboratory results, scholars in China have begun to search for potentially effective natural products based on these historical records of medical experience [8–10].

However, as the years passed, diseases and their names changed, leading to the disassociation between the traditional and modern medical terminologies. Given the voluminous content of the traditional Chinese medical literature, conducting searches to identify potential drug candidates is challenging. Additionally, the effects of classical formulae for

the treatment of modern diseases still need to be assessed. All of these aspects present obstacles to the effective and efficient use of the classical literature resources for therapeutic product discovery. Consequently, modern approaches that can mine these classical medical records of traditional Chinese medicine need to develop. Over the last five years, through the International Research Network for Traditional and Complementary Medicine (IRN-TCM), we have developed and refined methods for text mining of the traditional Chinese medicine classical literature to identify candidate herbs and herbal combinations that show potential for further research [11–13].

Diabetic nephropathy is the most common cause of end-stage renal disease around the world and is characterized by rapid progression and a poor prognosis [14]. With the standard therapy of angiotensin-converting enzyme (ACE) inhibitors or angiotensin II receptor blockers (ARB), combined with glucose, lipid, and blood pressure control [15], the outcome for patients with diabetic nephropathy remains poor [16]. There is a need for new therapies to improve the outcomes of diabetic nephropathy treatment. In China, after thousands of years of traditional medical practice, a great deal of valuable experience has accumulated regarding diabetic nephropathy. Therefore this study aimed to apply modern text-mining methods to identify candidate herbs and formulae for the treatment of diabetic nephropathy.

The project involved three parts: (1) identification of classical terms that could refer to diabetic nephropathy; (2) text mining of the classical Chinese medical literature; and (3) preliminary evaluation of the effect and safety of candidates on diabetic nephropathy and the selection of candidates for further drug discovery efforts.

2. Methods

In order to identify all the classical terms that could have referred to diabetic nephropathy, literature searches were conducted. Articles that focused on original researches related to classical medical terms and on the experience of venerable TCM doctors were retrieved from the Chinese databases CNKI, VIP, Wan Fang, CBM, and TCM online. Medical textbooks for undergraduate and postgraduate teaching issued by the state and medical monographs on diabetic nephropathy were also collected through the library of Guangzhou University of Chinese Medicine.

Two authors extracted the classical terms related to diabetic nephropathy that were mentioned in these sources and calculated the frequency of mention for each term. In order to obtain expert opinion on which terms were more corresponding with diabetic nephropathy, a questionnaire was designed and distributed to traditional medicine hospitals around China. Heads of the nephrology department in these hospitals who had more than 10 years of clinical experience in classical medical Chinese were consulted.

The consulting questionnaire included all the classical terms, classical medical records describing their clinical manifestations, and the clinical features of diabetic nephropathy according to the diagnostic criteria of modern medicine. Experts were required to gauge the degree of consistency between the classical term and the modern conception of diabetic nephropathy by comparing their clinical manifestations descriptions. Frequencies of each classical term mentioned in research articles, empirical articles, textbooks, and medical monographs were attached as a reference.

The degree of consistency was divided into five categories: completely consistent (5 points), mostly consistent (4 points), partly consistent (3 points), seldom consistent (2 points), and completely inconsistent (1 point). Experts had to tick only one category for each classical term. Total score of each classical term was calculated by adding the points experts ticked. Scoring rate of each classical term was full score divided by its total score and then multiplied by 100%. Full score was 5 points multiplied by the number of returned questionnaires.

These classical terms with scoring rate more than 50 percent were regarded as identified terms by expert consultation for further verification. Their corresponding modern diseases were retrieved in the textbooks and monographs of Chinese Internal Medicine, monographs of kidney disease of Chinese Medicine, and dictionaries of Chinese Medicine via the library of Guangzhou University of Chinese Medicine. The mentioned frequencies of each modern disease were counted.

Classical terms which have corresponding modern diseases not limited to diabetic nephropathy or targeting many organs not mainly in kidney were excluded. Classical terms with corresponding modern diseases which refer to kidney damages occurring in diabetes mellitus were included and used in ancient literature searching.

"Encyclopedia of Traditional Chinese Medicine" (CD-ROM version 4.0, published by Hunan Electronic and Audio-Visual Publishing House in 2006), which includes 1009 different Chinese medical books written before the emergence of the People's Republic of China (1949 AD) [13], was selected as the text mining resource.

The information about the treatments of these included classical terms was extracted, including the titles and completion dates of the books, all records related to therapies for disorders congruent with diabetic nephropathy, and the formulae used for treating these disorders. Ancient formulae targeting incongruent disorders with diabetic nephropathy confirmed by two authors, respectively, were excluded. Discrepancies were resolved by a third author, who made the final decision. The frequency of citation of each included formula was calculated. Formulae with higher recorded frequency were selected as candidates for further work in drug discovery for diabetic nephropathy.

A preliminary evaluation of the effect of candidates on diabetic nephropathy was conducted by searching the databases PubMed (January 1966 to June 2012), EMBASE (January 1985 to June 2012), the Cochrane Library, and clinicalTrials.gov to locate studies on the clinical application and experimental research on candidate formulae and their components.

3. Results

3.1. Classical Terms That Refer to Diabetic Nephropathy. Database searches resulted in the inclusion of 91 original

research articles and 25 articles on the empirical experience of venerable TCM doctors that mentioned classical terms for DN. 60 medical monographs and 11 textbooks that included sections on diabetic nephropathy were selected via the library of Guangzhou University of Chinese Medicine.

A total of 31 classical terms associated with diabetic nephropathy were collected for expert consultation (Table 1). Frequencies of each classical term mentioned in research articles, empirical articles, medical monographs, and textbooks were attached as a reference (Table 1).

Thirty-five questionnaires were returned from 4 municipalities, 17 provinces, and 3 autonomous regions in China. These did not include Shandong province, Hainan province, Gansu province, Hunan province, Qinghai province, Tibet autonomous region, and the Xinjiang Uygur autonomous region. Full score of each classical term was 175 points (5 points multiplied by 35 returned questionnaires). Scoring rates of Shui Zhong (水肿), Shen Xiao (肾消), Niao Zhuo (尿浊), Guan Ge (关格), Xu Lao (虚劳), Xia Xiao (下消), Xiao Ke (消渴), and Xiao Shen (消肾) were more than 50 percent (Table 2). Experts who marked one classical term at least 3 points were considered approving the consistency between this classical term and diabetic nephropathy and their provinces were listed in Table 2.

To further verify the consistency between classical terms with scoring rate more than 50 percent and diabetic nephropathy, 35 textbooks of Chinese Internal Medicine, 86 monographs of Chinese Internal Medicine, 57 monographs of kidney disease of Chinese Medicine, and 12 dictionaries of Chinese Medicine were retrieved via the library of Guangzhou University of Chinese Medicine. The correspondence between these ancient terms and diabetic nephropathy was overlapping (Table 3).

Corresponding modern diseases of Shui Zhong (水肿) include renal edema, cardiac edema, nutritional edema, endocrine edema, hepatic edema, and edema of unknown reason. Besides diabetic nephropathy, renal edema also refers to acute or chronic glomerulonephritis, nephrotic syndrome, other secondary glomerular diseases (such as lupus nephritis), and chronic renal failure. Xu Lao (虚劳) is considered as chronic and consumptive disease involving multisystems and multiorgans, especially organ function decline or failure. Guan Ge (关格) is regarded as chronic renal failure, acute renal failure, uremia period, ileus, and esophageal carcinoma. Niao Zhuo (尿浊) refers to chyluria, phosphaturia, filariasis, urinary system infection, urinary system cancer, tuberculosis, and so on. Xiao Ke (消渴) mainly refers to diabetes mellitus (Table 3).

Shen Xiao (肾消), Xia Xiao (下消), and Xiao Shen (消肾) were not regarded as independent diseases in textbooks and monographs of Chinese Internal Medicine, and monographs of kidney disease of Chinese Medicine. They were mentioned in Xiao Ke (消渴) when kidney damage occurs (Table 3).

The following three extracts are examples of descriptions consistent with DN [17]. In relation to Xiao Shen (消肾) the *Bei Ji Qian Jin Yao Fang,* written by Sun Si-miao during the Tang Dynasty (652 AD), provides the following description: *"Patients with symptoms such as fever due to deficiency, thirst but not drinking more water, frequent urination, turbid urine and thready pulse were often diagnosed as Xiao Shen (消肾) disease."* In the *Jing Yue Quan Shu,* written by Zhang Jie-bin during the Ming Dynasty (1640 AD), the following definition is provided: "*Xia Xiao (下消) with the symptoms of dark urine, turbid urine, gloomy complexion, muscle wasting, is also called Shen Xiao (肾消), as the disease location is in the kidney (Shen equals to kidney in Chinese).*" The *Cheng Fang Qie Yong,* which was written by Wu Yi-luo during the Qing Dynasty (1761 AD),

Table 1: Candidate classical terms related to diabetic nephropathy.

Classical term (Chinese name)	Frequency		
	Modern original research articles	Empirical articles by venerable TCM doctors	Medical monographs and textbooks
Shui Zhong (水肿)	45	16	24
Guan Ge (关格)	39	3	17
Niao Zhuo (尿浊)	35	9	5
Shen Xiao (肾消)	29	3	3
Xiao Ke (消渴)	28	12	0
Xiao Shen (消肾)	17	1	0
Xu Lao (虚劳)	17	10	14
Shen Lao (肾劳)	17	0	2
Xia Xiao (下消)	13	2	0
Yao Tong (腰痛)	11	3	0
Zhang Man (胀满)	10	1	3
Long Bi (癃闭)	6	0	0
Xiao Dan (消瘅)	5	0	1
Ni Du (溺毒)	5	0	0
Shui Bing (水病)	4	0	0
Tu Ni (吐逆)	4	0	0
Nei Xiao (内消)	3	0	0
Xuan Yun (眩晕)	2	3	6
San Xiao (三消)	2	0	0
Shen Feng (肾风)	1	0	0
Fei Xiao (肺消)	1	0	0
Shen Ke (肾渴)	1	0	0
Shen Shui (肾水)	1	0	0
Shen Dan (肾瘅)	1	0	0
Shen Zhuo (肾着)	1	0	0
Shen Jue (肾绝)	1	0	0
Lao Lin (劳淋)	1	0	0
Lin Zheng (淋证)	1	0	0
Xue Niao (血尿)	1	0	0
Pi Dan (脾瘅)	1	0	0
Shui Qi Bing (水气病)	1	0	0

Table 2: Results of the expert consultation.

Classical term (Chinese name)	Total score	Scoring rate (full score divided by total score)	Provinces of experts who chose completely consistent, mostly consistent, or partly consistent
Shui Zhong (水肿)	124	71.4%	Beijing, Guangdong, Guangxi, Guizhou, Hebei, Heilongjiang, Hubei, Jilin, Jiangsu, Jiangxi, Liaoning, Ningxia, Shanxi, Shaanxi, Shanghai, Tianjin, Yunnan, Zhejiang, Chongqing
Guan Ge (关格)	92	52.6%	Beijing, Guangdong, Guangxi, Guizhou, Hebei, Heilongjiang, Hubei, Jilin, Jiangxi, Liaoning, Ningxia, Shanghai, Chongqing
Niao Zhuo (尿浊)	95	54.3%	Beijing, Guangdong, Hebei, Heilongjiang, Hubei, Jilin, Jiangxi, Liaoning, Shanxi, Shanghai, Zhejiang
Shen Xiao (肾消)	111	63.4%	Beijing, Guangdong, Guangxi, Hebei, Heilongjiang, Hubei, Jiangsu, Jiangxi, Liaoning, Shanghai, Tianjin, Yunnan, Zhejiang
Xiao Ke (消渴)	90	51.4%	Beijing, Guangdong, Guangxi, Hebei, Heilongjiang, Hubei, Jilin, Jiangsu, Ningxia, Shanghai, Tianjin, Zhejiang
Xiao Shen (消肾)	88	50.2%	Beijing, Guangdong, Guangxi, Hebei, Heilongjiang, Hubei, Jilin, Liaoning, Ningxia, Shaanxi, Tianjin, Zhejiang
Xu Lao (虚劳)	91	52.0%	Beijing, Guangdong, Guangxi, Hebei, Heilongjiang, Hubei, Jiangxi, Liaoning, Ningxia, Shanxi, Shaanxi, Shanghai, Tianjin, Yunnan, Zhejiang
Xia Xiao (下消)	95	54.3%	Beijing, Guangdong, Hebei, Heilongjiang, Hubei, Jilin, Ningxia, Shaanxi, Shanghai, Tianjin, Yunnan
Shen Lao (肾劳)	85	48.5%	Guangdong, Guangxi, Hubei, Jilin, Jiangsu, Liaoning, Ningxia, Shanxi, Tianjin
Yao Tong (腰痛)	78	44.6%	Beijing, Guangdong, Hebei, Heilongjiang, Hubei, Jilin, Liaoning, Ningxia, Shanxi, Yunnan
Zhang Man (胀满)	63	36.0%	Beijing, Guangdong, Hebei, Heilongjiang, Hubei, Ningxia, Yunnan
Long Bi (癃闭)	70	40.0%	Beijing, Guangdong, Heilongjiang, Hubei, Liaoning, Shanghai, Chongqing
Xiao Dan (消瘅)	74	42.3%	Guangdong, Hebei, Hubei, Ningxia, Shanxi, Shaanxi, Shanghai, Tianjin, Zhejiang
Ni Du (溺毒)	83	47.4%	Beijing, Guangdong, Guizhou, Hebei, Hubei, Shanxi, Shanghai, Zhejiang
Shui Bing (水病)	84	48.0%	Beijing, Guangdong, Hebei, Heilongjiang, Hubei, Jilin, Liaoning, Ningxia, Shanxi, Shaanxi, Shanghai, Yunnan, Zhejiang, Chongqing
Tu Ni (吐逆)	59	33.7%	Guangdong, Guangxi, Shanxi, Shanghai
Nei Xiao (内消)	58	33.1%	Guangdong, Shanxi
Xuan Yun (眩晕)	56	32.0%	Guangdong, Hebei
San Xiao (三消)	68	38.9%	Beijing, Guangdong, Hebei, Ningxia, Shaanxi, Tianjin
Shen Feng (肾风)	57	32.6%	Guangdong, Hebei, Shanxi, Zhejiang
Fei Xiao (肺消)	41	23.4%	None
Shen Ke (肾渴)	66	37.7%	Guangdong, Hubei, Liaoning, Ningxia, Shaanxi
Shen Shui (肾水)	75	42.9%	Guangdong, Heilongjiang, Hubei, Jilin, Ningxia, Shanxi, Shaanxi, Zhejiang
Shen Dan (肾瘅)	67	38.3%	Guangdong, Hubei, Shanxi, Shaanxi, Zhejiang
Shen Zhuo (肾着)	55	31.4%	Guangdong, Shanxi, Tianjin
Shen Jue (肾绝)	46	26.3%	Hebei
Lao Lin (劳淋)	45	25.7%	Hebei
Lin Zheng (淋证)	43	24.6%	None
Xue Niao (血尿)	44	25.1%	Ningxia
Pi Dan (脾瘅)	45	25.7%	None
Shui Qi Bing (水气病)	77	44.0%	Guangdong, Hebei, Hubei, Jiangsu, Liaoning, Ningxia, Shanxi, Shaanxi, Tianjin, Chongqing

Table 3: Corresponding modern diseases of classical terms.

Classical terms	Corresponding modern diseases	Number of modern books mentioning modern disease			
		Textbooks of Chinese Internal Medicine	Monographs of Chinese Internal Medicine	Monographs of kidney disease of Chinese Medicine	Dictionaries of Chinese Medicine
Shui Zhong (水肿)	Renal edema	25	42	4	3
	Acute or chronic glomerulonephritis	21	40	3	Not mentioned
	Nephrotic syndrome	18	29	3	Not mentioned
	Secondary glomerular diseases (diabetic nephropathy, lupus nephritis)	3	3	Not mentioned	Not mentioned
	Chronic renal failure	Not mentioned	1	Not mentioned	Not mentioned
	Cardiac edema	23	37	4	3
	Nutritional edema	23	32	3	3
	Edema of unknown reason	6	5	2	Not mentioned
	Endocrine edema	22	30	4	3
	Hepatic edema	2	13	3	3
Xu Lao (虚劳)	Severe anemia	13	17	Not mentioned	1
	Immune function disorder, deficiency, or decrease	11	11	Not mentioned	Not mentioned
	Endocrine gland dysfunction	12	11	Not mentioned	Not mentioned
	Metabolic disorders	9	12	Not mentioned	Not mentioned
	Nutrition deficiency	12	11	Not mentioned	Not mentioned
	Nerve function depression or excessive suppression	9	10	Not mentioned	Not mentioned
	Organ function decline	8	4	Not mentioned	1
	Cachexia	1	Not mentioned	Not mentioned	Not mentioned
	Cancer	Not mentioned	4	Not mentioned	1
	Renal failure	Not mentioned	5	Not mentioned	1
	Heart failure	1	4	Not mentioned	Not mentioned
	Chronic respiratory disease	Not mentioned	2	Not mentioned	1
	Digestive system disease	Not mentioned	2	Not mentioned	Not mentioned
	Connective tissue diseases	Not mentioned	1	Not mentioned	Not mentioned
Guan Ge (关格)	Chronic renal failure	7	15	4	Not mentioned
	Acute renal failure	2	12	4	Not mentioned
	Uremia period	1	5	Not mentioned	2
	Ileus, esophageal carcinoma	Not mentioned	1	Not mentioned	Not mentioned
Niao Zhuo (尿浊)	Chyluria	6	9	3	Not mentioned
	Phosphaturia	Not mentioned	8	3	Not mentioned
	Filariasis	2	2	Not mentioned	Not mentioned
	Prostatitis	2	3	Not mentioned	Not mentioned
	Prostatic hyperplasia	Not mentioned	1	Not mentioned	Not mentioned
	Vesiculitis	Not mentioned	1	Not mentioned	Not mentioned
	Urinary system infection	Not mentioned	1	3	Not mentioned
	Urinary system cancer	Not mentioned	6	2	Not mentioned
	Tuberculosis	1	6	2	Not mentioned
Xiao Ke (消渴)	Diabetes mellitus	22	48	2	Not mentioned
Xia Xiao (下消)	Kidney damage occurring in Xiao Ke (消渴)	17	42	2	Not mentioned

Table 3: Continued.

Classical terms	Corresponding modern diseases	Number of modern books mentioning modern disease			
		Textbooks of Chinese Internal Medicine	Monographs of Chinese Internal Medicine	Monographs of kidney disease of Chinese Medicine	Dictionaries of Chinese Medicine
Shen Xiao (肾消)	Kidney damage occurring in Xiao Ke (消渴)	3	3	2	Not mentioned
Xiao Shen (消肾)	Kidney damage occurring in Xiao Ke (消渴)	2	1	Not mentioned	Not mentioned

provided the following linkage with diabetes: "*Shen Xiao (肾消) progresses from Xiao Ke (消渴), with the symptoms of polydipsia, polyuria and turbid urine*."

The relationship between the three ancient terms was described in 8 dictionaries of Chinese Medicine. Xia Xiao (下消) refers to Shen Xiao (肾消) and Xiao Shen (消肾).

Xiao Shen (消肾) refers to Xia Xiao (下消) and Shen Xiao (肾消). But besides Xia Xiao (下消), Shen Xiao (肾消) also refers to Qiang Zhong (强中), which is called priapism in modern times. Therefore, Xia Xiao (下消), Shen Xiao (肾消), and Xiao Shen (消肾) were considered more corresponding with diabetic nephropathy. However, ancient records about the symptoms of priapism should be excluded during the ancient formulae information extraction.

3.2. Discovery from the Classical Medical Literature Text Mining. This study searched ancient records of Xia Xiao (下消), Shen Xiao (肾消), and Xiao Shen (消肾) via "Encyclopedia of Traditional Chinese Medicine." Ancient records which were thought to be corresponding with the symptoms of priapism were not included for formulae extraction.

The search revealed a total of 80 Chinese formulae for treating disorders congruent with diabetic nephropathy recorded in medical books from Tang Dynasty (618 AD to 907 AD) to Qing Dynasty (1644 AD to 1912 AD). The earliest formulae for treating diabetic nephropathy recorded in Tang dynasty were Huang qi yin (黄芪饮), Xuan bu wan (宣补丸), and E jiao tang (阿胶汤). Eighteen formulae were recorded more than 5 times. The top eight formulae were, in the order, Liu wei di huang wan (六味地黄丸), Jia jian shen qi wan (加味肾气丸), Bai fu ling wan (白茯苓丸), Si wu tang (四物汤), Sao si tang (缫丝汤), Hui xiang san (茴香散), Lu rong wan (鹿茸丸), and Ren shen san (人参散) (Table 4).

The number of ingredients of the eighteen most frequent formulae was calculated in order to identify simple formulae that may be suitable for further drug discovery efforts (Table 5). The following formulae contained fewer than 5 ingredients: Sao si tang (缫丝汤), Hui xiang san (茴香散), Si wu tang (四物汤), Ge gen wan fang (葛根丸), and Gu ben wan (固本丸). Liu wei di huang wan (六味地黄丸), Jia jian shen qi wan (加减肾气丸), Lu rong wan (鹿茸丸), Hu fen san (胡粉散), and E jiao tang (阿胶汤) contain more than 5 and fewer than 10 ingredients. Bai fu ling wan (白茯苓丸), Shen li san (肾沥散), Xuan bu wan fang (宣补丸方), Cong rong wan (苁蓉丸), Shuang bu wan (双补丸), Gou qi zi wan (枸杞子丸), and Ping bu wan (平补丸) contained more than 10 ingredients (Table 5).

3.3. Preliminary Evaluation of the Effect and Safety of Candidates on Diabetic Nephropathy. After identification of the candidate formulae, preliminary evaluation of their effect on diabetic nephropathy was undertaken. This began with the simple, high frequency formulae. Among the 18 formulae, "Sao si tang (缫丝汤) (also called Reeling Silk Decoction)" ranked fifth and was the simplest since it only contained one ingredient—silkworm and/or silk cocoon.

The earliest record of its use was in *Yi Xue Zheng Zhuan* written by Yu Tuan during the Ming Dynasty (1515 AD). In reference to the inherited formula Reeling Silk Decoction, he wrote that "*it has an excellent effect on Shen Xiao with the symptoms of turbid urine, polydipsia and excessive appetite but the person loses weight…... the effect of the hot water used in reeling silk (i.e. Reeling Silk Decoction) is best. If this is not available, it can be replaced by a decoction of silkworm cocoon or silk floss*."—from *Yi Xue Zheng Zhuan* [17].

Based on this report and subsequent repeated citation of this remedy by other authors, we conducted the literature search of the modern studies regarding the silkworm, its related products, and its active ingredients, for treating diabetic nephropathy in order to investigate whether this simple formula could have the potential to be developed into a new agent for diabetic nephropathy.

No studies of Reeling Silk Decoction were located, but there have been considerable studies involving silkworm, its related products, and its active ingredients. 202 articles describing the active ingredients of the silkworm and its products for diabetic nephropathy were retrieved in a search of the modern literature (Figure 1).

According to modern studies, the silkworm and its products are rich in various active substances such as alkaloids, flavanoids, and silk protein hydrolysates.

1-Deoxynojirimycin (DNJ) is a major component of the alkaloids in silkworm [18]. A clinical study in Japan [19] showed that the N-hydroxyethyl derivative of 1-DNJ (miglitol) decreased the urinary albumin excretion rate in Japanese patients with type 2 diabetes. One possible mechanism is related to improved insulin resistance [20]. It was reported to be safe for patients with stage 3 diabetic nephropathy [21]. However, it is not recommended for patients with renal insufficiency (serum creatinine >2 mg/dL) because it is excreted primarily via the kidney [22].

Table 4: 80 ancient formulae for diabetic nephropathy.

Pin Yin names of ancient formulas (Chinese name)	Number of ancient formulae	Recorded frequency
Liu wei di huang wan (六味地黄丸)	1	44 times
Jia jian shen qi wan (加减肾气丸)	1	38 times
Bai fu ling wan (白茯苓丸)	1	17 times
Si wu tang (四物汤)	1	11 times
Sao si tang (缫丝汤), Hui xiang san (茴香散)	2	9 times
Lu rong wan (鹿茸丸)	1	8 times
Ren shen san (人参散)	1	7 times
Shen li san (肾沥散), Xuan bu wan fang (宣补丸方), Ge gen wan (葛根丸)	3	6 times
Cong rong wan (苁蓉丸), Shuang bu wan (双补丸), Gu ben wan (固本丸), Hu fen san (胡粉散), Gou qi zi wan (枸杞子丸), E jiao tang (阿胶汤), Ping bu wan (平补丸)	7	5 times
Xiao tu si zi wan (小菟丝子丸), Da bu yuan jian (大补元煎), You gui yin (右归饮), Gui pi tang (归脾汤), Huang lian wan fang (黄连丸方), Huang qi wan (黄芪丸)	6	4 times
Qing xin lian zi yin (清心莲子饮), Huang qi yin (黄芪饮), Ji long tang (荠茏汤), Jin ying bo wan (金银箔丸), Zhi bai ba wei wan (知柏八味丸), Mi yuan jian (秘元煎), Zuo gui yin (左归饮), Hua cong rong wan (花苁蓉丸), Ying long tang (引龙汤), Fu tu wan (茯菟丸), Shu yu wan (薯蓣丸), Shu gan di huang san (熟干地黄散), Tu si zi san (菟丝子散), Bu ying wan (补阴丸)	14	3 times
Yuan tu wan (元菟丸), Gu ying jian (固阴煎), Ren shen fu ling wan (人参茯苓丸), Bu shen di huang yuan (补肾地黄元), Shen xiao san (神效散), Zhu long san (竹笼散), Ge fen wan (葛粉丸), Gu wa tang (古瓦汤), Gua lou gen wan fang (栝蒌根丸方), Mu li wan fang (牡蛎丸方), Gan di huang wan (干地黄丸), Tie fen wan (铁粉丸), Sang piao xiao wan (桑螵蛸丸方), Shan zhu yu fang (山茱萸方), Ci shi yin (磁石饮), Ling shu tu si wan (苓术菟丝丸), Tian hua wan (天花丸), Sang bai pi tang (桑白皮汤), Ning fei tang (宁沸汤), Nv zhen tang (女贞汤), Hu tao wan (胡桃丸), Zhen zhu fen wan (珍珠粉丸)	22	2 times
Lin sha dan (灵砂丹), Xuan tu dan (玄兔丹), Tian wang bu xin dan (天王补心丹), Da bu di huang wan (大补地黄丸), Xia zuo yin (下左饮), Nei hua wan (内化丸), Dang gui liu huang tang (当归六黄汤), Di huang tang (地黄汤), Jin gui shun qi wan (金匮顺气丸), Liu shen yin (六神饮), Qian jin di Huang wan (千金地黄丸), ying su tang (罂粟汤), Dan sha san (丹砂散), Huang lian huang qi wan (黄连黄芪丸), Zhu yu huang qi wan (茱萸黄芪丸), Ren shen lu rong wan (人参鹿茸丸), Yuan zhi wan (远志丸), Tian xiong san (天雄散), Shen di ying zi (生地饮子), Wu Long tang (乌龙汤)	20	1 time

Among the flavanoids, which have been purified and identified from the sericin layer of silkworm cocoons [23], quercetin was reported to have renal protective effects. It suppressed glomerular mesangial cell hypertrophy, proliferation, and extracellular matrix accumulation, all of which occur in glomerular sclerosis [24]. Proposed mechanisms of action include inhibition of transforming growth factor-β1 (TGF-β1) expression [25] and amelioration of oxidative stress [26], which have been shown to be final common mediators of renal injury in diabetes [27]. Additionally, quercetin was reported to reduce nuclear factor-κB (NF-κB) expression, which may be involved in the pathogenesis of proteinuria in diabetic nephropathy [28, 29].

Additionally, the concentrations of 1-DNJ and the activities of quercetin in silkworm are higher than in mulberry leaves, which are the only food source of silkworm, because of the biotransformation in the silkworm body [30–35].

Therefore, components of Reeling Silk Decoction have demonstrated promising potential for development as new agents for the treatment of diabetic nephropathy. However, its safety for patients with renal insufficiency should be evaluated in further investigations.

4. Discussion

The methods used in classical traditional Chinese medicine, which have been "clinically" tested for thousands of years, continue to play an indispensable role in the treatment of chronic diseases in Asian countries. It has also become an important source of drug discovery for Western scholars and pharmacologists. However, barriers such as the disassociation between the traditional and modern medical terminologies, and the voluminous content of traditional Chinese medical literature, have slowed the pace of drug discoverer using the resources of the classical literature. The use of modern

Table 5: Ingredients of the eighteen formulae.

Classical formulae Pin Yin name (Chinese name)	Number of ingredients	Latin name of ingredients
Liu wei di huang wan (六味地黄丸)	6	Radix Rehmannia Preparata; Fructus Corni; Rhizoma Dioscoreae; Cortex Moutan Radicis; Poria; Rhizoma Alismatis
Jia wei shen qi wan (加味肾气丸)	10	Radix Rehmannia Preparata; Poria; Rhizoma Dioscoreae; Cortex Moutan Radicis; Fructus Corni; Rhizoma Alismatis; Radix Achyranthis Bidentatae; Semen Plantaginis; Cortex Cinnamomi; Radix Aconiti Lateralis Preparata
Bai fu ling wan (白茯苓丸)	11	Poria; Fructus Rubi; Rhizoma Coptidis; Radix Ginseng; Radix Trichosanthis; Radix Rehmannia Preparata; Endothelium Corneum Gigeriae Galli; Rhizoma Dioscoreae Septemlobae; Radix Scrophulariae; Herba Dendrobii; Fructus Cnidii
Si wu decoction (四物汤)	4	Radix Rehmannia Preparata; Radix Paeoniae Alba; Radix Angelicae Sinensis; Rhizoma Chuanxiong
Sao si tang (缫丝汤)	1	Bombyx Bombycis
Hui xiang san (茴香散)	2	Fructus Foeniculi; Fructus Toosendan
Lu rong wan (鹿茸丸)	7	Cornu Cervi Pantotrichum; Radix Scutellariae; Radix Ginseng; Radix Ipomoeae hungaiensis; Herba Cistanches; Endothelium Corneum Gigeriae Galli; Semen Cuscutae
Ren shen san (人参散)	9	Radix Ginseng; Cornu Cervi Pantotrichum; Radix Astragali; Fructus Trichosanthis; Ootheca Mantidis; Cortex Eucommiae; Endothelium Corneum Gigeriae Galli; Fructus Corni; Semen Cuscutae
Shen li san (肾沥散)	17	Endothelium Corneum Gigeriae Galli; Radix Polygalae; Radix Ginseng; Radix Astragali; Ootheca Mantidis; Rhizoma Alismatis; Radix Rehmannia Preparata; Cortex Cinnamomi; Radix Angelicae Sinensis; Os Draconis; Radix Glycyrrhizae; Radix Ophiopogonis; Fructus Schisandrae; Magnetitum; Poria; Rhizoma Chuanxiong; Radix Scrophulariae
Xuan bu wan (宣补丸)	12	Radix Astragali; Fructus Trichosanthis; Radix Ophiopogonis; Poria; Radix Ginseng; Radix Glycyrrhizae; Rhizoma Coptidis; Rhizoma Anemarrhenae; Radix Rehmannia Preparata; Gypsum Fibrosum; Herba Cistanches; Semen Cuscutae
Ge gen wan fang (葛根丸方)	4	Radix Puerariae; Fructus Trichosanthis; Plumbum Tetroxide; Radix Aconiti Lateralis Preparata
Cong rong wan (苁蓉丸)	20	Herba Cistanches; Radix Rehmannia Preparata; Radix Ophiopogonis; Rhizoma Alismatis; Fructus Schisandrae; Cortex Cinnamomi; Radix Morindae Officinalis; Cortex Lycii; Radix Angelicae Sinensis; Magnetitum; Radix Astragali; Radix Ginseng; Endothelium Corneum Gigeriae Galli; Halloysitum Rubrum; Semen Allii Tuberosi; Os Draconis; Radix Glycyrrhizae; Limonitum; Cortex Moutan Radicis; Ootheca Mantidis
Shuang bu wan (双补丸)	16	Colla Cornus Cervi; Lignum Aquilariae Resinatum; Rhizoma Alismatis; Fructus Rubi; Poria; Radix Ginseng; Fructus Chaenomelis; Semen Coicis; Radix Astragali; Radix Rehmannia Preparata; Herba Cistanches; Semen Cuscutae; Fructus Schisandrae; Herba Dendrobii; Radix Angelicae Sinensis; Moschus
Gu ben wan (固本丸)	5	Radix Ginseng; Radix Rehmanniae; Radix Rehmannia Preparata; Radix Asparagi; Radix Ophiopogonis

Table 5: Continued.

Classical formulae Pin Yin name (Chinese name)	Number of ingredients	Latin name of ingredients
Hu fen san (胡粉散)	7	Plumbum tetroxide; Galenitum; Fructus Trichosanthis; Radix Glycyrrhizae; Rhizoma Alismatis; Halloysitum Rubrum; Halloysitum Rubrum
Gou qi zi wan (枸杞子丸)	12	Fructus Lycii; Poria; Radix Astragali; Endothelium Corneum Gigeriae Galli; Fructus Trichosanthis; Rhizoma Alismatis; Cortex Moutan Radicis; Fructus Corni; Radix Ophiopogonis; Concha Ostreae; Ootheca Mantidis; Semen Plantaginis
E jiao tang (阿胶汤)	7	Colla Corii Asini; Rhizoma Zingiberis; Radix Polygalae; Radix Aconiti Lateralis Preparata; Radix Ginseng; Radix Glycyrrhizae; Fructus Cannabis
Ping bu wan (平补丸)	11	Semen Cuscutae; Fructus Corni; Radix Angelicae Sinensis; Fructus Alpiniae Oxyphyllae; Fructus Toosendan; Radix Achyranthis Bidentatae; Semen Trigonellae; Cortex Eucommiae; Radix Morindae Officinalis; Herba Cistanches; Olibanum

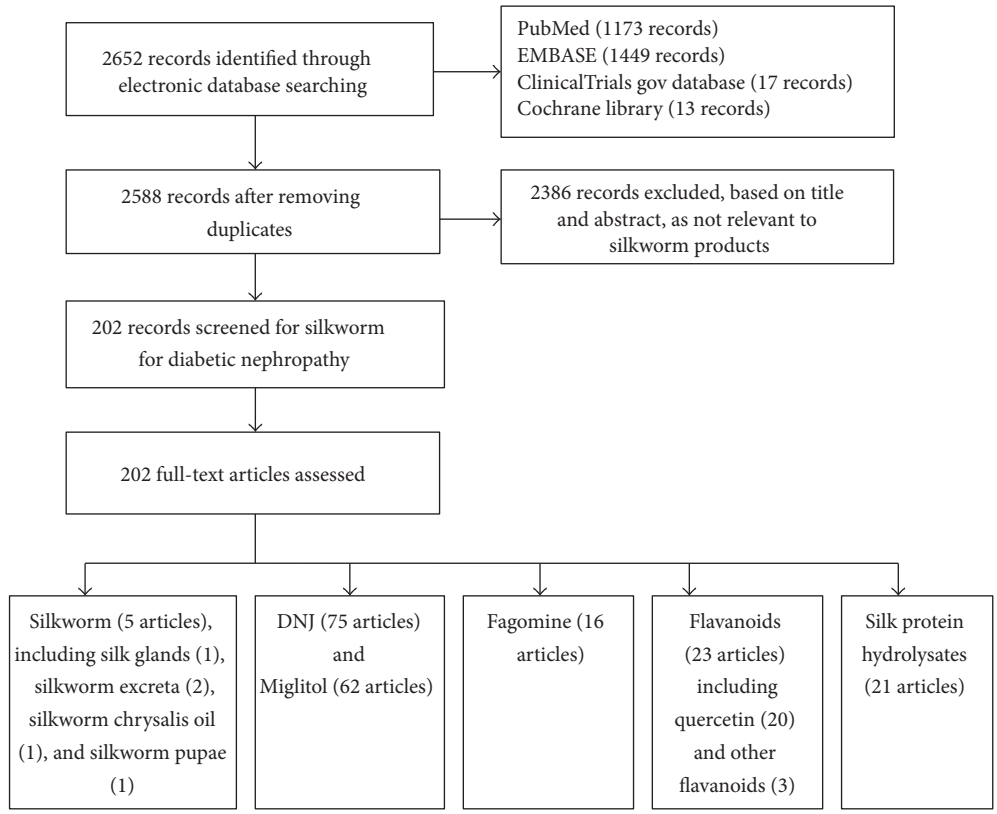

Figure 1: Flowchart detailing study selection process.

technology and methods for text mining of the traditional Chinese medicine classical literature can provide an approach to accelerating this process.

According to the method we developed, the process of drug discovery from the classical medical literature includes three main steps: (1) identification of candidate classical terms; (2) systemic search and analysis of classical medical records; (3) preliminary evaluation of the effects and safety of the candidates.

The usual method for identifying ancient terms corresponding with modern disease is based mainly on narrative reviews of the classical literature. However, the result in this study indicated that correspondence between ancient terms and modern disease was overlapping, rather than there being a one-to-one correspondence. This phenomenon also appeared in age-related dementia and memory impairment [12]. So the usual approach narrative review was not enough to identify the classical terms of modern disease. The two-way

confirmation of terminology correspondence was applied in our study. Expert consultation was used to identify the ancient terms related to diabetic nephropathy. And then the corresponding modern diseases of each term identified by expert opinion were retrieved in textbooks and monographs of Chinese Internal Medicine, monographs of kidney disease of Chinese Medicine, and dictionaries of Chinese Medicine.

Among these identified ancient terms, Shui Zhong (水肿) was named after symptom of a visible edema caused by discords in many systems. Besides diabetic nephropathy, chronic or acute glomerulonephritis, nephrotic syndrome, and other secondary glomerular diseases may result in renal edema as well, which is usually characterized by facial or lower limb swelling due to water-sodium retention or hypoproteinemia. Chronic renal failure was one of the modern diseases corresponding with Guan Ge (关格) and Xu Lao (虚劳). It was the serious end stage of all the progressed chronic kidney diseases, not only diabetic nephropathy. Xiao Ke (消渴) was regarded as diabetes mellitus, which referred more to diabetes without kidney damage. And the modern diseases of Niao Zhuo (尿浊) would prefer chyluria, tuberculosis, urinary system infection, and cancer, rather than diabetic nephropathy. Therefore, it was difficult to identify that if the ancient literature describing these classical terms referred to diabetic nephropathy or not. It deserved further researches specifically identifying treatment related to diabetic nephropathy in their ancient records for each of them. Xia Xiao (下消), Shen Xiao (肾消), and Xiao Shen (消肾) which meant kidney damage occurring in diabetes were considered more corresponding with diabetic nephropathy and used in ancient literature text mining. Because Shen Xiao (肾消) also referred to Qiang Zhong (强中), which meant priapism in modern times. Formulae targeted Qiang Zhong (强中) was excluded when formulae extracting.

The two-way confirmation of terminology correspondence showed the overlap between ancient terms and modern disease more clearly. It was helpful for consistency evaluation between classical text that described these ancient terms and diabetic nephropathy in ancient text mining. However, it would be more convincing if expert consultation was included in modern diseases retrieval, just as done in the classical terms identification of diabetic nephropathy.

The systematic search of full texts of medical book firstly required the identification of a suitable collection. Our previous work located fourteen collections of traditional Chinese medical literature that could be used as resources for systematic searches [36]. The most accessible of the large full-text collections is the Zhong Hua Yi Dian CD ("Encyclopedia of Traditional Chinese Medicine"), which allows electronic searches. So the Zhong Hua Yi Dian CD was used in our study.

Since reports about the nephrotoxicity of Chinese Medicine appeared in 1994, and a condition named "Chinese herbs nephropathy" [37] received attention, the effect and safety of Chinese Medicine on patients with chronic kidney disease have been constantly questioned. Therefore a preliminary evaluation of the effect and safety of a formula is an essential step in the drug discovery process. In this study, the primary evaluation was in the form of a review of the modern literature. This provided much useful data which had some implications for further clinical investigations and pharmacology and pharmacodynamics experiments. For example, the review indicated that the active ingredients of silkworm, such as 1-deoxynojirimycin (DNJ) and quercetin, may have a renoprotective function, but this still needs further clinical verification with a large sample and in-depth molecular mechanism research. We also learnt that the safety of silkworm in diabetic nephropathy patients with renal insufficiency had to be evaluated in further investigations because of the renal excretion of 1-DNJ.

We chose Reeling Silk Decoction, which contains only a single agent, as an example in this study, since most researchers pay more attention to individual agents than to compound formulae. This is because a single agent is simple and its effect on modern disease is easier to be elucidated using current technology. However, formulae consisting of only a single agent are not typical of the prescription used in ancient China. In fact, the compound formula containing multiple agents with different roles in treating the diseases is the essence and characteristic feature of traditional Chinese medicine [9]. In our study, a total of 80 classical formulae for treating conditions congruent with diabetic nephropathy were collected. Most of these formulae are multiherb formulae, comprising two or more herbs. If researchers only focus on single agent, it is likely that they would lose much useful information. However challenges such as the unpredictable pharmacokinetic properties of multiple components and the potential risks of agent-agent interactions in formula add to the difficulty in undertaking a preliminary evaluation of formula effect and safety. More effort is still needed to improve our modern techniques in the preliminary evaluation on the effect and safety of candidates.

5. Conclusions

This convergence of the results of text mining of the classical literature and searches of modern biomedical databases illustrates the value of this text-based approach to the selection of candidates for drug discovery endeavours. The use of modern technology for text mining the classical literature of traditional Chinese medicine shows potential and could be an important step towards a brighter future for drug discovery. The methods developed in this study offer a targeted approach to identifying traditional herbs and/or formulae as candidates for further investigation in the search for new drugs for modern diseases. However, more effort is still required to improve our techniques, especially with regard to compound formulae.

Appendix

Search Strategies

#1 ("kidney")

#2 ("glucose")

#3 ("nephropathy")

#4 ("diabetic nephropathy")

#5 ("diabetes")

#6 ("Bombyx"[Mesh] OR "chymotrypsin inhibitor 13 protein, Bombyx mori"[Supplementary Concept] OR "paralytic peptide, insect"[Supplementary Concept] OR "NUE protein, silkworm"[Supplementary Concept] OR "transcription factor TFIIIR, Bombyx mori"[Supplementary Concept] OR "Moths"[Mesh] OR "7,2′-dihydroxy-8-hydroxyethyl-4′-methoxyflavane-2′-O-beta-D-glucopyranoside"[Supplementary Concept] OR "sorbitol-6-phosphatase, Bombyx mori"[Supplementary Concept] OR "30Kc6 protein, Bombyx mori"[Supplementary Concept] OR "Edf1 protein, mouse"[Supplementary Concept] OR "fibroin, silkworm"[Supplementary Concept] OR "L-3, 4-dihydroxyphenylalanine decarboxylase, Bombyx mori"[Supplementary Concept] OR "BMCHIR1protein, Bombyx mori"[Supplementary Concept] OR "Bmdsx protein, Bombyx mori"[Supplementary Concept] OR "samui protein, Bombyx mori"[Supplementary Concept] OR "30kP protease A protein, Bombyx mori"[Supplementary Concept] OR "ACPIP protein, Bombyx mori"[Supplementary Concept] OR "fhx protein, Bombyx mori"[Supplementary Concept] OR "cecropin CMIV protein, Bombyx mori"[Supplementary Concept] OR "ZDD4 protein, Bombyx mori"[Supplementary Concept])

#7 ("1-Deoxynojirimycin")

#8 ("miglitol")

#9 ("fagomine")

#10 ("quercetin")

#11 ("silk fibroin")

#12 #1 OR #2 OR #3 OR #4 OR #5

#6 AND #12 482(pubmed)

#7 AND #12 385(pubmed)

#8 AND (#1 OR #3 OR #4) 4(pubmed)

#9 AND #12 9(pubmed)

#10 AND (#1 OR #3 OR #4) 271(pubmed)

#11 AND #12 22(pubmed)

Abbreviations

ACE: Angiotensin-converting enzyme
ARB: Angiotensin II receptor blocker
DN: Diabetic nephropathy
GFR: Glomerular filtration rate
DNJ: 1-Deoxynojirimycin
TGF-β1: Transforming growth factor
NF-κB: Nuclear factor.

Conflict of Interests

The authors declare that there is no conflict of interests regarding the publication of this paper.

Acknowledgments

This study was an industry special scientific research project funded by the State Chinese Medicine Administration Bureau (no. 201007005), part of the Research Project for Practice Development of National TCM Clinical Research Bases.

References

[1] R. Breinbauer, M. Manger, M. Scheck, and H. Waldmann, "Natural product guided compound library development," *Current Medicinal Chemistry*, vol. 9, no. 23, pp. 2129–2145, 2002.

[2] F. E. Koehn and G. T. Carter, "The evolving role of natural products in drug discovery," *Nature Reviews Drug Discovery*, vol. 4, no. 3, pp. 206–220, 2005.

[3] D. Greenwood, "The quinine connection," *The Journal of Antimicrobial Chemotherapy*, vol. 30, no. 4, pp. 417–427, 1992.

[4] R. Wang, H. Yan, and X.-C. Tang, "Progress in studies of huperzine A, a natural cholinesterase inhibitor from Chinese herbal medicine," *Acta Pharmacologica Sinica*, vol. 27, no. 1, pp. 1–26, 2006.

[5] J. G. Mahdi, A. J. Mahdi, A. J. Mahdi, and I. D. Bowen, "The historical analysis of aspirin discovery, its relation to the willow tree and antiproliferative and anticancer potential," *Cell Proliferation*, vol. 39, no. 2, pp. 147–155, 2006.

[6] D.-X. Kong, X.-J. Li, G.-Y. Tang, and H.-Y. Zhang, "How many traditional Chinese medicine components have been recognized by modern western medicine? A chemoinformatic analysis and implications for finding multicomponent drugs," *ChemMedChem*, vol. 3, no. 2, pp. 233–236, 2008.

[7] C. W. Wright, "Traditional antimalarials and the development of novel antimalarial drugs," *Journal of Ethnopharmacology*, vol. 100, no. 1-2, pp. 67–71, 2005.

[8] T. W. Corson and C. M. Crews, "Molecular understanding and modern application of traditional medicines: triumphs and trials," *Cell*, vol. 130, no. 5, pp. 769–774, 2007.

[9] D.-X. Kong, X.-J. Li, and H.-Y. Zhang, "Where is the hope for drug discovery? Let history tell the future," *Drug Discovery Today*, vol. 14, no. 3-4, pp. 115–119, 2009.

[10] I. Paterson and E. A. Anderson, "The renaissance of natural products as drug candidates," *Science*, vol. 310, no. 5747, pp. 451–453, 2005.

[11] H. M. Hügel, N. Jackson, B. H. May, and C. C. I. Xue, "Chinese herbs for dementia diseases," *Mini-Reviews in Medicinal Chemistry*, vol. 12, no. 5, pp. 371–379, 2012.

[12] B. H. May, C. Lu, L. Bennett, H. M. Hügel, and C. C. L. Xue, "Evaluating the traditional Chinese literature for herbal formulae and individual herbs used for age-related dementia and memory impairment," *Biogerontology*, vol. 13, no. 3, pp. 299–312, 2012.

[13] B. H. May, Y. Lu, C. J. Lu, A. L. Zhang, S. Chang, and C. C. Xue, "Systematic assessment of the representativeness of published collections of the traditional literature on Chinese Medicine," *The Journal of Alternative and Complementary Medicine*, vol. 19, no. 5, pp. 403–409, 2013.

[14] A. T. Reutens and R. C. Atkins, "Epidemiology of diabetic nephropathy," *Contributions to Nephrology*, vol. 170, pp. 1–7, 2011.

[15] R. C. Atkins and P. Zimmet, "World Kidney Day 2010: diabetic kidney disease—act now or pay later," *American Journal of Kidney Diseases*, vol. 55, no. 2, pp. 205–208, 2010.

[16] S. Vupputuri, G. A. Nichols, H. Lau, P. Joski, and M. L. Thorp, "Risk of progression of nephropathy in a population-based sample with type 2 diabetes," *Diabetes Research and Clinical Practice*, vol. 91, no. 2, pp. 246–252, 2011.

[17] R. Hu, *Encyclopaedia of Traditional Chinese Medicine*, Hunan Electronic and Audio-Visual Publishing House, Changsha, China, 4th edition, 2006, (Chinese).

[18] G.-X. Zhou, J.-W. Ruan, M.-Y. Huang, W.-C. Ye, and Y.-W. He, "Alkaloid constituents from silkworm dropping of Bombyx mori," *Zhong Yao Cai*, vol. 30, no. 11, pp. 1384–1385, 2007 (Chinese).

[19] H. Yokoyama, S. Kannno, I. Ishimura, and K. Node, "Miglitol increases the adiponectin level and decreases urinary albumin excretion in patients with type 2 diabetes mellitus," *Metabolism*, vol. 56, no. 11, pp. 1458–1463, 2007.

[20] W.-H. Kong, S.-H. Oh, Y.-R. Ahn, K.-W. Kim, J.-H. Kim, and S.-W. Seo, "Antiobesity effects and improvement of insulin sensitivity by 1-deoxynojirimycin in animal models," *Journal of Agricultural and Food Chemistry*, vol. 56, no. 8, pp. 2613–2619, 2008.

[21] T. Uzu, H. Yokoyama, H. Itoh et al., "Elevated serum levels of interleukin-18 in patients with overt diabetic nephropathy: effects of miglitol," *Clinical and Experimental Nephrology*, vol. 15, no. 1, pp. 58–63, 2011.

[22] L. K. Campbell, D. E. Baker, and R. K. Campbell, "Miglitol: assessment of its role in the treatment of patients with diabetes mellitus," *The Annals of Pharmacotherapy*, vol. 34, no. 11, pp. 1291–1301, 2000.

[23] H.-Y. Wang, Y.-J. Wang, L.-X. Zhou, L. Zhu, and Y.-Q. Zhang, "Isolation and bioactivities of a non-sericin component from cocoon shell silk sericin of the silkworm Bombyx mori," *Food and Function*, vol. 3, no. 2, pp. 150–158, 2012.

[24] D.-Q. Tang, Y.-Q. Wei, X.-X. Yin et al., "In vitro suppression of quercetin on hypertrophy and extracellular matrix accumulation in rat glomerular mesangial cells cultured by high glucose," *Fitoterapia*, vol. 82, no. 6, pp. 920–926, 2011.

[25] P.-B. Lai, L. Zhang, and L.-Y. Yang, "Quercetin ameliorates diabetic nephropathy by reducing the expressions of transforming growth factor-β1 and connective tissue growth factor in streptozotocin-induced diabetic rats," *Renal Failure*, vol. 34, no. 1, pp. 83–87, 2012.

[26] R. Babujanarthanam, P. Kavitha, U. S. Mahadeva Rao, and M. R. Pandian, "Quercitrin a bioflavonoid improves the antioxidant status in streptozotocin: induced diabetic rat tissues," *Molecular and Cellular Biochemistry*, vol. 358, no. 1-2, pp. 121–129, 2011.

[27] F. N. Ziyadeh and D. C. Han, "Involvement of transforming growth factor-β and its receptors in the pathogenesis of diabetic nephropathy," *Kidney International, Supplement*, vol. 51, no. 60, pp. S7–S11, 1997.

[28] P. Chen, J. B. Chen, W. Y. Chen, ZhengQL, Y. Q. Wang, and X. J. Xu, "Effects of quercetin on nuclear factor-κB p65 expression in renal ubiquitin-proteasome system of diabetic rats," *Zhonghua Nei Ke Za Zhi*, vol. 51, no. 6, pp. 460–465, 2012 (Chinese).

[29] P. Chen, Q. Shi, X. Xu, Y. Wang, W. Chen, and H. Wang, "Quercetin suppresses NF-κB and MCP-1 expression in a high glucose-induced human mesangial cell proliferation model," *International Journal of Molecular Medicine*, vol. 30, no. 1, pp. 119–125, 2012.

[30] N. Asano, "Glycosidase inhibitors: update and perspectives on practical use," *Glycobiology*, vol. 13, no. 10, pp. 93R–104R, 2003.

[31] S. Taniguchi, N. Asano, F. Tomino, and I. Miwa, "Potentiation of glucose-induced insulin secretion by fagomine, a pseudo-sugar isolated from mulberry leaves," *Hormone and Metabolic Research*, vol. 30, no. 11, pp. 679–683, 1998.

[32] K. Nakagawa, K. Ogawa, O. Higuchi, T. Kimura, T. Miyazawa, and M. Hori, "Determination of iminosugars in mulberry leaves and silkworms using hydrophilic interaction chromatography-tandem mass spectrometry," *Analytical Biochemistry*, vol. 404, no. 2, pp. 217–222, 2010.

[33] T. Daimon, C. Hirayama, M. Kanai et al., "The silkworm green b locus encodes a quercetin 5-O-glucosyltransferase that produces green cocoons with UV-shielding properties," *Proceedings of the National Academy of Sciences of the United States of America*, vol. 107, no. 25, pp. 11471–11476, 2010.

[34] C. Hirayama, H. Ono, Y. Tamura, and M. Nakamura, "C-prolinylquercetins from the yellow cocoon shell of the silkworm, Bombyx mori," *Phytochemistry*, vol. 67, no. 6, pp. 579–583, 2006.

[35] C. Hirayama, H. Ono, Y. Tamura, K. Konno, and M. Nakamura, "Regioselective formation of quercetin 5-O-glucoside from orally administered quercetin in the silkworm, Bombyx mori," *Phytochemistry*, vol. 69, no. 5, pp. 1141–1149, 2008.

[36] B. H. May, C. Lu, and C. C. Xue, "Collections of traditional Chinese medical literature as resources for systematic searches," *Journal of Alternative Complementary Medicine*, vol. 18, no. 12, pp. 1101–1107, 2012.

[37] J.-P. Cosyns, M. Jadoul, J.-P. Squifflet, J.-F. De Plaen, D. Ferluga, and C. van Ypersele de Strihou, "Chinese herbs nephropathy: a clue to Balkan endemic nephropathy?" *Kidney International*, vol. 45, no. 6, pp. 1680–1688, 1994.

Hindawi Publishing Corporation
Evidence-Based Complementary and Alternative Medicine
Volume 2013, Article ID 459390, 9 pages
http://dx.doi.org/10.1155/2013/459390

Research Article

In Vitro Screening for Antihepatic Steatosis Active Components within Coptidis Rhizoma Alkaloids Extract Using Liver Cell Extraction with HPLC Analysis and a Free Fatty Acid-Induced Hepatic Steatosis HepG2 Cell Assay

Hui Fan,[1,2] Yuan-yuan Chen,[1] Wei-jian Bei,[1] Lai-you Wang,[1] Bao-tian Chen,[2] and Jiao Guo[1]

[1] *Key Unit of Modulating Liver to Treat Hyperlipemia SATCM (State Administration of Traditional Chinese Medicine), SATCM Level 3 Lab of Lipid Metabolism, Guangdong TCM Key Laboratory for Metabolic Diseases, Institute of Chinese Medicinal Sciences, Guangdong Pharmaceutical University, Guangzhou Higher Education Mega Centre, Guangzhou 510006, China*
[2] *College of TCM, Southern Medical University, Guangzhou 510515, China*

Correspondence should be addressed to Jiao Guo; jguozyy@hotmail.com

Received 13 October 2013; Accepted 22 October 2013

Academic Editor: Calvin Yu-Chian Chen

A high-throughput method was developed and applied to screen for the active antihepatic steatosis components within Coptidis Rhizoma Alkaloids Extract (CAE). This method was a combination of two previously described assays: HepG2 cell extraction with HPLC analysis and a free fatty acid-induced (FFA) hepatic steatosis HepG2 cell assay. Two alkaloids within CAE, berberine and coptisine, were identified by HepG2 cell extraction with HPLC analysis as high affinity components for HepG2. These alkaloids were also determined to be active and potent compounds capable of lowering triglyceride (TG) accumulation in the FFA-induced hepatic steatosis HepG2 cell assay. This remarkable inhibition of TG accumulation ($P < 0.01$) by berberine and coptisine occurred at concentrations of 0.2 μg/mL and 5.0 μg/mL, respectively. At these concentrations, the effect seen was similar to that of a CAE at 100.0 μg/mL. Another five alkaloids within CAE, palmatine, epiberberine, jateorhizine, columbamine, and magnoline, were found to have a lower affinity for cellular components from HepG2 cells and a lower inhibition of TG accumulation. The finding of two potent and active compounds within CAE indicates that the screening method we developed is a feasible, rapid, and useful tool for studying traditional Chinese medicines (TCMs) in treating hepatic steatosis.

1. Introduction

Hepatic steatosis, a condition characterized by excessive fat accumulation within hepatocytes, is becoming a serious global health threat. Despite this, there are currently no effective treatments available for this condition [1, 2]. Traditional Chinese medicines (TCMs) serve as an excellent alternative and/or complementary treatment for hepatic steatosis [3]. Previous work in China studying extracts classified as TCMs has found them effective as antihepatic steatosis agents [4–9]. However, due to the uncertainty concerning the active components of these extracts as well as the possible role of multiple components, clinical application has been limited [10]. Therefore, determining the active ingredients within these clinically applicable extracts is an important avenue of study.

In order to determine the active components against hepatic steatosis within these TCMs extracts, a high-throughput screening protocol was developed. One method within this protocol involves using cell extraction of the component of interest combined with HPLC analysis to identify which component from multicomponent materials has an affinity for cellular components [11]. This method is based on the affinity of the active component for the living cell, where the active components have the highest affinity for the cells and, therefore, can be extracted after the drug has been incubated with the cell line. The general procedure for cell extraction with HPLC analysis is as follows: the cells are

cultured, the drug is incubated with the cells, an elution is performed to remove any thing binding with low specificity binding, and a targeted extraction is done for high-affinity binding to cellular components followed by identification by HPLC analysis. This method has previously been successfully applied to screen active components from TCMs [12, 13].

Another screening assay available for determining antihepatic steatosis agents uses an *in vitro* free fatty-acid- (FFA-) induced hepatic steatosis HepG2 cell model. Oil Red O staining and intracellular triglyceride (TG) contents are used in this assay to evaluate the activity of the compounds of interest on lowering the lipid levels within the cells. This method has been used previously to validate the activity of components in TCMs [14, 15].

In this study, these two assays, HepG2 cell extraction with HPLC analysis and FFA-induced hepatic steatosis in HepG2 cells, were combined to develop a new method to screen for the antihepatic steatosis active components from Coptidis Rhizoma alkaloid extracts (CAE). The HepG2 cell extraction with HPLC analysis was used to screen for CAE components with high-affinity for hepatocytes. Then, the FFA-induced hepatic steatosis HepG2 cell assay verified the antisteatosis activity of the identified components.

Recent studies using high-fat feed induced hyperlipidemia animal models revealed that CAE may reduce total cholesterol (TC) and triglyceride (TG) levels [16]. Also, CAE has a hepatoprotective effect on CCl_4 induced acute liver injuries [17, 18]. These studies suggest that CAE has significant hepatoprotective effects and can be used to treat hepatic steatosis. However, CAE is composed of multiple components [19], predominantly several alkaloids: berberine, palmatine, jateorhizine, epiberberine, coptisine, columbamine, and magnoflorine. Presently, only berberine, the alkaloid present in the highest amount in CAE, has been paid much attention, whereas other alkaloids remain unstudied. We therefore used our screening method in order to explore the possible antihepatic steatosis active components in CAE.

2. Material and Reagents

Berberine, palmatine, coptisine, jateorhizine, and magnoflorine (Figure 1), purity of >98%, were purchased from Chengdu Herbpurify Co., LTD (Chengdu, China) for use as standards. Epiberberine and columbamine were supplied by the Chongqing Academy of Chinese Materia Medica. Sodium oleic and sodium palmitic were purchased from Sigma (Madrid, Spain). HPLC-grade acetonitrile was purchased from Honeywell International Inc. (Burdick & Jackson, Muskegon, MI, USA). Deionized water was purified using a PURELAB Ultra GE MK2 water system (ELGA, High Wycombe, UK). DMEM medium was from Gibco. Triglyceride enzymatic assay kits were from Nanjing Jiancheng Bioengineering Institute (Nanjing, China). All other reagents used were of analytical grade at minimum. Samples of Coptidis Rhizoma were provided by the Zhixin Chinese Herbal Medicine Co., Ltd. (Guangzhou, China) and authenticated by Professor Shuyuan Li, pharmacognosist of the School of Chinese Medicinal Sciences, Guangdong Pharmaceutical University.

3. Methods

3.1. The Preparation and Chromatographic Analysis of CAE. To prepare the CAE, a method mimicking the TCM approach was used [20]. Briefly, the dry rhizomes were cut into pieces, and 100 g was added to 600 mL of 70% ethanol and immersed for 30 min at 25°C. This mixture was heated under reflux for 120 min. Following filtration, the extraction was repeated on the residue twice for a total of three times. The three extract solutions were then combined and evaporated until the volume was 75 mL under reduced pressure. The alcohol extract was reconstituted with 1% acetic acid, adjusted to a pH of 3.0 using 1.0 mmol/L HCl and salted by adding in 6% NaCl. The precipitate from this step was dried at 40°C under a DZF-6021 vacuum drying oven (Hangzhou Lihui Environmental Testing Equipment Co. Ltd., Hangzhou, China).

For the chromatographic analysis, the HPLC system Dionex UltiMate 3000 (Dionex, Germany) used came equipped with Chromeleon software (Dionex) and was comprised of a quaternary pump, an online vacuum degasser, an autosampler, a thermostated column compartment, and DAD. All separations were carried out on a DIONEX Acclaim C_{18} column (250 mm × 4.6 mm, 5.0 μm) with the column temperature maintained at 30°C. The isocratic mobile phase was used and consisted of acetonitrile-potassium dihydrogen phosphate solution (0.015 mol/L) (40/60, v/v) (1.7 g/L sodium dodecyl sulfate, phosphoric acid to adjust to pH 3.0) pumped at a flow rate of 1.0 mL/min. The injection volume was 10 μL and the detection wavelength was 270 nm.

3.2. Cell Culture. HepG2 cells, a human hepatoblastoma cell line, were cultured at 37°C in a humidified 5% CO_2 atmosphere in high glucose Dulbecco's modified Eagle's medium (DMEM) supplemented with 10% fetal bovine serum (FBS) and an 1% antibiotic mixture of penicillin (100 U/mL) and streptomycin (100 mg/mL). This media was changed every 2 days until the cells were 70% confluent, usually 5–7 days after initial seeding. Prior to each experiment, the cells were cultured in the absence of FBS for 24 h.

3.3. Liver Cell Extraction. HepG2 cells were grown in a cell culture flask for at least 24 h prior to treatment with alkaloids. Once the HepG2 cells were 70% confluent, they were treated with a working solution of different alkaloids or DMEM alone as a negative control at 37°C for 24 h. A cell suspension was made from each experimental flask and was centrifuged at 210 ×g for 10 min. The supernatant was then removed and the remaining pellet was washed five times with 2 mL of PBS (pH 7.4) followed by centrifugation at 210 ×g for 10 min to remove any compounds binding with low affinity. The last one of PBS washes was collected and used as a low specificity reference for HPLC analysis. Finally, the cell pellet was lysed by adding 2 mL of 75% ethanol and repeatedly freeze-thawed. This solution was centrifuged at 8000 ×g for 10 min and the supernatant was filtered through a 0.22 μm membrane and analyzed by HPLC.

CAE was used at a working concentration of 100.0 μg/mL and incubated with HepG2 cells following the cell viability

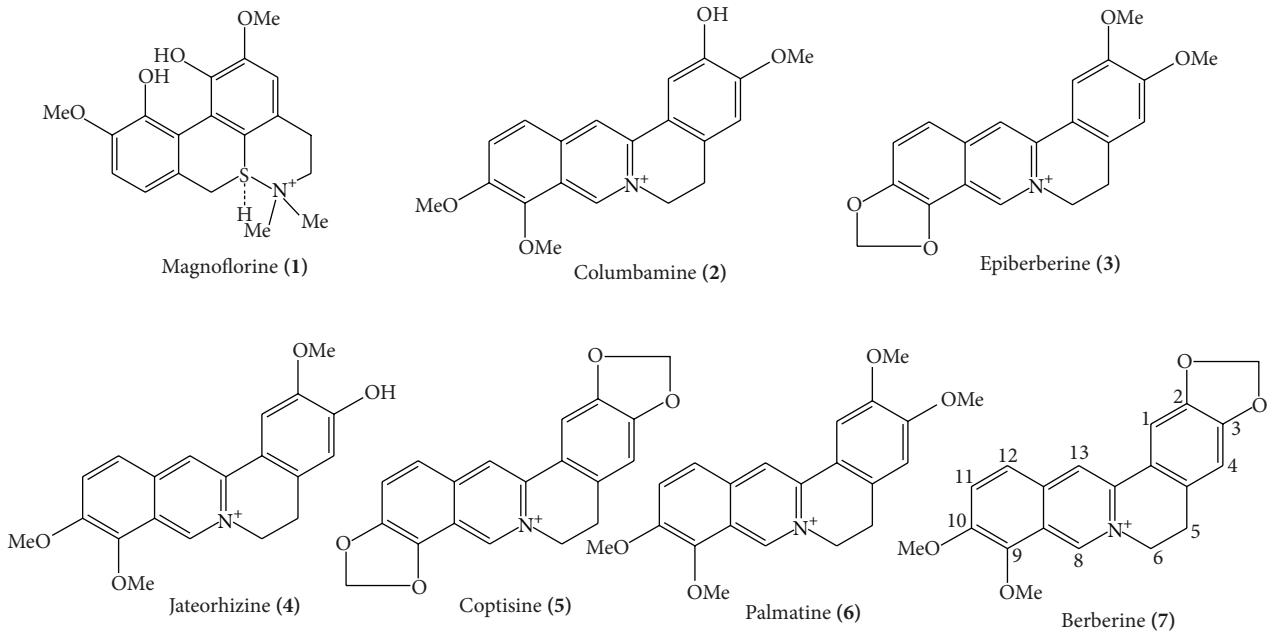

Figure 1: The chemical structure of seven alkaloids.

assay. A mixed standard working solution composed of the seven alkaloids in equal concentrations was prepared and incubated with HepG2 cells at 10 μg/mL. In addition, gemfibrozil, a lipid regulator, was used as a positive control for liver cell extraction at a working concentration of 100.0 μg/mL as previously described [21].

3.4. Cell Viability Assay. FFA-induced cytotoxicity of HepG2 cells was assessed by the (MTT) assay in the presence or absence of the alkaloids. After incubating for 24 h, 20 μL of MTT solution was added to each well and the plates were further incubated at 37°C for 4 h. The media was then removed, 100 μL of DMSO was added and the plates were gently shaken for 5 min. An enzyme-linked immunosorbent assay was performed and the optical absorbance was determined at 485 nm (Mithras LB 940, Berthold Technologies, Germany). Each condition was performed in triplicate.

3.5. In Vitro Antihepatic Steatosis Assay. HepG2 cells were seeded in 6-well plates at a density of 2×10^5 cells in 2.0 mL/well of 10% FBS-DMEM medium and incubated for 48 h. Upon reaching 80–90% confluency, the cultured cells were incubated with 0.5 mmol/L FFA (sodium oleic/sodium palmitic, 2 : 1) plus the different alkaloid solutions for 24 h. The alkaloid solutions were applied to the cells at different concentrations and each sample was treated with preventive administration in the medium. One control consisted of cells exposed to the 0.5 mmol/L FFA in media in the absence of additional alkaloids or CAE and was designated the "model group." Another control consisted of cells treated with FFA-free medium. There were 6 parallel holes at every group.

All alkaloid reference standards were dissolved in DMSO. The appropriate concentrations of CAE were prepared in 0.1% hydrochloric acid. In order to investigate the dose-dependent effect of alkaloids on antihepatic steatosis, a series of concentrations of each alkaloid and the CAE were prepared.

3.6. Intracellular TG Content and Oil Red O Staining. The amount of lipid accumulation in HepG2 cells was investigated by measuring TG content and Oil Red O staining. Intracellular TG content was determined using the EnzyChrom triglyceride assay kit according to the manufacturer's instructions and was normalized to the total protein content of each experimental sample. Protein content was measured using the BCA Protein Assay Kit (Cwbiotech, China) according to the manufacturer's instructions. TG accumulation inhibition rates were calculated using the following equation:

$$\begin{aligned}&\text{TG accumulation on inhibition rate (\%)}\\&= \big((\text{TG contents of model group}\\&\qquad - \text{TG content of sample group})\\&\qquad \times (\text{TG content of model group})^{-1} \big) \times 100.\end{aligned} \tag{1}$$

The Oil Red O staining was performed by fixing the samples in 4% paraformaldehyde and then staining with Oil Red O for 15 min. The samples were washed with isopropanol for a few seconds, followed by three distilled water washes. Results were determined by inverted fluorescence microscopy (HAL-100 Zeiss, Germany).

3.7. Statistical Analysis. The data is displayed as mean ± SD. Statistical significance between each experimental group was determined by Student's test using SPSS software (version 16.0), where $P < 0.05$ was considered statistically significant.

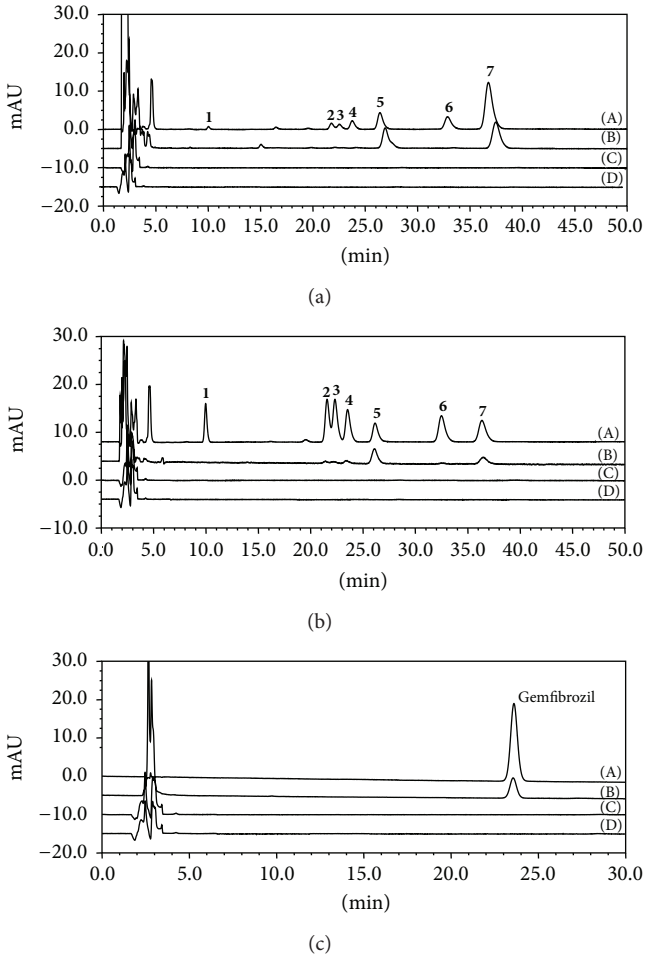

Figure 2: The HPLC chromatograms of HepG2 cell extracts analyzed at 270 nm following treatment with (a) CAE, (b) a mixed standard of seven alkaloids, or (c) gemfibrozil. The lines for ((A)–(D)) represent the (A) sample work solution, (B) the denatured desorption elute of HepG2 cells incubated with sample, (C) the final washing elute of HepG2 cells incubated with sample, and (D) the denatured desorption eluate of HepG2 cells cultured in medium without sample (blank). Peaks identified as (**1**) magnoflorine, (**2**) columbamine, (**3**) epiberberine, (**4**) jateorhizine, (**5**) coptisine, (**6**) palmatine, and (**7**) berberine.

4. Results

4.1. The Chromatographic Analysis of CAE. The chromatographic parameters were optimized to achieve high resolution of all seven alkaloids in the CAE solution. The seven alkaloids were able to be clearly separated and detected by UV detector at 270 nm as shown in Figure 2(a)-Line (A). The reference standards were used to quantify each alkaloid within CAE at the 100.0 μg/mL concentration. The data showed that the alkaloid present at the highest amount was berberine at 31.74 μg/mL. The next most abundant were coptisine and palmatine at 10.64 μg/mL and 9.10 μg/mL, respectively. The other alkaloids were present at lower concentrations with epiberberine at 4.56 μg/mL, columbamine at 1.44 μg/mL, magnoflorine at 1.30 μg/mL, and jateorhizine at 1.10 μg/mL. The comparison of the chromatogram of CAE in Figure 2(a)-Line (A) and the mixed reference standard in Figure 2(b)-Line (A) indicated that the seven alkaloids are the major peaks seen in CAE and make up 59.88% of the CAE solution.

4.2. Cytotoxic Effect on HepG2 Cells. HepG2 cells were treated with 0–2.0 mmol/L FFA mixture (sodium oleic/sodium palmitic, 2 : 1) for 24 h and the FFA-induced cytotoxicity of HepG2 cells was measured by MTT assay. FFA was not cytotoxic at concentrations lower than 1.0 mmol/L. The cytotoxicity of different concentrations of the alkaloids and CAE combined with FFA (0.5 mmol/L) were subsequently measured by MTT assay. It was found that CAE had no toxicity on HepG2 cells in the tested concentrations of up to 100.0 μg/mL. Also, there were no cytotoxic effects of each alkaloid on HepG2 cells at concentrations of less than 50.0 μg/mL during 24 h incubation.

4.3. Liver Cell Extraction. Chromatograms of CAE liver cell extractions are shown in Figure 2(a). There were two peaks detected by HPLC at 270 nm in the extract of denatured HepG2 cells (Figure 2(a)-Line (B)). By comparing each peak's retention time with the corresponding standard (Figure 2(b)-Line (B)), peaks 5 and 7 were identified as coptisine at 26.4 min and berberine at 36.8 min. The chromatogram of the low-specificity elution was used (Figure 2(a)-Line (C)) to discount any confounding peaks that the eluting process may produce. Meanwhile, the blank liver cell extraction without added CAE or alkaloids was performed to discount any peaks from the cell components themselves (Figure 2(a)-Line (D)). The peaks that were determined to be from CAE or the alkaloids were absent from both the low-specificity elution and the blank cell extraction as berberine and coptisine are the two most abundant components of CAE. The next step was to explore whether the affinity of the tested compounds for the cells was related to the concentration of each component. Therefore, the mixed reference alkaloid solution was prepared containing the same concentration of each alkaloid, 10.0 μg/mL, and was used to treat HepG2 cells as previously described. Using this reference solution, we confirmed that berberine and coptisine, the same high-affinity components previously identified, were extracted from denatured HepG2 cells (Figure 2(b)-Line (B)). This suggests there is no correlation between the concentration of the substance and its binding affinity. Additionally, the peak areas ratio of berberine to coptisine following extraction was 1.22 higher than the 0.72 before extraction. It was suggested that the binding ability of coptisine to HepG2 cells is possibly stronger than that of berberine, regardless of the concentration of berberine in CAE. Berberine and coptisine were defined as components capable of binding with high-affinity to liver cells, while the other five alkaloids can bind with low affinity. The gemfibrozil used as a positive control demonstrated that the extraction from HepG2 cells was successful (Figure 2(c)).

4.4. FFA-Induced Hepatic Steatosis HepG2 Cells Model. A hallmark of hepatic steatosis is abnormal TG accumulation

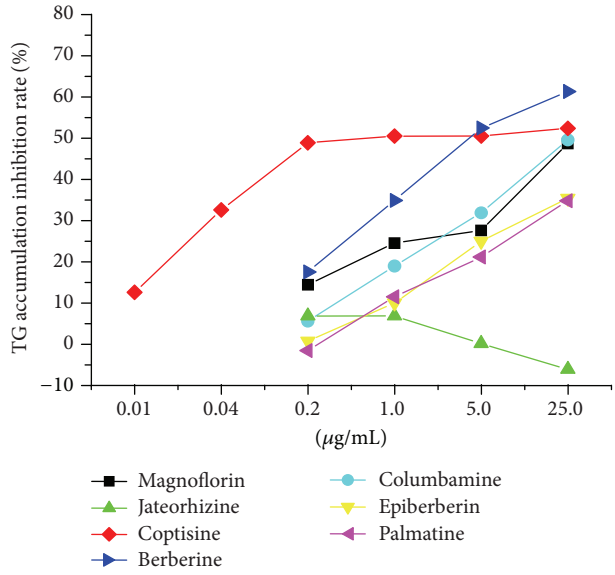

FIGURE 3: The trend chart of the rate of TG accumulation inhibition following treatment with alkaloids at different concentrations on a hepatic steatosis HepG2 cell model.

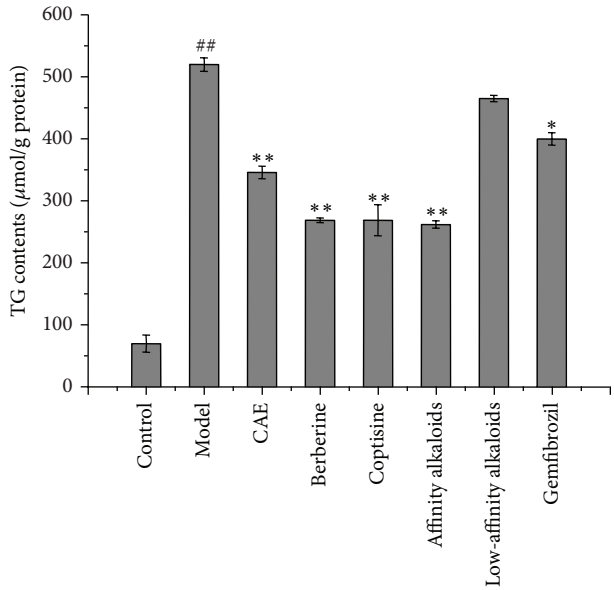

FIGURE 4: The combinatorial analysis of seven alkaloids: 50.0 μg/mL CAE, 15.87 μg/mL of berberine, 5.32 μg/mL of coptisine, a high-affinity alkaloid group composed of 15.87 μg/mL berberine, 5.32 μg/mL coptisine, a low-affinity alkaloid group composed of 4.55 μg/mL palmatine, 2.28 μg/mL epiberberine, 0.55 μg/mL jateorhizine, 0.72 μg/mL columbamine, 0.65 μg/mL magnoline, and 100.0 μg/mL gemfibrozil. The selected concentration of alkaloids was based on the concentration ratio within 50.0 μg/mL CAE.

within liver cells. An *in vitro* FFA-induced hepatic steatosis HepG2 cell assay has been previously employed and acknowledged as an effective screening model. FFA consisting of oleic acid/palmitic acid added exogenously at a 2 : 1 ratio has been reported to be optimum for inducing this condition [22]. In order to increase the solubility of oleic acid and palmitic acid in the growth medium, the FFA mixture of sodium oleic/sodium palmitic at a 2 : 1 ratio was used and then the concentration was further optimized. It was found that FFA treatment at concentrations from 0.1 to 2.0 mmol/L for 24 h resulted in a dose-dependent intracellular TG level increase that was significant ($P < 0.01$) up to 0.5 mmol/L FFA as compared to the control group. When administering the combination of alkaloids, the concentration of 0.5 mmol/L FFA (sodium oleic/sodium palmitic at 2 : 1) was decided on as the induction concentration of the model group. Oil Red O staining (Figure 5(b)) shows that lipid droplets accumulated significantly in the HepG2 cell cytoplasm at 0.5 mmol/L FFA.

4.5. TG Reduction by CAE and Alkaloids. First, a series of CAE concentrations was used to treat the hepatic steatosis HepG2 cell model for 24 h. It was found that CAE treatment at concentrations ranging from 12.5 μg/mL to 100.0 μg/mL had a TG reducing effect in a dose-dependent manner, whereas 50.0 μg/mL achieved the significant inhibitory effect ($P < 0.01$) shown in Figure 4. This indicated that CAE had anti-TG accumulation activity.

We previously found that seven alkaloids make up the main marker peaks in chromatographic analysis of CAE. Therefore, the TG reduction ability of every alkaloid was evaluated using a series of concentrations for each alkaloid. The concentrations of each alkaloid were determined based on their relative content within 100.0 μg/mL CAE. Each alkaloid was applied at concentrations of 0.2, 1.0, 5.0, and 25.0 μg/mL, and the inhibition of TG accumulation was evaluated. Table 1 shows the TG inhibition activity of each alkaloid concentration series. Several major results were found. (1) Berberine exhibited a potent inhibitory effect on the intracellular TG levels in a dose-dependent manner at 0.2 μg/mL with a significance of $P < 0.05$ and 1.0 μg/mL with a significance

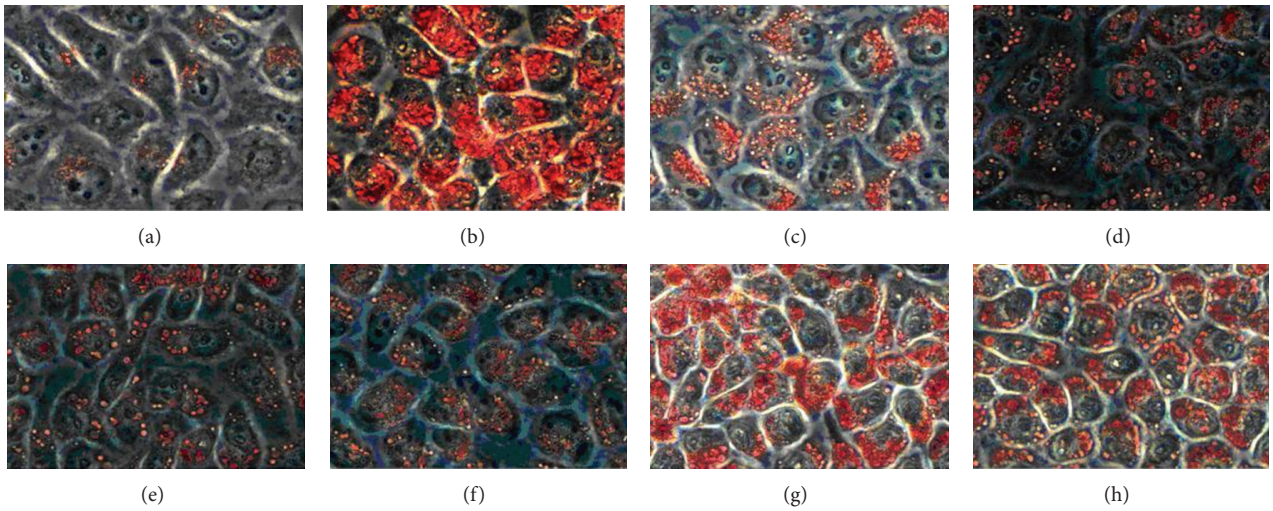

Figure 5: The Oil Red O staining (400x) effect of combinatorial treatment: (a) control cells, (b) 0.5 mmol/L FFA-induced steatosis model cells, (c) 50.0 μg/mL CAE, (d) 15.87 μg/mL berberine, (e) 5.32 μg/mL coptisine, (f) a high-affinity alkaloid group composed of 15.87 μg/mL berberine and 5.32 μg/mL coptisine, (g) a low-affinity alkaloid group composed of 4.55 μg/mL palmatine, 2.28 μg/mL epiberberine, 0.55 μg/mL jateorhizine, 0.72 μg/mL columbamine, and 0.65 μg/mL magnoline, and (h) 100.0 μg/mL gemfibrozil.

of $P < 0.01$. The highest concentration tested, 25.0 μg/mL, had a remarkable ability to inhibit 61.3% of TG accumulation. (2) Coptisine demonstrated the strongest inhibitory effect on the intracellular TG levels; however, there was no dose-dependent effect seen from concentrations of 0.2 μg/mL to 25 μg/mL. At a 0.2 μg/mL concentration, coptisine already significantly ($P < 0.01$) reduced TG accumulation by 48.9%. However, a dose-dependent effect was seen at the lower end of the concentration gradient, 0.01 μg/mL ($P < 0.05$) to 0.2 μg/mL ($P < 0.01$), during additional treatments. (3) Although palmatine, columbamine, epiberberine, and magnoflorine also exhibited a dose-dependent relationship with intracellular TG level reduction, it was only at the highest concentration, 5.0 μg/mL, that this reduction was significant ($P < 0.01$). (4) Jateorhizine failed to inhibit the FFA-induced hepatic steatosis model at concentrations ranging from 0.2 μg/mL to 25.0 μg/mL and had no dose-dependent effect. To better understand the inhibition activity of the seven alkaloids, the TG inhibition rate for each alkaloid at each concentration tested was expressed as a trend graph (Figure 3). At a 5.0 μg/mL concentration, the alkaloids ware differentiated into two groups: a high activity group consisting of coptisine and berberine, and a low activity group consisting of the rest of the alkaloids. The inhibition by coptisine was more potent than berberine at lower concentrations ranging from 0.2 μg/mL to 1.0 μg/mL. Compared to coptisine and berberine, the other alkaloids tested, not including jateorhizine, showed a weaker inhibition of TG accumulation. Jateorhizine failed to measurably inhibit TG accumulation.

4.6. TG Reduction Capabilities of Alkaloid Combinations. A combinatorial analysis was carried out to further verify the TG accumulation inhibition activity of coptisine and berberine, as well as evaluate whether the alkaloids have any synergistic or antagonistic effects with one another. The coptisine and berberine were combined to make a high-affinity alkaloid group, while the other five alkaloids were combined to make a low-affinity alkaloid group at concentrations based on their abundance in 50.0 μg/mL CAE. The TG reduction results are shown in Figure 4. The high-affinity alkaloid group had a potent inhibitory effect on TG reduction ($P < 0.01$), whereas the low-affinity alkaloid group still showed no significant inhibition. Compared with coptisine and berberine alone, the combination coptisine and berberine group had no increase in TG reduction, indicating there are no synergistic effects by these alkaloids on TG accumulation. Supporting these results, Oil Red O staining (Figure 5) showed that the lipid droplets were decreased significantly in the high activity component treatment groups, including CAE, berberine, coptisine, and the combination coptisine and berberine group, whereas the low-affinity alkaloid combined group showed a weak effect.

5. Discussions

The metabolism of oral drugs starts with absorption into the bloodstream, where the drugs are maintained in their ingested form or metabolized and then delivered into organs and cells. In this study, a comprehensive pharmacokinetic study was undertaken. Prototype alkaloids, including jateorhizine, berberine, coptisine, and palmatine have previously been identified and quantified in rat plasma following oral administration by Wuji Pill using LC-MS/MS [23]. Further investigation by Xiexin Decoction in rats found that three of these, alkaloids, coptisine, palmatine, and berberine, remained in their nascent form when measured in rat urine [24]. These results demonstrate that berberine and coptisine do not get metabolized in the blood and are excreted in their original form from the urine. This suggests that berberine and

Table 1: Intracellular TG content of hepatic steatosis cell model treated with alkaloids.

Sample group	Magnoflorine	Columbamine	Jateorhizine	Epiberberine	Coptisine	Palmatine	Berberine
Control group	37 ± 03	42 ± 12	57 ± 06	79 ± 10	39 ± 07	70 ± 14	47 ± 13
Model group	464 ± 34$^{\#\#}$	456 ± 32$^{\#\#}$	510 ± 15$^{\#\#}$	520 ± 31$^{\#\#}$	485 ± 29$^{\#\#}$	520 ± 11$^{\#\#}$	473 ± 12$^{\#\#}$
0.01 μg/mL					424 ± 15		
0.04 μg/mL					327 ± 12*		
0.2 μg/mL	397 ± 22	438 ± 06	475 ± 07	516 ± 09	248 ± 09**	528 ± 15	390 ± 04*
1.0 μg/mL	350 ± 19*	376 ± 23*	475 ± 01	468 ± 29	240 ± 03**	460 ± 06*	308 ± 08**
5.0 μg/mL	336 ± 06*	316 ± 13**	509 ± 19	390 ± 13*	240 ± 15**	410 ± 27**	225 ± 12**
25.0 μg/mL	276 ± 25**	234 ± 21**	541 ± 14	336 ± 11**	231 ± 06**	339 ± 24**	183 ± 03**

*Indicates a significant difference compared with model group cells, and # indicates a significant difference compared with control group cells. Values were mean ± SD ($n = 6$) and expressed in μmol/g protein.
$^{*}P < 0.05$, $^{**}P < 0.01$, $^{\#\#}P < 0.01$.

coptisine could reach the hepatic and liver cells. Therefore, the high-affinity interaction we demonstrated in our work should occur. The other alkaloids studied here would either fail to enter into blood or have no affinity for liver cells.

Previous work has found evidence that berberine affects glucose metabolism, leading to an increase in insulin secretion, suppression of adipogenesis, inhibition of mitochondrial function, and activation of the 5′ adenosine monophosphate-activated protein kinase (AMPK) pathway [25–28]. This antidiabetic and insulin sensitizing effect of berberine has been confirmed in a few relatively small, short-term clinical trials [29]. To date, very few reports on the lipid regulation by the other alkaloids derived from CAE have been published. In our experiments, coptisine had a superior lipid reducing effect compared with berberine. Several studies of the pharmacologic activity of coptisine have reported vasorelaxant action [30], a cardioprotective effect [31], an antidiabetic effect [32], and an antimicrobial effect [33]. This suggests that coptisine deserves to be further explored as an antihepatic steatosis agent. However, other alkaloids, including palmatine, jateorhizine, epiberberine, columbamine, and magnoflorine, also have a certain degree of lipid reduction activity. Our work demonstrated that the five other alkaloids had weak activity as antihepatic steatosis agents singularly and no observable synergistic effect.

The relationship between the structure and activity of the seven alkaloids in CAE is very interesting. All seven are derivatives of benzyl tetrahydroisoquinoline alkaloids. However, there are subtle differences between them due to substitution groups (Figure 1) that result in the affinity and activity differences observed in our experiments. Structural analysis revealed that berberine and coptisine possess a common methylenedioxy group at C2, C3, differing from the other alkaloids. The reports on the relationship between the structure and function have proven that when methylenedioxy groups were substituted in, an enhancement of the antibacterial activity of the alkaloids was seen. Meanwhile, there was an increased toxic effect when substituted with methoxyl groups [34, 35]. Berberine studies have also showed that methylenedioxy groups at C2, C3 are important groups for antimicrobial [33] and antifungal properties [36]. In addition, the methylenedioxy group plays an important role in hepatic mitochondrial-reduced glutathione (GSH) stimulatory activity as shown from schisandrin studies [37]. These results suggest that methylenedioxy could be a key active group in antihepatic steatosis. Moreover, besides a common methylenedioxy group at C2, C3, coptisine has another methylenedioxy group at C9, C10, while berberine has a methoxyl group at the C9, C10.

Lipid metabolism in hepatocytes is primarily regulated by the homeostasis of intracellular lipid within the cells. Fatty acid β-oxidation and VLDL equipment are both located within the cytoplasm. The nuclear receptors regulating lipogenesis, also located in the cytoplasm, include SREBP-1C, PPAR-α, and LXR [1, 2]. Therefore, antihepatic steatosis agents must display an affinity for the cell membrane or become intracellular to have an effect. Liver cell extraction with HPLC analysis is a method of screening for components with a high-affinity towards hepatocytes, suggesting that this method is suitable for screening for antihepatic steatosis studies. In order to increase the specificity of this method, *in vitro* FFA-induced hepatic steatosis of HepG2 liver cells was also used as an evaluative tool after liver cell extraction. Because the same type of cells was used in both the screening and evaluation, an agreement between the two methods was guaranteed. It believed that this method will be applicable and a strong tool for studying other multicomponential extracts from TCMs, such as flavonoids, saponins, and terpenes acid.

Conflict of Interests

The authors declare no competing financial interests.

Acknowledgments

This work was financially supported by a collaboration in industry, education, and research of Guangdong province and Ministry of Education of P.R. China (2011B090400379), by the team project of Nature Science Foundation of Guangdong Province, China (10351022401000000), and by the Natural Science Foundation of Guangdong Province, China (S2012010009288 and S2013010015021).

References

[1] S. C. Matherly and P. Puri, "Mechanisms of simple hepatic steatosis: not so simple after all," *Clinics in Liver Disease*, vol. 16, no. 3, pp. 505–524, 2012.

[2] B. W. Smith and L. A. Adams, "Nonalcoholic fatty liver disease and diabetes mellitus: pathogenesis and treatment," *Nature Reviews Endocrinology*, vol. 7, no. 8, pp. 456–465, 2011.

[3] K. Q. Shi, Y. C. Fan, W. Y. Liu et al., "Traditional Chinese medicines benefit to nonalcoholic fatty liver disease: a systematic review and meta-analysis," *Molecular Biology Reports*, vol. 39, no. 10, pp. 9715–9722, 2012.

[4] Z.-Q. Xie, G. Liang, L. Zhang et al., "Molecular mechanisms underlying the cholesterol-lowering effect of *Ginkgo biloba* extract in hepatocytes: a comparative study with lovastatin," *Acta Pharmacologica Sinica*, vol. 30, no. 9, pp. 1262–1275, 2009.

[5] X. Gu, Z. Xie, Q. Wang et al., "Transcriptome profiling analysis reveals multiple modulatory effects of *Ginkgo biloba* extract in the liver of rats on a high-fat diet," *FEBS Journal*, vol. 276, no. 5, pp. 1450–1458, 2009.

[6] S.-Y. Pan, Z.-L. Yu, H. Dong, C.-J. Xiang, W.-F. Fong, and K.-M. Ko, "Ethanol extract of fructus schisandrae decreases hepatic triglyceride level in mice fed with a high fat/cholesterol diet, with attention to acute toxicity," *Evidence-Based Complementary and Alternative Medicine*, vol. 2011, Article ID 729412, 6 pages, 2011.

[7] J.-Q. Wang, J. Li, Y.-H. Zou et al., "Preventive effects of total flavonoids of *Litsea coreana* leve on hepatic steatosis in rats fed with high fat diet," *Journal of Ethnopharmacology*, vol. 121, no. 1, pp. 54–60, 2009.

[8] X. Hong, H. Tang, L. Wu, and A. Li, "Protective effects of the *Alisma orientalis* extract on the experimental nonalcoholic fatty liver disease," *The Journal of Pharmacy and Pharmacology*, vol. 58, no. 10, pp. 1391–1398, 2006.

[9] H.-D. Yuan, H.-Y. Yuan, S.-H. Chung, G.-Z. Jin, and G.-C. Piao, "An active part of *Artemisia sacrorum* ledeb. Attenuates hepatic lipid accumulation through activating AMP-activated protein kinase in human HepG2 cells," *Bioscience, Biotechnology, and Biochemistry*, vol. 74, no. 2, pp. 322–328, 2010.

[10] Y. Feng, X. Lin, L. Shen, and Y. L. Hong, "Pharmaceutical study on multi-component traditional Chinese medicines," *China Journal of Chinese Materia Medica*, vol. 38, no. 5, pp. 629–632, 2013.

[11] S.-L. Li, P. Li, L.-H. Sheng, R.-Y. Li, L.-W. Qi, and L.-Y. Zhang, "Live cell extraction and HPLC-MS analysis for predicting bioactive components of traditional Chinese medicines," *Journal of Pharmaceutical and Biomedical Analysis*, vol. 41, no. 2, pp. 576–581, 2006.

[12] X. X. Yang, Y. L. Zhang, X. X. Zhang, and X. N. Li, "Cell membrane chromatography and its application in the analysis of bioactive ingredients of TCMs," *Journal of Chinese Pharmaceutical Sciences*, vol. 20, no. 1, pp. 20–25, 2011.

[13] M. Hong, H.-Y. Ma, X.-R. Wu, Y.-Q. Hua, Q. Zhu, and H.-W. Fan, "A method of hepatocyte extraction conjugated with HPLC is established for screening potential active components in chinese medicines—probing *Herba Artemisiae Scopariae* as an exemplifying approach," *Molecules*, vol. 17, no. 2, pp. 1468–1482, 2012.

[14] Y. Liu, D. Wang, D. Zhang et al., "Inhibitory effect of blueberry polyphenolic compounds on oleic acid-induced hepatic steatosis in vitro," *Journal of Agricultural and Food Chemistry*, vol. 59, no. 22, pp. 12254–12263, 2011.

[15] J.-F. Liu, Y. Ma, Y. Wang, Z.-Y. Du, J.-K. Shen, and H.-L. Peng, "Reduction of lipid accumulation in HepG2 Cells by luteolin is associated with activation of AMPK and Mitigation of oxidative stress," *Phytotherapy Research*, vol. 25, no. 4, pp. 588–596, 2011.

[16] W. Xie, D. Gu, J. Li, K. Cui, and Y. Zhang, "Effects and action mechanisms of berberine and *Rhizoma coptidis* on gut microbes and obesity in high-fat diet-fed C57BL/6J mice," *PLoS ONE*, vol. 6, no. 9, Article ID e24520, 2011.

[17] Y. Feng, N. Wang, X. Ye et al., "Hepatoprotective effect and its possible mechanism of *Coptidis rhizoma* aqueous extract on carbon tetrachloride-induced chronic liver hepatotoxicity in rats," *Journal of Ethnopharmacology*, vol. 138, no. 3, pp. 683–690, 2011.

[18] X. Ye, Y. Feng, Y. Tong et al., "Hepatoprotective effects of *Coptidis rhizoma* aqueous extract on carbon tetrachloride-induced acute liver hepatotoxicity in rats," *Journal of Ethnopharmacology*, vol. 124, no. 1, pp. 130–136, 2009.

[19] D. Wang, Z. Liu, M. Guo, and S. Liu, "Structural elucidation and identification of alkaloids in Rhizoma Coptidis by electrospray ionization tandem mass spectrometry," *Journal of Mass Spectrometry*, vol. 39, no. 11, pp. 1356–1365, 2004.

[20] Y. Cao, W. Bei, Y. Hu et al., "Hypocholesterolemia of Rhizoma Coptidis alkaloids is related to the bile acid by up-regulated CYP7A1 in hyperlipidemic rats," *Phytomedicine*, vol. 19, no. 8-9, pp. 686–692, 2012.

[21] K. Pahan, M. Jana, X. Liu, B. S. Taylor, C. Wood, and S. M. Fischer, "Gemfibrozil, a lipid-lowering drug, inhibits the induction of nitric-oxide synthase in human astrocytes," *The Journal of Biological Chemistry*, vol. 48, no. 277, pp. 45984–45991, 2002.

[22] J.-H. Chu, H. Wang, Y. Ye et al., "Inhibitory effect of schisandrin B on free fatty acid-induced steatosis in L-02 cells," *World Journal of Gastroenterology*, vol. 17, no. 19, pp. 2379–2388, 2011.

[23] J. Yuan, Y. Wang, R. An et al., "Simultaneous determination of six alkaloids and one monoterpene in rat plasma by liquid chromatography-tandem mass spectrometry and pharmacokinetic study after oral administration of a Chinese medicine Wuji Pill," *Journal of Chromatography B*, vol. 895-896, pp. 154–161, 2012.

[24] B. Tan, Y. Ma, R. Shi, and T. Wang, "Simultaneous quantification of three alkaloids of Coptidis Rhizoma in rat urine by high-performance liquid chromatography: application to pharmacokinetic study," *Biopharmaceutics and Drug Disposition*, vol. 28, no. 9, pp. 511–516, 2007.

[25] L.-J. Xing, L. Zhang, T. Liu, Y.-Q. Hua, P.-Y. Zheng, and G. Ji, "Berberine reducing insulin resistance by up-regulating IRS-2 mRNA expression in nonalcoholic fatty liver disease (NAFLD) rat liver," *European Journal of Pharmacology*, vol. 668, no. 3, pp. 467–471, 2011.

[26] X. Chang, H. Yan, J. Fei et al., "Berberine reduces methylation of the MTTP promoter and alleviates fatty liver induced by a high-fat diet in rats," *Journal of Lipid Research*, vol. 51, no. 9, pp. 2504–2515, 2010.

[27] J. Tang, Y. Feng, S. Tsao, N. Wang, R. Curtain, and Y. Wang, "Berberine and Coptidis Rhizoma as novel antineoplastic agents: a review of traditional use and biomedical investigations," *Journal of Ethnopharmacology*, vol. 126, no. 1, pp. 5–17, 2009.

[28] F.-M. Ho, Y.-H. Liao, A.-J. Yang et al., "Anti-atherosclerotic action of Ger-Gen-Chyn-Lian-Tang and AMPK-dependent lipid lowering effect in hepatocytes," *Journal of Ethnopharmacology*, vol. 142, no. 1, pp. 175–187, 2012.

[29] A. F. Cicero and E. Tartagni, "Antidiabetic properties of berberine: from cellular pharmacology to clinical effects," *Hospital Practice*, vol. 40, no. 2, pp. 56–63, 2012.

[30] L. L. Gong, L. H. Fang, H. L. Qin, Y. Lv, and G. H. Du, "Analysis of the mechanisms underlying the vasorelaxant action of coptisine in rat aortic rings," *The American Journal of Chinese Medicine*, vol. 40, no. 2, pp. 309–320, 2012.

[31] L.-L. Gong, L.-H. Fang, S.-B. Wang et al., "Coptisine exert cardioprotective effect through anti-oxidative and inhibition of RhoA/Rho kinase pathway on isoproterenol-induced myocardial infarction in rats," *Atherosclerosis*, vol. 222, no. 1, pp. 50–58, 2012.

[32] H. A. Jung, N. Y. Yoon, H. J. Bae, B.-S. Min, and J. S. Choi, "Inhibitory activities of the alkaloids from Coptidis Rhizoma against aldose reductase," *Archives of Pharmacal Research*, vol. 31, no. 11, pp. 1405–1412, 2008.

[33] D. Yan, C. Jin, X.-H. Xiao, and X.-P. Dong, "Antimicrobial properties of berberines alkaloids in *Coptis chinensis* Franch bymicrocalorimetry," *Journal of Biochemical and Biophysical Methods*, vol. 70, no. 6, pp. 845–849, 2008.

[34] C.-C. Lin, L. T. Ng, F.-F. Hsu, D.-E. Shieh, and L.-C. Chiang, "Cytotoxic effects of *Coptis chinensis* and *Epimedium sagittatum* extracts and their major constituents (berberine, coptisine and icariin) on hepatoma and leukaemia cell growth," *Clinical and Experimental Pharmacology and Physiology*, vol. 31, no. 1-2, pp. 65–69, 2004.

[35] Y. Han, D. Yan, Y. Zhao, C. Peng, and X. Xiao, "Toxic effects of protoberberine alkaloids from *Rhizoma Coptidis* on *Tetrahymena thermophila* BF_5 growth based on microcalorimetry: a reliable evaluation method of structure-function relationship," *Journal of Thermal Analysis and Calorimetry*, vol. 108, no. 1, pp. 341–346, 2012.

[36] Y. Zhao, D. Yan, J. Wang, P. Zhang, and X. Xiao, "Anti-fungal effect of berberine on *Candida albicans* by microcalorimetry with correspondence analysis," *Journal of Thermal Analysis and Calorimetry*, vol. 102, no. 1, pp. 49–55, 2010.

[37] K. M. Ko and P. Y. Chiu, "Structural determinants of schisandrin B which enhance mitochondrial functional ability and glutathione status as well as heat shock protein expression in rat hearts and H9c2 cells," *Molecular and Cellular Biochemistry*, vol. 276, no. 1-2, pp. 227–234, 2005.

Hindawi Publishing Corporation
Evidence-Based Complementary and Alternative Medicine
Volume 2013, Article ID 674305, 10 pages
http://dx.doi.org/10.1155/2013/674305

Review Article

Cerebrospinal Fluid Pharmacology: An Improved Pharmacology Approach for Chinese Herbal Medicine Research

Yan-qing Wu,[1,2] Ying-wu Zhou,[3] Xiu-de Qin,[2] Sheng-yu Hua,[1] Yu-lian Zhang,[2] and Li-yuan Kang[1]

[1] *Institute of Traditional Chinese Medicine, Tianjin University of Traditional Chinese Medicine, Tianjin 300193, China*
[2] *The Second Hospital Affiliated to Tianjin University of Traditional Chinese Medicine, Tianjin 300150, China*
[3] *The Gu Lou Hospital of Traditional Chinese Medicine of Beijing, Beijing 100009, China*

Correspondence should be addressed to Li-Yuan Kang; klyzm@163.com

Received 19 September 2013; Revised 2 November 2013; Accepted 14 November 2013

Academic Editor: Calvin Yu-Chian Chen

Despite many successful applications of Chinese herbal medicine (CHM) in the treatment and prevention of neurological diseases (ND), the fully scientific understanding of CHM's action mechanisms had been hampered for lack of appropriate methods to explore the combinatorial rules, the synergistic mechanisms, and the molecular basis of CHM. As an improved pharmacology approach, cerebrospinal fluid pharmacology (CSFP), based on the fact that cerebrospinal fluid plays an important role in the health maintenance of specific survival environment for neurons and glial cells, has been constructed and applied to CHM research for treating ND. In the present review, the concept and advantages of CSFP are briefly introduced. The approaches and key technologies of CSFP in CHM research are also collated and analyzed. Furthermore, the developing tendency of CSFP is summarized, and its framework in CHM research is also proposed. In summary, CSFP provides a new strategy not only to eliminate some barriers of CHM research for treating ND, but also to broaden the pharmacology research for bridging the gap between CHM and modern medicine. Moreover, the advancements in CSFP will bring about a conceptual move in active ingredients discovery of CHM and make a significant contribution to CHM modernization and globalization.

1. Introduction

Many neurological diseases (ND) are caused or exacerbated by disparate physiological, pathological, environmental, and lifestyle factors. It is obvious that the hypothesis to search for highly selective single-target drugs interacting with a well-defined molecular target is meeting the challenges owing to the complex etiology and pathogenesis of ND. As the leading cause of disability, ND has attracted unprecedented attention from medical researchers around the world, and different types of drugs and medications are used for treating ND, such as intensive medication, rehabilitation therapy, and traditional Chinese medicine (TCM). TCM has been reevaluated and considered as one of the most important complementary or alternative medicine in most western countries and has been increasingly accepted worldwide [1]. Pharmaceutical companies have increasingly shifted their attention toward TCM for novel lead compounds, and increasing efforts have been devoted to study TCM, from which a large number of bioactive compounds have been isolated and studied [2–6]. Chinese herbal medicine (CHM), with the concept of multitarget or multicomponent therapy, has accumulated rich experience in treating ND and a large number of medical records [7–11] and drug design studies [12–16] published in international journals. These records not only enable people to understand the mechanisms of CHM with a new perspective, but also provide a modern theoretical basis for clinical applications. As an important potential source for the discovery of bioactive molecules with therapeutic effects, CHM is gaining increased attention for designing multitargets drugs, and domestic and foreign scholars have been devoted to elucidating the efficacy mechanisms and the material basis of CHM which belong to natural products and have already been proved to possess clear therapeutic action

on public health in the clinical setting [17–26]. However, the fully scientific understanding of CHM's action mechanisms has been hampered by the lack of appropriate methods that can explore the combinatorial rules, the synergistic pharmacological mechanisms, and the complex nature of CHM at the cellular and molecular levels. Thus how to make the cell biology technique in vitro coincides with the characteristics of CHM treatment is one of the major issues that need to be addressed.

Serum pharmacology is an external testing method to explore the mechanism of CHM at the cellular and molecular levels. However, owing to the presence of blood-brain barrier and the specific survival environment of neurons and glial cells in central nervous system (CNS), serum pharmacology has some limitations in CHM researches for treating ND. As a methodology and technology, cerebrospinal fluid pharmacology (CSFP) is an emerging pharmacological method mainly to the research of drugs for treating ND [27]. Since CSFP imitated the survival microenvironment of neurons and glial cells in CNS, the application of this method could improve the credibility of CHM pharmacology by eliminating the interference caused by the physical and chemical properties of the other solvent itself containing CHM. In addition, CSFP, as an improved pharmacology method in vitro, not only provides a new scientific research method to the effectiveness evaluation system of CHM, but also brought new ideas in studying the material basis and the efficacy mechanism of CHM. Moreover, this principle obviously coincides with the synergistic effects of multiple compounds and herbal formula, which are mainly based on the integrative and holistic ways.

In this present review, the concept and significance of CSFP are briefly introduced. Its application and potential role in CHM research are also collated and analyzed. Furthermore, the limitations and problems of CSFP are also discussed, and its framework for bridging the gap between CHM and modern medicine is proposed.

2. Concept and Approaches of CSFP in CHM Research

Pharmacology has provided fresh insight into the drug discovery. However, addressing the scientific suspense on the material basis and the efficacy mechanism of CHM is urgent in order to develop a pharmacological methodology based on the characteristics of CHM. Yan et al. [28] proposed that the methodology in CHM research must follow three principles of these combinations, that is, the combination of systems theory and reductionism, the combination of macroeconomic research and microscopic studies, and the combination of analysis in vivo and analysis in vitro, which pointed out the overall direction and principles of CHM research.

In order to investigate the action mechanism of CHM at the cellular level in vitro, serum pharmacology was adopted in the pharmacological investigation and the drug screening of the CHM [29]. serum pharmacology provides profitable approach to address some scientific suspense of CHM studies in vitro. However, along with the deepening of CHM research, there are some obvious flaws when using serum pharmacology to study CHM for treating ND. Therefore, the pharmacological method reflecting the material basis and mechanism of CHM for treating ND is really becoming the focus in modern CHM research. In 1999, to explore an effective method by which the pharmacological effects of CHM for treating ND could be correctly investigated, Mei et al. [30], inspired by the idea of serum pharmacology and based on the innovation and improvement of early methodology in the course of CHM research, created a novel concept of CSFP, which built on the fundamental concept that cerebrospinal fluid (CSF) is the immediate survival environment of neurons and glial cells in CNS.

The CSFP was informally established based on the study of Qingnao Yizhi prescription's effect on neurons damaged by glutamate. CSF and serum were, respectively, taken in 1–1.5 h after administration of CHM and added into the culture medium of astrocytes. After 48 h, a certain amount of the incubated medium was transferred into the neuron culture medium. The serum, but not the CSF, showed a certain degree of cytotoxicity on the astrocytes. The astrocytes medium stimulated by the CSF containing Qingnao Yizhi prescription could promote the neuron axon growth. The experiment verified the superiority of CSF to serum and the validity of the CSFP to evaluate the action mechanism of CHM in vitro, thus indicating that the CSFP is suitable CHM study [27]. Briefly, the CSFP is using CSF extracted from animals after administration of drugs to explore the material basis and the efficacy mechanism in vitro experiment. CSFP coincides with the fundamental characteristics of CHM in neurological therapeutic areas that many active substances are the metabolites or secreted products passed through blood-brain barrier to the CSF. It affords a rewarding assistance to the authenticity and reliability of the experimental results at a higher efficiency, and to improve the potency for drug discovery.

3. Advantages of CSFP in CHM Research

CSFP provided a new method to broaden the pharmacology research of CHM. This method has the following advantages. Firstly and most obviously, the physical and chemical properties of CSF are very similar to the survival environment of neurons and glial cells in CNS. CSFP could eliminate the interference caused by the physicochemical properties of the other solvent itself containing CHM, thus improving the credibility of CHM pharmacology. Secondly, metabolic inactivation, without being absorbed into the body, indirectly exert their therapeutic effects through signaling cascades such as 2, 3 messenger, which are the major pathways transformed into active ingredients from chemical ingredients of CHM. Thus makes the research for material basis and action mechanisms of CHM very difficult [31]. Both the active ingredients produced by a series of vivo biotransformation of CHM and the endogenous active ingredients produced by the body under the action of CHM are the pharmaceutical ingredients in CSF containing CHM. CSFP not only simulates the interaction between drugs and the body, but also precludes various confounding factors in these crude extracts

of CHM, thus improving scientific authenticity and feasibility in the research to clarify the efficacy material basis and action mechanisms of CHM for treating ND in vitro experiments. Thirdly, these factors affecting the experimental results in vitro, such as the toxic effects of the serum itself and the various questions on whether and which active ingredients of CHM passed through the blood brain barrier could be eliminated by using CSFP to explore the efficacy of CHM for treating ND, thus contributing to confirm the active components and the bioactive ingredients based on the efficacy of CHM for treating ND. Finally, using CSFP to explore the efficacy relationship and the dynamic changes of the active ingredients in CSF contributs to clarify the essence of CHM compatibility, thus providing a new method to promote the basic theory research of CHM.

4. Key Technologies of CSFP in CHM Research

As an emerging pharmacology used mainly to evaluate the material basis and action mechanisms of CHM in treatment of ND, the experimental conditions for CSFP are very immature and needed further improvement.

4.1. Selection of Animals Used to Extract CSF. The first key of CSFP is how to obtain effective CSF containing CHM. Theoretically, the animal used to extract CSF and the animal used to isolated cells should belong to the same genus, thus narrowing the differences in the physical, chemical, and biological characteristics of the two kinds of CSF and reducing the immune response owing to the species differences. Ma and Tian [32] explored the effect of the CSF containing Liuwei Dihuang pills (LDP) components extracted from different species (human, rabbit, and rat) on PC12 cell injured by $A\beta_{1-40}$. Surprisingly, there is no evident difference of the cell viability among the CSF containing LDP extracted from human group, the CSF containing LDP extracted from rabbit group, and the CSF containing LDP extracted from rat group. Furthermore, further studies on selection of animals in CSFP are needed to be validated.

4.2. Optimal Dose and Timing of Administration to Animals. In order to obtain the high-quality CSF containing drug, determining the timing of administration to animals should depend on the half-life of drug. CSF was taken from rabbits mainly in the period of 1–1.5 h [27], 1 d [33], 3 d [34–37], 3.5 d [38, 39], 7 d [40], and 15 d [41] after consecutive administration of CHM in currently CSFP studies. CSF was taken from rats after consecutive administration of CHM for 3 d and 3.5 d. CSF was taken from beagle dogs after administration of CHM for 2 months [42]. Owing to the complex composition of CHM, the time-effect relationship of CHM was probably used to determine the optimal time period. Studies demonstrated that CSF extracted from rat after administering Danggui Shaoyao powder or Nimodipine repetitiously (2 times/d × 3.5 d) exerted higher protective efficacy on PC12 cell than that after single administration of Danggui Shaoyao powder or Nimodipine [43, 44]. It is proposed that the CSF containing drugs should be extracted from animals after administerting drugs repetitiously.

In order to obtain CSF containing higher concentration drugs, most of the experimental researches intend to increase the dose to administration. It is noted that simply increasing the dose of administration to the animals is not necessarily a benefit to absorption, distribution, and metabolism of CHM, and thus increasing the CHM components in CSF. Conversely, CSF containing very high concentrations of drugs inhibited the vitality of neurons [45]. Therefore, in order to make the test conditions closer to the environment of the drug effect in the body, the optimal dose administrated to related animals should be converted according to the standard conversion rules of the adult dosage [34, 46].

4.3. Acquisition Time of CSF Containing Drugs. Since the different process of absorption, distribution, and metabolism are caused by various features of CHM and its multiple pharmaceutical formulations, thus, the active ingredients and thier amounts in CSF containing drugs are different to collect at different times. To verify the optimal acquisition time of CSF containing Tongsaimai tiny pill extracted from rats, Zhang et al. [47] explored the efficacy of CSF containing Tongsaimai tiny pill, collected at range from 0.5 to 3 hours after the last administration, following consecutively administration for 3 days on injured PC12 cells. The results demonstrated that the optimal acquisition time of CSF containing Tongsaimai tiny pill is at 2 hours after the last administration. Cui et al.'s experiment demonstrated that the optimal acquisition time of CSF containing Qingxin Kaiqiao decoction is also at 2 hours after the last administration [48]. In addition, Zhang et al.'s studies showed that 1.5 hour after the last administration is the optimal acquisition time of CSF containing Danggui Shaoyao powder [43].

4.4. Acquisition Methods of CSF Containing Drugs. Precise location for puncture is the key point of drawing CSF from experimental animals. Fu et al. [49] observed anatomic structure of cerebellomedullary cistern in rabbit and rat to decide the optimal percutaneous puncture position and direction. The district of cerebral dura mater covering over the cerebellomedullary cistern was thin, soft, and frangible to be pierced. The district projected on the skin of neck is in between external occipital protuberance and first cervical vertebra. The optimal percutaneous puncture positions for rabbit and rat were about 1.0–1.2 cm and 0.6–0.7 cm below the center of external occipital protuberance, respectively, when animals' head bended to thorax. The pinhead paralleled the parietal bone to pierce the skin and cerebral dura mater, and then reached cerebellomedullary cistern. The percutaneous puncture to this direction can effectively avoid injuring the medulla oblongata and blood vessels. Further studies [50, 51] also demonstrated that the method to collect CSF from foramen magnum is visual and convenient to operate, causing less injury and complications and possessing a high rate of success. In addition, the collection volume and the pass rate of using microinjector via spinal dura mater puncture under direct vision were much higher than those of

the cerebellomedullary cistern via percutaneous puncture and the gashed spinal dura mater under direct vision ($P < 0.01$) [52].

4.5. Preservation, Processing, and Additive Amount of CSF. The impact probably caused by preservation, processing, and additive amount of CSF containing drugs cannot be ignored at some main approaches in the drug development process. To establish the standard conditions in preservation, processing, and additive amount of CSF is very important to the CSFP method. How to process CSF is the first issue to consider. Surprisingly, The study of Zhang et al. [44] illustrated that there was no obvious statistical difference among the raw CSF containing Nimodipine and the CSF containing Nimodipine treated by heat (56°C), ethanol, or acetone, through the experiment to explore the protective effect of CSF containing Nimodipine on injured PC12 cells induced by the hydrogen peroxide under different conditions. Meanwhile, there was also no significant statistical difference of the protective effects on injured PC12 cells among the raw CSF containing optimized Danggui Shaoyao powder and the CSF containing Danggui Shaoyao powder treated by heat (56°C), ethanol, or acetone, through the experiment to explore the protective effect of CSF containing optimized Danggui Shaoyao powder on PC12 cells injured by the hydrogen peroxide under different conditions [43]. Thence, it is not necessary for the processing of CSF containing drugs after extracting from animals.

Preservation of CSF containing drugs is the key point of ensuring the authenticity with the experiment results. The study of Zhang et al. [44] demonstrated that the protective rates of CSF containing drugs preserved for 1 d, 15 d, and 30 d at −20°C cryopreservation were, respectively, 65.43%, 50.18% and 24.86% in the experiment to explore the protective effect of CSF containing drugs on PC12 cells injured by hydrogen peroxide. It is no doubt that the protective rates declined with the prolonging of the preserved time. It is suggested that the CSF containing drugs at −20°C cryopreservation are preserved no more than 30 days. In addition, the general added amount of CSF containing drugs is 10% or 20% of the medium in current studies [43, 44].

In summary, in order to make the test conditions closer to the environment of the drug effect in the body, it is suggested that the CSF containing drug may be prepared with 10% or 20% CSF without treating after being extracted from animals and preserved at −20°C no more than 30 days.

5. Application of CSFP in CHM Research

CHM, the ancient traditional treatment methodology popular in China and surrounding areas, has been recognized as a potential important pharmaceutical area of TCM and holds promise for preventing diseases in a holistic way [53]. In a very long period of clinical practice, it is known for its effectiveness and beneficial contribution to public health and disease control. However, the modern pharmacological mechanisms of CHM have not been fully established [54]. With increasing knowledge of the genes and molecular interactions, the researchers intend to adopt some pharmacology for CHM research and development. Up till now, CSFP in CHM research has been frequently reported. Figure 1 shows the developing tendency of CSFP studies from the data available in PubMed and China National Knowledge Infrastructure (CNKI) databases from 1999 to August 2013. The applications of CSFP, focused on the studies of CHM from classic and commonly used prescriptions for treating ND, were systematically summarized to demonstrate the significant value.

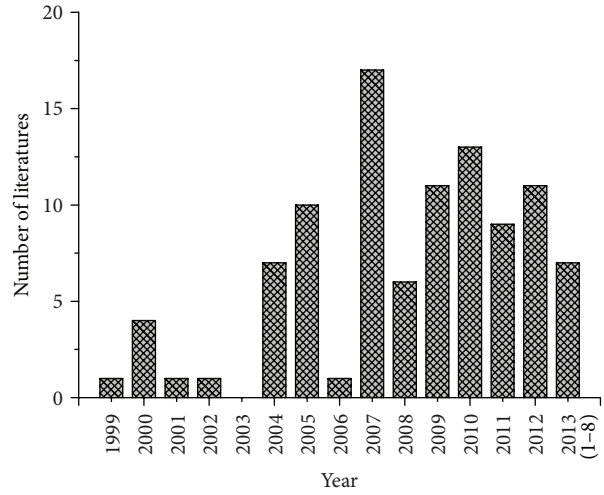

Figure 1: Developing tendency of CSF pharmacology study for CHM research. The publications of CSF pharmacology for CHM research in PubMed and CNKI databases from 1999 to August 2013. All results were screened in manual way.

5.1. Verify the Efficacy and Action Mechanism of CHM for Treating ND. To explore the efficacy and action mechanism of Qingnao Yizhi formula (QYF) for treating vascular dementia and multiinfarct dementia, Mei et al. [55, 56] utilized CSFP to investigate the effect of CSF-QYF on the cultured rabbit neurons injured by glutamate. CSF was taken at 1–1.5 h after administration of CHM and added into the culture medium of astrocytes. After 48 h, the incubated medium was transferred into the neuron culture medium according to a certain proportion. The results demonstrated that QYF could increase the survival rate of injured neuron, decrease LDH content in the culture medium, and increase the neuron survival activity in the culture medium. Meanwhile, it had no effect on the proliferation of astrogliocytes. These results showed that QYF can protect neurons from glutamate-induced injury by stimulating the secretion of neurotrophic factors from the astrogliocytes.

To investigate the protective effects of Jiawei Wuzi Yanzong formula (JWYF) on hippocampal neurons injured by beta-amyloid, an experimental model of Alzheimer's disease in vitro, Zeng et al. [57] used CSFP method to investigate the effect of CSF extracted from SD rats, respectively, fed with various components of JWYF (total formula, total flavonoids, or total polysaccharides) on beta-amyloid protein-induced

neurons. CSF containing JWYF showed significant neuroprotective effect, and the protection of CSF containing total flavonoids or total polysaccharides was significantly greater than that of CSF containing total formula. The results showed that some flavonoids and polysaccharide components in JWYF can pass through the blood-brain barrier and protect neurons from beta-amyloid protein-induced neuron injury to some extent.

To investigate the protective effects of the CSF with ancient prescriptions on PC12 cells injured by β-amyloid protein ($A\beta_{25-35}$), an experimental model of Alzheimer's disease in vitro, several studies manifested that CSF containing Dihuang decoction (CSF-DHD) can effectively reduce calcium ion internal flowing, reduce the protein expression of c-jun, c-fos, bax, caspase-3, and APP, enhance the expression of bcl-2, and improve the survival condition and the vitality of PC12 cells, following injury by $A\beta_{25-35}$, thus indicating that CSF-DHD has a protective effect on injured PC12 cell induced by $A\beta_{25-35}$ [58–62]. In addition, CSF-DHD can effectively decrease the releasing of LDH and increase the live activity of cultured hippocampal neurons injured by $A\beta_{25-35}$ [63].

PC12 cell induced by MPP+, an experimental model of Parkinson disease in vitro, was utilized to investigate the mechanism of ancient prescriptions on Parkinson disease. Studies showed that CSF containing Zhengan Xifeng decoction (CSF-ZGXFD) could remarkably restrain the expression of caspase-3 mRNA, Cyt c protein, phospho c-jun protein, mRNA and protein of Bax, and mRNA and protein of Bcl-2 and significantly upregulate mRNA and protein expression of Bcl-2 in PC12 cell induced by MPP+, thus indicating that CSF-ZGXFD has protective effects on injured PC12 cell induced by MPP+ [64–66].

The injured PC12 cells, cell models of ischemic stroke induced by hydrogen peroxide, sodium dithionite and glutamic acid respectively, was used to clarify the mechanisms of CHM on ischemic stroke. Yan et al.'s [67] experiment showed that CSF containing Tongsaimai tiny pill has a protective effect on injured PC12 cell by inhibiting intracellular calcium overload, free radical oxidative damage, and glutamate excitotoxicity.

Astrogia CRL-2541 cell injured by the high ammonia, a cell model of hepatic encephalopathy (HE), was utilized to explore mechanism of Ruhuang pill on hepatic encephalopathy. Studies [67, 68] showed that CSF containing Ruhuang pill increased the vitality of CRL-2541 cells injured under high ammonia and upregulated the GFAP expression, indicating that Ruhuang pill could enter in BBB and protect the injured astroglia in high ammonia, which suggests that astroglia is one of the targets of Ruhuang pill for treating HE.

5.2. Clarify Effective Constituents of CHM. Effect of CHM on neurological disease is based on comprehension of effective constituents of CSF containing CHM, which utilizes the CSFP analysis to speculate and estimate effects of drugs. It focuses on the specific component comparison between CSF containing CHM and serum containing CHM and provides assistance for drug effective evaluation and research. To confirm the main effective constituents in Sinisan freeze-dry powder with the improving sedative-hypnotic function, Li et al. [69, 70] used CSFP to explore the main active constituents of Sinisan freeze-dry powder. Surprisingly, the study identified that there were no other constituents of Sinisan freeze-dry powder absorbed into blood except for the pentobarbital natrium. However, the endogenous substance in CSF containing Sinisan freeze-dry powder was increased obviously. Synephrine, paeoniflorin, saikosaponin C, and glycyrrhetinic acid could make the peak area of endogenous substance (5-hydroxytryptamine, 5-HT) in CSF larger than that in blank CSF. But all their effects were less than those of Sinisan freeze-dry powder. The increasing peak area of 5-HT in CSF containing the mixture (synephrine : paeoniflorin : saikosaponin C : glycyrrhetinic acid = 17 : 2 : 3 : 13) was 3.2 times as much as that of Sinisan freeze-dry powder, thus indicating that the active constituents (synephrine, paeoniflorin, saikosaponin C, and glycyrrhetinic acid) in Sinisan freeze-dry powder are confirmed and could improve the sedative function.

5.3. Determine the Therapeutic Time Window of CHM. The chronomedicine theory of TCM is an integral part of the treatment in CHM [71–73]. From a macroperspective, it reflects the rhythm of human physiological activities and organs activities to regulate body functional imbalances and disorders. CSFP could be used for determining the therapeutic time window of CHM to guide clinic treatment, which integrates the information of "heaven corresponding humans" and emphasizes the close relationship between the body's natural rhythms.

The injured neurons induced by thrombin and hypoxic-ischemic, a cell model of acute intracerebral hemorrhage (AICH) in vitro, were used to observe the therapeutic time window of AICH intervened by Beagle dog CSF containing DSQ-03 herbal medicine. Guo et al.'s experiment revealed that beagle dog's CSF containing DSQ-03 was able to inhibit the neural apoptosis; the therapeutic time window of AICH treated with DSQ-03 was at a time from 0 h to 24 h following intracerebral hemorrhage. Meanwhile, the study laid the foundation to further investigate the efficacy mechanism and to determine the clinical dose [74].

5.4. Verify Drug Association and Perfect Quality Standard in CHM Prescription. Monarch, minister, assistant, and guide in CHM prescription contain many principles of system theory, and the aim of coordination and cooperation in several kinds of CHM is to regulate body functional imbalances and disorders [54]. CSFP could be used to verify drug association and perfect quality standard of CHM prescription based on "the mechanisms of multicomponent efficiency in CHM" model. Shen et al. [75] used CSFP method to describe the properties of the effective constituents in Dachuanxiong prescription. The result revealed that senkyunolide I is the only ingredient found both in plasma and in CSF, thus indicating that senkyunolide I is the guide component to upstream of effective ingredients. Research on key ingredients of active components in Dachuanxiong prescription is favorable to the clarification of its active substance basis and perfection of quality standard. CSFP offered valuable information to

Table 1: Brief introduction of mainly experimental techniques in CSFP.

Technique	Application fields	Advantage	Literatures
Percutaneous puncture	The acquisition of CSF containing drugs in rabbit and rat	Effectively avoid injuring the medulla oblongata, and blood vessel, significantly increase the rate of success in drawing CSF	[49]
Foramen magnum puncture	The acquisition of CSF containing drugs in SD rats	More visual and convenient to operate, causing less injury and complications and possessesing high rate of success	[50, 51]
Using microinjector via spinal dura mater puncture under direct vision	The acquisition of CSF containing drugs in SD rats	A fast, convenient, and clean technique for collecting CSF, increase the collection volume of CSF	[52]
The optimization to acquisition time of CSF containing drugs	The acquisition of CSF containing drugs in SD rats	Obtain optimal CSF containing drug	[43, 47, 48]
Analysis on transitional composition of drug in cerebrospinal fluid	Clarify main effective constituents	Convenient to clarify the true active ingredients	[69, 70]
Analysis on transitional composition association of drug in cerebrospinal fluid	Verify constituents or drug association and perfect quality standard	Simplify the complexity of constituents or drug and find out potential association	[75]

identify the effective constituents and potential effect of known compounds in a complex system.

Due to limited space, only 4 kinds of literature reports related to CSFP containing CHM were provided, each of which was published by mainly Chinese scholars in recent years. Although the studies introduced in this paper are not thorough and systematic enough, there is still no doubt that the CSFP plays an effective role in studying the efficacy mechanism of CHM and solving the problems of administration in vitro experiment. Brief information of CSFP technologies and tools is shown in Table 1.

6. Discussion and Conclusion

CHM has a unique theoretical system which belongs to the dialectical and philosophical medical system and mainly reflects the features of the experience-based medicine. Its clinical practice is based on the theory of the holistic concept and syndrome differentiation [76]. In terms of TCM theory, the pharmacological effect of CHM has the advantages of the overall adjustment, bidirectional regulation, and multiple prevention-treatment-repairing in physiological and pathological conditions. That is to say, CHM has multitarget actions, rather than single effect, which are completely different from the modern medical system [11]. Therefore, if the research ideas of TCM completely follow the research methods of the modern medicine such as the separation of the chemical composition and screening of the active ingredient which could be directly used in vitro experiment, there are some problems and flaws ignoring TCM characteristics of the multitarget synergistic overall effect in the methodology contrary to the basic theory of TCM, thus affecting the authenticity and reliability of the experimental results. Unclear material basis, unclear action mechanism, and low-level quality control are the main problems more or less existing in CHM preparations. The evaluation and validation of the safety and efficacy of CHM, CHM prescriptions, and treatment techniques are key points. Therefore, we should attach great importance to basic research on material basis and compatibility law of CHM combined with modern medical indexes at the cellular level. The biggest obstacles of CHM development are lack of appropriate methods to really explain the effective mechanisms and the scientific connotation of the CHM formulae.

Owing to the presence of blood-brain barrier and the specific survival environment of neurons and glial cells, it is no doubt that serum pharmacology is not suitable to evaluate the effects of CHM for treating ND. Fortunately, as a novel approach, CSFP imitated the survival microenvironment of neurons and glial cells to optimize the discovery of drug for treating ND. Since the CSFP was proposed, it is gradually becoming an important approach to explore the details of drug-target, material basis, and efficacy mechanism of multiple active components in CHM for treating ND. As seen in the above studies, CSFP was suitable to such studies, providing a robust basis and direction for basic research. In addition, CSFP can truly reflect pharmacological effect and increase the relevance of active ingredients and should be adopted in the pharmacological investigation and the drug screening of CHM. So it is thought that CSFP has an important scientific significance at the cellular level.

The application of CHM is inseparable from the guiding of CHM theory. It does not matter whether CHM could pass through BBB, it is likely to play a role in treating ND [77], thus also consistent with the theory that CHM has the multitarget actions of the overall adjustment. Yao et al.'s [60] experiment proved the authenticity of this theory.

We can draw a conclusion that all these roles may be the result of maintaining balance and harmony of the internal environment through the regulation of neuro-endocrine-immune network. However, the precise mechanism is still unclear. Here we want to emphasize that CSFP belongs to a new pharmacological experimental method, which is preliminary to solve the problems in vitro experiments of CHM

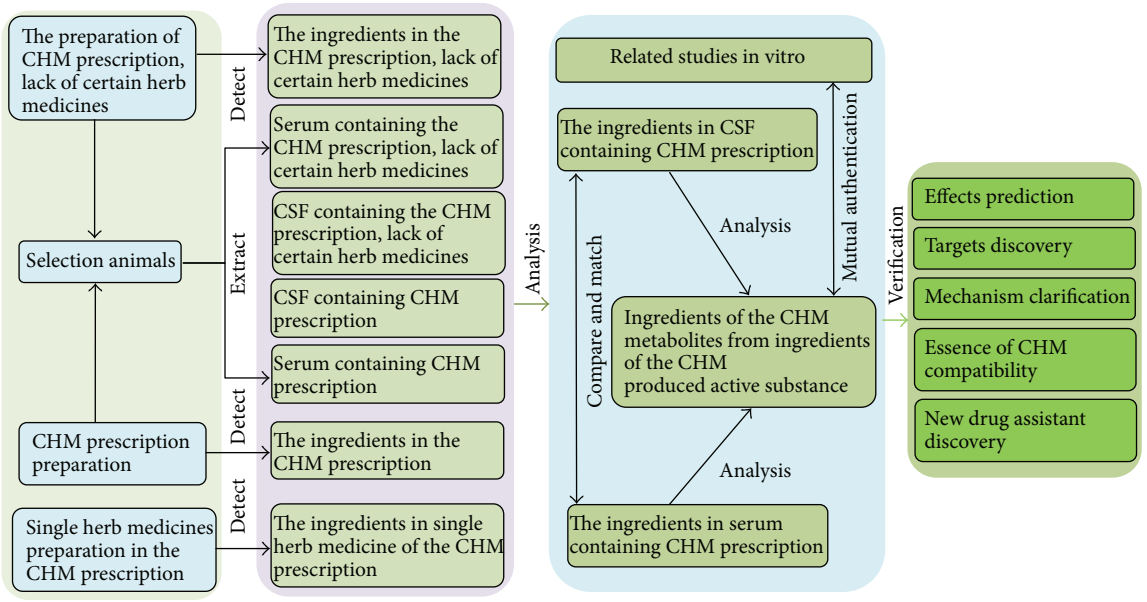

Figure 2: CSFP approaches for CHM research. It analyzes the ingredients of CHM, metabolites from ingredients of the CHM, and produced active substance in CSF containing CHM. Finally, it carries out experimental verifications to mutual authentication for the discovery of CHM-derived targets, effect prediction, mechanism clarification, and new drug assistant discovery using CSFP approach.

for treating ND and needed further to clarify its action mechanisms.

CSFP has become a helpful tool in understanding the fine details of drug-target interactions, efficacy, and mechanism of drugs. However, the CSFP still has some limitations. Firstly, whether the donor animals to extract CSF containing drugs are necessary for modeling, the difference of herbal ingredients in CSF between normal animal and model animal are still an unresolved issue. Secondly, in view of the complexity of CSF ingredients, more studies are required for better understanding the mechanism whereby the CSFP works. Finally, how to make an effective of these active ingredients in CHM, which could not passed through the blood-brain barrier, is still a puzzling question. Using CSFP to investigate CHM pharmacological effects and drug targets, attention should be paid to verify the results of CSFP analysis and mutual authentication. A diagram is proposed to exhibit the research approach of CSFP for CHM research (Figure 2). This approach is a combination of serum pharmacology, which comprises the core values for reflecting the ingredients, metabolites, and active substance correlated with CHM. The appropriate cellular models are also conducive to evaluate the effectiveness of CHM, which could be used to verify the results of CSFP analysis and mutual authentication. By integrating the chemical predictor, target predictor, and mutual authentication, a system of CSFP in CHM research was constructed. It systematically revealed the potential mechanisms of TCM. CSFP could be helpful to confirm the effective ingredients and promote drug discovery of CHM.

In summary, CSFP, as an improved pharmacology method to explore the material basis and action mechanism in vitro, not only breaks the theory that pharmacokinetics studies are limited to the overall function, but also offers new ideas for the selection of the appropriate cells in vitro culture system to study material basis and efficacy mechanism of CHM for treating ND. Moreover, the advancements in CSFP undoubtedly bring about a conceptual move in active ingredients discovery of CHM, make an operational shift in CHM research, and make a significant contribution to CHM modernization and globalization.

Conflict of Interests

The authors declare that there is no conflict of interests.

Authors' Contributions

Yan-qing Wu and Li-yuan Kang contributed equally to this work.

Acknowledgments

The authors thank their tutor Bo-li ZHANG, an academician of the Chinese Academy of Engineering, who provided good work conditions and a highly qualified work team for them. This work was supported by 973 Project for Basic Research of Traditional Chinese Medicine (Project batch no. 2010CB530405), the National Natural Science Foundation of China (Project batch nos. 81273815 & 81202798), and the China Postdoctoral Science Foundation (Project batch no. 2012M520587).

References

[1] M. Jiang, J. Yang, C. Zhang et al., "Clinical studies with traditional Chinese medicine in the past decade and future

research and development," *Planta Medica*, vol. 76, no. 17, pp. 2048–2064, 2010.

[2] W. I. Tou and C. Y.-C. Chen, "In silico investigation of potential Src kinase ligands from traditional chinese medicine," *PLoS ONE*, vol. 7, no. 3, Article ID e33728, 2012.

[3] K. Y. Chen, S. S. Chang, and C. Y. Chen, "In silico identification of potent pancreatic triacylglycerol lipase inhibitors from traditional Chinese medicine," *PLoS One*, vol. 7, no. 9, Article ID e43932, 2012.

[4] S.-C. Yang, S.-S. Chang, H.-Y. Chen, and C. Y.-C. Chen, "Identification of potent EGFR inhibitors from TCM Database@Taiwan," *PLoS Computational Biology*, vol. 7, no. 10, Article ID e1002189, 2011.

[5] C.-H. Lin, T.-T. Chang, M.-F. Sun et al., "Potent inhibitor design against H1N1 swine influenza: Structure-based and molecular dynamics analysis for M2 inhibitors from traditional Chinese medicine database," *Journal of Biomolecular Structure and Dynamics*, vol. 28, no. 4, pp. 471–482, 2011.

[6] T.-T. Chang, K.-C. Chen, K.-W. Chang et al., "In silico pharmacology suggests ginger extracts may reduce stroke risks," *Molecular BioSystems*, vol. 7, no. 9, pp. 2702–2710, 2011.

[7] T. Li and T. Peng, "Traditional Chinese herbal medicine as a source of molecules with antiviral activity," *Antiviral Research*, vol. 97, no. 1, pp. 1–9, 2012.

[8] W.-F. Li, J.-G. Jiang, and J. Chen, "Chinese medicine and its modernization demands," *Archives of Medical Research*, vol. 39, no. 2, pp. 246–251, 2008.

[9] L. C. Lo, C. Y. Chen, S. T. Chen et al., "Therapeutic efficacy of traditional Chinese medicine, Shen-Mai San, in cancer patients undergoing chemotherapy or radiotherapy: study protocol for a randomized, double-blind, placebo-controlled trial," *Trials*, vol. 13, no. 1, p. 232, 2012.

[10] C. Ritenbaugh, R. Hammerschlag, S. F. Dworkin et al., "Comparative effectiveness of traditional Chinese medicine and psychosocial care in the treatment of temporomandibular disorders-associated chronic facial pain," *The Journal of Pain*, vol. 13, no. 11, pp. 1075–1089, 2012.

[11] Z. L. Ren and P. P. Zuo, "Neural regeneration: role of traditional Chinese medicine in neurological diseases treatment," *Journal of Pharmacological Sciences*, vol. 120, no. 3, pp. 139–145, 2012.

[12] C. Y. Chen, "A novel integrated framework and improved methodology of computer-aided drug design," *Current Topics in Medicinal Chemistry*, vol. 13, no. 9, pp. 965–988, 2013.

[13] C. Y.-C. Chen, "TCM Database@Taiwan: the world's largest traditional Chinese medicine database for drug screening in silico," *PLoS ONE*, vol. 6, no. 1, Article ID e15939, 2011.

[14] K.-C. Chen, M.-F. Sun, S.-C. Yang et al., "Investigation into potent inflammation inhibitors from traditional Chinese medicine," *Chemical Biology and Drug Design*, vol. 78, no. 4, pp. 679–688, 2011.

[15] K.-C. Chen, K.-W. Chang, H.-Y. Chen, and C. Y.-C. Chen, "Traditional Chinese medicine, a solution for reducing dual stroke risk factors at once?" *Molecular BioSystems*, vol. 7, no. 9, pp. 2711–2719, 2011.

[16] W. I. Tou, S. S. Chang, C. C. Lee et al., "Drug design for neuropathic pain regulation from traditional Chinese medicine," *Scientific Reports*, vol. 3, p. 844, 2013.

[17] R. Xue, Z. Fang, M. Zhang et al., "TCMID: traditional Chinese medicine integrative database for herb molecular mechanism analysis," *Nucleic Acids Research*, vol. 41, no. 1, pp. D1089–D1095, 2013.

[18] R. Wang, A. Z. Xiong, Z. Q. Teng et al., "Radix paeoniae rubra and radix paeoniae alba attenuate CCl4-induced acute liver injury: an ultra-performance liquid chromatography-mass spectrometry (UPLC-MS) based metabolomic approach for the pharmacodynamic study of traditional Chinese medicines (TCMs)," *International Journal of Molecular Sciences*, vol. 13, no. 11, pp. 14634–14647, 2012.

[19] Y. Zhang, P. Jiang, M. Ye et al., "Tanshinones: sources, pharmacokinetics and anti-cancer activities," *International Journal of Molecular Sciences*, vol. 13, no. 10, pp. 13621–13666, 2012.

[20] Z. Cao, W. Lin, Z. Huang et al., "Ethyl acetate extraction from a Chinese herbal formula, Jiedu Xiaozheng Yin, inhibits the proliferation of hepatocellular carcinoma cells via induction of G0/G1 phase arrest in vivo and in vitro," *International Journal of Oncology*, vol. 42, no. 1, pp. 202–210, 2013.

[21] W. Wang, X. P. Mei, L. Chen et al., "Triptolide prevents and attenuates neuropathic pain via inhibiting central immune response," *Pain Physician*, vol. 15, no. 6, pp. E995–E1006, 2012.

[22] W. J. Miao, Q. Wang, T. Bo et al., "Rapid characterization of chemical constituents and rats metabolites of the traditional Chinese patent medicine Gegen-Qinlian-Wan by UHPLC/DAD/qTOF-MS," *Journal of Pharmaceutical and Biomedical Analysis*, vol. 72, pp. 99–108, 2013.

[23] D. S. Liu, Y. H. Zhou, E. S. Liang et al., "Neuroprotective effects of the Chinese Yi-Qi-Bu-Shen recipe extract on injury of rat hippocampal neurons induced by hypoxia/reoxygenation," *Journal of Ethnopharmacology*, vol. 145, no. 1, pp. 168–174, 2013.

[24] Q. Zhang, C. C. Fong, W. K. Yu et al., "Herbal formula Astragali Radix and Rehmanniae Radix exerted wound healing effect on human skin fibroblast cell line Hs27 via the activation of transformation growth factor (TGF-β) pathway and promoting extracellular matrix (ECM) deposition," *Phytomedicine*, vol. 20, no. 1, pp. 9–16, 2012.

[25] Y. X. Deng, X. J. Zhang, Q. Z. Shi et al., "Anti-hyperglycemic effects and mechanism of traditional Chinese medicine Huanglian Wan in streptozocin-induced diabetic rats," *Journal of Ethnopharmacology*, vol. 144, no. 2, pp. 425–432, 2012.

[26] Q. F. Xie, J. H. Xie, T. T. Dong et al., "Effect of a derived herbal recipe from an ancient Chinese formula, Danggui Buxue Tang, on ovariectomized rats," *Journal of Ethnopharmacology*, vol. 144, no. 3, pp. 567–575, 2012.

[27] J. X. Mei and B. L. Zhang, "A Preliminary attempt to develop the new cerebrospinal fluid pharmacology of Chinese materia medica on neurotrophic effects of astrocytes," *Chinese Traditional and Herbal Drug*, vol. 31, no. 7, pp. 523–526, 2000.

[28] S. K. Yan, J. Zhao, S. S. Dou et al., "Methodology of modernization research in traditional Chinese medicine based on systems biology and network biology," *Chinese Journal of Natural Medicines*, vol. 7, no. 4, pp. 249–259, 2009.

[29] W. Bochu, Z. Liancai, and C. Qi, "Primary study on the application of Serum Pharmacology in Chinese traditional medicine," *Colloids and Surfaces B*, vol. 43, no. 3-4, pp. 194–197, 2005.

[30] J. X. Mei, B. L. Zhang, and R. Lu, "Established the cerebrospinal fluid pharmacology approach: neuroprotective effect of cerebrospinal fluid of qingnao yizhi decotion on injured neurons in vitro," *Tianjin Traditional Chinese Medicine*, vol. 16, no. 6, p. 25, 1999.

[31] C. Yan and L. Y. Kang, "Advance in search for cerebrospinal fluid pharmacology in Chinese materia medic," *The Chinese Journal of Clinical Pharmacology*, vol. 25, no. 3, pp. 257–259, 2009.

[32] F. Ma and J. Y. Tian, "The study on the neuroprotection of cerebrospinal fluid containing LDP components," *Ningxia Medical Journal*, vol. 28, no. 3, pp. 165–167, 2006.

[33] W. Ma, F. Ma, Z. H. Miao et al., "Study on the protective effect of CSF containing LDD components on the AD model with deficits of α7nAChR induced by Aβ1–40," *Ningxia Medical Journal*, vol. 30, no. 4, pp. 289–291, 2008.

[34] T. Liu Tao, H. Y. Jiang, Q. Dong et al., "Cerebrospinal fluid containing modified San Jia San's effect on cell injury related gene of the Aβ-induced hippocampal neuronal," *Jiangsu Journal of Traditional Chinese Medicine*, vol. 42, no. 10, pp. 72–74, 2010.

[35] C. P. Zou, X. Chen, and L. Yan, "Protective effect of buyanghuanwu decoction in cerebrospinal fluid on damaged cortical neurocyte," *Jiangsu Journal of Traditional Chinese Medicine*, vol. 26, no. 11, pp. 9–12, 2008.

[36] Y. Y. Zhou, N. Xie, X. M. Yao et al., "The experimental study on the antioxidative effect of the DHYZ on the AD cell," *China Journal of Chinese Medicine*, vol. 25, no. 147, pp. 249–250, 2010.

[37] X. F. Duan, W. Y. Li, and N. Xie, "Protective effect of modified Dihuang Yinzi on the nerve cell in rats with focal cerebral ischemia," *Journal of Shandong University of TCM*, vol. 33, no. 4, pp. 335–337, 2009.

[38] H. Y. Hu, D. Z. Xi, L. Lei et al., "Protective mechanism of cerebrospinal fluid containing Qingxin Kaiqiao recipe on PC12 cell injury induced by glutamate," *China Journal of Chinese Materia Medica*, vol. 38, no. 12, pp. 1997–2000, 2013.

[39] W. M. Zhu, H. Y. Hu, X. Chen et al., "Protective effect of cerebrospinal fluid containing Qianxin Kaiqiao decoction on PC12 cell injury induced by hydrogen peroxide," *Chinese Archives of Traditional Chinese Medicine*, vol. 31, no. 3, pp. 466–469, 2013.

[40] Y. P. Hu, P. Wang, Y. N. Hu et al., "Cerebrospinal fluid containing modified Wendan Decoction for protection against β-amyloid25-35-induced injury in NG108-15 cells," *Chinese Journal of Experimental Traditional Medical Formulae*, vol. 13, no. 7, pp. 26–28, 2007.

[41] Y. Ben, X. L. Wang, F. H. Zhang et al., "Effects of huanglian wendan decoction on experimental autoimmune neuritis in lewis rats," *Chinese Journal of Experimental Traditional Medical Formulae*, vol. 18, no. 9, pp. 237–242, 2012.

[42] J. W. Guo, Y. C. He, S. H. Chen et al., "The protection effect of Beagle dog cerebrospinal fluid on the neuron," *Journal of Chinese Medicinal Materials*, vol. 28, no. 10, pp. 927–930, 2005.

[43] Q. C. Zhang, J. P. Kou, D. N. Zhu et al., "Preliminary studies on standardization of cerebrospinal fluid pharmacological experimental methods:protective effect of CSF of optimized Danggui Shaoyao San on PC12 cells," *Chinese Journal of Experimental Traditional Medical Formulae*, vol. 13, no. 8, pp. 10–13, 2007.

[44] Q. C. Zhang, J. P. Kou, D. N. Zhu et al., "Neuroprotective effect of cerebrospinal fluid of nimodipine on various PC12 cell injuries in vitro," *Chinese Journal of Modern Applied Pharmacy*, vol. 26, no. 5, pp. 345–348, 2009.

[45] J. W. Guo, Y. C. He, and S. H. Chen, "The researches on the optimal dose of Beagle dog cerebrospinal fluid containing drugs to protect the injured neurons," *Traditional Chinese Medicine Journal*, vol. 4, no. 4, pp. 54–58, 2005.

[46] Y. Y. Zhou, X. M. Yao, X. L. He et al., "Effect of Dihuang Yinzi decoction on expression of SOD mRNA in PC12 cells induced by β-amyloid," *Chinese Journal of Integrative Medicine on Cardio/Cerebrovascular Disease*, vol. 9, no. 6, pp. 704–706, 2011.

[47] X. Z. Zhang, X. L. Zhao, and L. Q. Di, "The effect of cerebrospinal fluid containing tongsaimai tiny pill on injured PC12 cells," *Journal of Nanjing University of TCM*, vol. 26, no. 2, pp. 123–125, 2010.

[48] Z. H. Cui, H. Y. Hu, X. Chen et al., "Protective effect of cerebrospinal fluid containing Qingxin Kaiqiao decoction on PC12 cell injured by hydrogen peroxide," *Zhejiang Chinese Medicine Journal*, vol. 48, no. 7, pp. 478–481, 2013.

[49] H. Fu, Y. H. Tao, X. M. Wang et al., "Method of drawing cerebrospinal fluid from cerebellomedullary cisterm of experimental animals via percutaneous puncture," *Chinese Journal of Comparative Medicine*, vol. 16, no. 11, pp. 684–687, 2006.

[50] Y. D. Cao, L. Z. Zhang, M. S. Wang et al., "Two methods to collect cerebrospinal fluid in SD rats," *Acta Academiae Medicinae Xuzhou*, vol. 25, no. 4, pp. 317–319, 2005.

[51] W. Ma, F. Ma, and J. Y. Tian, "A simple and practical cerebrospinal fluid collection method of experimental animals," *Journal of Ningxia Medical College*, vol. 29, no. 4, pp. 436–437, 2007.

[52] Z. Yang, G. C. Lai, G. B. Wang et al., "Method improvement of collecting cerebrospinal fluid of SD rats," *China Occupational Medicine*, vol. 38, no. 2, pp. 117–119, 2011.

[53] F. Cheung, "TCM: made in China," *Nature*, vol. 480, no. 7378, pp. S82–S83, 2011.

[54] G. B. Zhang, Q. Y. Li, Q. L. Chen et al., "Network pharmacology: a new approach for Chinese herbal medicine research," *Evidence-Based Complementary and Alternative Medicine*, vol. 2013, Article ID 621423, 9 pages, 2013.

[55] J. X. Mei, B. L. Zhang, and R. Lu, "In vitro protective effect of qingnao yizhi formula on glutamic-acid-induced neuron injury," *Traditional Chinese Drug Research and Clinical Pharmacology*, vol. 12, no. 4, pp. 252–255, 2001.

[56] J. X. Mei, B. L. Zhang, and R. Lu, "Vitro study of cerebrospinal fluid containing Chinese medicine's protective effect on injuried neurons," *Tianjin Journal of Traditional Chinese Medicine*, vol. 17, no. 5, pp. 36–38, 2000.

[57] K. W. Zeng, X. M. Wang, H. Fu et al., "Protective effect of cerebrospinal fluid containing Jiawei Wuzi Yanzong Formula on β-amyloid proteininduced injury of hippocampal neurons," *Chinese Journal of Integrated Traditional and Western Medicine*, vol. 30, no. 8, pp. 851–856, 2010.

[58] X. L. He, H. L. Sun, Y. Y. Zhou et al., "PC12 cells injured by amyloid-protein and effected by the cerebrospinal fluid with drug-containing Dihuangyinzi," *Information on Traditional Chinese Medicine*, vol. 26, no. 2, pp. 52–54, 2009.

[59] X. L. He, F. Meng, Y. Y. Zhou et al., "PC12 cells injured by amyloid protein and affected by the APP mRNA through cerebrospinal fluid containing dihuangyinzi," *Information on Traditional Chinese Medicin*, vol. 28, no. 4, pp. 26–28, 2011.

[60] X. M. Yao, Y. Y. Zhou, X. L. He et al., "Effect of decoration of Rehmanniae on the survived condition and the vitality of PC12 induced by Aβ25-35," *Acta Chinese Medicine and Pharmacology*, vol. 37, no. 6, pp. 16–17, 2009.

[61] N. Xie, F. Meng, X. M. Yao et al., "Effect of decoction of Rehmanniae on immediate early gene c-jun and c-fos of PC12 model injury induced by Aβ25-35," *Lishizhen Medicine and Materia Medica Research*, vol. 18, no. 12, pp. 2875–2877, 2007.

[62] N. Xie, X. M. Yao, F. Meng et al., "Effect of decoration of rehmanniae on apoptosis gene bax bcl-2 and caspase-3 of hippocampal neurons model injury," *Chinese Archives of Traditional Chinese Medicine*, vol. 25, no. 9, pp. 1770–1773, 2007.

[63] C. P. Zou, N. Xie, C. Z. Song et al., "Study on influence of decoction of rehmanniae on releasing of LDH and live activity of cell on cultured hippocampal neurons injury," *Journal of Harbin*

University of Commerce Natural Sciences Edition, vol. 20, no. 1, pp. 1–3, 2004.

[64] Y. T. Geng, J. M. Li, G. Wang et al., "Expression of caspase-3 mRNA and Cyt c protein in PC12 cell induced by MPP + and the Effect of Cerebrospinal Fluid containing Zhenganxifeng decoction," *Liaoning Journal of Traditional Chinese Medicine*, vol. 37, no. 9, pp. 1834–1836, 2010.

[65] C. C. Li, J. M. Li, G. W. Gang et al., "Protective effect of cerebrospinal fluid containing Zhenganxifeng decoction on PC12 cell injury induced by MPP+," *Chinese Journal of Experimental Traditional Medical Formulae*, vol. 16, no. 9, pp. 134–137, 2010.

[66] Y. Zou, Z. Y. Li, Q. Li et al., "Effect of cerebrospinal fluid containing zhenganxifeng decoction on C-jun phosphorylation in PC12 cell induced by MPP+," *China Foreign Medical Treatment*, vol. 24, pp. 6–7, 2010.

[67] X. S. Yan, Y. Q. Peng, and C. Z. Zhang, "Effect of Ruhuang Pill on the activity and GFAP expression of rat CRL-2541 cells under high ammonia," *Herald of Medicine*, vol. 27, no. 4, pp. 371–373, 2008.

[68] Y. Q. Peng, J. M. Chen, X. S. Yan et al., "Effect of ruhuang pill on the activity and GFAP expression of astrocyte induce by high ammonia," *Chinese Archives of Traditional Chinese Medicine*, vol. 24, no. 11, pp. 2046–2047, 2006.

[69] Y. F. Li, Y. M. Su, T. L. Li et al., "Material basis of Sini Powder with sedative-hypnotic effect," *Chinese Traditional and Herbal Drugs*, vol. 43, no. 7, pp. 1361–1365, 2012.

[70] Y. F. Li and T. L. Li, "Study on main active constituents of cerebrospinal fluid with SiNiSan freeze-dry powder in rats," *The Chinese Journal of Clinical Pharmacology*, vol. 26, no. 8, pp. 619–621, 2010.

[71] W. Q. Peng, W. F. Shang, and Z. P. Li, "On relation of TCM chronomedicine theory and gastrointestinal dynamics," *World Chinese Medicine*, vol. 8, no. 4, pp. 460–462, 2013.

[72] X. Y. Pan, Z. D. Huang, and H. L. Qiu, "Investigation of theory of chronomedicine in Yellow Emperor's Inner Canon," *Hunan Journal of Traditional Chinese Medicine*, vol. 29, no. 5, pp. 3–5, 2013.

[73] B.-S. Yu, "Several controversial problems of time science in traditional Chinese medicine," *Chinese Journal of Clinical Rehabilitation*, vol. 10, no. 15, pp. 159–161, 2006.

[74] J. W. Guo, Y. C. He, S. H. Chen et al., "The protection effect of Beagle dog cerebrospinal fluid on the neuron," *Chinese Journal of Integrative Medicine on Cardio-/Cerebrovascular Disease*, vol. 3, no. 10, pp. 884–886, 2005.

[75] L. Shen, X. Lin, Y. L. Hong et al., "Study on HPLC characteristic fingerprint of active components of Dachuanxiong fang in plasma and cerebrospinal fluid," *China Journal of Chinese Materia Medica*, vol. 37, no. 13, pp. 2017–2021, 2012.

[76] B. L. Zhang, J. H. Zhang, and J. Q. Hu, "Thinking about translational medicine and traditional Chinese medicine," *Journal of Translational Medicine*, vol. 10, supplement 2, p. 33, 2012.

[77] C. Y.-C. Chen, Y.-F. Chen, C.-H. Wu, and H.-Y. Tsai, "What is the effective component in suanzaoren decoction for curing insomnia? Discovery by virtual screening and molecular dynamic simulation," *Journal of Biomolecular Structure and Dynamics*, vol. 26, no. 1, pp. 57–64, 2008.

Hindawi Publishing Corporation
Evidence-Based Complementary and Alternative Medicine
Volume 2013, Article ID 590698, 6 pages
http://dx.doi.org/10.1155/2013/590698

Research Article

Microcirculation Perfusion Monitor on the Back of the Health Volunteers

Yanqi Li,[1] Xiaomei Li,[2] Dan Zhou,[1] Kang Wang,[3] Yangyang Liu,[1] Yi Guo,[1] Shuang Qiu,[4] Tianchen Zhai,[4] Shuang Liu,[4] Jingjing Liu,[4] and Dong Ming[4]

[1] *Experimental Acupuncture Research Center of Tianjin University of Traditional Chinese Medicine, Tianjin 300193, China*
[2] *Shenzhen Renren Health Management Co., LTD, Shenzhen 518000, China*
[3] *The 2nd Clinical Medical College of Beijing University of Chinese Medicine, Beijing 100078, China*
[4] *Neural Engineering & Rehabilitation Lab of Tianjin University, Tianjin 300072, China*

Correspondence should be addressed to Yi Guo; guoyi_168@163.com

Received 27 September 2013; Revised 1 November 2013; Accepted 15 November 2013

Academic Editor: Calvin Yu-Chian Chen

Objective. To observe the dermal microcirculation blood perfusion characterization of meridians channels (acupoints). *Methods*. 20 healthy human subjects were monitored using Pericam Perfusion Speckle Imager (PSI) for the changes in dermal microcirculation blood perfusion on governor meridian and other respective dermal regions as a control. *Result*. The microcirculation blood perfusion on Governor Meridian is higher than its control area. *Conclusion*. The dermal microcirculation blood perfusion on certain parts of Governor Meridian of healthy human subjects showed specifics.

1. Introduction

The meridian doctrine is one of the core theories of traditional Chinese medicine. After a half century's exploring and studying, prominent achievements have been gained in the field of the meridian doctrine and the specificity of meridians has been proved from various aspects. Biological characteristics of the meridians (acupoints) were monitored physiologically and pathologically by Contemporary scholars with many methods, including LDF and infrared spectrum detection [1]. For example, under the physical condition, ATP [2, 3], the oxygen partial pressure [4–9], transcutaneous CO_2 emission (TCE) [10–17], temperature, and the microcirculation perfusion [18–31] at the acupoints were higher than that at the nonacupoints. Meanwhile, the corresponding indexes changed after the intervention measures like acupuncture stimulation, moxibustion, and pressure. Xu et al. [24] had found out that the dermal areas and deep tissues along the governor meridian had a higher microcirculation blood perfusion than nonmeridian controlled dermal regions on the healthy adults. In addition, the usage of electroacupuncture would result in a higher microcirculation blood perfusion. However, the current researches now were mainly focused on the distinction between the acupoints and nonacupoints instead of the meridians and nonmeridians.

At present, most of the studies on the microcirculation were proceeded with the LDF. However, the LDF had its own limitations that could not achieve a large area and real time simultaneous monitoring at the same time. This study was carried on with the PeriCam PSI System (PSI). It is a blood perfusion imager based on the Laser Speckle Contrast Analysis (LASCA) technology. It is a method that visualizes tissue blood perfusion in real-time and combine dynamic response and spatial resolution in one instrument, providing both real-time graphs and video recordings of the area of interest. LASCA provides new means to study the microcirculation in ways that were not possible in the past.

Nonlinear analysis has been applied more and more in the microcirculation analysis and provided strong supports for the microcirculation researches. Several nonlinear analysis strategies, such as fractal analysis [32] and complexity analysis [33] on the microcirculation signals, provided statistical evidence for the further understanding of the microcirculation either under the physiological or pathological

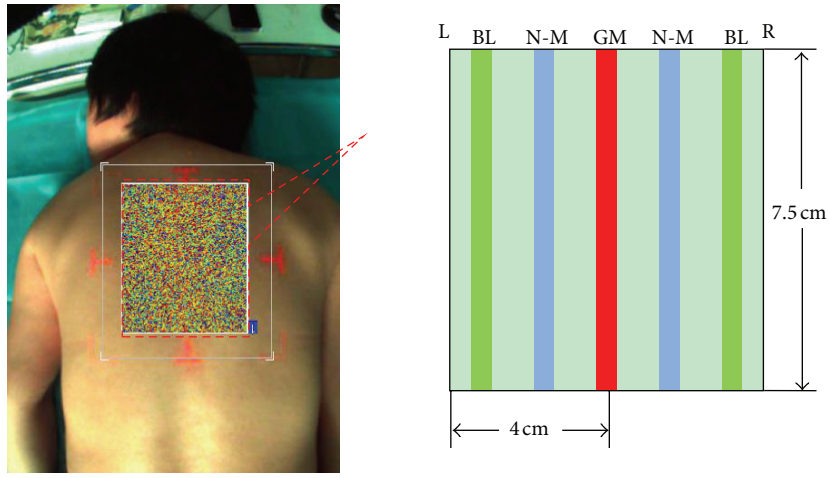

Figure 1: Diagram for the data acquisition.

conditions. The energy amount by Fourier transformation, support vector machine (SVM), and the fuzzy c-means algorithm are applied in this study. All of the three methods can describe and provide ample biological information in the microcirculation characters and provide evidences from different aspects.

The purpose of this study is to monitor the blood of the microcirculation in the back with the PeriCam PSI System (PSI) in a large area and real time, analyze data by nonlinear analysis, and compare the blood features between the governor meridian and nonmeridians so as to confirm that whether there is a difference in the dermal blood perfusion along the governor meridian.

2. Methods

2.1. Ethics Statement. This study was authorized by the Institutional Review Board of Acupuncture and Moxibustion institution, Tianjin University of Traditional Chinese Medicine (TCM). Each participant approved and signed the informed consent form before the study.

2.2. Subjects. Our study was conducted at the experimental acupuncture research center of Tianjin University of TCM between June and September, 2012. 20 healthy participants (10 males and 10 females) aged from 24 to 28 were recruited from Tianjin University of TCM. Smokers and alcoholics, people under recent emotional stress or have taken vasoactive drugs that may affect microcirculation, and people with skin lesions such as scars and acne on the experimental region were excluded. Participants were all informed and agreed to our study procedures.

2.3. Methodology

2.3.1. Experiment Conditions. In our study, room temperature was controlled around $26 \pm 1^{\circ}$C, and the relative humidity was maintained at 50%–60%. No direct sunlight or obvious indoor air convection was allowed during experiment.

The PSI parameter was set as follows: sample rate of 1 frame per second and detecting distance of 20 ± 1 cm with the whole monitoring area of $14 \times 14\,\text{cm}^2$. The monitoring area was also called the Region of Interest (ROI); in this study, we chose T5 as the center of the ROI. Perfusion data was recorded in real time, and the perfusion unit (PU) of the ROI was calculated and finally analyzed by the PSI System.

2.3.2. Location. We chose governor meridian (GM) and the two medial branches of bladder meridian (BM) as the study group; meridians were located according to the international standard. Besides, two nonmeridians (N-M), the middle line between the governor meridian, and the medial branch of bladder meridian were cited as the control group (Figure 1).

2.3.3. Experiment Flow. ROI was marked and exposed to air before sampling so as to adapt to the environment; participants were in prone position and told to be relaxed. 20 min later, the blood perfusion data of the marked spot was recorded for 10 min.

2.3.4. Statistics. All data was transformed, calculated, and compared using Fourier transformation, support vector machine, and fuzzy c-means algorithm.

3. Experiment Results

3.1. Experiment Subjects. 20 healthy participants were included from June to September, 2012, and all of them completed the study.

3.2. Data Process. An area of $7.5 \times 8\,\text{cm}^2$ of the ROI was chosen for analysis, which was basically from T2 to T9. GM, BL, and N-M (the midline of the governor meridian and bladder meridian) were marked in this filed. For further data analysis, each rectangle was separated into 15 points with 0.5 cm diameter, respectively (Figure 2).

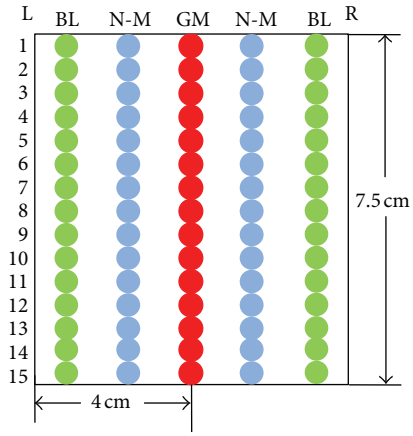

Figure 2: Diagram for the data acquisition.

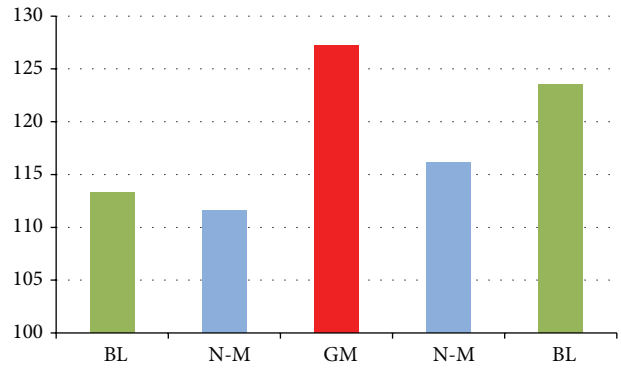

Figure 3: Microcirculation perfusion monitor on the back of the health volunteers. $P_{\text{GM: left BL}} = 0.061$; $P_{\text{GM: right BL}} = 0.679$; $P_{\text{GM: left N-M}} = 0.014$; $P_{\text{GM: right N-M}} = 0.016$.

3.2.1. Energy Amount by Fourier Transformation. Based on the theory of Fourier transformation, the acquired perfusion data was transformed into energy signals. The amount of energy of the five groups was calculated, respectively, and then compared (Figure 3).

The result of the energy amount showed that the governor meridian had the highest amount of energy, which followed by the medial branches of the bladder meridian and the nonmeridians. Moreover, the meridian and nonmeridian on the right side had higher energy than the left side. When compared statistically, there was significant statistical difference between the governor meridian and the two nonmeridians, while no statistical difference was observed between the governor meridian and the two bladder meridians or between the two bladder meridians and the nonmeridians. Therefore, the microcirculation blood perfusion on the governor meridian was obviously more activated than the other four lines.

3.2.2. Support Vector Machine (SVM). Support vector machine (SVM) is a kind of pattern recognition method based on statistical theories; it helps building a higher-dimensional space, the maximum separation hyperplane, to present all the vector data. In our study, we used this method to map the

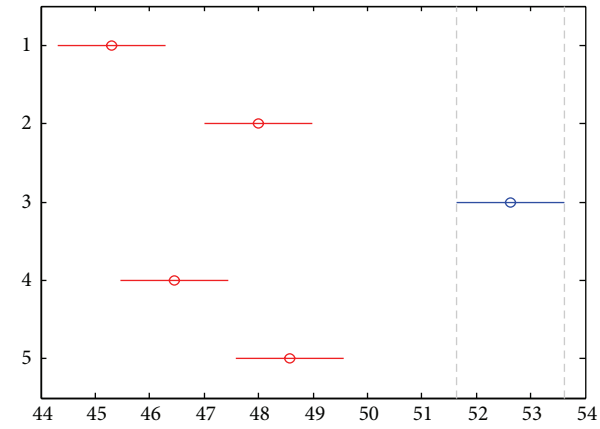

Figure 4: Microcirculation perfusion monitor on the back of the health volunteers; 1 denotes the left medial branch of the BL meridian; 2 denotes the left control line; 3 denotes the right control line; and 4 denotes the right medial branch of the BL meridian.

perfusion data of the five lines (governor meridian, bilateral medial branches of the bladder meridian, and the nonmeridians) into the maximum separation hyperplane. In this higher-dimensional space (Figure 4), overlapped vectors stand for no statistical difference, such as the two nonmeridians; while disoverlapped vectors imply for the existence of statistical differences, such as the governor meridian and nonmeridian. Therefore, we found out that the governor meridian had higher perfusion than either the medial branch of the bladder meridian or the nonmeridian practically and statistically.

3.2.3. Fuzzy c-Means Algorithm (FCM). Fuzzy c-means algorithm (FCM) was an algorithm which divides the limit numbered data into different clusters using membership function and the iterative algorithm on the premise of a defined cluster number. There were 3 clustering centers in each matrix, therefore, together $N = 45$ (15×3) samplings were analyzed in 20 dimensions. Perfusion data was finally output into 45×20 matrices, and each matrix represented the average blood perfusion of the sampling area. We mapped all the matrixes into a 20-dimensional coordinate as shown in Figures 5 and 6.

Governor meridian and the two medial branches of the bladder meridian were cited as the 3 clustering centers and samplings on governor meridian; the left and right medial branch of the bladder meridian were marked into green, blue, and red, respectively. By using FCM, a 20-dimensional chart of the 3 clustering centers was generated (as shown in Figure 5), and separated samplings in this chart stood for statistically difference of the corresponding meridians. It is clear that the PU of the green samplings (governor meridian) is significantly different from the other two colors (two bladder meridians), which means that the PU of governor meridian is statistically different from the two bladder meridians, while there is no difference between the two bladder meridians.

Use the same method to compare governor meridian with bilateral nonmeridians; similarly, mark governor meridian

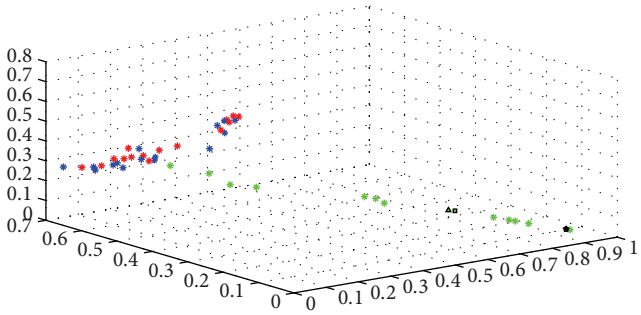

Figure 5: Microcirculation perfusion monitor on the back of the health volunteers. Green ones denote the governor meridian; blue ones denote the left medial branch of the BL meridian; and red ones denote the right medial branch of the BL meridian.

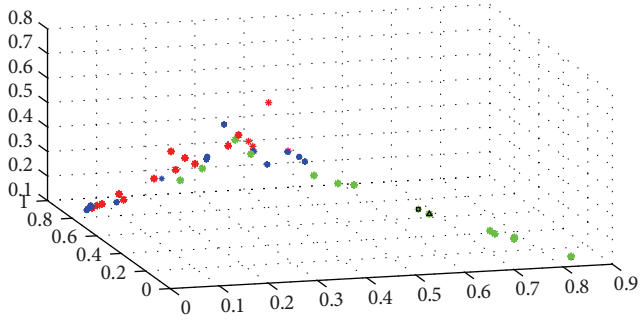

Figure 6: Microcirculation perfusion monitor on the back of the health volunteers. Green ones denote the governor meridian; blue ones denote the left control line; abd red ones denote the right control line.

and the left and right nonmeridian into green, blue, and red (as shown in Figure 6). The PU of the governor meridian was significantly statistically different from the two nonmeridians, while no difference was observed between the two nonmeridians.

4. Discussion

4.1. Results. Our study showed that governor meridian had a better microcirculation blood perfusion in healthy adults and its perfusion was higher than not only the two bilateral medial bladder meridians but also the nonmeridians, which reflected the characteristics of the microcirculation of the governor meridian directly. And the results were consistent with the previous researches [23].

The microcirculation of meridians is affected by numerous factors; the permeability of capillaries as well as vasoactive agent is of great importance. During the prestage of our study, we [34] found that, by injecting EB coloring agent into the veins surrounding the ears of healthy rabbits, the EB exudation along the governor meridian on the back was higher than nonmeridian lines on the bilateral of governor meridian; it indicated that the blood vessels along the governor meridian have exceptionally high permeability. Moreover, other researchers have shown that chemicals which affect the activation of blood vessels such as CGRP, Substance P, and NO might have their own respective dispersion characteristics. For example, a study by Ma et al. [35] on the correlation between temperature changes in tissues along meridians and CGRP concentration has found that there was higher CGRP concentration in tissues along meridians with elevated temperature than in area without elevated temperatures. Cao et al. [36] have shown that electrical stimulation of "Zusanli" acupoint on rats resulted in elevated SP concentrations in the dermal layer along the stomach meridian as well as in the colon, indicating that SP is involved in both the meridian activity from acupoint stimulation and the response of the respective organ. Ma [37] has found that NO concentration is significantly higher in tissues of acupoints; histochemistry test has shown that there is elevated NO expression in nerve fibers, axons, neurons, and hair follicles of acupoints.

4.2. Statistical Method. In recent years, the use of bioinformatic and nonlinear dynamic analysis methods has been increasingly widespread in medical field [38–40]. For example, Li et al. [41] used bioinformatic analysis methods to illustrate the tonifying and reduction techniques from a microcirculation point of view, which effectively distinguished the difference between the lifting-thrusting reinforcing method and lifting-thrusting reducing method of acupuncture. Wang et al. [42] used system identification algorithm to obtain biological characteristics of both left and right "he gu" acupoint, demonstrating the single side nature of acupoints. In our study, we applied the nonlinear dynamic method to analyze the perfusion data. This method was also successfully used in our other researches to analyze the effect of acupuncture on nerve impulses [43] and have found that the nerve tracts discharging sequence responding to different acupuncture techniques might have respective characteristic and could be differentiated by "time span," "frequency," and so forth, which was an elementary step to the establishment of a scientific description of the various acupuncture techniques.

In this study, multiple nonlinear analyzing methods were applied in order to distinguish the features of the governor meridian and nonmeridian from different views and verify the specificity of the microcirculation in the physiological status, which is suitable for this study. The application of nonlinear analysis could supplement the limitations of the general medical statistical analysis and is conductive to mining more biological information, which may explain the biological meanings reflected by the experimental data.

At present, we have observed part of the characteristics of the dermal microcirculation blood perfusion of the governor meridian. The whole features of the governor meridian have not been shown. In the further research, we plan to accomplish the whole features of the governor meridian as well as other twelve regular meridians and draw the specific dermal microcirculation blood perfusion chromatogram of the fourteen meridians in order to provide evidences to the microcirculation blood changes after the interventions or under the pathological conditions.

5. Conclusion

Governor meridian has the feature of a high microcirculation blood perfusion in healthy people.

Conflict of Interests

All of the authors declare that they have no conflict of interest.

Acknowledgments

This work is supported by the Grant (no. 81302916) from the National Natural Science Foundation of China. Sincerely, thanks goes to Zhang Yue for the text proofreading. Thanks goes to the team led by Professor Dong Ming from Neural Engineering & Rehabilitation Lab of Tianjin University. Shuang Qiu, Tianchen Zhai, Shuang Liu, and Liujing from this team helped with the data analysis. Thank goes to all of the participants. Yanqi Li and Xiaomei Li planned the study, recruited subjects, and performed the experiments. Yanqi Li and Kang Wang finished the paper. Yangyang Liu and Dan Zhou provided advices on the experiments and the paper. Yi Guo was the authority for the study planning as well as giving advice on the experiment.

References

[1] H. Hsiu, S. M. Huang, P. T. Chao et al., "Study on the microcirculatory blood velocity of acupoint monitored by laser Dopplesignal," in *Proceedings of the IEEE Engineering in Medicine and Biology Society Conference*, 2007.

[2] L.-H. Tan, C.-H. Ma, D. Zhang, S.-Y. Wang, and H.-M. Ma, "Changes of cutaneous temperature and the activity of Ca^{2+}- and Mg^{2+} -ATPase in the tissues along the running course of meridians in rabbit," *Acupuncture Research*, vol. 32, no. 5, pp. 330–333, 2007.

[3] Q. H. Han, G. H. Ding, and X. Y. Shen, "Infrared radicalization spectrum of human surface and the relationship with ATP energy metabolize," *Shanghai Journal of Biomedical Engineering*, vol. 26, no. 4, pp. 198–200, 2005.

[4] H. Wang, H. P. Zhang, and Y. X. Liu, "Test and analysis on deep meridian oxygen partial pressure," *Hubei College of Traditional Chinese Medicine*, vol. 16, no. 2, pp. 30–31, 1994.

[5] M. Chen, Z. X. Wu, X. L. Hu, and J. S. Xu, "Effect of acupuncture on partial oxygen pressure and temperature of deep tissues along large intestine channel in 30 normal volunteer subjects," *Chinese Journal of Basic Medicine in Traditional Chinese Medicine*, no. 5, pp. 553–555, 2011.

[6] M. Chen, X.-L. Hu, and Z.-X. Wu, "Effect of acupuncture on partial oxygen pressure of deep tissue along the Governor Vessel in 31 normal volunteer subjects," *Acupuncture Research*, vol. 33, no. 6, pp. 402–405, 2008.

[7] Y. J. Xie, X. L. Hu, and B. H. Wu, "Observation on the tissue po_2 after acupuncture," *Chinese Journal of Traditional Medical Science and Technology*, vol. 7, no. 6, pp. 353–354, 2000.

[8] H. Wang, H. P. Zhang, Y. X. Liu, Y. M. Chen, and Z. H. Liang, "Observation on the po_2 of the acupoints off the acupoint on the meridian and off the meridian," *Shanghai Journal of Acupuncture and Moxibustion*, vol. 16, no. 1, pp. 3–5, 1997.

[9] X. Y. Xu, X. L. Hu, and B. H. Wu, "Influence of mechanical pressing on partial pressure of oxygen in three points along the large intestine meridian during acupuncture," *Acupuncture Research*, vol. 25, no. 4, pp. 276–279, 2000.

[10] A. Eory, "In vivo skin respiration (CO_2) measurements in the acupuncture loci," *Acupuncture and Electro-Therapeutics Research*, vol. 9, no. 4, pp. 217–223, 1984.

[11] "The phenomena expressed by skin respiration (CO_2 emission) along the lung channel," Compilation of the Abstracts of Acupuncture Moxibustion Paper, Beijing, China: WFAS, 1987.

[12] W. B. Zhang, X. H. Jing, R. M. Xu, Z. X. Zhu, C. H. Li, and H. Li, "Characters on the Li meridian and the ST meridian on the of tagmata derma," *Chinese Journal of Integrated Traditional and Western Medicine*, vol. 15, no. 10, pp. 625–627, 1995.

[13] W. B. Zhang, H. Li, and R. M. Xu, "Observation of the TCE for the acupuncture on the meridian derma," *Chinese Acupuncture & Moxibustion*, vol. 16, no. 1, pp. 39–42, 1996.

[14] W. B. Zhang and H. Li, "Research on the TCE mechanism on the dermal," *Beijing Biomedical Engineering*, vol. 15, no. 4, pp. 221–226, 1996.

[15] W.-B. Zhang, L.-L. Wang, T. Huang et al., "Laser Doppler perfusion imaging for assessment of skin blood perfusion after acupuncture," *Medical Acupuncture*, vol. 20, no. 2, pp. 109–118, 2008.

[16] R.-H. Wang, T. Huang, Y.-Y. Tian et al., "[Influence of mechanical pressure on the change of acupuncture-induced transcutaneous CO_2 emission]," *Chinese Acupuncture & Moxibustion*, vol. 29, no. 7, pp. 565–568, 2009.

[17] T. Huang, R. H. Wang, W. B. Zhang et al., "Relationship between needle sensation and periphery transcutaneous CO_2 emission," *Chinese Journal of Basic Medicine in Traditional Chinese Medicine*, vol. 15, no. 8, pp. 615–618, 2009.

[18] X.-L. Hu, J.-S. Xu, P.-Q. Wang, X.-Y. Xu, L.-Y. Gao, and B.-H. Wu, "Preliminary exploration on the mechanism underlying the formation of infrared radiant track along meridian courses over human body surface," *Journal of Infrared and Millimeter Waves*, vol. 22, no. 3, pp. 175–243, 2003.

[19] X.-L. Hu, P.-Q. Wang, J.-S. Xu, B.-H. Wu, and X.-Y. Xu, "Main characteristics of infrared radiant rack along meridian courses over human body surface and the condition of its appearance," *Journal of Infrared and Millimeter Waves*, vol. 20, no. 5, pp. 325–328, 2001.

[20] X.-L. Hu, J.-S. Xu, L. Ye, J. Yang, P.-Q. Wang, and B.-H. Wu, "Elicitation of infrared radiant track along meridian courses over human body surface by local heating," *Journal of Infrared and Millimeter Waves*, vol. 21, no. 1, pp. 6–83, 2002.

[21] J.-S. Xu, X.-L. Hu, P.-Q. Wang, and B.-H. Wu, "Influence of electroacupuncture on infrared radiant track along meridian courses over human body surface," *Chinese Journal of Clinical Rehabilitation*, vol. 9, no. 29, pp. 251–253, 2005.

[22] J. S. Xu, X. Sh. Zheng, X. H. Pan, X. L. Hu, and Z. Y. Sa, "Influence of electro acupuncture on infrared radiant track along meridian courses over human body surface and microcirculation blood perfusion," *Journal of Fujian University of Traditional Chinese Medicine*, vol. 20, no. 1, pp. 13–73, 2010.

[23] J.-S. Xu, X.-H. Pan, X.-L. Hu, and B.-H. Wu, "Comparison between governor meridian and its bilateral control points in microcirculatory blood perfusion in 53 volunteer subjects," *Acupuncture Research*, vol. 33, no. 5, pp. 321–325, 2008.

[24] J. S. Xu, X. L. Hu, X. H. Pan, and S. Z. Sa, "Influence of electro acupuncture on infrared radiant track along meridian

courses over human body surface and microcirculation blood perfusion," in *Proceedings of the 12th National Infrared Heating and Infrared Medical Development Seminar Papers and Abstract Set, Nanjing, Infrared Electric Parts Professional Committee of Chinese Optical Society*, pp. 22–25, 2009.

[25] D. Zhang, "Observation on the effects of moxibustion by laser Doppler perfusion imaging," *Shanghai Journal of Acupuncture and Moxibustion*, vol. 23, no. 5, pp. 37–40, 2004.

[26] D. Zhang, H. M. Ma, and S. H. .Y. Wang, "Infrared thermo gram observation on the blood circulation for the dermal temperature," *Chinese Journal of Medical Imaging*, vol. 9, no. 2, pp. 140–142, 2001.

[27] X. J. Wang, Ch.Ch. Zeng, H. P. Liu, S. H. Liu, and L. G. Liu, "The effects of laser acupuncture on temperature and blood flow perfusion rate of the point tissue," *Acta Laser Biology Sinica*, vol. 14, no. 4, pp. 260–264, 2005.

[28] H. Zhao, W. B. Zhang, and F. Y. Zhuang, "Effect of acupuncture at Zuanli on subcutaneous microcirculatory flow at point along meridian," *Chinese Journal of Microcirculation*, vol. 8, no. 1, pp. 41–45, 1998.

[29] H. Hsiu, W.-C. Hsu, B.-H. Chen, and C.-L. Hsu, "Differences in the microcirculatory effects of local skin surface contact pressure stimulation between acupoints and nonacupoints: possible relevance to acupressure," *Physiological measurement*, vol. 31, no. 6, pp. 829–841, 2010.

[30] G. Litscher, L. Wang, G. Schwarz, and D. Schikora, "Increases of intracranial pressure and changes of blood flow velocity due to acupressure, needle and laserneedle acupuncture?" *Forschende Komplementarmedizin und Klassische Naturheilkunde*, vol. 12, no. 4, pp. 190–195, 2005.

[31] K. Kubo, H. Yajima, M. Takayama, T. Ikebukuro, H. Mizoguchi, and N. Takakura, "Changes in blood circulation of the contralateral achilles tendon during and after acupuncture and heating," *International Journal of Sports Medicine*, vol. 32, no. 10, pp. 807–813, 2011.

[32] F. Esen, G. S. Aydin, and H. Esen, "Detrended fluctuation analysis of laser Doppler flowmetry time series," *Microvascular Research*, vol. 78, no. 3, pp. 314–318, 2009.

[33] H. Hsiu, W. CH. Hsu, C. H. .L. Hsu, J. G. Bau, C. H. .T. Chen, and Y. S. Liu, "Complexity analysis of the microcirculatory-blood-flow response following acupuncture stimulation," *Microvascular Research*, no. 89, pp. 34–39, 2013.

[34] D. Zhou, Y. Guo, Y.-M. Guo, S. Zhang, and P. Pan, "Distribution and permeability of capillaries at the skin of the conception vessel and the governor vessel in healthy rabbits," *Journal of Traditional Chinese Medicine*, vol. 31, no. 4, pp. 356–359, 2011.

[35] C. H. H. Ma, L. H. Tan, X. J. Zhao, Y. S. Wang, H. M. Ma, and D. Zhang, "Relationship between the change of temperature and the contents of CGRP and at II in the tissues along the meridian in rabbits," *Acupuncture Research*, no. 2, pp. 149–151, 2002.

[36] D. Y. Cao, H. Z. Niu, and Y. Zhao, "Stimulation of acupoint induces release of substance P through primary afferent reflex," *Chinese Acupuncture & Moxibustion*, vol. 21, no. 10, pp. 623–625, 2001.

[37] S.-X. Ma, "Enhanced nitric oxide concentrations and expression of nitric oxide synthase in acupuncture points/meridians," *Journal of Alternative and Complementary Medicine*, vol. 9, no. 2, pp. 207–215, 2003.

[38] T.-T. Chang, K.-C. Chen, K.-W. Chang et al., "In silico pharmacology suggests ginger extracts may reduce stroke risks," *Molecular BioSystems*, vol. 7, no. 9, pp. 2702–2710, 2011.

[39] C. Y. C. Chen, "A novel integrated framework and improved methodology of computer-aided drug design," *Current Topics in Medicinal Chemistry*, vol. 13, no. 9, 2013.

[40] C. Y.-C. Chen, "Computational screening and design of traditional Chinese medicine (TCM) to block phosphodiesterase-5," *Journal of Molecular Graphics and Modelling*, vol. 28, no. 3, pp. 261–269, 2009.

[41] X. M. Li, Y. Q. Li, J. Z. Chen et al., "The influence of skin microcirculation blood perfusion at Zusanli acupoint by stimulating with lift-thrust reinforcing and reducing acupuncture manipulation methods on healthy adults," *Evidence-Based Complementary and Alternative Medicine*, vol. 2013, Article ID 452697, 7 pages, 2013.

[42] G. J. Wang, J. G. Han, G. Litscher, and W. B. Zhang, "System identification algorithm analysis of acupuncture effect on mean blood flux of contralateral Hegu acupoint," *Evidence-Based Complementary and Alternative Medicine*, vol. 2012, Article ID 951928, 7 pages, 2012.

[43] Z. Zheng, Y. Liu, Y. Guo et al., "Preliminary exploration of research method for studying the influence of acupuncture manipulations on electrical signals of spinal dorsal root nerve in rats," in *Proceedings of the 6th International Conference on Natural Computation (ICNC' 10)*, pp. 509–513, August 2010.

Hindawi Publishing Corporation
Evidence-Based Complementary and Alternative Medicine
Volume 2013, Article ID 828754, 7 pages
http://dx.doi.org/10.1155/2013/828754

Research Article

A Brief Analysis of Traditional Chinese Medical Elongated Needle Therapy on Acute Spinal Cord Injury and Its Mechanism

Mengxuan Du,[1] Rongliang Chen,[1] Renfu Quan,[1] Liang Zhang,[2] Jinwei Xu,[1] Zhongbao Yang,[3] and Disheng Yang[4]

[1] *Research Institute of Acupuncture and Moxibustion, Xiaoshan Traditional Chinese Medical Hospital, Zhejiang 311200, China*
[2] *Research Institute of Acupuncture and Moxibustion, Zhejiang Chinese Medical University, Hangzhou 31012, China*
[3] *Research Institute of Acupuncture and Moxibustion, Medical College of Xiamen University, Xiamen 361005, China*
[4] *Department of Acupuncture and Moxibustion, The Second Affiliated Hospital, Medical College of Zhejiang University, Hangzhou 310009, China*

Correspondence should be addressed to Renfu Quan; quanrenfu8@yahoo.com

Received 26 September 2013; Revised 22 October 2013; Accepted 22 October 2013

Academic Editor: Calvin Yu-Chian Chen

Acute spinal cord injury is one of the most common and complicated diseases among human spinal injury. We aimed to explore the effect of point-through-point acupuncture therapy with elongated needles on acute spinal cord injury in rabbits and its possible mechanism. Adult rabbits were randomly divided into a model group, elongated needle therapy group, and blank group. Immunohistochemical staining showed that the protein levels of Fas and caspase-3 in the model group were significantly higher than those in the blank group at each time point ($P < 0.05$) and significantly lower than those in the elongated needle therapy group on the 3rd and 5th days after operation ($P < 0.05$). RT-PCR showed that Fas and caspase-3 mRNA levels in the model group and elongated needle therapy group were significantly higher than those in the blank group ($P < 0.05, 0.01$). The mRNA levels of Fas and caspase-3 in the elongated needle therapy group were significantly lower than those in model group on the 3rd day ($P < 0.05, 0.01$). Therefore, we confirmed that elongated needle therapy has an obvious effect on acute spinal cord injury in rabbits. Its mechanism is made possible by inhibiting the expression of the Fas → caspase-3 cascade, thereby inhibiting cell apoptosis after spinal cord injury.

1. Introduction

Traditional Chinese medicine has centralized Chinese medical wisdom from all ages, which has led to a huge quantity of information. Acupuncture is a traditional Chinese medical therapy that uses elongated needles and modern penetration needling. This therapy has excellent results in both clinical care and acupuncture studies. Compared with other medical skills in China and abroad, elongated needle therapy is famous for its better economic efficiency, progressiveness, and representativeness.

The symptoms, morbidity, conditions, pathogenesis, and pathology of spinal cord injury (SCI) are complex. SCI is one of the most serious diseases endangering human health and its mechanisms are complicated. Recent studies have found that apoptosis and various genes have a role after spinal cord injury [1]. There are clinical reports [2, 3]. That claim adopting acupuncture to treat spinal cord injury has a curative effect. However, its curative mechanism is still unclear. We used a modified Allen's film forming method of spinal cord injury to build a spinal cord jury model called rabbit T13-L1 and coupled it with elongated needling acupuncture point therapy. Then through shape changes of the rabbit spinal cord after injury, we tested the Fas receptor for apoptosis, protein Caspase-3, and the expression of mRNA.

2. Materials and Methods

2.1. Model Establishment. Urethane at 20%, 1 g/kg was injected into the ear vein for anesthetization. Then, rabbits were fixed in the prone position on the operating table,

and under sterile conditions, with T13 as the center, the middle of rabbit's back was cut open about 2-3 cm. The T13-L1 spinous process and all the vertebral plates were broken off, and a 3 mm wide dura mater was exposed. A modified Allen's striking device was used to impact the T13-L1 spinal cord with an 80 gram cm force. Successful model establishment was considered when there was spastic swinging of the tail, fluttering of both lower extremities and body, and lower extremity flaccid paralysis. After operation, Crede's manipulation was used to massage the rabbit's abdomen every day to help defecation and uresis 2–4 times. For three consecutive days, 800,000 units of penicillin were injected to prevent wound infection.

2.2. Animal Preparation and Group of Experiments. Eighty-four purebred Japanese rabbits, of unknown gender, body weight 2.5 ± 0.25 kg were obtained from the Zhejiang Chinese Medical University Animal Experiment Research Center. Rabbits were randomly assigned into three groups: a model group, in which the SCI model was established without elongated needle therapy; elongated needle group; and control group. For elongated needle therapy, both sides of elongated needles were used to penetrate "Chihpien," "Flume," "Qihai," and "Intermediate" daily. Meanwhile, "Chihpien" and "Flume" formed a loop and were connected with a JL2B electric pulse stimulator for 15 min at a rate of 20–40 beats/min at an intensity of 1.5–3 V. For the sham operation group, we operated on the T13-L1 spinous process and all vertebral plates, and a 3 mm wide dura mater was opened but the spinal cord was not touched and there was no electrical stimulation. We found the acupuncture point locations for experimental animals in the "*Subject of Experimental.*"

2.3. Slice Preparation. Each animal group was sacrificed on the 1st, 3rd, and 5th days after operation. After anesthesia, a longitudinal cut was made in the middle of chest; the heart was exposed. Then, the left ventricle and right atrium were opened, and from the left ventricle, a tube was inserted along the aorta. Then, physiological saline was injected until the perfusate became clear and bright. Next, the heat was rapidly filled with 4% paraformaldehyde PD solution (pH = 7.4) at a flow rate of 50 mL/min for 3-4 min, followed by a flow rate of 10 mL/min for 20 min. Later, a 1 cm T13-L1 vertebral segment of spinal cord was removed. Finally, 4% paraformaldehyde solution was used to fix specimens for 24–48 h. Samples were routinely embedded in paraffin and sliced at a thickness of 4 μm for preservation.

2.4. Hematoxylin and Eosin (HE) Dyeing. Slices were taken from each rabbit randomly and stained normally with hematoxylin and eosin. Then, the shape changes of the spinal cord were observed through a light microscope.

2.5. Immunohistochemical Staining Method (SP). Sections from each rabbit were randomly selected and dyed according to the manufacturer's instruction. The antibody concentration of Fas was 1 : 100 and caspase-3 was 1 : 4000. DAB coloration was used with hematoxylin as a counterstain. Xylene was used to make tissue transparent and sections were mounted. PBS was used as a negative control. Both the positive cells and endochylema are pale brown. With an OLYMPUS BX-50 light microscope at 400 fields, three fields were randomly chosen per section to observe the expression of all positive cells in the anterior and posterior horns of spinal cord (there are cells of pale brown in endochylema and karyon). Image analysis software Image-Pro Plus was then used to count the optical density.

2.6. Semiquantitative RT-PCR to Testify the Expression of Fas and Caspase-3 mRNA. Three rabbits were chosen from each group at each time point and TRIzol (Invitrogen, Carlsbad, CA, USA) was used to extract total RNA of each spinal cord tissue. OD was also determined. A reverse transcription kit (all from Applied Biosystems, Foster City, CA) was used to make cDNA, and PCR amplification was performed. Gre-pro was used to analyze the electrophoresis grey level of Fas and caspase-3 mRNA and calculate relative expression. Relative expression amount = experimental grey level/internal reference grey level.

According to GenBank sequences, we used Primer 5.0 software (Premier company, Canada) to design primers for Fas and caspase-3. Primer sequences are shown in Table 1. β-actin was used as an internal reference.

2.7. Statistical Treatment. Statistical software SPSS17.0 (SPSS company, Chicago, IL, USA) was used to analyze data, and results are presented as $\overline{x} \pm s$. Variance analysis and LSD were used. When $P < 0.05$, the difference was considered statistically significant.

3. Experimental Results

3.1. Result of HE Staining. On the 5th day after sham-operation, a gray-white boundary of the spinal cord and the nuclei of the neurons were shaped like waves with two sharp peaks, glial cells were scattered, and nuclear Nissl body were clear (HE ×400, Figure 1(a)). On the 1st day after model group operation, the normal structure of the spinal cord tissue was lost; there was hemorrhaging, edema, and necrosis; the boundary between the grey and white matter was unclear; part of the neuronal nuclei decreased; and there was cavity disappearance. Glial cells proliferated, and there was local lymphocytic infiltration (HE ×200, Figure 1(b)). On the 1st day after elongated needle therapy, the normal structure of the spinal cord tissue was lost; there was hemorrhaging, edema, necrosis, and demyelination; the boundary between the grey and white matter was unclear; part of the neuronal nuclei decreased; and gliocytes proliferated around damaged areas (HE ×200, Figure 1(c)). On the 5th day after model group operation, the structure of the spinal cord tissue was disorganized, there was serious karyopyknosis, and a bigger cavity was formed with excessive gliocyte proliferation (HE ×400 Figure 1(d)). On the 5th day after elongated needle therapy, there were still some complete neuronal nuclei. There was a clear boundary between grey and white matter,

Table 1: Gene primer sequence table of Fas and Caspase-3.

Gen	Primer	Oligonucleotide sequences (5′-3′)	Length (bp)
Fas	Front	5′-GCAGACAAGCGATTTACTTCT-3′	581
	Rear	5′-ATCAGAACAGTGAAGCGTACA-3′	
Caspase-3	Front	5′-GCTGTGTGGGCTTGCTAAGTT-3′	749
	Rear	5′-TCACGTATCCTGGCGACTGTC-3′	
β-actin	Front	5′-GAGTACGCCAACATGGTGCTGTC-3′	146
	Rear	5′-CGTTCATGAGCCACACTTAGC-3′	

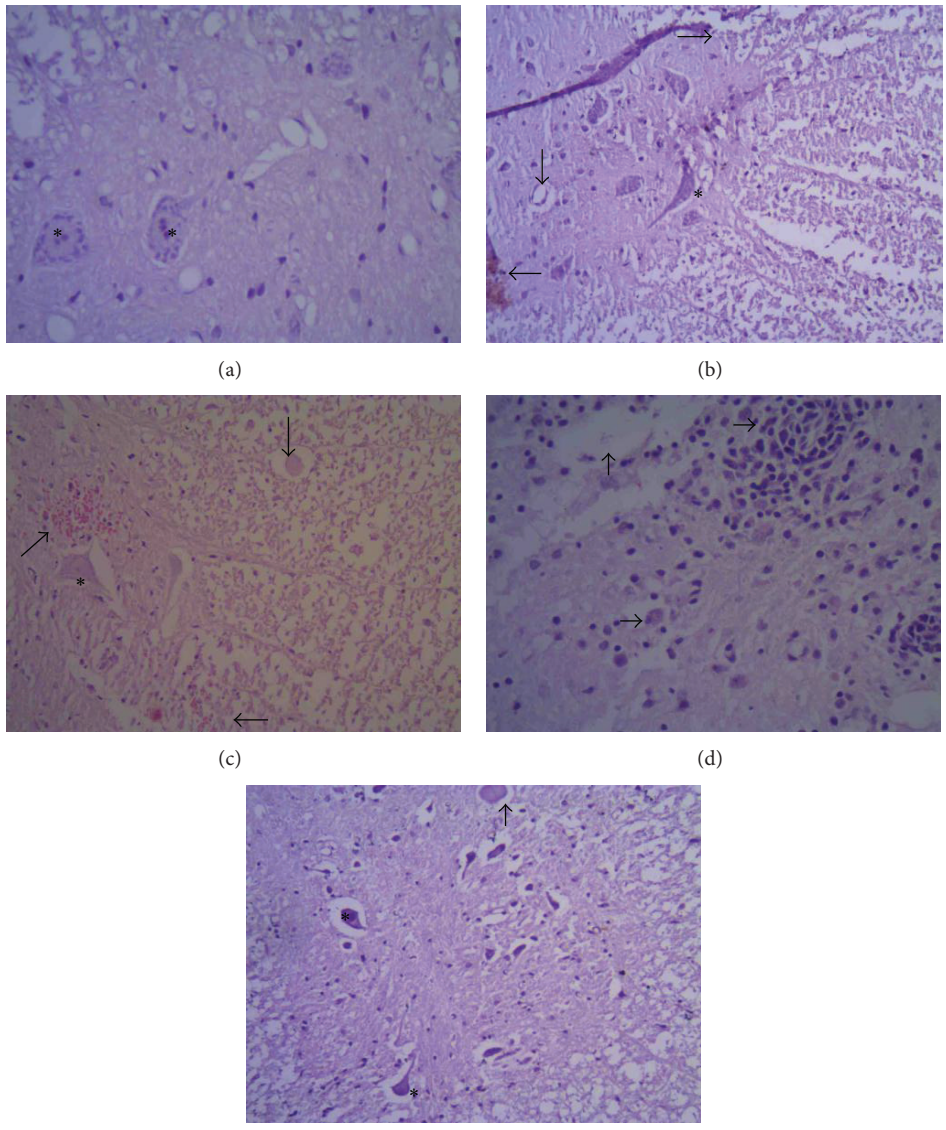

Figure 1: (a) On the 5th day after sham operation, a gray-white boundary of the spinal cord and the nuclei of the neurons were shaped like waves with two sharp peaks; glial cells were scattered; and nuclear Nissl body were clear (HE ×400). (b) On the 1st day after model group operation, the normal structure of the spinal cord tissue was lost; there was hemorrhaging, edema, and necrosis; the boundary between the grey and white matter was unclear; part of the neuronal nuclei decreased; and there was cavity disappearance. Glial cells proliferated, and there was local lymphocytic infiltration (HE ×200). (c) On the 1st day after elongated needle therapy, the normal structure of the spinal cord tissue was lost; there was hemorrhaging, edema, necrosis, and demyelination; the boundary between the grey and white matter was unclear; part of the neuronal nuclei decreased, and gliocytes proliferated around damaged areas (HE ×200). (d) On the 5th day after model group operation, the structure of the spinal cord tissue was disorganized; there was serious karyopyknosis; and a bigger cavity was formed with excessive gliocyte proliferation (HE ×400). (e) On the 5th day after elongated needle therapy, there were still some complete neuronal nuclei. There was a clear boundary between grey and white matter and less gliocyte proliferation (HE ×200).

less gliocyte proliferation (HE ×200, Figure 1(e)), and no bleeding.

3.2. Results of Immunohistochemistry. The results of Fas and caspase-3 optical density values of rabbit spinal cord tissue among each group at different time points is presented in Table 2. Positive expression of each sample point in the model group was significantly different than the sham operation group. Positive expression of each Fas albumen sampling point in elongated needle group was significantly different than the model group. Positive expression of caspase-3 on the 3rd and 5th days after operation in the elongated needle group was significantly different than with the model group.

3.2.1. Results of Fas Immunohistochemistry. There was little positive expression of each sampling point in the sham operation group (SP ×400; Figure 2(a)). Some positive expression appeared on the 1st day after operation in both the model and elongated needle groups (Table 2). Expression reached a peak on the 3rd day after operation. The positive cells in the model group were scattered with damaged grey and white neurons, and the inner white matter expressed more positive cells. The positive signal was found inside ectoenzymes and endochylema (SP ×400; Figure 2(b)). The elongated needle group had a much smaller expression area of visible positive cells in the grey matter than that in the model group (SP ×400, Figure 2(c)).

3.2.2. Results of Caspase-3 Immunohistochemistry. There was little positive expression of each sampling point in the sham-operation group (SP ×400; Figure 2(d)). There was positive expression on the 1st day after operation in both the model and elongated needle groups (Table 2). Expression reached a peak on the 3rd day after operation. The positive cells in the model group were mainly scattered in the damaged dorsal horn grey matter. The positive signal was found inside ectoenzymes and endochylema (SP ×400; Figure 2(e)). In the elongated needle group, there was positive expression in the dorsal horn region of the spinal cord grey matter. However, the expression of positive cells was more scattered than that of the model group (SP ×400; Figure 2(f)).

3.2.3. Results of Semiquantitative RT-PCR for Expression of Fas and Caspase-3 mRNA. Table 3 shows the expression of Fas and caspase-3 mRNA after spinal cord injury. The integrity of RNA extraction is shown in Figure 3. The results of the electrophoresis are presented in Figure 4. Fas and caspase-3 mRNA expressions of each sampling point in the model and elongated needle groups significantly increase more than in the sham operation group. The expression of Fas mRNA on the 1st and 3rd days after operation in the elongated needle group is significantly different than that in the model group. The expression of caspase-3 mRNA on the 3rd and 5th days after operation in the elongated needle group significantly decrease more than in the model group.

4. Discussion and Analysis

The term "elongated needle" is derived from the long needle of the "nine classical needles" in *Huangdi Neijing* (the internal canon of medicine), famous for its wheat-like shape. Elongated needles are the thinnest needle in acupuncture, and penetration needling is a novel style of deep needling. Elongated needle therapy could help dredge Qi-blood of internal organs and main and collateral channels. Then, through the induction of main and collateral channels, Qi reaches the affected area. The effect of this therapy reaches beyond ordinary filiform needles. Mao [4] has summarized clinical reports of using elongated needle therapy and states that the emphasis of elongated needle therapy should be on deep penetration. Thus, elongated needle therapy applies to diseases of deep nerves, muscles and ligaments. The hand-manipulating route of Chihpien and Flume, accompanied with vascular anatomy, could confirm that ample blood vessels and nerve tracts that exist in the pelvic autonomic nerve. Elongated needles used to stimulate the pelvic autonomic nerve can adjust bladder detrusor and urethra sphincterismus, and it also has an effect on coordinating muscles. Moreover, it can reach the spinal center or cerebral cortex, and this conduction of neural signal has an influence on repairing damaged spinal cord tissue.

In our experiment, we found that nerve cell apoptosis co exists with necrosis after spinal cord injury. During the primary period of damage, there was organelle damage or dissolving, regional structure in a mass, and apoptosis, karyopyknosis, and apoptotic body formation. There were also one or several apoptotic areas around the spinal cord tissue. Therefore, apoptosis is one of the factors causing lesion area expansion, which agrees with previous studies [5, 6]. Using elongated needles to penetrate "Chihpien-Flume" points could save more spinal cord injury tissue neurons than that of the model group. The technique also clarifies nerve cell structure and decreases edema and necrosis, compared with the model group. There is also less proliferation of glial cells, less Fas and caspase-3 protein expressions, and less Fas and caspase-3 mRNA expressions in the elongated needle group than in the model group. Therefore, the elongated needle technique is effective at curing spinal cord injury, and apoptosis reduction is one of mechanisms of its curative effect.

Spinal cord injury includes two types, one is primary spinal cord injury and the other is sequential spinal cord injury. Primary spinal cord injury is caused by mechanical pressure, hemorrhage, or electrolytic changes inside cells. Primary spinal cord injury occurs in several hours and is irreversible. Sequential spinal cord injury refers to a series of biochemical changes, which include ischemia reperfusion, inflammation, apoptosis, immune response, blood spinal cord barrier damage, intracellular and extracellular ion disturbance, and free radical reaction. The delayed death of nerve cells from spinal cord injury may be reversible [7]. Medications, physicotherapeutics, and operations can treat secondary damage after SCI and can promote the regeneration of the spinal cord. The effective treatment of sequential spinal cord injury can improve patient prognosis and quality

Table 2: The Fas and Caspase-3 optical density values of rabbit spinal cord tissue among each group at different time points.

Group	n	Fas			Caspase-3		
		1 d	3 d	5 d	1 d	3 d	5 d
Sham-operation group	9	0.040 ± 0.009	0.041 ± 0.010	0.049 ± 0.009	0.0412 ± 0.0217	0.0247 ± 0.0129	0.0358 ± 0.0125
Model group	9	0.372 ± 0.047$^{\bullet\bullet}$	0.743 ± 0.068$^{\bullet\bullet}$	0.256 ± 0.040$^{\bullet}$	0.4050 ± 0.0554$^{\bullet\bullet}$	0.7468 ± 0.0486$^{\bullet\bullet}$	0.2723 ± 0.0404$^{\bullet\bullet}$
Elongated needle group	9	0.314 ± 0.089$^{\blacktriangle}$	0.465 ± 0.045$^{\blacktriangle\blacktriangle}$	0.216 ± 0.063$^{\blacktriangle}$	0.3935 ± 0.0767	0.5540 ± 0.0439$^{\blacktriangle\blacktriangle}$	0.226 ± 0.0749$^{\blacktriangle}$

compared with sham-operation group $^{\bullet}P < 0.05$ and $^{\bullet\bullet}P < 0.001$; compared with model group $^{\blacktriangle}P < 0.05$ and $^{\blacktriangle\blacktriangle}P < 0.01$.

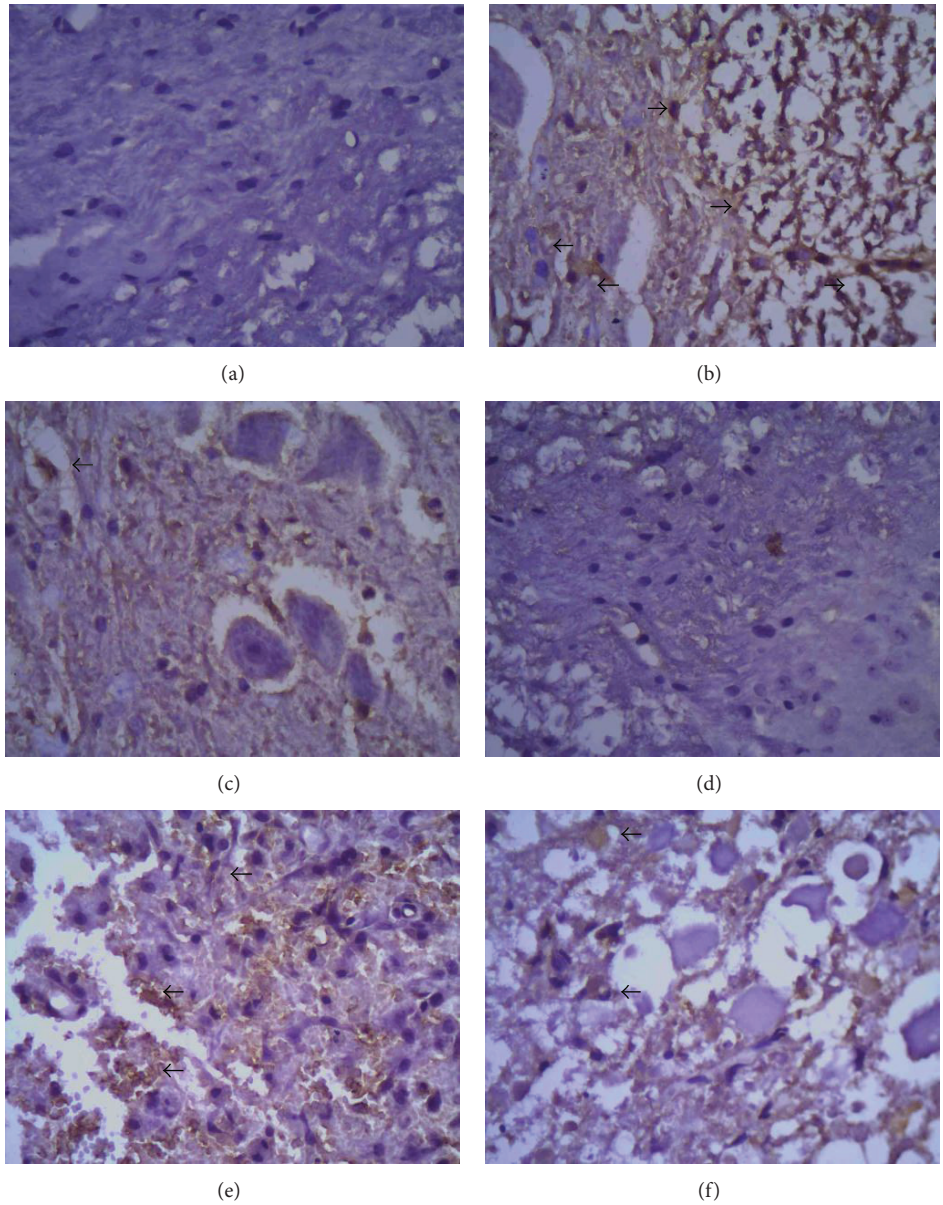

Figure 2: Use immunohistochemistry staining method to observe the positive cells expression in anterior and posterior horns of spinal cord. (a) On the 3rd day in the sham operation group, there was little positive cells expression of Fas protein (SP ×400). (b) On the 3rd day in the model operation group, positive cells of Fas protein scatter on damaged grey and white neuron, most of the positive cells scatter on white matter. There are positive signals inside ectoenzyme and endochylema (SP ×400). (c) On the 3rd day in the elongated needle therapy, the grey matter of Fas protein positive cells are less when comparing with the model group (SP ×400). (d) On the 5th day in the sham operation group, there is no evidence to show the positive cells expression of Caspase-3 protein. (e) On the 5th day in the model operation group, Caspase-3 protein positive cells are scattered on damaged grey matter dorsal horn neurons, and there are positive signals inside ectoenzyme and endochylema (SP ×400). (f) On the 5th day in the elongated needle therapy, there is expression of Caspase-3 positive cells in dorsal horn region of spinal cord grey matter, but the expression of positive cells is more scattered than that of the model group (SP ×400).

Table 3: The FasmRNA and Caspase-3mRNA relative expression level of rabbit spinal cord tissue among each group at different time points.

Group	n	Fas			Caspase-3		
		1 d	3 d	5 d	1 d	3 d	5 d
Sham-operation group	9	0.1034 ± 0.0085	0.1125 ± 0.0133	0.1357 ± 0.0272	0.1906 ± 0.0290	0.2176 ± 0.0132	0.1928 ± 0.0150
Model group	9	0.5069 ± 0.0687$^{\bullet\bullet}$	0.7223 ± 0.0257$^{\bullet\bullet}$	0.3147 ± 0.0142$^{\bullet}$	0.4074 ± 0.0310$^{\bullet\bullet}$	0.8583 ± 0.0402$^{\bullet\bullet}$	0.6534 ± 0.0273$^{\bullet\bullet}$
Elongated needle group	9	0.4075 ± 0.0216$^{\blacktriangle}$	0.5992 ± 0.0396$^{\blacktriangle}$	0.2834 ± 0.0216	0.4289 ± 0.0151	0.6236 ± 0.0223$^{\blacktriangle\blacktriangle}$	0.3478 ± 0.0258$^{\blacktriangle\blacktriangle}$

Note: compared with sham-operation group $^{\bullet}P < 0.05$, $^{\bullet\bullet}P < 0.001$; compared with model group $^{\blacktriangle}P < 0.05$, $^{\blacktriangle\blacktriangle}P < 0.01$.

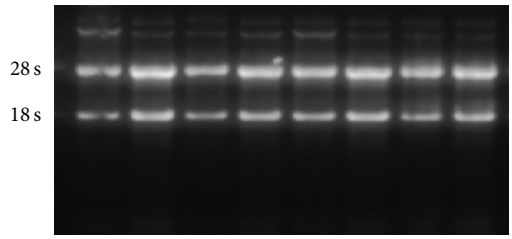

Figure 3: RNA extraction integrity.

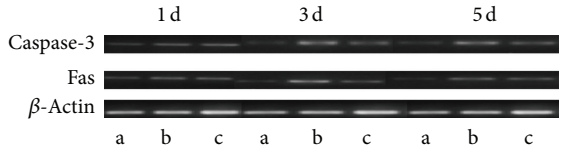

Figure 4: Fas mRNA and Caspase-3mRNA electrophoresis. *Note*: a: sham-operation group, b: model group, and c: elongated needle group.

of life [8]. Therefore, nerve recovery after sequential spinal cord injury is also the focus of our research.

Apoptosis is an essential part of sequential spinal cord injury. From the pathological point of view, mechanical force can cause bleeding, which is followed by tissue angiospasm, thrombus formation inside capillaries and ischemia in local nerve tissue. Mechanical force and ischemia in local nerve tissues can reinjure capillary endothelial cells, which causes expression of inflammatory mediators and activation of the glial cells and monocyte macrophage system. Then, inflammatory cells aggregate and clog capillaries, which aggravates the local ischemia [9]. After spinal cord injury, changes in the stability of factors that participate in pathological changes, such as oxygen free radicals and excitatory amino acids, could arouse oxygen free radical reaction, lipid peroxidation, and excitotoxicity. This can lead to changes in cell membrane permeability, intracellular calcium, sodium ion overload, and cellular edema [10]. These changes can eventually lead to apoptosis. Massive expression of inflammatory mediators and tumor necrosis factors can also induce apoptosis in the death receptor Fas/TNFR mediated pathway [11].

Fas is a 45 kDa membrane protein receptor, which belongs to tumor necrosis factor receptor family (TNFR) [12]. Fas can combine with caspase-8 to form a death-inducing signaling complex. Therefore, the expression of Fas can promote apoptosis [13]. The common pathway in the anaphase of apoptosis is caspase activation. Cysteine proteinase caspase functions as a final hub in apoptosis with several activated factors. Activated caspase-3 can cut many protein substrates, including cytoskeletal proteins (α-spectrin, β-spectrin, actin, and tau proteins), proteins participating in the regulation of the cytoskeleton, and enzymes participating in DNA repair such as PARP, DNA-PKcs, and apoptosis albumen Bcl-2. This finally may lead to cell death [14, 15]. In our experiments, we observed less expression of Fas and caspase-3 protein and weaker Fas and caspase-3 mRNA expressions in semiquantitative RT-PCR than that of the model group. Fas mRNA expression on 1st, 3rd, and 5th days in the model group are 2.1, 4.0 and 3.4 times that of the sham operation group. Through statistical analysis, this corresponds to homogeneity of variance. We observed that the peak-expression of Fas mRNA is earlier than that of caspase-3 mRNA. This shows that the mechanism of elongated needle therapy is to firstly activate Fas, and after a cascade of reactions, activate the caspase-3 cascade. Elongated needle acupuncture has a curative effect on spinal cord injury, and restraining apoptosis is one of its mechanisms. The Fas → caspase-3 cascade is probably the method by which apoptosis is restrained after spinal cord injury when using elongated needles. This provides new evidence for SCI and provides new clues to curing spinal cord injury.

5. Conclusions

Encouraging comprehensive treatment is the common clinical method for treatment of SCI, and acupuncture as a traditional and economic skill has an effect in curing spinal cord injury [16]. This study attempts to build up a new theoretical base of using elongated needle therapy to cure spinal cord injury.

Acknowledgment

The authors would like to gratefully acknowledge the financial support from the Zhejiang Provincial and Hangzhou City the Science and Technology Program.

References

[1] G. T. Williams and C. A. Smith, "Molecular regulation of apoptosis: genetic controls on cell death," *Cell*, vol. 74, no. 5, pp. 777–779, 1993.

[2] I. Heo, B.-C. Shin, Y.-D. Kim, E.-H. Hwang, C. W. Han, and K.-H. Heo, "Acupuncture for spinal cord injury and its complications: a systematic review and meta-analysis of randomized controlled trials," *Evidence-Based Complementary*

and Alternative Medicine, vol. 2013, Article ID 364216, 18 pages, 2013.

[3] S.-F. Huang, Y. Ding, J.-W. Ruan et al., "An experimental electro-acupuncture study in treatment of the rat demyelinated spinal cord injury induced by ethidium bromide," *Neuroscience Research*, vol. 70, no. 3, pp. 294–304, 2011.

[4] L. Mao, "Analysis on spectrum of using elongated needle therapy to curing diseases," *Chinese Medicine Research*, vol. 22, no. 1, pp. 61–62, 2009.

[5] E. D. Crown, Z. Ye, K. M. Johnson, G.-Y. Xu, D. J. McAdoo, and C. E. Hulsebosch, "Increases in the activated forms of ERK 1/2, p38 MAPK, and CREB are correlated with the expression of at-level mechanical allodynia following spinal cord injury," *Experimental Neurology*, vol. 199, no. 2, pp. 397–407, 2006.

[6] C. E. Hulsebosch, B. C. Hains, E. D. Crown, and S. M. Carlton, "Mechanisms of chronic central neuropathic pain after spinal cord injury," *Brain Research Reviews*, vol. 60, no. 1, pp. 202–213, 2009.

[7] H. Li, H. Zhu, C.-J. Xu, and J. Yuan, "Cleavage of BID by caspase 8 mediates the mitochondrial damage in the Fas pathway of apoptosis," *Cell*, vol. 94, no. 4, pp. 491–501, 1998.

[8] K. R. Byrnes, B. A. Stoica, S. Fricke, S. di Giovanni, and A. I. Faden, "Cell cycle activation contributes to post-mitotic cell death and secondary damage after spinal cord injury," *Brain*, vol. 130, no. 11, pp. 2977–2992, 2007.

[9] K. Nakamura, E. Bossy-Wetzel, K. Burns et al., "Changes in endoplasmic reticulum luminal environment affect cell sensitivity to apoptosis," *Journal of Cell Biology*, vol. 150, no. 4, pp. 731–740, 2000.

[10] D. Siniscalco, C. Fuccio, C. Giordano et al., "Role of reactive oxygen species and spinal cord apoptotic genes in the development of neuropathic pain," *Pharmacological Research*, vol. 55, no. 2, pp. 158–166, 2007.

[11] R. V. Rao, E. Hermel, S. Castro-Obregon et al., "Coupling endoplasmic reticulum stress to the cell death program. Mechanism of caspase activation," *Journal of Biological Chemistry*, vol. 276, no. 36, pp. 33869–33874, 2001.

[12] W. R. Yu and M. G. Fehlings, "Fas/FasL-mediated apoptosis and inflammation are key features of acute human spinal cord injury: implications for translational, clinical application," *Acta Neuropathologica*, vol. 122, no. 6, pp. 747–761, 2011.

[13] K. Kandasamy, S. M. Srinivasula, E. S. Alnemri et al., "Involvement of proapoptotic molecules Bax and Bak in tumor necrosis factor-related apoptosis-inducing ligand (TRAIL)-induced mitochondrial disruption and apoptosis: differential regulation of cytochrome c and Smac/DIABLO release," *Cancer Research*, vol. 63, no. 7, pp. 1712–1721, 2003.

[14] R. Eguchi, S. Toné, A. Suzuki et al., "Possible involvement of caspase-6 and -7 but not caspase-3 in the regulation of hypoxia-induced apoptosis in tube-forming endothelial cells," *Experimental Cell Research*, vol. 315, no. 2, pp. 327–335, 2009.

[15] H. Khalil, N. Peltzer, J. Walicki et al., "Caspase-3 protects stressed organs against cell death," *Molecular and Cellular Biology*, vol. 32, no. 22, pp. 4523–4533, 2012.

[16] B. C. Shin, M. S. Lee, J. C. Kong, and I. Jang, "Acupuncture for spinal cord injury survivors in Chinese literature: a systematic review," *Complementary Therapies in Medicine*, vol. 17, no. 5, pp. 316–327, 2009.

Hindawi Publishing Corporation
Evidence-Based Complementary and Alternative Medicine
Volume 2013, Article ID 767290, 12 pages
http://dx.doi.org/10.1155/2013/767290

Research Article

Modeling and Simulating Dynamics of Complete- and Poor-Response Chronic Hepatitis B Chinese Patients for Adefovir and Traditional Chinese Medicine Plus Adefovir Therapy

Lequan Min,[1,2] Xiao Chen,[2,3] Yongan Ye,[4] Qun Zhang,[2] Shuying Ru,[4] and Xiaoke Li[4]

[1] *School of Mathematics and Physics, University of Science and Technology Beijing, Beijing 100083, China*
[2] *School of Automation and Electrical Engineering, University of Science and Technology Beijing, Beijing 100083, China*
[3] *School of Informatics, Linyi University, Linyi 276005, China*
[4] *Traditional Chinese Internal Medicine Key Laboratory of China Education Ministry, Dongzhimen Hospital, Beijing University of Chinese Medicine, Beijing 100700, China*

Correspondence should be addressed to Lequan Min; minlequan@gmail.com

Received 6 July 2013; Accepted 30 August 2013

Academic Editor: Gerhard Litscher

ChiCTR-TRC-11001263 study was the first large-scale double-blind randomized placebo-controlled traditional Chinese medicines (TCMs) and adefovir (ADV) antihepatitis B virus (HBV) infection trial in the world. A total of 560 hepatitis B e antigen- (HBeAg-) positive Chinese patients with chronical HBV were randomly classified, in 1 : 1 ratio, into two groups: experimental group (EXG) receiving TCMs + ADV and controlled group (CTG) receiving ADV + TCM-placebo treatment for 48 weeks. This paper introduces two models to model and simulate the evolutions of dynamics for the complete-response patients and the poor-response patients in EXG and CTG, respectively. The stimulated mean HBV DNA and alanine aminotransferase (ALT) levels were close to the patients' experimental data. Analysis and simulations suggest that the activated patients' immune functions by TCMs + ADV may not only clear infected hepatocytes, but also clear HBV, which made the complete-response patients' mean serum HBV DNA levels in EXG reduce rapidly 12 weeks' earlier than the ones in CTG. One can assume that both the TCMs and ADV have the function of preventing complete-response patients' infected hepatocytes from being injured by cytotoxic T lymphocytes (CTLs); the patients' activated immune cells may also block HBV replications.

1. Author Summary

Nucleoside analogues (NAs), such as lamivudine, adefovir, entecavir, and telbivudine, suppress HBV replication and result in the improvement of the liver architecture. Some TCMs are able to activate patients' immune function because patients' serum HBeAg levels may reduce rapidly much earlier before their serum HBV DNA levels decrease significantly. ChiCTR-TRC-11001263 was the first international registered ADV + TCM-placebo (control group CTG) and TCM + ADV-placebo switching to TCM + ADV (experimental group EXG) anti-HBV infection therapy trial. Based on Nowak et al.'s uninfected cell-infected cell-free virus basic virus infection model, this paper introduces two models with additional immune variable and alanine aminotransferase loads to describe and understand the two group patients' dynamics for anti-HBV infection therapy. The results include the determinations of the model parameters, predicting the outcome of the long-term treatment, finding that both the TCMs and ADV may have the function of preventing complete-response patients' infected hepatocytes from being injured by CTLs; activated CTLs may also play the role of blocking HBV replications; HBeAg seroconversion may be defined as a predictor that patients can keep their activated immune function via one-year additional treatment, then ending their therapy.

2. Introduction

Hepatitis B is a life-threatening liver infection caused by hepatitis B virus (HBV), which can cause chronic liver disease and make people die of cirrhosis of the liver and liver cancer. Two billion people worldwide have been infected with HBV and more than 400 million have chronic (long-term) liver infections. An estimated 1 million people die every year due to the consequences of hepatitis B [1].

The goal of anti-CHB infection treatment is to achieve sustained suppression of HBV DNA and remission of liver disease [2]. Nucleoside analogues, such as lamivudine, adefovir, entecavir, and telbivudine, are popular drugs to treat HBV infection. The main role of nucleoside analogues is to block the replication of HBV DNA in vivo.

Some TCMs anti-HBV infection therapies have the advantages of rare viral mutation, rare side, and cheap price. Lines of evidence show that TCMs can regulate CHB patients' immune functions [3].

Monotherapy may have low response rates. Most CHB patients need long-term medication, which can maintain a low response rate after withdrawing drugs and result in higher rate of drug resistance [4–8]. The disadvantages of some NA monotherapies limit the clinical application of CHB patients' treatments.

NA + TCM therapy has better efficacy than monotone treatment, which is able to increase proportion of patients' achieving HBeAg loss and clear HBV directly without damaging patients' hepatocytes [3, 9].

Modelling the dynamics of HBV infection and other virus infections has attracted considerable attentions. Mathematical models play a significant role in improving understanding of the dynamics of the HBV infections in vivo. The models typically used to study HBV dynamics in vivo tend to focus on healthy cells, free virus, and infected cells [10, 11].

The basic viral infection dynamic mathematical model (BVIM) proposed by Nowak et al. [12, 13] has been widely used in the study of the dynamic of infectious agents such as hepatitis B, C and HIV. The BVIM has the following form [12]:

$$\begin{aligned} \dot{x} &= \lambda - dx - bvx, \\ \dot{y} &= bvx - ay, \\ \dot{v} &= ky - uv, \end{aligned} \tag{1}$$

where x, y, and v are the numbers of uninfected cells, virus-infected cells, and free virus, respectively. Uninfected cells are produced at a constant rate λ, die at rate dx, and become infected at rate bvx. Virus-infected cells are produced at rate bvx and die at rate ay. Free virus is produced from virus-infected cells at rate ky and is removed at rate uv.

Equation (1) has an infection free-steady state Q_1:

$$Q_1 = \left(\frac{\lambda}{d}, 0, 0\right), \tag{2}$$

representing an infected person's complete recovery. Equation (1) has also an endemic steady state Q_2:

$$Q_2 = \left(\frac{au}{\beta k}, \frac{\lambda}{a}\left(1 - \frac{1}{R_0}\right), \frac{d}{\beta}\left(R_0 - 1\right)\right), \quad R_0 = \frac{\lambda bk}{adu} \tag{3}$$

representing an infected person's persistent infection. Here, R_0 is called the basic virus reproductive number of model (1).

It has been proved that if $R_0 \leq 1$, then the infection-free steady state of the model (1) is globally attractive; otherwise the endemic steady state of the model (1) is globally attractive [14].

Since λ/d in R_0 represents the total number of uninfected cells of the patient's target organ, this implies that an individual with a larger liver will be more difficult to be cured than a person with a smaller one. The meaning of R_0 is questionable. Recently, some amended basic viral infection models (ABVIM) [10, 15, 16] are established. One of them takes the following form [15]:

$$\begin{aligned} \dot{x} &= \lambda - dx - \frac{bvx}{x + y}, \\ \dot{y} &= \frac{bvx}{x + y} - ay, \\ \dot{v} &= ky - uv, \end{aligned} \tag{4}$$

where the meanings of the variables x, y, and v and the parameters λ, d, a, k, and u are the same as those given in model (1). $(bvx)/(x+y)$ is the viral infected rate of uninfected cells by free virus and produced rate of virus from virus-infected cells.

The ABVIM has a basic virus reproductive number $R_0 = bk/(au)$, which is independent on the total number of cells of the patient's target organ. It has been proved that if $R_0 \leq 1$, then the infection free steady state is globally attractive; otherwise the endemic steady state is globally attractive [15, 17].

During the process of viral infections, the immune response has been shown to be universal and necessary to eliminate or control the disease [18, 19]. Actually, in most virus infections, cytotoxic T lymphocytes (CTLs) play a critical role in antiviral defense by attacking virus-infected cells [20].

Therefore, many viral infection dynamic mathematical models with immune response have been studied in recent years [3, 13, 20–22]. One of them has the following form [13]:

$$\begin{aligned} \dot{x} &= \lambda - dx - bvx, \\ \dot{y} &= bvx - ay - k_1 ye, \\ \dot{v} &= ky - uv, \\ \dot{e} &= k_2 y - k_3 e, \end{aligned} \tag{5}$$

where the meanings of the variables x, y, and v and the parameters λ, d, b, a, k, and u are the same as those given in model (1). The variable e represents the number of cytotoxic T lymphocytes (CTLs). CTLs are produced at rate $k_2 y$ and die at rate $k_3 e$. The term $k_1 ye$ is the death rate of virus-infected cells caused by immune response. Model (5) has a basic virus reproductive number $R_0 = \lambda bk/(adu)$, which is also dependent on the total number of cells of the patient's target organ. The infection free-steady state $Q_1 = (\lambda/d, 0, 0, 0)$ of model (5) is independent on the parameters k_2 and k_3 which relate to the production of CTLs.

Based on the experimental data and previous researches on the dynamics of virus infection model [3, 10, 12, 13, 15, 16, 20–22], this paper introduces two mathematical models to model, simulate, and analyze the dynamics of the evolutions of patients' mean serum HBV DNA and ALT levels and make long-term prediction for the complete-response patients and the poor-response patients for ADV monotherapy and TCM + ADV combination therapy.

3. Methods

3.1. Experiment. ChiCTR-TRC-11001263 study was a double-blind randomized placebo-controlled trial. ADV and two kinds of TCMs, Tiaoganjianpihuoxue grain (TCM1) and Tiaoganjieduhuashi grain (TCM2), were used in the trial. TCM1 consists of 13 herbal ingredients, and TCM2 consists of 15 herbal ingredients. A total of 560 Chinese HBeAg-positive CHB patients were randomly classified into, in 1 : 1 ratio, two groups: control group (CTG) and experimental group (EXG).

The patients' plasma HBV DNA level baselines were 3 $\log_{10}$copies/mL ~ 8 $\log_{10}$ copies/mL by PCR assay. And the alanine aminotransferase (ALT) level baselines were 2 ULN~ 12 ULN (Disease: ULN, upper limit of normal), where the abbreviation ULN represents "upper limit of normal". Total bilirubin (TBIL) load baselines were less or equal to 3ULN.

The patients in CTG received ADV (10 mg, once daily) + TCM-placebo (twice daily) for 48 weeks. The patients in EXG were divided into 3 subgroups as follows.

(a) Group EXG1 has 207 patients whose ALT levels were larger than 2 ULN and less than 6 ULN.

(b) Group EXG2 has 39 patients whose ALT levels were larger than 6 ULN and less than 12 ULN.

(c) Group EXG3 has 34 patients whose HBeAg levels were less than 60 S/CO.

The patients' numbers of the corresponding three subgroups in CTG are 206, 35, and 39, respectively. The control group and the experimental three subgroups have the same characteristics (ITT).

The experimental schemes of the three sub-EXGs were designed as follows.

(a) The patients in EXG1 received TCM1 (twice daily) + ADV-placebo (10 mg once daily) for the first 24 weeks and then switched to TCM2 + AD for additional 24 weeks.

(b) The patients in EXG2 received TCM2 (twice daily) + ADV-placebo (10 mg once daily) for the first 24 weeks and then switched to receive TCM2 + AD for additional 24 weeks.

(c) The patients in EXG3 continuously received TCM2 (twice daily) + ADV (10 mg once daily) for 48 weeks.

(d) During the first 24-week therapy if a patient's ALT level in EXG2 was larger than 8 × ULN, then the patient switched to receive TCM2 + ADV-placebo until the 24th week and then switched to receive TCM2 + ADV for additional 24 weeks.

Table 1: Virologic and biochemical responses at week 48.

Group	HBeAg loss	DNA < 10^3	ALT < 1 ULN
EXG1 *N* (%)	47/207 (22.71%)	62/207 (29.95%)	118/207 (57%)
CTG1 *N* (%)	26/206 (12.62%)	55/205 (26.83%)	121/206 (58.74)
P value	0.0106	0.5529	0.7972
EXG2 *N* (%)	15/39 (38.46%)	21/39 (53.85%)	28/39 (71.70%)
CTG2 *N* (%)	11/35(31.43%)	20/35 (57.14%)	24/35 (68.57%)
P value	0.6974	0.9596	0.9616
EXG3 *N* (%)	21/34 (61.76%)	17/34 (50.00%)	24/34 (70.59%)
CTG3 *N* (%)	13/39 (33.33%)	23/39 (58.97%)	29/39 (74.36%)
P value	0.0282	0.5942	0.9225

(e) For any one in EXG1 or EXG2, if a patient's HBeAg level was less than 60 S/CO, or ALT level was larger than 12×ULN, or TBIL level was larger than 3× ULN, then the patient switched to receive the scheme of EXG3 for therapy.

The main function of TCM1 is to regulate patients' immune abilities, and the main role of TCM2 is to block the repletion of HBV. However, efficacy of TCM2 is limited, and it needs NA (e.g., ADV) for combination therapy to increase its efficacy.

The therapy scheme suggests that the patients with lower immune abilities whose ALT levels were less than 6 ULN or HBeAg levels were larger than 60 S/Co or TBIL levels were less than 3 ULN should receive only TCM1 therapy to regulate their immune functions for the first 24 weeks if their tested items did not change to the levels given in item (e).

The conditions item (e) may be a criterion which makes corresponding patients switch to use TCM2 + ADC scheme for further therapy.

Consequently, the purpose of the above therapy scheme was to expect that the 24-week therapy would make some patients in groups EXG1 and EXG2 achieve the conditions in item (e). And then the patients in the three groups received the TCM2 + ADV combination treatment for additional 24 weeks.

Some virologic and biochemical responses of the six subgroups are listed in Table 1 (also see [9]). The results show that TCM + ADV anti-HBV combination therapy resulted in increased proportion of patients achieving HBeAg loss in the EXG1 and EXG3 versus the CTG1 and CTG3 at week 48. The other virologic and biochemical responses of the controlled group and the experimental group had not significant differences.

At week 48, there were 28 and 31 patients in EXG and CTG who achieved complete response (denoted by CEXG and CCTG), respectively. Meanwhile, there were 42 and 55 patients in EXG and CTG responded poorly (denoted by PEXG and PCTG). Here complete response is defined as HBV DNA level being lower than undetectable level (<1000 copies/mL) and HBeAg seroconversion (HBeAg < 1 and anti-HBe < 1); poor response is defined as less than 1 $\log_{10}$ copies/mL decrease in HBV DNA level from the baseline at the 48th week.

Table 2: Mean HBV DNA levels, ALT levels, and HBeAg levels at different weeks.

Group	Item	Weeks				
		0	12	24	36	48
CEXG	DNA	$4.46e+7$	$7.41e+7$	$6.49e+6$	63004	<1000
CCTG	DNA	$5.83e+7$	$3.62e+7$	$1.25e+6$	$7.97e+5$	<1000
CEXG	ALT	180.06	79.918	57.518	44.221	23.939
CCTG	ALT	198.02	42.329	30.235	28.439	23.784
CEXG	HBeAg	349.95	143.1	97.988	25.741	0.53036
CCTG	HBeAg	306.35	46.831	15.215	23.508	0.45258
PEXG	DNA	$2.67e+8$	$1.83e+8$	$1.15e+8$	$6.47e+7$	$6.14e+7$
PCTG	DNA	$1.85e+8$	$1.15e+8$	$8.37e+7$	$3.72e+7$	$9.59e+7$
PEXG	ALT	127.47	112.55	139.13	150.21	140.82
PCTG	ALT	128.36	113.18	126.19	144.36	155.41
PEXG	HBeAg	728.45	788.87	565.44	566.79	732.34
PCTG	HBeAg	703.73	672.5	488.11	510.91	690.28

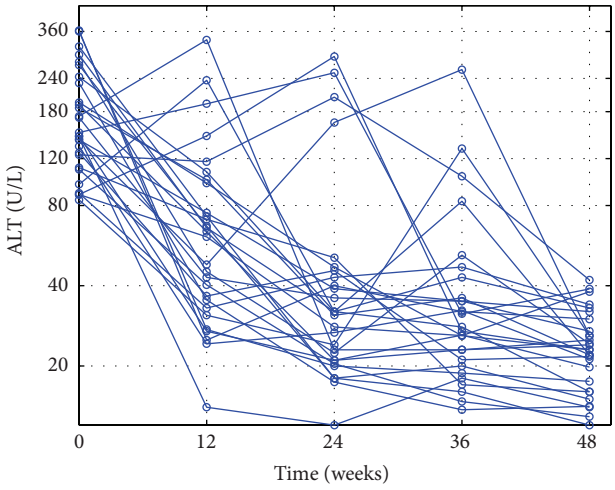

Figure 1: Outcomes of the complete-response patients' ALT loads in the experimental group during the 48-week therapy.

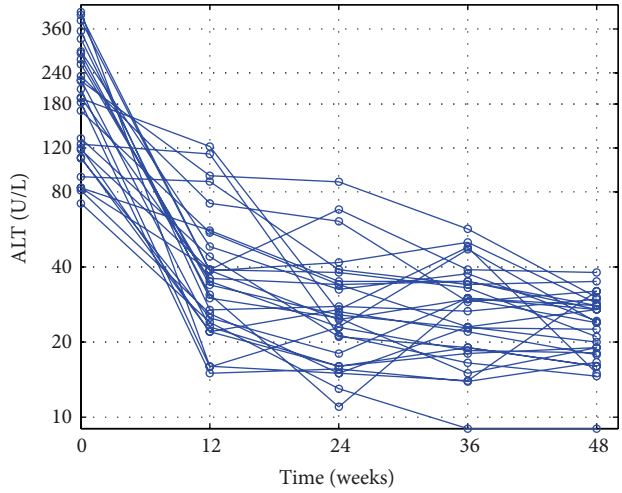

Figure 2: Outcomes of the complete-response patients' ALT loads in the control group during the 48-week therapy.

The outcomes of the patients' ALT loads in CEXG and CCTG are shown in Figures 1, 2, 3, and 4, respectively. The patients' mean HBV DNA levels, ALT loads, and HBeAg levels are listed in Table 2 (also see [23]).

Figures 1–4 and the data in Table 2 suggest that the main function of the TCMs is to regulate the patients' immune functions. The additional 24-week TCM + ADV therapy speeded up the patients' enhancement of immune functions. This observation motivates us to introduce two models to describe the dynamics of anti-HBV infection with ADV and TCMs + ADV in the next section.

3.2. Models. Based on the previous work [3, 10, 12, 13, 15, 16, 20–22] and the above analysis, we use model (6) to describe the dynamics of the CTG with the ADV anti-HBV infection therapy (similar to that proposed in [22] which does not include the ATL level variable w):

$$\begin{aligned}
\dot{x} &= \lambda - dx - (1-m)\frac{bvx}{x+y},\\
\dot{y} &= (1-m)\frac{bvx}{x+y} - ay - \frac{k_1 ye}{x+y},\\
\dot{v} &= (1-n)ky - uv,\\
\dot{e} &= k_2(x+y) - k_3 e,\\
\dot{w} &= k_5 + k_6\left(\frac{k_1 ye}{x+y}\right)^3 - k_7 w.
\end{aligned} \tag{6}$$

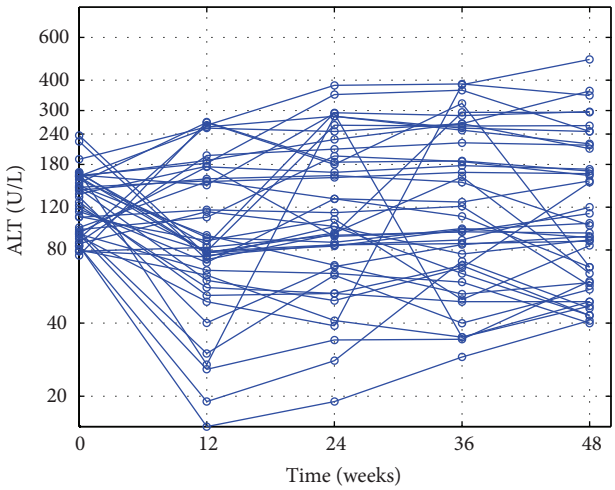

FIGURE 3: Outcomes of the poor-response patients' ALT loads in the experimental group during the 48-week therapy.

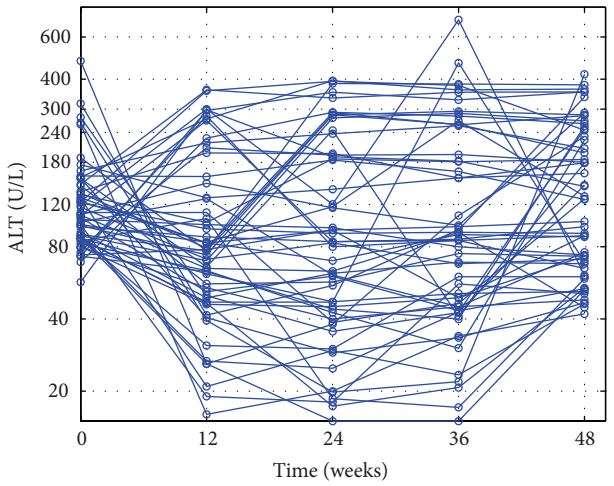

FIGURE 4: Outcomes of the poor-response patients' ALT loads in the control group during the 48-week therapy.

By the similar reasons, we introduce model (7) to describe the dynamics of the EXG with the TCM + ADV anti-HBV infection therapy (similar to [3, 24]):

$$\begin{aligned}
\dot{x} &= \lambda - dx - (1-m)\frac{bvx}{x+y},\\
\dot{y} &= (1-m)\frac{bvx}{x+y} - ay - \frac{k_1 ye}{x+y},\\
\dot{v} &= (1-n)ky - uv - \frac{k_4 ve}{x+y},\\
\dot{e} &= k_2(x+y) - k_3 e,\\
\dot{w} &= k_5 + k_6\left(\frac{k_1 ye}{x+y}\right)^3 - k_7 w.
\end{aligned} \tag{7}$$

Here, the meanings of the variables x, y, v, and e and the parameters λ, d, b, a, k, and u are the same as those given in model (1); e represents the number of CTLs which are produced at rate $k_2(x+y)$ and die at rate $k_3 e$; $(k_1 ye)/(x+y)$ is the death rate of virus-infected cells generated by immune killing; $(k_4 ve)/(x+y)$ is the clearing rate of virus generated by some specific immune abilities activated via antivirus infection therapy. The variable w represents the serum ALT levels. A liver without immune attacking produces ALT at rate k_5, and ALT dies at rate $k_7 w$. A CHB patient's liver produces ALT at rate $k_5 + k_6(k_1 ye/(x+y))^3$. m, n $(0 < m, n < 100\%)$ are the treatment efficacy variables during the anti-HBV treatment.

Model (6) and model (7) both have the same infection-free equilibrium Q_1:

$$Q_1 = \left(\frac{\lambda}{d}, 0, 0, \frac{k_2\lambda}{k_3 d}, \frac{k_5}{k_7}\right). \tag{8}$$

Model (6) has an endemic equilibrium Q_2^1:

$$Q_2^1 = (\overline{x}, \overline{y}, \overline{v}, \overline{e}, \overline{w}), \tag{9}$$

representing persistent virus infection, where

$$\begin{aligned}
\overline{x} &= \frac{\lambda u(1+c_1)}{du(1+c_1) + bkc_1}, \qquad \overline{y} = c_1\overline{x},\\
\overline{v} &= \frac{kc_1\overline{x}}{u}, \qquad \overline{e} = \frac{k_2\overline{x}(1+c_1)}{k_3},\\
\overline{w} &= \frac{1}{k_3 k_7}(k_3 k_5 + kk_2 k_6 c_1\overline{x}),\\
c_1 &= \frac{R_0 - 1 - c_2}{1+c_2}, \qquad R_0 = \frac{bk}{au}, \qquad c_2 = \frac{k_1 k_2}{ak_3}.
\end{aligned} \tag{10}$$

Model (7) has an endemic equilibrium Q_2^2:

$$Q_2^2 = (\overline{x}, \overline{y}, \overline{v}, \overline{e}, \overline{w}), \tag{11}$$

where

$$\begin{aligned}
\overline{x} &= \frac{\lambda}{d + (bc_1c_2)/1 + c_2}, \quad \overline{y} = c_2\overline{x},\\
\overline{v} &= c_1c_2\overline{x}, \qquad \overline{e} = \frac{k_2(1+c_2)\overline{x}}{k_3},\\
\overline{w} &= \frac{k_5(\overline{x}+\overline{y}) + k_1k_6\overline{y}\,\overline{e}}{k_7(\overline{x}+\overline{y})},\\
c_1 &= \frac{kk_3}{uk_3 + k_2k_4}, \qquad c_2 = \frac{bc_1k_3 - ak_3 - k_1k_2}{ak_3 + k_1k_2}.
\end{aligned} \tag{12}$$

For model (6), the basic virus reproductive number is

$$R_0 = \frac{kb(1-m)(1-n)}{au(1 + (k_1k_2/ak_3))}. \tag{13}$$

For model (7), the basic virus reproductive number is

$$R_* = \frac{kb(1-m)(1-n)}{au\left(1+\left(k_1k_2/ak_3\right)\right)\left(1+\left(k_2k_4/uk_3\right)\right)}. \quad (14)$$

Similar to [22], we can prove the following theorems.

Theorem 1. *Let R_0 be defined by (13). If $R_0 < 1$, then the infection-free equilibrium Q_1 of (6) is locally stable.*

Theorem 2. *If*

$$\frac{kb(1-m)(1-n)}{au} < 1, \quad (15)$$

then the infection-free equilibrium Q_1 of (6) is globally asymptotically stable.

Similar to [3, 24], we can prove the following theorems

Theorem 3. *Let R_* be defined by (14). If $R_* < 1$, then the infection-free equilibrium Q_1 of (7) is locally stable.*

Theorem 4. *If*

$$\frac{kb(1-m)(1-n)}{au} < 1, \quad (16)$$

then the infection free equilibrium Q_2 of (7) is globally asymptotically stable.

4. Numerical Simulation

In this subsection, in order to interpret more clearly the specific role of TCM in the anti-HBV infection therapy, we use model (7) and model (6) to simulate the dynamics of the evolutions of mean serum HBV DNA and ALT levels and make long-term prediction for the CRP and PRP in CTG and EXG anti-HBV infection therapies, respectively.

4.1. Simulations for Complete-Response Patients' Dynamics in EXG. Model (7) is used to simulate complete-response patients' dynamics for TCM + ADV anti-HBV infection therapy. Use the methods in [3, 15, 17, 22] to determine approximately the parameters in model (7) as follows.

(1) Because a human liver contains about 2×10^{11} hepatocytes [13], we obtain

$$\frac{\lambda}{d} \approx 2 \times 10^{11}. \quad (17)$$

(2) Since the half-life of a hepatocyte is about half a year [25], we get

$$d = -\frac{\ln(0.5)}{183}. \quad (18)$$

(3) Assuming the natural death rate of infected hepatocytes is the same as that of uninfected hepatocytes, hence we obtain

$$a = d. \quad (19)$$

(4) A CHB patient typically has between $\delta = 5\%$ and $\delta = 40\%$ infected hepatocytes [13]. Different CHB patient's serum HBV DNA load varies ranging from $\overline{v} = 10^3$ cps/mL to $\overline{v} = 10^{12}$ cps/mL. Hence, we assume that δ and $\overline{v}$ have the following relation:

$$\delta = p + q\overline{v}. \quad (20)$$

We can calculate p and q via the following equations:

$$\begin{aligned} 5\% &= p + q \times 10^3, \\ 40\% &= p + q \times 10^{12}. \end{aligned} \quad (21)$$

Consequently, we obtain

$$\delta = 0.05 + 3.5 \times 10^{-13}\overline{v}. \quad (22)$$

(5) In the complete-response patients in EXG for TCM + ADV anti-HBV infection therapy, $\overline{v} = 4.4556 \times 10^7$ cps/mL. Hence, we calculate

$$\delta \approx 0.050016. \quad (23)$$

(6) Chronic HBV infection makes some infected hepatocytes undergo apoptosis and be replaced by hepatic stellate cells [26]. Define a parameter δ_0, and the patient's hepatocytes are reduced by $(1-\delta_0) \times 100$ percent. Hence, we get

$$\overline{x} + \overline{y} = \delta_0 \frac{\lambda}{d}, \quad (24)$$

where we choose $\delta_0 = 0.95$. Furthermore, we obtain

$$\begin{aligned} \overline{x} &= (1-\delta)\,\delta_0 \frac{\lambda}{d}, \\ \overline{y} &= \delta\delta_0 \frac{\lambda}{d}. \end{aligned} \quad (25)$$

(7) Assuming the half-life of a virus is about one day [13], we obtain

$$u = 0.67. \quad (26)$$

(8) Assuming that the baseline $k_4 = 0$, we get

$$k = \frac{u\overline{v}}{\overline{y}}. \quad (27)$$

(9) Since the half-life of CTLs is about 77 days [27], we obtain

$$k_3 = -\frac{\ln(0.5)}{77}. \quad (28)$$

(10) Because the half-life of ALT is about 2~3 days [28], we select

$$k_7 = -\frac{\ln(0.5)}{2.5}. \quad (29)$$

(11) We assume that 22 U/L is the mean normal ALT level because the complete response patients' mean ALT level was

Table 3: Parameter values in different weeks for the complete-response patients' model in EXG.

Weeks	n	k	k_1	k_2	k_4
0~12	0.00	$1.1k$	$0.65k_1$	k_2	k_1
13~24	0.75	k	$0.60k_1$	$1.5k_2$	$4k_1$
25~36	0.995	k	$0.60k_1$	$3k_2$	$20k_1$
37~48	0.9998	k	$0.60k_1$	$3k_2$	$20k_1$

about 24 U/L at the week 48. When a human is healthy, $k_1 = 0$ in model (7). Hence, we can obtain that

$$k_5 = 22 \times 3 \times k_7 \tag{30}$$

because an individual has about about 3-liter serum.

(12) Solving the equilibrium point equation gives

$$b = \frac{\lambda - d\overline{x}}{\overline{v}(1-\delta)}, \qquad k_1 = \frac{b\overline{v}(1-\delta) - a\overline{y}}{\delta\overline{e}},$$
$$k_2 = \frac{k_3\overline{e}d}{\delta_0\lambda}, \qquad k_6 = \frac{(k_7\overline{w} - k_5)(\overline{x} + \overline{y})}{k_1\overline{y}\,\overline{e}}. \tag{31}$$

(13) Because a healthy Chinese has about 600 ± 300 counts/μL CD8 + T cells, we assume that

$$e_0 = 200 \times 3 \times 10^6. \tag{32}$$

(14) Select the mean serum HBV DNA level 4.4556×10^7 copies/mL at week 0 as the initial value, and an individual have 3-liter serum; hence we determine

$$v_0 = 4.4556 \times 10^7 \times 3 \times 10^3. \tag{33}$$

(15) Select the mean serum ALT level value 180.06 U/L (see Table 2) at week 0 as the initial value, and an individual have 3-liter serum; hence we obtain

$$w_0 = 180.06 \times 3. \tag{34}$$

(16) Select $m = 0$ since none of the available nucleoside analogues inhibitors have been shown to prevent infection of uninfected hepatocytes [29].

In order to agree with the experimental data, the parameters n, k, k_1, k_2, and k_4 need to be changed during the treatment. Their values are listed in Table 3.

Selecting the following initial condition

$$(x_0, y_0, v_0, e_0, w_0) = \left((1-\delta)\delta_0\frac{\lambda}{d}, \delta\delta_0\frac{\lambda}{d}, 4.4556 \times 10^7 \times 3 \times 10^3, 200 \times 3 \times 10^6, 180.06 \times 3\right), \tag{35}$$

then one can simulate the dynamics of the complete-response group in EXG for TCM + ADV anti-HBV infection therapy.

Table 4: Parameter values in different weeks for the complete-response patients' model in CTG.

Weeks	n	k_1	k_2
0~12	0.40	$0.55k_1$	k_2
13~24	0.95	$0.55k_1$	$1.5k_2$
25~36	0.95	$0.55k_1$	$2k_2$
37~48	0.9999	$0.55k_1$	$3k_2$

4.2. Simulations for Complete-Response Patients' Dynamics in CTG. Model (6) is used to simulate the complete-response patients' dynamics in CTG for ADV anti-HBV infection therapy. The parameters $\lambda/d, d, a, \delta_0, u, k, b, k_1, k_2, k_3, k_5, k_6$, and k_7 in model (6) have the same values as those given in (1) ~ (3) and (6) ~ (13) in the above section. Consider the following.

(1) Substituting $\overline{v} = 5.8337 \times 10^7$ cps/mL into formula (22) gives $\delta = 0.05002$.

(2) Since the mean serum HBV DNA load value at week 0 is 5.8337×10^7, it follows that $v_0 = 5.8337 \times 10^7 \times 3 \times 10^3$ via (14) in the above section.

(3) Since the mean serum ALT level value at week 0 is 198.02 U/L (see Table 2), it follows that $w_0 = 198.02 \times 3$ via (15) in the above section.

The parameters n, k_1, and k_2 have changed during the treatment. Their values are listed in Table 4.

Selecting the following initial condition:

$$(x_0, y_0, v_0, e_0, w_0) = \left((1-\delta)\delta_0\frac{\lambda}{d}, \delta\delta_0\frac{\lambda}{d}, 5.8337 \times 10^7 \times 3 \times 10^3, 200 \times 3 \times 10^6, 198.02 \times 3\right), \tag{36}$$

then one can simulate the complete-response patients' dynamics in CTG.

4.3. Simulations for Poor-Response Patients' Dynamics in EXG. Model (7) is used to simulate the poor-response patients' dynamics of in EXG for TCM + ADV anti-HBV infection therapy. The parameters $\lambda/d, d, a, \delta_0, u, k, b, k_1, k_2, k_3, k_4, k_5, k_6$, and k_7 in model (7) have the same values as those given in (1) ~ (3) and (6) ~ (13) in the above section. Consider the following.

(1) Substituting $\overline{v} = 2.6685 \times 10^8$ cps/mL into formula (22) gives $\delta = 0.050093$.

(2) Since the mean serum HBV DNA load value at week 0 is 2.6685×10^8, it follows that $v_0 = 2.6685 \times 10^8 \times 3 \times 10^3$.

(3) Since the mean serum ALT level value at week 0 is 127.47 U/L, it follows that $w_0 = 127.47 \times 3$.

The parameters n, k, k_2, and k_4 have changed during the treatment. Their values are listed in Table 5.

Table 5: Parameter values in different weeks for the poor-response patients' model in EXG.

Weeks	n	k	k_1	k_2	k_4
0~12	0.20	k	$0.90k_1$	$1.4k_2$	$2k_1$
13~24	0.30	k	$0.80k_1$	$2.4k_2$	$2k_1$
25~36	0.44	$1.2k$	k_1	$4.5k_2$	$2k_1$
37~48	0.18	$3k$	k_1	$4.0k_2$	$9k_1$

Table 6: Parameter values in different weeks for the poor-response patients' model in CTG.

Weeks	n	k	k_1	k_2
0~12	0.20	k	$0.9k_1$	$1.4k_2$
13~24	0.30	k	$0.8k_1$	$2.4k_2$
25~36	0.44	$1.3k$	k_1	$4.5k_2$
37~48	0.40	$3.5k$	k_1	$4.0k_2$

Selecting the following initial condition:

$$\begin{aligned}&(x_0, y_0, v_0, e_0, w_0)\\&= \left((1-\delta)\,\delta_0\frac{\lambda}{d}, \delta\delta_0\frac{\lambda}{d},\ 2.6685\times 10^8\times 3\times 10^3,\right.\\&\qquad \left. 200\times 3\times 10^6, 127.47\times 3\right),\end{aligned} \tag{37}$$

then one can simulate the poor-response patients' dynamics in EXG for TCM + ADV anti-HBV infection therapy.

4.4. Simulations for Poor-Response Patients' Dynamics in CTG. Model (6) is used to simulate the poor-response patients' dynamics in CTG for ADV anti-HBV infection therapy. The parameters $\lambda/d, d, a, \delta_0, u, k, b, k_1, k_2, k_3, k_5, k_6$, and k_7 in model (6) have the same values as those given in (1)~(3) and (6) ~ (13) in the above section. Consider the following.

(1) Substituting $\overline{v} = 1.8504 \times 10^8$ cps/mL into formula (22) gives $\delta = 0.050065$.

(2) Since the mean serum HBV DNA level at week 0 is 1.8504×10^8, it follows that $v_0 = 1.8504 \times 10^8 \times 3 \times 10^3$ via (14) in the above section.

(3) Since the serum ALT level value at week 0 is 128.36 U/L, it follows that $w_0 = 128.36 \times 3$.

The parameters m, n, k, k_1, and k_2 have changed during the treatment. Their values are listed in Table 6.

Selecting the following initial condition:

$$\begin{aligned}&(x_0, y_0, v_0, e_0, w_0)\\&= \left((1-\delta)\,\delta_0\frac{\lambda}{d}, \delta\delta_0\frac{\lambda}{d},\ 1.8504\times 10^8\times 3\times 10^3,\right.\\&\qquad \left. 200\times 3\times 10^6, 128.36\times 3\right),\end{aligned} \tag{38}$$

then one can simulate the dynamics of the poor response patients in CTG for ADV anti-HBV infection therapy.

5. Results

The numerical simulations of the evolution dynamics of patients mean serum HBV DNA and ALT levels for the four subgroups are shown in Figures 5 and 6, respectively. Observe that the stimulated evolutions of the mean serum HBV DNA levels and ALT levels are close to the experimental data.

The numerical simulations of the patients' dynamics of the anti-HBV infection therapies give the following results.

(1) At the week 0 (baseline), the basic virus reproductive numbers $R_*'s$ and $R_0's$ of the 4 subgroups CEXG, CCTG, PEXG, and CTG are 1.0526, 1.0527, 1.0527, and 1.0527, respectively. This can interpret why they become virus-persistent CHB patients.

After the 48-week therapy, the basic virus reproductive numbers R_* and R_0 of the two subgroups CEXG and CCTG were reduced to 1.1×10^{-4} and 7.9×10^{-5}, respectively. Further simulations show that it needs about 6.5 and 6.8 years of treatment to make all infected hepatocytes be replaced by normal ones, respectively.

After the 48-week therapy, the basic virus reproductive numbers R_* and R_0 of the two subgroups PEXG and PCTG were only reduced to 0.84085 and 0.87121, respectively. Further simulations show that the poor-response patients in EXG and CTG cannot be recovered completely until 20 years of treatments.

(2) Figure 5 and Table 2 show that the complete-response patients' mean serum HBV DNA levels in CEXG have reduced rapidly during week 24 and week 36, which was 12 weeks earlier than the complete response patients in CCTG.

In order to model this phenomenon, the parameter k_2 in model (7) related to the production rate of CTLs has increased from $2k_2$ to $4k_2$ while the parameter k_4 in model (7) has been designed to increase form $4k_1$ to $20k_1$ during week 24 and week 36. k_4 represents the clearing rate of virus generated by some specific immune abilities activated via anti-HBV infection therapy, which can clear HBV directly.

Combining the trial data listed in Tables 1 and 2 and the modeling data given in Tables 3 and 4 follows that the TCMs + ADV combination therapy may offer superior efficacy for suppressing HBV replications than monotone ADV therapy.

(3) Comparing the model parameters given in Tables 3–6 gives the following.

(a) At week 48, the poor-response patients' parameter value on n is much smaller than the complete-response patients' one.

(b) During weeks 25 to 48, the poor-response patients' parameter value on k increased while the complete-response patients' one kept unchanged.

The above results imply that for the poor-response patients, the drug resistance made the therapy efficacy (parameter n) reduce rapidly, and the virus replication rate (parameter k_1) was increased quickly.

6. Discussion

Based on the experimental data of CHB patients' serum HBV DNA levels and ALT levels, this paper introduces

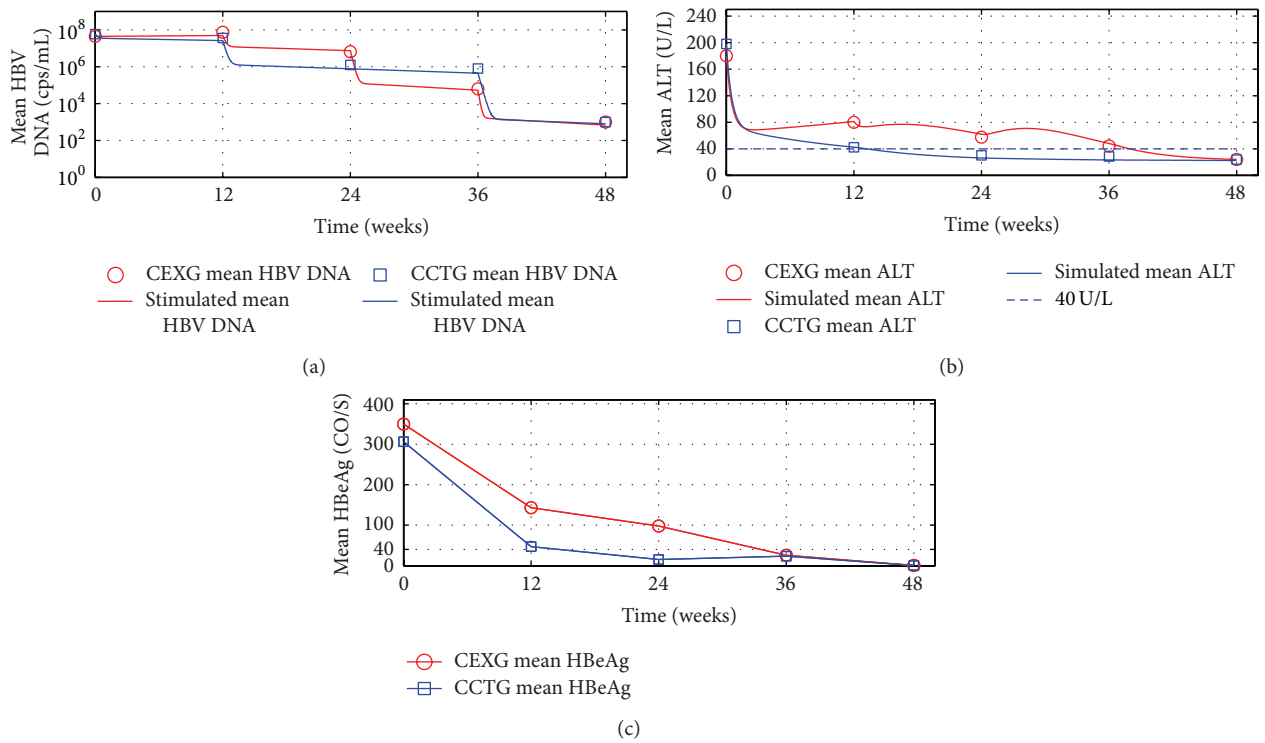

FIGURE 5: The outcomes of the complete-response patients' therapy efficacy in EXG and CTG. For 104-week treatments and 136-week followup: mean serum HBV DNA, ALT, and HBeAg levels. Solid lines: simulations of models (6) and (7). Circles and squares: complete-response patients' mean value experimental data in EXG and CTG, respectively. (a) Mean HBV DNA levels. (b) Mean ALT levels.

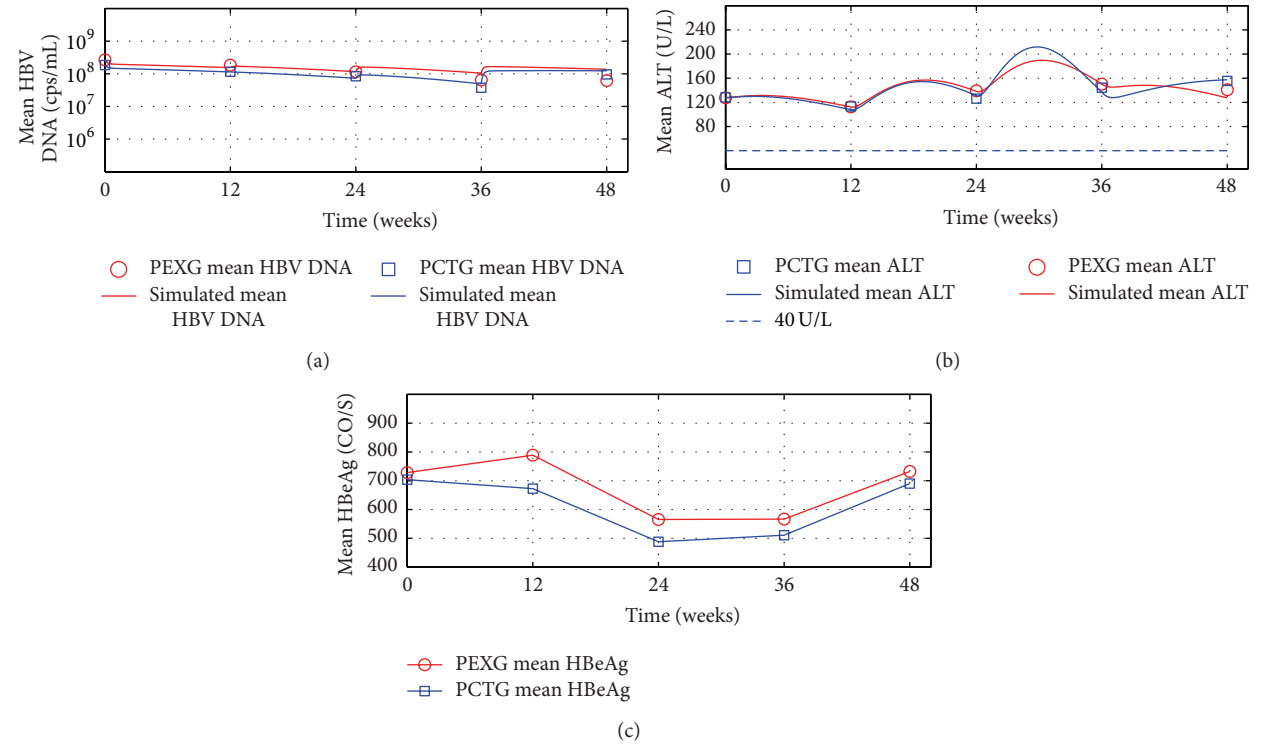

FIGURE 6: Outcomes of the complete-response patients' therapy efficacy in EXG and CTG. Mean serum HBV DNA, ALT, and HBeAg levels. Solid lines: simulations of models (6) and (7). Circles and squares: complete-response patients' mean value experimental data in EXG and CTG, respectively. (a) Mean HBV DNA levels. (b) Mean ALT levels. (c) Mean HBeAg levels.

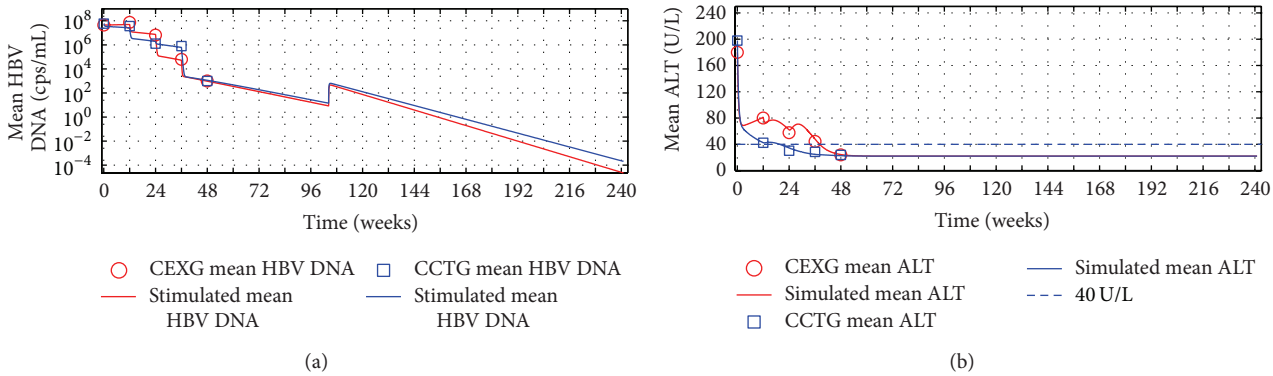

Figure 7: Outcomes of the poor-response patients' therapy efficacy in EXG and CTG. Mean serum HBV DNA, ALT, and HBeAg levels. Solid lines: simulations of models (6) and (7). Circles and squares: poor-response patients' mean value experimental data in EXG and CTG, respectively. (a) Mean HBV DNA levels. (b) Mean ALT levels. (c) Mean HBeAg levels.

two differential equation models (6) and (7) to describe the CHB patients' dynamics for the ADV monotone treatment and the TCMs + ADV combination therapy. An amended term $k_6(k_1 ye/(x + y))^3$ related to the ability for killing infected hepatocytes is included in the models to describe the evolution of the patients' ALT levels.

Making some simplified assumptions, one can determine 11 of the 13 parameters in (6) and (7). The simulation results are close to the patients' mean HBV DNA levels and mean ALT levels.

Based on the experimental data (see Table 2) and the simulation results, one can propose the following hypotheses.

Hypothesis (a). Both the TCMs and ADV have the function that prevents complete-response patients' infected hepatocytes from being injured by CTLs; that is, the killing parameter $k_1's$ in (6) and (7) becomes smaller than its baseline values.

This hypothesis may interpret why the complete-response patients' ALT loads decreased quickly while their HBV DNA levels decreased slowly or increased during the first 12-week therapy (see Tables 2, 3, and 4 and Figure 5).

Clinically, some patients with NA or TCM treatments may show serum HBV DNA levels to rebound higher than their baseline levels after cessation treatments. Hypothesis (a) may interpret that the patients kept the function of preventing infected hepatocytes from being injured by CTLs after stopping therapy.

The experimental data (see Table 2) and the simulation results (see Figure 6) suggest that the Chinese patients with high baseline HBV DNA levels, as well as HBeAg loads, and low baseline ALT levels may not obtain complete responses for the ADV or the CTMs + ADV treatments in 48 weeks.

The numerical simulations show that for the complete-response patients in EXG and CTG, it needs about 6.5 and 6.8 years of treatment to make all infected hepatocytes be replaced by normal if no virus mutations will appear and the efficacy of the therapy will be kept.

Clinically, a complete response CHB patient with nucleoside analogues treatment usually needs much longer times to obtain hepatitis B surface antigen loss. This fact suggests that patients' activated immune abilities may decrease as patients' HBV DNA levels decrease to very low levels.

At week 48, the very high efficacy (see n given in Tables 3 and 4 and Figure 5) of suppressing HBV replications makes us propose the second hypothesis.

Hypothesis (b). The efficacy of blocking HBV replications is not generated via TCMs and/or ADV alone. The CTLs (represented by variable e in (6) and (7)) efficiently control HBV replication by noncytolytic mechanisms [30] contributing also to block HBV replications.

This hypothesis may interpret why some patients' HBV DNA levels reduced rapidly at some specific time during their treatments because the activated noncytolytic mechanisms of CTL may play roles.

Based on a review article on the endpoints of hepatitis B treatment [31] and hypothesis (b), one can propose the following.

Hypothesis (c). For complete-response CHB patients with nucleoside analogues treatments, additional one-year consolidation therapy can make most patients keep their activated immune abilities (parameter k_2 in (6) and (7)), contributing to the treatment efficacy (parameter n) after finishing the consolidation treatment.

This hypothesis may interpret Recommendation 9 given in the Chronic Hepatitis B Guideline of the Asian-Pacific Association for the Study of the Liver.

For oral antiviral agents, in HBeAg-positive patients, treatment can be stopped when HBeAg seroconversion with undetectable HBV-DNA has been documented on 2 separate occasions at least 6 months apart [32].

Based on hypothesis (c), we assume that after finishing two-year treatment, the complete-response patients in EXG and CTG keep their immune parameter k_2 unchanged, k_1 returns to baseline, $k_4 = 0$, and efficacy parameter n reduces to 0.99. The simulated evolutions dynamics of HBV DNA levels and ALT levels are shown in Figure 7. Observe that the treatment benefits are kept.

Modeling the dynamics for the ADV monotone treatment and the TCMs + ADV combination therapy may also provide some theoretical interpretation for the medical statistic results (see Table 1).

Since the TCMs + ADV therapy made the patients have an additional immune term (see the third equation in (7)), the TCMs + ADV therapy significantly resulted in increased proportion of the patients achieving HBeAg loss in the experimental group (see Table 1).

The modeling analysis with the experimental data analysis motivates to propose the previous three hypotheses, which may interpret some clinical experience judgements. The dynamics of anti-HBV infection therapy are very complex. It is difficult to set up mathematical model to describe them accurately. However, modelling dynamics of anti-HBV infection therapy would enable a better understanding, prediction, and design of anti-HBV infection treatments.

Conflict of Interests

The authors have no conflict of interests to declare.

Acknowledgments

The authors would like to thank the referees for their valuable comments. The authors wish also to thank the following people who performed the experiments: Fengzhen Zhao (The First Hospital affiliated to Tianjin University of Chinese Medicine), Daqiao Zhou (Shenzhen College of Chinese Medicine), Mingxiang Zhang (Shenyan 6th People Hospital), Jingdong Xue (Shanxi Provincial Hospital of Chinese Medicine), Tiejun Liu (Hospital affiliated to Changchun University of Chinese Medicine), Xiaoling Chi (Guangdong Provincial Hospital of Chinese Medicine), Xianbo Wang (Ditan Hospital Affiliated to Capital University of Medicine), Bingjiu Lu (Liaoning Provincial Hospital of Chinese Medicine), Jun Li (302 Military Hospital of China), Qin Li (Fuzhou Infection Disease Hospital), Dewen Mao (The First Hospital affiliated to Guangxi College of Chinese Medicine), Huasheng Yang (Youan Hospital affiliated to Capital University of Medicine), Hongzhi Yang (The Third Hospital affiliated to Zhongshan University), Wenxia Zhao (The First Hospital affiliated to Henan College of Chinese Medicine), Yong Li (The Hospital Affiliated to Shandong University of Chinese Medicine), Guoliang Zhang (Anhui Provincial Hospital of Chinese Medicine), and Feng Jiang (Dongzhimen Hospital affiliated to Beijing University of Chinese Medicine).

References

[1] World health Organization, "Hepatitis B: Fact Sheet," 2013, http://www.who.int/mediacentre/factsheets/fs204/en/.

[2] A. S. Lok and B. J. McMahon, "Chronic hepatitis B," *Hepatology*, vol. 45, no. 2, pp. 507–539, 2007.

[3] X. Chen, L. Min, Y. Ye, and Y. Zheng, "Modeling and simulation for dynamics of anti-HBV infection therapy," *Lecture Notes in Electrical Engineering*, vol. 123, no. 2, pp. 557–566, 2011.

[4] E. B. Keeffe, S. Zeuzem, R. S. Koff et al., "Report of an International workshop: roadmap for management of patients receiving oral therapy for chronic hepatitis B," *Clinical Gastroenterology and Hepatology*, vol. 5, no. 8, pp. 890–897, 2007.

[5] F. Zoulim and R. Perrillo, "Hepatitis B: reflections on the current approach to antiviral therapy," *Journal of Hepatology*, vol. 48, supplement 1, pp. S2–S19, 2008.

[6] Y. F. Liaw, "On treatment outcome prediction and adjustment during chronic hepatitis B therapy: now and future," *Antiviral Therapy*, vol. 14, no. 1, pp. 13–22, 2009.

[7] A. S. Lok and B. J. McMahon, "Chronic hepatitis B: update 2009," *Hepatology*, vol. 50, no. 3, pp. 661–662, 2009.

[8] European Association for The Study of The Liver, "EASL clinical practice guidelines: management of chronic hepatitis B," *Journal of Hepatology*, vol. 50, no. 2, pp. 227–242, 2009.

[9] Y. Ye, L. Min, Q. Zhang et al., "Evaluation of 48 week adefovior dipvoxl (AD) and Chinese hebral medicine plus AD treatment in HBeAg(+) chronic hepatitis B Chinese patients: a doublebind randomized trial," in *Proceedings of the 62st Annual Meeting of the American Association for the Study of Liver Diseases: The Liver Meeting 2011*, vol. 54, p. 1047A, San Francisco, NC, USA, 2011.

[10] S. Eikenberry, S. Hews, J. D. Nagy, and Y. Kuang, "The dynamics of a delay model of hepatitis B virus infection with logistic hepatocyte growth," *Mathematical Biosciences and Engineering*, vol. 6, no. 2, pp. 283–299, 2009.

[11] S. Hews, S. Eikenberry, J. D. Nagy, and Y. Kuang, "Rich dynamics of a hepatitis B viral infection model with logistic hepatocyte growth," *Journal of Mathematical Biology*, vol. 60, no. 4, pp. 573–590, 2010.

[12] M. A. Nowak, S. Bonhoeffer, A. M. Hill et al., "Viral dynamics in hepatitis B virus infection," *Proceedings of the National Academy of Sciences of the United States of America*, vol. 93, no. 9, pp. 4398–4402, 1996.

[13] M. A. Nowak and R. M. May, *Virus Dynamics: Mathematical Principles of Immunology and Virology*, Oxford University, Oxford, UK, 2000.

[14] P. D. Leenheer and H. L. Smith, "Virus dynamics: a global analysis," *SIAM Journal on Applied Mathematics*, vol. 63, no. 4, pp. 1313–1327, 2003.

[15] L. Min, Y. Su, and Y. Kuang, "Mathematical analysis of a basic virus infection model with application to HBV infection," *Rocky Mountain Journal of Mathematics*, vol. 38, no. 5, pp. 1573–1585, 2008.

[16] S. A. Gourley, Y. Kuang, and J. D. Nagy, "Dynamics of a delay differential model of hepatitis B virus infection," *Journal of Biological Dynamics*, vol. 2, no. 2, pp. 140–153, 2008.

[17] Y. Zheng, L. Min, Y. Ji, Y. Su, and Y. Kuang, "Global stability of endemic equilibrium point of basic virus infection model with application to HBV infection," *Journal of Systems Science and Complexity*, vol. 23, no. 6, pp. 1221–1230, 2010.

[18] D. Kägi and H. Hengartner, "Different roles for cytotoxic T cells in the control of infections with cytopathic versus noncytopathic viruses," *Current Opinion in Immunology*, vol. 8, no. 4, pp. 472–477, 1996.

[19] J. E. Schmitz, M. J. Kuroda, S. Santra et al., "Control of viremia in simian immunodeficiency virus infection by CD8+ lymphocytes," *Science*, vol. 283, no. 5403, pp. 857–860, 1999.

[20] Q. Z. Xie, D. W. Huang, S. D. Zhang, and J. Cao, "Analysis of a viral infection model with delayed immune response," *Applied Mathematical Modelling*, vol. 34, no. 9, pp. 2388–2395, 2010.

[21] D. Wodarz, J. P. Christensen, and A. R. Thomsen, "The importance of lytic and nonlytic immune responses in viral infections," *Trends in Immunology*, vol. 23, no. 4, pp. 194–200, 2002.

[22] Y. Zheng, L. Min, X. Chen, and Y. Ye, "Dynamic analysis of HBV infection model with simulations for anti-HBV infection therapy," in *2011 IEEE International conference on Intelligent Computation and Bio-Medical Instrumentation, ICBMI 2011*, pp. 291–295, chn, December 2011.

[23] L. Min, X. Chen, Y. Ye et al., "Modeling and simulating dynamics of complete and poor response hbeag positive chronic hepatitis B chinese patients for adefovir (adv) and traditional chinese medicine plus adv therapy," in *Proceedings of the 22st Conference of the Asian Pacific Association for the Study of the Liver, Hepatology Intenational*, vol. 6, p. 62, Taipei, Taiwan, February 2012.

[24] X. Chen, L. Min, Y. Zheng et al., "Modeling and simulation for dynamics of anti-HBV infection therapy," *Computer Engineering and Applications*, vol. 48, pp. 20–27, 2012 (Chinese).

[25] A. S. Perelson, "Modelling viral and immune system dynamics," *Nature Reviews Immunology*, vol. 2, no. 1, pp. 28–36, 2002.

[26] R. Bataller and D. A. Brenner, "Liver fibrosis," *Journal of Clinical Investigation*, vol. 115, no. 2, pp. 209–218, 2005.

[27] M. Hellerstein, M. B. Hanley, D. Cesar et al., "Directly measured kinetics of circulating T lymphocytes in normal and HIV-1-infected humans," *Nature Medicine*, vol. 5, no. 1, pp. 83–89, 1999.

[28] S. L. Stockham and M. A. Scott, *Fundamentals of Veterinary Clinical Pathology*, Iowa State University Press, Ames, Iowa, USA, 2002.

[29] F. Zoulim, M. Buti, and A. S. Lok, "Antiviral-resistant hepatitis B virus: can we prevent this monster from growing?" *Journal of Viral Hepatitis*, vol. 14, no. 1, pp. 29–36, 2007.

[30] J. J. Chang, A. J. V. Thompson, K. Visvanathan et al., "The phenotype of hepatitis B virus-specific T cells differ in the liver and blood in chronic hepatitis B virus infection," *Hepatology*, vol. 46, no. 5, pp. 1332–1340, 2007.

[31] W. Chotiyaputta and A. S. F. Lok, "Endpoints of hepatitis B treatment," *Journal of Viral Hepatitis*, vol. 17, no. 10, pp. 675–684, 2010.

[32] Y. Liaw, N. Leung, J. Kao et al., "Asian-Pacific consensus statement on the management of chronic hepatitis B: a 2008 update," *Hepatology International*, vol. 2, no. 3, pp. 263–283, 2008.